Universität Augsburg University

# Statistical Downscaling to Analyze the Impacts of Climate Change on Future Water Resources of the Indus River Basin of Pakistan

**by**

**Muhammad Saleem Pomee**

A cumulative dissertation submitted in the fulfillment of the requirements for the degree of Doctor in natural sciences at the University of Augsburg

**Faculty of Applied Computer Sciences and Faculty of Medicine**

**University of Augsburg**
**Germany**

May 2022

Universität Augsburg
University

# Statistisches Downscaling zur Analyse der Auswirkungen des Klimawandels auf die zukünftigen Wasserressourcen des Indus in Pakistan

**by**

**Muhammad Saleem Pomee**

Kumulative Dissertation zur Erlangung des naturwissenschaftlichen Doktorgrades
(Dr. rer. nat.) der Universität Augsburg

**Fakultät für Angewandte Informatik und Medizinische Fakultät**

**Universität Augsburg**
**Germany**

Mai 2022

| | |
|---|---|
| First Reviewer: | Prof. Dr. Elke Hertig, University of Augsburg |
| Second Reviewer: | Prof. Dr. Harald Kunstmann, University of Augsburg |
| Member Examination Committee: | Prof. Dr. Matthias Schmidt, University of Augsburg |
| Date of Oral Examination: | May 9, 2022 |

# Executive Summary

The Indus River system derives the bulk of its runoff from complex processes operating simultaneously at various scales within the cryosphere-dominated Upper Indus Basin (UIB) to support the livelihood of a large population. However, the mountain climate of the UIB has shown conflicting signals to draw uncertain inferences about its future hydrology and cryosphere stability. This implicates rational adaptation planning across the basin. The UIB is a known climate hotspot, and observational and general circulation model (GCM) simulation challenges influence its meteo-hydrological uncertainties.

The current PhD study used an advanced statistical downscaling framework to improve climate simulations over Pakistan's Indus River basin by focusing on the UIB within available observational constraints. Besides precipitation, both maximum and minimum temperatures were modeled due to their distinct influence on regional water balance and glacial stability. Given their relatively skillful representation in the GCMs, large-scale atmospheric dynamics rather than precipitation were used in the downscaling process as modeled precipitation is affected by a lack of reliability associated with its complex generating mechanism and high spatial variability. Such model limitations manifest over high mountain regions like the UIB, where orography results in additional precipitation variation. Severe observational constraints further restrict the ability to correct such GCM biases adequately over the UIB.

The downscaling focused on the spatiotemporal variability of the regional climate, reference and GCM level of uncertainties, and statistical skills of regression models using an observational profile that the recent high altitude (HA) observatories have significantly improved. K-means clustering initially helped identify homogeneous precipitation regions by using observed precipitation variability on seasonal scales. The clustering process established how relatively low altitude stations could be used to explain the precipitation dynamics over HA regions. Avoiding downscaling over the recently established HA stations is advantageous for circumventing temporal and quantitative biases associated with shorter data and erroneous precipitation measurements over these regions.

Atmospheric drivers of the sub-regional precipitation (temperature) were then identified from the ERA-Interim reanalysis dataset by implementing a robust cross-validation framework. The identified ERA-predictors were compared separately with two additional reanalysis datasets (ERA5 and NCEP-NCAR-II) to estimate their suitability for regional analysis by quantifying reference uncertainties. Such predictor comparisons with GCMs' historical simulations helped rank the models and quantify uncertainties (model uncertainty) according to the ability of models to simulate precipitation (temperature) predictors.

Predictors under two Representative Concentration Pathway scenarios (i.e., RCP4.5 and RCP8.5) were used in the respective regression models to assess future precipitation and temperatures over the basin. Overall, significantly wetter and warmer conditions could dominate the basin hydrology throughout the 21st century compared to the base climate (1976-2005). These multi-model (median) signals intensified towards the end of the century (2071-2100) under the RCP8.5 scenario. Signal-to-noise ratio (SNR) and better-performing GCMs further validated these findings. Seasonally, the future winter (DJFM) would experience the highest precipitation and ($T_{min}$ dominated) warming. The Karakoram region would experience the highest precipitation increase. Meanwhile, significant decreases in precipitation as well as ($T_{max}$ dominated) increased warming was projected during the pre-monsoon (AMJ) period. The future monsoon (JAS) season showed increased precipitation and a striking feature of low-warming conditions over the UIB. The Lower Indus showed more warming compared to the UIB during all seasons.

These typical climatic changes would exert tremendous influence on the hydrology of the basin. For instance, the liquid precipitation proportion may significantly increase due to rising nighttime temperatures in winter. Decreasing spring precipitation may be compensated to some extent by increased melting (glacial and previously accumulated snow) and favorable climatic changes over the eastern tributaries. Increased winter precipitation could increase base flows, which may cause heavy flooding under the projected monsoon strengthening. Increased minimum temperatures could also trigger avalanches and ice mass redistribution, affecting water resources, infrastructure, and communities. Increased warming over the Lower Indus may prompt an early start of the agricultural seasons and a tremendous increase in future water demand.

Such favorable meteorological changes over the UIB may significantly increase future water availability to help meet water demand. Contrary to some downscaling studies, an increased water supply may remain possible without a rapid glacial retreat, particularly over the Karakoram region. Therefore, the continuation of the Karakoram anomaly until the end of the 21st century is possible even under the RCP8.5 forcing. Increased albedo, aerosol forcing, and cloud radiative feedbacks associated with stronger and further northward penetrating westerly (monsoon) circulations may induce glacial stability in the future**.** Adopting uniform lapse rates without considering spatial heterogeneity within the UIB and improper representation of the monsoon-topography internal feedbacks in GCMs may induce warm biases, which overestimate glacier retreats in such bias-corrected (downscaling) studies.

Such predictor-predictand modeling to estimate future climate response and associated robustness at finer scales was never performed in the region, presenting an alternate simulation perspective. Such a statistical framework may influence future climate research in the region and other complex and data constraint settings to support regional adaptations.

# Zusammenfassung

Das Indus-Flusssystem gewinnt den Großteil seines Abflusses auf Basis komplexer Prozesse, die zeitgleich auf verschiedenen Ebenen innerhalb des von der Kryosphäre dominierten Oberen Indus-Beckens (engl. Upper Indus Basin, UIB) ablaufen, um den Lebensunterhalt einer großen Bevölkerung zu sichern. Das Gebirgsklima des UIB, einem bekannten Klimahotspot, hat bisher jedoch widersprüchliche Signale gezeigt, die zuverlässige Rückschlüsse auf die künftige Hydrologie und die Stabilität der Kryosphäre erschweren und eine rationale, zukunftsgerichtete Anpassungsplanung im gesamten Einzugsgebiet erforderlich machen. Die Beschaffenheit des Untersuchungsgebietes erschwert sowohl eine zuverlässige Messung als auch die Simulation von klimatischen Parametern, welche weitestgehend für die bestehenden meteorologischen und hydrologischen Unsicherheiten verantwortlich sind.

In der vorliegenden Arbeit wurde ein innovatives statistisches Downscaling-Verfahren angewandt, um die Klimasimulationen über dem pakistanischen Indus-Einzugsgebiet zu verbessern, wobei der Schwerpunkt auf dem UIB im Rahmen der verfügbaren Beobachtungen lag. Neben dem Niederschlag wurden auch die Maximal- und Minimallufttemperaturen modelliert, da diese einen großen Einfluss auf den regionalen Wasserhaushalt und die Gletscherstabilität aufweisen. Die großräumige atmosphärische Dynamik wurde anstelle des Niederschlags, den es aufgrund von komplexen Entstehungsmechanismen und einer hohen räumlichen Variabilität noch immer an Zuverlässigkeit in den neuesten globalen Klimamodellen (GCMs) mangelt, in den Downscaling-Prozess einbezogen, da diese vergleichsweise relativ gut dargestellt wird. Solche Modellbeschränkungen zeigen sich besonders in Hochgebirgsregionen wie der UIB, wo die Orographie einen zusätzlichen Einfluss auf Niederschlagsbildung, -mengen und -variabilität darstellt. Darüber hinaus führen die komplexen lokalen Bedingungen zu Ungenauigkeiten bei der Erhebung von Messdaten, wodurch die Möglichkeiten zur Korrektur solcher GCM-Bias über dem UIB entsprechend weiter eingeschränkt werden.

Beim Downscaling lag ein besonderer Schwerpunkt auf der räumlich-zeitlichen Variabilität des regionalen Klimas, den Unsicherheiten auf Messdaten- und GCM-Ebene und den statistischen Fähigkeiten der Regressionsmodelle unter Verwendung von Beobachtungsdaten, die durch den zusätzlichen Einbezug von Observationen aus der Hochgebirgsregion (engl. high altitude, HA) deutlich für die Anwendung verbessert wurden.

Basierend auf der beobachteten saisonalen Niederschlagsvariabilität wurde zunächst eine K-Means-Clusteranalyse zur Ermittlung von homogenen Niederschlagsregionen durchgeführt. Der Clustering-Prozess zeigte dabei auch das Potential auf, inwieweit anhand von relativ niedrig gelegenen Messstationen die HA-Niederschlagsdynamik erklärt werden kann. Die Vermeidung von den erst kürzlich installierten HA-Stationen beim Downscaling ist von Vorteil, um, mit kürzeren Datenzeitreihen

und Niederschlagsmessungen verbundene, zeitliche und quantitative Bias zu umgehen. Durch die Anwendung eines robusten Kreuzvalidierungsverfahrens wurden die atmosphärischen Einflussfaktoren auf den subregionalen Niederschlag (Temperatur) anhand des ERA-Interim-Reanalysedatensatzes ermittelt. Die identifizierten ERA-Prädiktoren wurden separat mit zwei weiteren Reanalysedatensätzen (ERA5 und NCEP-NCAR-II) verglichen, um ihre Eignung für die regionale Analyse basierend auf der Quantifizierung der Referenzunsicherheiten zu bewerten. Solche Vergleiche der Prädiktoren mit den historischen Simulationen der GCMs halfen bei der Beurteilung der Modelle (Modellunsicherheit) entsprechend ihrer Fähigkeit, Niederschlags- (Temperatur-) Prädiktoren zu simulieren.

GCM-Prädiktoren für zwei repräsentative Konzentrationspfadszenarien (RCP4.5 und RCP8.5) wurden in den jeweiligen Regressionsmodellen verwendet, um die künftigen Niederschläge und Temperaturen im Einzugsgebiet abzuschätzen. Die Ergebnisse zeigen, dass im Vergleich zur Referenz (1976-2005) deutlich nassere und wärmere Bedingungen die Hydrologie des Einzugsgebiets im 21. Jahrhundert dominieren werden. Diese Multimodell-Signale (Median) verstärken sich unter dem RCP8.5-Szenario und gegen Ende des Jahrhunderts (2071-2100) unter dem RCP8.5-Szenario. Das Signal-Rausch-Verhältnis und die besser abschneidenden GCMs bestätigten zusätzlich diese Ergebnisse. In der Karakorum-Region würde saisonal betrachtet der Winter (DJFM) in Zukunft die stärksten Niederschläge und die (von $T_{min}$ dominierte) stärkste Erwärmung erfahren. Für den Vormonsun (AMJ) wurden dagegen deutlich geringere Niederschläge und eine starke Erwärmung (dominiert von $T_{max}$) projiziert. Die künftige Monsun-(JAS)Saison zeigte erhöhte Niederschläge und eine moderate Erwärmung der UIB-Region. Die untere Indus-Region erwärmte sich stärker im Vergleich zur UIB in allen Jahreszeiten.

Diese projizierten klimatischen Veränderungen würden einen enormen Einfluss auf die Hydrologie des Einzugsgebiets haben. So könnte sich beispielsweise der Anteil des flüssigen Niederschlags aufgrund steigender nächtlicher Temperaturen im Winter deutlich erhöhen. Abnehmende Frühjahrsniederschläge könnten bis zu einem gewissen Grad durch einen zunehmenden Schmelzwasseranteil (Gletscherschmelze und zuvor akkumulierter Schnee) und günstige klimatische Veränderungen über den östlich gelegenen Nebenflüssen kompensiert werden. Erhöhte Winterniederschläge führen möglicherweise zu einem Anstieg des Basisabflusses, was bei der projizierten Verstärkung des Monsuns zu schweren Überschwemmungen führen könnte. Erhöhte Minimumtemperaturen könnten auch Lawinenabgänge und die Umverteilung von Eismassen begünstigen und somit auch Wasserressourcen, Infrastruktur und die ansässige Bevölkerung beeinflussen. Die starke Erwärmung über dem unteren Indus könnte zu einem früheren Beginn der landwirtschaftlichen Saison und einem enormen Anstieg des zukünftigen Wasserbedarfs führen.

Solche meteorologischen Veränderungen über der UIB könnten die künftige Wasserverfügbarkeit erheblich steigern und dazu beitragen, den Wasserbedarf im Untersuchungsgebiet zu decken. Im

Gegensatz zu einigen Downscaling-Studien zeigen die Ergebnisse der vorliegenden Arbeit, dass eine erhöhte Wasserversorgung auch ohne einen raschen Gletscherrückgang möglich sein kann, insbesondere in der Karakorum-Region. Daher wäre eine Fortsetzung der Karakorum-Anomalie bis zum Ende des 21. Jahrhunderts möglich, selbst unter dem RCP8.5-Szenario. Eine erhöhte Albedo, der Einfluss von Aerosolen und Wolkenstrahlungsrückkopplungen in Verbindung mit stärkeren und weiter nach Norden vordringenden westlichen (Monsun-)Zirkulationen führen gegebenenfalls zu einer zukünftigen Gletscherstabilität. Die Annahme einheitlicher Schmelzraten ohne Berücksichtigung der räumlichen Heterogenität innerhalb der UIB und die unsachgemäße Darstellung der internen Rückkopplungen zwischen Monsun und Topographie in den GCMs können für zu warme Bias und damit einhergehend für zu hoch geschätzte Gletscherrückgänge in bisher veröffentlichten Biaskorrektur-basierten (Downscaling) Studien verantwortlich sein.

Eine in dieser Arbeit durchgeführte Prädiktor-Prädiktand-Modellierung zur Abschätzung der künftigen Klimareaktion und der damit verbundenen Robustheit auf feineren Skalen wurde in der Region noch nie durchgeführt, was eine alternative Perspektive für Simulationen darstellt. Die hier entwickelte statistische Methodik könnte die künftige Klimaforschung in der Region und in anderen komplexen und von eingeschränkter Datenverfügbarkeit betroffenen Umgebungen positiv beeinflussen, um regionale Anpassungen an den zu erwartenden Klimawandel zu unterstützen.

# Table of Contents

# List of Acronyms used in this Thesis

| | |
|---|---|
| UIB | Upper Indus Basin |
| GCM | General Circulation Model |
| HA | High Altitude/ High Elevation |
| HKH | Hindukush, Karakoram, and Himalayans |
| SNR | Signal to Noise Ratio |
| $T_{max}$ | Maximum Temperature /Daytime Temperature |
| $T_{min}$ | Minimum Temperature /Nighttime Temperature |
| RCP | Representative Concentration Pathway |
| UN | United Nations |
| EDW | Elevation Dependent Warming |
| RCM | Regional Climate Model |
| $km^2$ | Square Kilometres |
| bcm | Billion Cubic Meter |
| RR | Regional Representative |
| zg | Geopotential Height |
| va | Meridional Wind Component |
| ua | Zonal Wind Component |
| hus | Specific Humidity |
| hur | Relative Humidity |
| ta | Air Temperature |
| hPa | Hectopascal |
| °E | Degree East |
| °N | Degree North |
| PCA | Principal Component Analysis |
| PC | Principal Component |
| GLM | Generalized Linear Model |
| MLR | Multiple Linear Regression |
| MSESS | Mean Squared Error Skill Score |
| MSE | Mean Squared Error |
| CMIP5 | Phase 5 of the Coupled Model Intercomparison Project |
| PS | Performance Score |
| CR | Pattern Correlation |
| NSD | Normalized Standard Deviation |
| RMSE | Root Mean Squared Error |
| RCP4.5 | Representative Concentration Pathway, Radiative Forcing Scenario 4.5 |

| | |
|---|---|
| RCP8.5 | Representative Concentration Pathway, Radiative Forcing Scenario 8.5 |
| PARC | Pakistan Agricultural Research Council |
| WCA | West Central Asian |
| PhD | Doctor of Philosophy |
| ELA | Equilibrium Line Altitude/ Summer Freezing Line |
| WMO | World Meteorological Organisation |
| LI | Lower Indus |
| CORDEX-SA | Coordinated Regional Climate Downscaling Experiment for South Asia |
| HAR | High Asia Refined Analysis |
| PMD | Pakistan Meteorological Department |
| WAPDA | Water and Power Development Authority |
| CAK | Cultural Areas Karakoram |
| WS | Winter Season (DJFM) |
| PMS | Pre-monsoon Season (AMJ) |
| MS | Monsoon Season (JAS) |
| K-S | Kolmogorov-Smirnov |
| dd | Decimal Degrees |
| Long | Longitude |
| Lat | Latitude |
| PDF | Probability Density Function |
| SPM | Single Predictor Model |
| SSE | Sum of Squared Error |
| R1 | Region 1 |
| HA-UIB | High Altitude -UIB |
| NAO | North Atlantic Oscillation |
| ENSO | El Niño-Southern Oscillation |
| Hi-AWARE | Himalayan Adaptation, Water and Resilience Research |
| CARIAA | Collaborative Adaptation Research Initiative in Africa and Asia |
| ORNL | Oak Ridge National Laboratory |
| DAAD | Deutscher Akademischer Austauschdienst (German Academic Exchange Service) |
| PARC | Pakistan Agricultural Research Council |
| Hi-AWARE | Himalayans Adaptation, Water and Resilience Research |
| CMIP3 | Phase 3 of the Coupled Model Intercomparison Project |
| FAO | Food and Agriculture Organisation |
| MME | Multi-Model Ensemble |
| SI | Supporting Information |
| DTR | Diurnal Temperature Range |
| WRF | Weather Research and Forecasting |

# List of Figures

# Acknowledgments

I am indebted to Almighty ALLAH, worthy of all praises, for blessing me with the opportunity, skills, and passion for achieving this professional triumph.

As a water resources manager, I extensively learned and worked on how to improve water-use efficiency in the agriculture sector, which is the backbone of Pakistan's economy. From hydrology, I already knew how to estimate future water supplies and needs for water resources planning. However, I was always keen to learn how climate change would influence water balance over large spatial scales. In particular, I was interested in learning physical mechanisms that control spatial precipitation and serve as input for hydrological assessments. In 2015, a regional project Himalayan Adaptation, Water and Resilience Research (HI-AWARE), was approved to support science-based climate adaptations across all major Himalayan River basins. The UK and Canada provided funding for this project, which included PARC, my parent organization, to implement it over the Indus Basin in Pakistan. This project provided the opportunity to meet my professional ambitions by offering a PhD position in Germany. This is how I was in Germany. I am very grateful to PARC and HI-WARE Project for supporting my PhD research. In particular, the support extended by the then Chairman of PARC, Dr. Ifitikhar Ahmad (late), Dr. Bashir Ahmad, HI-AWARE Project In-charge at PARC, and Dr. Philippus Wester, the HI-AWARE project coordinator at ICIMOD-Nepal, is greatly acknowledged. I also want to recognize Irfan Ali (PARC) for managing my personal affairs during my absence from Pakistan. Thank you, buddy.

I would like to especially acknowledge the role of Prof Dr. Elke Hertig, who supervised this research at Augsburg University. Often we had long discussions on research scoping, identifying researchable issues, and formulating work plans. She was always encouraging and provided valuable technical guidance during the lengthy research period. She also helped arrange financial support, short-term skill development programs, and opportunities to present the research outputs on different platforms. Besides, she also helped me find a house in Pfersee and my son in learning initial German. Dr. Elke, thank you very much for your consistent technical and social help, without which my successful journey to achieve PhD would have remained a dream.

Without station observations, this research was not possible. I want to thank different organizations and individuals who helped me acquire such data. In particular, Pakistan Meteorological Department (PMD) and Water and Power Development Authority (WAPDA) need to be sincerely appreciated for collecting and sharing their data. I would also like to thank Dr. Abdul Wahid Jasra, the then country-head ICIMOD at Pakistan, and Dr. Asim Rauf Khan from WAPDA, for their special favor in acquiring high altitude observations. Zakir Hussain Dahri (PARC) and Dr. Ghazala Qasir (PMD) were also helpful in data acquisition. I would also like to acknowledge Bilal Iqbal (CEWRI-PARC) for preparing different maps on short notice. The financial support provided by DAAD and Augsburg University to support various research phases also needs due appreciation.

On the long way, many other colleagues and friends helped in different capacities. I am grateful to PD Dr. Christoph Beck for making his R course mainly in English at my request, which helped me complete my studies. Sincere gratitude is also extended to Dr. Irena Kaspar-Ott, Dr. Christian Merkenschlager, and Ms. Sally Jahn at our chair. They were helpful in one way or the other during the research period. Especially their help in translating the executive summary of this thesis into German was outstanding. Thank you all for your consistent support and friendly attitude throughout my stay at the university. I would also like to thank Dr. David and Dr. Bin for their quick proofreading of the thesis.

Without mentioning Paulina Simkin and Wolfgang Merkel, the good memories at the University will remain incomplete. Both were very nice fellows and often crossed over coffee/or lunch breaks to have chit-chats. Here I would like to mention Paulina's exceptional help in choosing a Gymnasium school for my son. Paulina, this was unforgettable support, and we want to thank you and wish you a very bright future. Never forget Dr. Florian Wilken, who was friendly and helpful along with Paulina, and my children always liked to play games with both. I wish you both a pleasant time ahead.

We had a great time in Augsburg city, where we met with many Pakistani families and friends. Often we hang out together on day trips, BBQ parties, and participate in social and religious festivals. This made our lives much more comfortable in a foreign country. Among many friends, I want to especially thank Khalil Ur Rehman, Arif Bhutta, and their families for always extending warm gestures.

I want to remember the instrumental role my parents have played throughout my life and professional career. Without their support, prayers, and encouragement, no success would have been possible. I pray for their good health and thank them for their consistent support. My brothers and sister also boosted confidence in lean times, and I pray for their future success. The support of my in-laws was also outstanding and needed due appreciation. The sincerest acknowledgment goes to my wife, who worked full time to support our comfortable stay in Germany. Without her hard work, management skills, and devotion to the family, my studies, the education of our children, domestic peace, and Europe-wide traveling was not possible. Thank you, Madeeha, for doing so much for all of us. My Son, Faiz, and daughter, Soha, could not get the attention they deserved due to my lengthy research work; Thank you for your understanding. You made our stay in Germany memorable with your innocence and making great academic progress despite language barriers. I am proud of you both and wish you a blessed time ahead.

# 1

# Introduction

## 1.1 Problem Statement

High-mountains often serve as the world's water towers (Immerzeel et al., 2010) and are experiencing some of the earliest and greatest impacts of climate change (e.g., Beniston, 2005). Steep topography and biological gradients combined with sharp seasonal contrasts in these regions can trigger climatic and geomorphic events that affect the ecological and human environments far beyond these landscapes (Körner, 2013; Hoy et al., 2016). Assessing mountain climate is essential to infer the future of their essential services (e.g., freshwater supply) for adaptation planning. However, mountain climates are characterized by several complex processes and observational constraints, which restrict accurate simulations.

The Upper Indus Basin (UIB) is marked by the confluence of the three high mountain ranges: the Hindukush, Karakoram, and Himalayans (HKH), and is a challenging region for climate simulation. These mountains host the largest glaciers outside the Polar Regions (Bocchiola et al., 2011; Soncini et al., 2015) and serve as headwater regions for many large Asian rivers, including the Indus River in Pakistan (Kaab et al., 2012; Immerzeel et al., 2010). The regional cryosphere, a buffer against famine, is influenced by the winter snowfall, monsoon precipitation, and melting of the accumulated snow and glacial ice mass. Among all HKH rivers, the Indus River system depends heavily on the snow and glacier melting (Sharif et al., 2013) to help sustain nearly 215 million people (Bolch et al., 2012). On the contrary, the Lower Indus predominantly experiences an arid to semi-arid climate and depends heavily on water availability from the UIB.

Considering global warming (IPCC, 2014), projected changes in large-scale circulations, concerns of elevation-dependent warming (Peppin et al., 2015), cryosphere sustainability (Kumar et al., 2019), and the dependency of a large and rapidly growing population (UN, 2019) on Indus waters, a pragmatic hydrological assessment at the basin-scale is imperative for future water resources planning. The Indus hydrology, unlike other basins, depends both on precipitation and temperature dynamics, as precipitation alone cannot explain melt-dominated river flows. These hydrological variables can help assess future water availability, cryosphere stability, and irrigation demand across the basin, which are primary concerns for sustainable development in the region.

However, the projected climate has shown conflicting signals, particularly within the UIB (e.g., Fowler and Archer 2006). For instance, contrary to the global retreat of glaciers and icefields (WGMS, 2020), a glacial expansion or at least stability has been reported in the Karakoram region since the late 1990s, a response known as "The Karakoram Anomaly" (Hewitt, 2005, Brun et al., 2017; Hewitt, 2014).

Similarly, the notion of elevation-dependent warming (EDW) is well-accepted globally (Pepin et al., 2015). However, some recent studies (e.g., Latif et al., 2020) using fresh evidence from a few High Altitude (HA) stations have argued its relevance over the UIB. Besides, regional studies differ substantially in change signal magnitude, direction, seasonality, and progression of the projected climate over the UIB. For example, more than 6 $^{o}$C year-round warming (Shafeeq and Lu, 2021; Almazroui et al., 2020) suggests rapid glacial retreats over the UIB. In contrast, Bashir et al. (2017) estimated monsoon cooling tendencies over the UIB using five decades of synoptic observations to support the future continuation of the Karakoram anomaly. These contrasting signals have massive implications for developing appropriate policy responses to ensure water-dependent regional prosperity under climate change. There is a dire need to improve climate simulations, particularly over the UIB, to facilitate informed decision-making on future water resources. Identifying primary uncertainty sources and their appropriate treatments should help in this regard.

General circulation models (GCMs) provide quantitative inferences about the future climate to perform impact assessment studies (Reichler and Kim, 2008). Despite significant improvements in numerical models and spatial resolutions, the GCM output still requires statistical or dynamic downscaling to support sensible adaptations at regional to sub-regional scales (e.g., Hertig et al., 2018). Statistical downscaling is a cost-effective alternative to its dynamical counterpart. During statistical downscaling, the climate uncertainties may stem from; i) the adopted observational profile (e.g., Palazzi et al., 2013), ii) selected GCM simulations (e.g., Heo et al., 2014), and iii) the choice of downscaling method. These uncertainties are exceptionally high within the UIB, where intricate topography-climate interaction defines sharp climate gradients (e.g., Palazzi et al., 2014, Solomon et al., 2007). For instance, the available long-term meteorological network is sparse and limited to lower elevations, while data quality and continuity issues are inherent in such harsh environments. Indus Hydrology depends mainly on HA precipitation, which remains one of the largest unknowns (Immerzeel et al., 2015). Gridded products (e.g., reanalysis, satellite measurements) often serve as de facto observations; however, their reliability over the snow-covered mountains of the UIB is poor (Cannon et al., 2015, Immerzeel et al., 2015).

Both GCMs and regional climate models (RCMs) have shown significant limitations in representing critical dynamical and thermodynamical processes over the region and induce significant wet and cold biases (e.g., Ashfaq et al., 2017; Hasson et al., 2019, Mishra, 2015; Dar et al., 2020). Therefore, an arbitrarily selected single climate model (e.g., Mahmood and Babel, 2012; Akhtar et al., 2008; Khan et al., 2015) or an ensemble identified using raw model precipitation (e.g., Ali et al., 2020, Lutz et al., 2016b) may lack the accuracy required for regional adaptations. Even the bias-corrected model output may contain significant uncertainties due to observational limitations over the UIB. The available observations (long-term data at valleys and short-term HA observations) could induce either spatial (Ali et al., 2015) or temporal biases (Hasson, 2016) in future simulations. Besides, using HA precipitation for bias correction and downscaling could induce additional errors because the precipitation

measurements over these regions are unrepresentative of the actual precipitation. Some studies (e.g., Armastrang, 2010) estimated HA precipitation measurement errors up to 60% under the influence of wind drift. Interestingly, when most bias-corrected downscaling studies project rapid glacier meltings (e.g., Ali et al., 2020), it was found that trend-analysis studies reported glacial stability (Khattak et al., 2011). These methodological biases further highlight the need for an alternative and more robust approach for climate change analysis over the UIB.

A statistical downscaling framework based on large-scale atmospheric circulations offers a promising alternative since the latest GCMs have shown more skills in their simulations compared to precipitation outputs (Kaspar et al., 2019). The GCMs struggle to accurately capture the complex precipitation phenomena and associated high spatiotemporal variability (Trigo et al., 2001). Such model limitations manifest over the high-mountain regions like the UIB, where orography results in additional variation at sub-grid scales.

The current research aims to provide an alternative climate simulation perspective over the basin using large-scale atmospheric patterns within an advanced statistical downscaling framework. Both methodological considerations and the fresh evidence from 23 recent HA stations in the downscaling process can improve the quality of climate simulations, particularly within the UIB. Firstly, the atmospheric drivers (predictors) of the key hydrological variables (predictands) were identified from a reanalysis dataset by accounting for high climate variability on spatiotemporal scales. These predictors were then used to quantify the reference and GCM level of uncertainties as well as future climatic changes at finer scales. The robustness of these change signals was evaluated using regression models' statistical skills, observational and GCM uncertainties, multi-model ensemble, signal-to-noise ratio (SNR), and physical consistency of the statistical models. Extending analysis further into the Lower Indus would simultaneously assess the future water demand required for integrated water management at the basin scale.

To the best of our knowledge, such predictor-driven statistical downscaling that accounts for high climate variability, observational limitations, and GCM simulation challenges over high mountains is unique over the basin. This analysis can potentially influence future climate research in the region and beyond, serving the wide-ranging interests of the scientific community and other stakeholders.

## 1.2 Study Area and Indus Hydrological Regime

The trans-Himalayan Indus River (**Figure 1a**) originates from the southwestern Tibetan Plateau and traverses approximately 3200 km to drain an estimated 1.12 million square kilometers ($km^2$) transboundary basin into the Arabian Sea (e.g., Jain et al., 2007). The Indus River system annually distributes 153 billion cubic meters (bcm) of freshwater through the world's largest contiguous irrigation

system to sustain the water, renewable energy, and food security of nearly 215 million people (Archer et al., 2010; Lutz et al., 2016b).

The UIB covers an area of approximately $4.03 \times 10^5$ km$^2$ (Dahri et al., 2016) which includes several mountain peaks above 7000 m elevations, including K2. Snow and ice melting in this region govern the Indus hydrological regime. Generally, the glacier melting from HA regions (glacial regime), snow thawing from mid-altitude catchments (nival regime), and concurrent seasonal rainfall over the lower-elevation watersheds (pluvial regime) determine the runoff. The relative contributions of the glacial, nival, and pluvial regimes vary with hypsometry and the dominant mode of large and regional-scale circulations (e.g., Pitchard et al., 2019, Hewitt, 2005) that regulate year-round moisture and energy supplies into the basin.

Orographic processes largely determine the precipitation distribution over the UIB. Precipitation generally increases with elevation up until a specific point, after which it sharply decreases (Hewitt, 2014). About two-thirds of the UIB precipitation is received between October and April and covers nearly 70% of the area with snow. Winter western disturbances are eastward propagating extratropical cyclones that govern winter moisture accumulation over the UIB (Cannon et al., 2015). These cyclonic systems advect moisture from the Atlantic, Mediterranean, Caspian, and Arabian Seas (e.g., Barlow et al., 2005). During the pre-monsoon period (AMJ), the west Tibetan High becomes active to displace the sub-tropical jet further northward, allowing solar radiation to penetrate the UIB and initiate melting over mid-altitudes (de Kok and Immerzeel, 2019). However, the river flows are only maximum during the monsoon (Jul- Sep), when HA melting starts under rising summer temperatures. Consequently, the summer glacial cover reduces to approximately 13 % of the UIB (Khan et al., 2014). Monsoon moisture is mainly sourced from the Arabian Sea, the Bay of Bengal, and the Indian ocean due to differential land-ocean heating during the boreal summer (e.g., Bolch et al., 2012). Often high floods are experienced in the region when a warm and moist monsoon follows an excessively wet winter season. Besides, moisture recycling (evapotranspiration from irrigated plains and snow-packed HKH mountains) also significantly influences the regional climate (de Kok et al., 2018; Curio and Scherer, 2016).

The current research focuses on the basin area controlled by Pakistan (**Figure 1b**) due to constraints on updated data from other countries. The study region is the largest basin fraction entailing maximum orography and cryosphere volumes to mimic the complexities of the entire basin in the simulation.

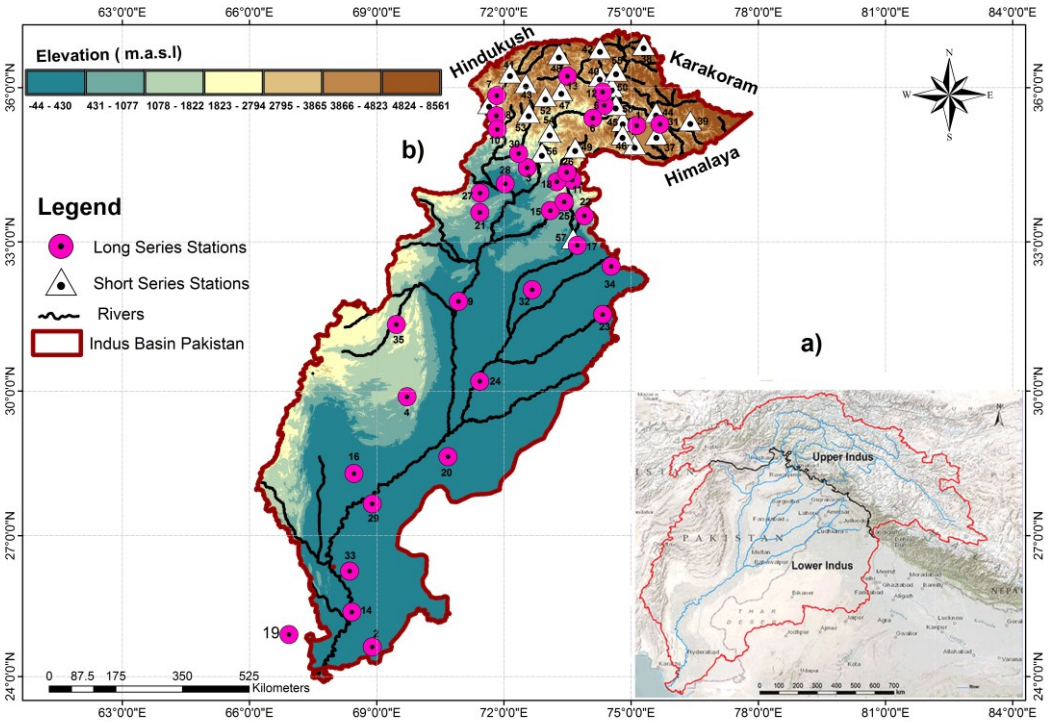


**Figure 1. a)** The transboundary Indus River Basin and demarcation of the Upper Indus and Lower Indus regions. The major river network flowing across the basin is also shown. **b)** Spatial distribution of the meteorological stations over the Indus basin of Pakistan used in the current analysis. The circlers (triangles) represent the historical (recent HA) observatories. The color scheme in **b)** denotes the elevation variation over the study basin.

## 1.3 Research Aims: Scope and Questions

The Indus climate has changed considerably and will continue to transform drastically because of changes in the precipitation form, amount, seasonality, and melt contributions. An accurate climate assessment, variability, and future evolution remain a scientific challenge due to observational constraints, particularly over UIB. HA monitoring requires extensive financial resources, while methodological considerations to better exploit the available observations can impact the quality of climate simulations.

The current PhD study aims to improve climate assessments over the entire study basin to infer future hydrological responses by addressing common uncertainty sources within a statistical downscaling framework. Besides precipitation, both maximum ($T_{max}$ ) and minimum ($T_{min}$) temperatures were considered due to their distinct influence on regional precipitation, cryosphere, runoff, and water

demand. A greater focus was on the precipitation and UIB assessments due to their significance for regional water balance. The study has the following specific objectives;

- Model future precipitation and temperatures (Tmax and $T_{min}$) changes on seasonal scales within available observational constraints by using a more suitable statistical downscaling approach.
- To explain physical mechanisms underlying the statistical models that govern the anomalous precipitation over the UIB.
- Propose a promising method to quantify reference and GCM uncertainties at finer scales to facilitate robust climate change analysis over complex regions.

Although regional analysis using full moisture-energy balance is essential to represent the melt-dominated Indus hydrology accurately, observational limitations do not permit such research (e.g., Pritchard et al., 2019). Like many other studies (e.g., Archer, 2003; Ali et al., 2015), the regional precipitation and temperatures are considered practical proxies of moisture and energy fluxes over the basin in this study. These specific objectives were further translated into the following research questions;

- Why is climate characterization of the basin essential, and how could it be performed?
- Can relatively low-altitude stations explain orography within the UIB, and why is that essential?
- How physical are the statistical models in explaining complex precipitation phenomena over the UIB?
- Is spatial temperature analysis using precipitation classification justified?
- How to select GCMs by circumventing modeled precipitation and temperature simulations that are highly biased?
- How to account for model democracy and variable GCM performances simultaneously in future simulations?
- What are the seasonal precipitation and temperature changes and their robustness?
- How would future moisture and energy fluxes as approximated by the precipitation and temperatures influence the regional cryosphere?
- Do seasonal changes follow elevation-dependent patterns?
- Would future water supplies be enough to meet its demand?

A specific experimental design helped to answer these research questions and achieve the study objective.

# 2

# Research Approach

## 2.1 Predictands and Precipitation Regionalization

The monthly time series of precipitation and temperature ($T_{max}$ and $T_{min}$) observations from 58 meteorological stations across the basin (**Figure 1b**) served as the predictands. These stations provide the historical (35 stations, 1979-2015) and relatively short-term (23 stations, 1994-2015) climatology over the low and HA regions. Despite shorter data length, the HA stations have significantly enhanced the altitudinal coverage from the existing below 2400 m to above 4700 m in elevation over the UIB to improve the understanding of orographic processes regulating the basin hydrology.

Climate analyses that treat the topographically heterogeneous basin as a single spatial unit (e.g., Lutz et al., 2016a) or using arbitrarily selected sub-regions (e.g., Hasson et al., 2017) may not accurately account for its high climate variability, particularly within the UIB. Moreover, downscaling/ bias correction using short-term HA observations (e.g., Hasson, 2016) may not be suitable for long-term planning requirements. The unadjusted HA precipitation observations (e.g., Wolf et al., 2017, Dahri et al., 2019) may induce additional uncertainties in future projections. However, downscaling using low-altitude stations (e.g., Ali et al., 2015 may not provide any quantifiable inferences about the HA climate.

Basin classification using a time and space differentiated climate analysis could account for profound seasonality, spatial variability, and typical observational constraints (e.g., variable data lengths, quality issues). Furthermore, the precipitation would provide a more rational basis for basin characterization due to its high spatial variation over the temperature fields. Thus, precipitation regionalization would identify more sub-regions than corresponding temperatures and facilitate a finer-scale analysis over the mountain regions, which is advantageous.

Since precipitation is not a point phenomenon and covers a minimum spatial scale, some joint variability should exist between the low and high altitudes on at least seasonal scales when the region is under the same climate forcing. In other words, though the precipitation amounts would differ substantially over the UIB, their altitudinal distributions may vary linearly under the orographic forcing. Such joint precipitation variability, if present, could allow using relatively low-altitude stations that offer historical data to make quantifiable inferences about precipitation variability over the HA regions.

K-means clustering analysis was employed to test the hypothesis of joint precipitation variability and define its spatial extent. The assumption would be supported if many HA stations could cluster around nearby historical stations in the UIB. Before clustering, three major precipitation seasons covering the winter (DJFM), pre-monsoon (APJ), and monsoon (JAS) seasons were identified. These seasons cover

the primary accumulation (winter) and melt seasons (monsoon) to infer cryosphere dynamics. The station-level time series were grouped into these seasons and checked for completeness (Moberg et al., 2006), homogeneity (Wijngaard et al., 2003), and the underlying distribution (e.g., KS, Shapiro, and Anderson-Darling tests) to identify appropriate statistical treatments. Subsequently, K-means clustering was performed on the precipitation correlation matrix to group the stations depicting similar co-variability. Precipitation clustering by avoiding actual precipitation amounts is advantageous over the high mountain regions due to erroneous measurements over HA regions (e.g., Curio and Scherer, 2016; Tahir et al., 2011). Spearman correlation estimates served as the distance measure (Wilks, 2006) during the clustering process. During clustering, the correlations were maximized (minimized) within (across) the regions to define regional boundaries sharply. After the cluster identification, cluster-centroids were computed to describe the mean precipitation features of individual clusters and correlated with each corresponding member. Finally, the stations offering spatially coherent (high station-centroid correlation), temporarily complete, homogeneous, and historical data were selected as regional representatives (RR). The time series of these RR stations served as predictands. Thus, downscaling only over the RR stations could help draw reliable spatial (horizontal and verticle) inferences over a region. Another regionalization experiment covering only HA parts of the UIB was also separately performed to account for these regions' high uncertainty and hydrological significance.

The precipitation regions were also adopted for temperature downscaling to ensure the spatiotemporal consistency of the moisture-energy fluxes that simultaneously regulate the basin hydrology. Since temperatures show less spatial variation, precipitation regions can provide more fine-scale temperature inferences to the analysis.

## 2.2 Predictor Data and Principal Component Analysis (PCA)

Initially, different variables from ERA-Interim reanalysis (Dee et al., 2012) were selected using a literature review to model observed precipitation and temperature dynamics over the study basin. These variables included the geopotential height (zg), meridional and zonal wind components (va and ua), air temperatures (ta), and the specific and relative humidities (hus and hur) at different pressure levels. The ERA5 could not be used since it was unavailable at the start of this research in 2016.

A large predictor domain (10° E to 100° E, 10° N to 60° N) was selected to include dynamic (zg, va, ua) and thermal influences (ta) of the Atlantic and Indian Oceans and the Siberian High on regional climate (e.g., Syed et al., 2010, Ashfaq et al., 2017). While, a smaller domain (64° E to 80° E, 22° N to 40° N) was considered for the humidity variables used to investigate the role of more localized thermodynamic forcing (e.g., evapotranspiration) on these predictands. After re-griding to $2^{o}$ x $2^{o}$ spatial resolution, the monthly averages of the predictors were grouped into seasons.

S-mode Varimax-rotated PCA was performed separately on each predictor field for dimension reduction (e.g., Preisendorfer, 1988). The number of retained PCs was determined using a modified dominance criterion (Philipp, 2003) with some additional constraints. The resulting PC scores (loadings) defined the predictor time series (centers of variations) for constructing downscaling models.

## 2.3 Downscaling Framework: Model Development and Selection

Generalized linear model (GLM) (McCullagh and Nelder, 1989) and multiple linear regression (MLR) framework were adopted to model observed precipitation and temperature ($T_{max}$ and $T_{min}$) distributions at the RR stations. Within the GLM framework, Tweedie exponential dispersion models (e.g., Dunn, 2004) were selected for those predictand cases containing exact zeros in their time series. The GLM gamma models were used for RR stations containing non-zero precipitation.

A cross-validation framework by randomly subsetting the available predictand/predictor time series into 1000 calibration/ validation iterations were used to identify robust atmospheric drivers (predictors) that skillfully resolve predictand distributions. During the modeling process, two-thirds (remaining one-third) of the data length was used for calibration(validation) purposes, and mean squared error scores (MSESS) (Wilks, 2006) served as a performance measure. Multi-collinearity among predictors was considered to choose simpler models by avoiding duplicating predictor influences. The regression models that exhibited maximum MSESS (minimum mean squared errors, MSE) using relatively independent predictors were selected for downscaling.

## 2.4 Precipitation Composites

Analyzing physical mechanisms underlying the statistical models could further improve the confidence in subsequent projections. Since precipitation over the UIB is more uncertain and essential for the basin's water cycle, it was decided to analyze the physics of selected precipitation models using composite analysis. For this purpose, the monsoon and winter season precipitation distributions were analyzed over a larger and the wettest part of the UIB. Sample composites were constructed using a PC with the highest regression coefficient (in respective regression models) to explain atmospheric circulations during the anomalous precipitation over the UIB in two main precipitation seasons.

A threshold of ±1.5 PC score was used to subset the precipitation and relevant atmospheric circulations during the dry and wet periods. Standardized predictor anomalies were then computed from these subsets and plotted to explain precipitation supporting (suppressing) climatologies. The difference between the dry and wet regimes helped identify circulation anomalies that support above-normal precipitation over the UIB.

## 2.5 Quantification of Climate Uncertainties

### 2.5.1 GCM ranking and selection process

Because of precipitation reliability issues over high mountain regions, a new GCM selection procedure devoid of modeled precipitation was proposed. Precipitation governing predictors were instead used to rank the available GCMs that belong to the 5th phase of coupled model intercomparison project (CMIP5) according to their simulation ability for these large-scale patterns. For this purpose, a similar S-mode PCA was performed on each relevant GCM predictor field and compared with ERA-Interim counterparts using Taylor diagrams (Taylor, 2001). Such model-reference predictor correspondence was evaluated during the historical period. A performance score (PS) derived using two summary statistics of Taylor diagrams (i.e., pattern correlation and the normalized ratio of variance) helped to quantify the strength of predictor correspondence as follows;

$$PS = |CR| - |NSD - 1| \qquad (1)$$

Under ideal conditions, the PS will attain its highest unit value due to the maximization of phase correspondence (i.e., CR =1) and the same magnitude of predictor spread (the term NSD - 1 becomes zero) between the reference and GCM simulations. Similarly, a smaller PS value will demonstrate a weaker correspondence. The PS magnitude will also intuitively influence the third summary statistics (i.e., standardized RMSE), as its maximum value (PS = 1) will ensure zero errors and vice versa. In PS computations, the regression coefficients were further used as a weight to identify GCMs that better simulate more important predictors (i.e., predictors with high regression coefficients).

GCMs' predictor simulation abilities were tested over different sub-regions, identified through K-means clustering, to select GCMs that outperform over spatial scales. Thus, GCM depicting the highest (lowest) PS in different sub-regions could be identified as the best (worst) GCM. Using PS, the model (ensemble) level uncertainties (1-PS)*100 were also computed to assess the reliability of subsequent projections at sub-regional scales.

### 2.5.2 Reference level

Using ERA-Interim predictors for GCM ranking requires the regional robustness of these variables in the first place. To evaluate the usefulness of ERA-Interim predictors for regional simulations, these were compared (separately) with predictors from the latest ERA5 (Hersbach et al., 2018) and NCEP-NCAR-II) (Kalnay et al., 1996) reanalysis datasets. The PS was again used to quantify the inter-reference predictor correspondence. Thus ERA-Interim PS against these additional reanalysis datasets can specify the range and average magnitude of the reference-level uncertainty at different scales. A high PS and a

narrow range could indicate more confidence in using ERA-Interim predictors for regional analysis and vice versa.

## 2.6 Future Projections and Signal Robustness

GCM predictors from two different representative concentration pathway scenarios- RCP (RCP4.5 and RCP8.5) were considered to model the future precipitation-temperature response of the Indus basin. These RCPs represent the managed (RCP4.5) and unabated (RCP8.5) societal response towards greenhouse gas emissions and are suitable for supporting regional adaptations (Sanford et al., 2014). After accounting for their variable spatial resolutions, the model predictors were standardized over the historical and future time-slices (separately for each scenario). These standardized variables were projected onto the corresponding PC loadings of the ERA-Interim to generate new predictor time series. These new predictors containing climate change information were then used through the regression models to derive the downscaled historical and future projections. The difference between downscaled historical and two future time slices (separately for each RCP and time slice) was used to compute median precipitation and temperature changes over the basin under selected global warming scenarios.

A signal-to-noise ratio (SNR) was used to evaluate the strength of change signals against the observational uncertainty. The ratio used median changes (signal) simulated by the individual models (ensemble) and corresponding standard deviations of the historical period (noise). SNR > 1 indicated that the change signal exceeds the internal climate variability (robustness) and vice versa. A non-parametric Wilcoxon signed-rank test was also used to evaluate the statistical significance of the ensemble (medians) changes during 2071–2100 compared to 1976–2005 under both RCP scenarios.

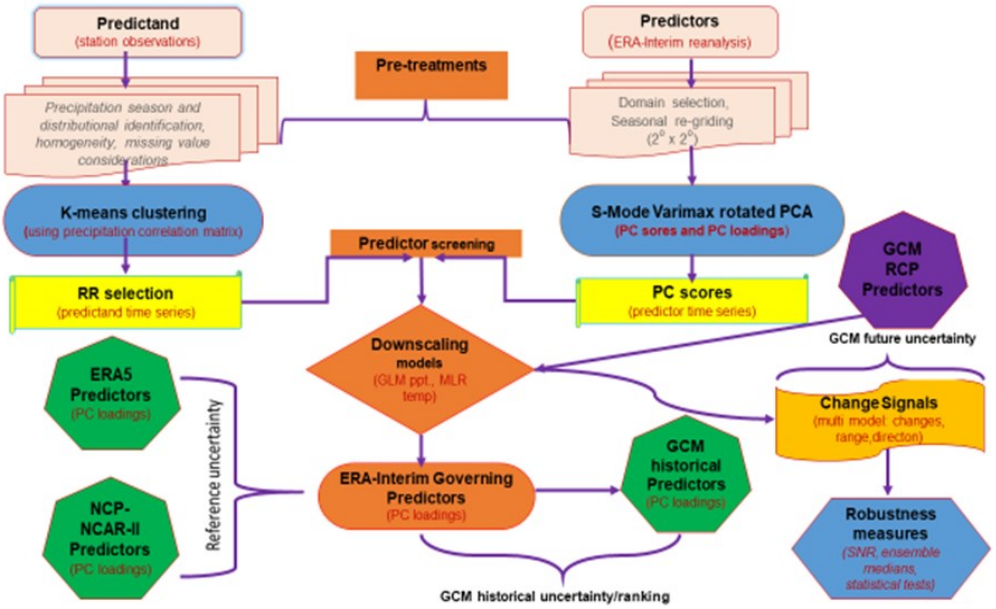


**Figure. 2** Flowchart detailing the statistical downscaling framework implemented in the current study.

# 3

# Results and Discussion

## 3.1 Precipitation Regionalization

K-means cluster analysis successfully captured the spatial variability of seasonal precipitation and topographic heterogeneity within the basin, which justified adopting a sub-regional approach. The regionalization scheme identified six (winter), seven (pre-monsoon), and seven (monsoon) sub-regions to explain a large proportion of observed precipitation variability in respective seasons. The clustering process recognized high precipitation variability over the UIB by identifying, on average, four different clusters per season compared to the two sub-regions over the Lower Indus. Within the UIB, the clustering process identified the unique precipitation variation over the southern and trans-Himalayan regions (including the Karakoram) and northwestern Hindukush regions by grouping these areas into different clusters. These regions serve as the primary water supply nodes for the Indus River system. Similarly, the main water demand reflectors (e.g., irrigated plains and coastal areas) were also identified during the basin-wide regionalization experiment. Thus, the adopted regionalization scheme and basin-wide considerations provided a unique opportunity to simultaneously analyze the basin's future water supply and demand.

Clustering of many recent HA stations around relatively low-altitude stations during the regionalization process further validated the hypothesis of joint precipitation variability among the low and HA regions. Therefore constructing downscaling models over the relatively low elevation stations to draw HA precipitation inferences was justified. Such downscaling could support long-term planning needs by avoiding temporal or quantitative biases in the projections.

## 3.2 Downscaling Models: Predictors' Contributions and Physical Relevance

The downscaling framework skillfully modeled the observed precipitation and temperature distributions over the basin using different lower tropospheric dynamical (winds) and thermodynamical (humidities) predictors. However, some upper-tropospheric variables (va200, zg200) also explained monsoon precipitation variation over the UIB. Seasonally the monsoon models were the most complex, requiring many predictors over different pressure levels. Spatially, the trans-Himalayan regions (also covering the Karakoram region) mainly required both dynamic and thermodynamic forcing (complicated models) to resolve their precipitation effectively. On the other hand, the Lower Indus models were most simplified for all three predictands.

Final downscaling models demonstrated significant validation skills, particularly over the UIB. Validation performance reflects a downscaling model's ability to transfer statistical relationships to

other (unknown) periods and, therefore, strongly influences the projection reliability. Compared to precipitation, the predictive skills of the temperature models were very high because relatively simplified processes regulate temperature distributions. Interestingly the downscaling models demonstrated higher skills in simulating precipitation over the UIB compared to different Lower Indus regions. High climate variability over the UIB may reduce climatological models' usefulness; hence the downscaling models outperform. The opposite is true in the Lower Indus, where in addition, a strong land-atmosphere coupling (due to extensive irrigation) may cause localized climate variability, not explained by the large-scale forcing. Although regional scale humidities were considered, the adopted predictor resolution ($2^o$ x $2^o$) seemed too coarse to capture appropriately such finer-scale irrigation feedbacks.

The statistically identified predictors also represented seasonally varying regional climatology. For instance, the overturning of the local Hadley-cell circulations during the monsoon was well captured by the presence of meridional winds at the lower (850 hPa) and upper troposphere (200 hPa) in precipitation models. Similarly, the dynamic forcing associated with westerly and easterly circulations was represented by the dominance of different wind predictors in winter and monsoon models. In contrast, the dominance of humidity predictors during the pre-monsoon simulations could describe increased moisture advection (Cannon et al., 2015b) and convection (due to regional heating) over the region. The humidity becomes important when dynamic forcing loses strength during the pre-monsoon periods (Cannon et al., 2015b). Similarly, the specific humidity explaining most $T_{min}$ distributions over the basin might be connected to cloud radiative and soil moisture feedbacks. Overall, statistically skillful and physically plausible precipitation (temperature) regression models provided a solid platform to assess future water availability, cryosphere stability, and water demands over the basin.

## 3.3 Precipitation Governing Mechanisms

Besides statistical skills, the reliability of precipitation models was also complemented by explaining the underlying physical mechanisms using composite analysis. An upper level (200 hPa) high-pressure anomaly over West Central Asia (WCA) and a low-pressure anomaly over the Indian Peninsula mark a strong reversal of the local Hadley-Cell circulations during monsoon. Additionally, the lower-level circulation anomalies (850 hPa) exhibited stronger than normal westerlies over the Arabian Sea and south-westerlies over the Bay of Bengal. These upper and lower tropospheric pressure and wind anomalies should significantly enhance moisture advection from the oceanic sources and dynamic forcing over the UIB. The corresponding precipitation composites confirmed these physical mechanisms by indicating more than double precipitation over the UIB under such circulation patterns. Meanwhile, the upper level High's weakening and further eastward shift should reduce the moisture and dynamic forcing over the UIB to cause excessive dryness. The associated composites indicated three times less than average precipitation over the UIB under such monsoon circulations.

During winter, the sea level pressure composites exhibited a high-pressure (low-pressure) anomaly over northern Siberia and Europe (North Africa) to facilitate cyclogenesis activities around the Mediterranean, Europe, and the Middle East. These storm tracks propagate eastward and further intensify over the WCA region due to the presence of a low-pressure anomaly to support excessive precipitation over the UIB. Moreover, increased cyclonic activity over the Bay of Bengal and the southern Arabian Sea further helps moisture advection into the UIB. These dynamic and thermodynamic forces should promote intense winter precipitation in the region. Similarly, a reversal of these conditions should promote excessive dryness over the UIB. The corresponding precipitation composites confirmed these winter season precipitation controlling physical mechanisms.

Such physically consistent and statistically skillful models could better explain future precipitation changes over the UIB during the primary precipitation seasons. Therefore, the reliability of future precipitation changes may increase.

## 3.4 Uncertainty Quantification

### 3.4.1 Reference level assessments

High predictor correspondence (weighted PS) among different reanalysis datasets strongly justified using ERA-Interim predictors for regional precipitation and temperature analysis. However, inter-reference predictor robustness (uncertainty) varied with seasons, spatial scales, and predictor types. For instance, different dynamical predictors showed increased correspondence than the thermodynamic variables. Spatially, the predictor correspondence remained stronger over the UIB than in the Lower Indus regions, improving confidence in subsequent simulations over hydrologically important mountains. In particular, Tmax predictors showed stronger inter-reference robustness over most HA regions. Since Tmax regulates cryosphere melting, their robust simulations could improve the reliability of subsequent inferences about cryosphere dynamics and associated water availability.

Seasonally, the reference uncertainty was low during the primary melt (monsoon) and accumulation seasons (winter) despite regression model complexities. Compared to precipitation models, the dominance of lower tropospheric winds and relatively high thermodynamic contributions slightly increased the temperature uncertainties over the basin. The interpolation issues over the mountainous regions (Palazzi et al., 2013) and boundary-layer influences may cause increased disparities among lower-level predictors.

### 3.4.2 GCM level uncertainties

After establishing the robustness of ERA-Interim predictors, these atmospheric patterns were used to estimate GCM level uncertainty and identify better-performing models. The available GCMs were

ranked according to their abilities for simulating ERA-Interim precipitation (temperature) predictors. The reference-model predictor comparison (i.e., PS) showed that no single GCM could adequately capture climate variability over the basin without making significant simulation compromises. Besides, the average GCM uncertainty was nearly double the corresponding reference uncertainty in most cases. Modeled precipitation predictors, in particular, showed more differences with reanalysis counterparts to highlight variable skills of the GCMs in simulating precipitation structure over the region. Spatially, the modeled uncertainty remained high over the UIB compared to the Lower Indus regions to indicate GCM limitations in representing mountain climate. A broader uncertainty range also justified the ensemble diversity for regional simulations despite its smaller size.

The GCMs demonstrated significantly improved skills in representing regional thermodynamic structures but showed more differences for dynamic circulations. Therefore unlike reference, the GCM uncertainty was mainly controlled by the lower-level wind forcing. Such predictor matching patterns may also influence the seasonal reliability of GCMs. Generally, the GCMs better modeled the westerly dominated periods (Dec to Jun) due to the dominance of humidity predictors in their downscaling models. In contrast, the GCM monsoon uncertainty was high due to the increased wind predictors in downscaling models. Many previous studies also highlighted poor representation of the monsoon circulations over the study region (e.g., Ashfaq et al., 2017; Sperber et al., 2013). A relatively high reference uncertainty during the monsoon would also restrict accurate GCM evaluations.

Differences in horizontal resolution, domain size, and numerical models may contribute to model-level uncertainties. For example, a better resolution agreement between GCMs and adopted ERA-Interim fields ($2^o$ x $2^o$) may reduce interpolation needs over the mountain terrains, improving correspondence among humidity predictors. The humidity domain focused on the study area, and many PCs were spatially located over or in the surroundings of high mountains. Such resolution impact could also be realized in reference datasets where finer-scale ($0.25^o$) ERA5 showed more differences than the coarse resolution ($2^o$) NCEP-NCAR-II for simulating ERA-Interim humidity predictors. Ashfaq et al. (2016) have also shown that increased resolution may not improve GCMs' systematic biases over this region.

However, seasonally varying dynamic forcing is more complex and sourced from distant terrestrial and oceanic sources (larger predictor domain). Often GCMs fail to accurately represent dynamic aspects like trajectories, strength, timing, and orography due to mountain blocking (e.g., McSweeney et al., 2015), which may increase simulation uncertainty about these processes. The PS, measuring grid by grid predictor correspondence, may also be negatively influenced by the larger domain (pattern matching over more cells is required) and vice versa to explain modeled predictors' typical patterns. However, the current study did not quantify the underlying influences of the domain, resolution, and numerical models on modeled uncertainty. Further research could explain these gaps.

The model ranking helped identify GCMs exhibiting significantly higher skills than other ensemble members for simulating past climate despite regional complexities. Unlike other studies (e.g., Khan and Koch, 2018, Lutz et al., 2016a), the selection process avoided excessive subjective decisions to provide a more rational basis for model ranking (i.e., atmospheric pattern matchings). Such GCM selections have never been implemented in the region and can influence future climate research.

## 3.5 Weighted GCM Ensemble

The need for an ensemble analysis was obvious since no single GCM could simultaneously outperform in representing observed precipitation and temperature dynamics over the study basin. However, using an ordinary ensemble where the so-called bad and good models are used indiscriminately may not be logical as GCMs differ significantly in their regional simulations. On the other hand, only using the so-called best model(s) may eliminate many GCMs from the analysis. Such model elimination is often criticized (e.g., Hasson et al., 2019; McScweeney et al., 2015) by arguing the complex nature of the climate system and its unknown future evaluation.

A weighted GCM ensemble could ensure both model democracy (e.g., Knutti, 2010 ) and variable GCM abilities for regional analysis. The specific weights could represent an individual model's simulation performance during the historical period (e.g., PS in this study). Thus, a better-performing GCM (with higher PS) would influence change signals more than the poor-performing models (smaller PS) in an ensemble setting and vice versa. Of course, it requires stationarity assumption, which remains fundamental to most statistical downscaling approaches. The weighted ensemble would also avoid physical inconsistencies and boundary forcing issues that may arise from adopting different GCMs for different sub-regions (e.g., Lutz et al., 2016a). Model weighting impact was also evaluated by comparing the weighted and unweighted ensemble changes. In many instances, the weighting refined the seasonal signals and particularly projected stronger (weaker) westerlies during the winter (pre-monsoon ) and monsoon circulations over the HA regions. Since actual precipitation over the HA regions remains very high (Immerzeel et al., 2015), these minor changes could still strongly influence the basin hydrology. Therefore, ensemble analysis that acknowledges the model's regional suitability and follows an inclusive GCM approach could provide a different and more rational perspective. Since most GCMs show significant biases over the high mountain regions, using their known performance for adjusting future simulations could be advantageous in such complex regional settings.

## 3.6 Projected Changes and Impacts on Water Resources

### 3.6.1 Winter changes

The downscaling output showed a significantly wet and warmer winter over the study basin throughout the 21st century compared to the baseline period (1976-2005) under RCP4.5 and RCP8.5 scenarios. Increased warming (RCP8.5) would strengthen these changes, which become more distinct during the end of the 21st century. However, these changes and associated reliability varied greatly over the spatial and elevation scales.

Future precipitation followed an elevation-dependent pattern, where large parts of the trans-Himalayan HA regions would receive significantly high precipitation. The highest precipitation increase (~ 80%) was estimated over the Karakoram region. Increased warming could strengthen future westerlies and their northward penetration, increasing dynamic forcing over the UIB to justify such spatial changes. However, a large inter-model spread indicated more uncertainty about the change magnitude to implicate future hydrological assessments. Variable representation of the UIB topography and its complex interaction with climate forcing may govern such simulation divergence among GCMs. In contrast, the Lower Indus showed mixed precipitation signals with an overall positive outlook.

Significantly positive $T_{min}$ changes would govern projected seasonal warming over the entire basin. Spatially, high warming over the northwestern and Lower Indus regions was robust among GCMs. Strikingly, both temperature changes could not follow the EDW notion at the basin scale. However, the mean temperature changes (average of $T_{max}$ and $T_{min}$) over the UIB followed the EDW pattern. High statistical skills of the downscaling models and reduced reference uncertainty may induce confidence in such temperature changes.

A significantly increased precipitation over the UIB, which is robust among regional studies (e.g., Almazroui et al., 2020, Lutz et al., 2016b; Forsythe et al., 2015, Khattak et al., 2011), could trigger negative feedbacks (e.g., cloud radiative forcing, increased surface albedo, and soil moisture dynamics). These feedback processes may increase shading over the UIB to reduce daytime heating and trape the solar radiation within the boundary layer during nights to justify more significant $T_{min}$ warming. Specific humidity served as a single predictor to exexplain winter $T_{min}$ patterns and hinted at the dominant role of atmospheric humidity/ shading on regional temperatures.

In contrast, erratic precipitation over the Lower Indus may increase daytime warming (e.g., Ali et al., 2020) to substantially increase irrigation needs and evapotranspiration. Such daytime warming could also warm the Arabain sea. Consequently, the afternoon cloudiness may increase over the Lower Indus to justify rising $T_{min}$ patterns. These interconnected mechanisms could explain Lower Indus warming contributed simultaneously by $T_{max}$ and $T_{min}$ changes.

Rising nighttime temperatures would also significantly increase the liquid precipitation proportion over the UIB. Such favorable temperature and precipitation changes would substantially increase seasonal water availability from the UIB. A lesser increase in maximum temperatures, very high precipitation rates, and prevailing severe cold conditions, particularly over the Karakoram region, may not drastically reduce glacial sustainability. However, increased liquid precipitation may trigger future avalanches to endanger downstream communities and infrastructure. Nighttime warming over the Lower Indus may also reduce wheat crop maturity time, a staple food grown over vast areas, allowing crop intensification in the agricultural calendar.

### 3.6.2 Pre-monsoon changes

Changes in large and regional scale circulations could promote a significantly drier and warmer pre-monsoon climate over the study basin during the 21st century. The maximum dryness was projected over the northwestern regions that continued further over the southwestern highlands and irrigated plains in the Lower Indus. Many previous studies (e.g., Ashfaq et al., 2020, Hasson et al., 2017) have also estimated similar climatic changes in this season. Contrary to the winter season, the Tmax changes mainly regulated pre-monsoon warming. The temperature changes ($T_{max}$ and $T_{min}$) could not validate EDW at the basin or UIB scales and instead demonstrated a west-east gradient that intensified over the lower elevations.

Weaker than normal and further northward-penetrating westerlies may reduce moisture advection from distant sources, explaining precipitation reduction over the lower northwestern regions. Since relative humidity served as the primary precipitation predictor over the northwestern areas, its future reduction should induce regional dryness. Projected strengthening of the West Tibetan High that essentially regulates moisture-energy fluxes into the region at this time of the year (e.g., de Kok et al., 2019) could trigger such westerly circulations response. The intensification of Tibetan anticyclone may promote clear-sky conditions to allow greater penetration of the solar radiation into the UIB and justify more significant daytime heating. While agreeing on the link between anticyclone and seasonal warming, the studies differ on whether the Tibetan High is a cause (Forsythe et al., 2018) or a response to regional heating (de Kok and Immerzeel et al., 2019). Further research could explain the interconnection between westerlies and Tibetan High.

Increased daytime warming could also reduce atmospheric moisture (i.e., relative humidity) to explain excessive dryness, particularly in northwestern regions. Using synoptic observations of the five decades, Bashir et al. (2017) showed an increasing afternoon cloudiness trend over the UIB. It is argued that the projected winter precipitation and temperature increase over the UIB could enhance liquid precipitation, melting, and soil moisture in the UIB. Such carryover soil moisture could evaporate under daytime heating during the pre-monsoon to promote afternoon cloudiness over the UIB. Therefore, negative

feedback processes associated with afternoon cloudiness could justify rising $T_{min}$ temperatures despite decreasing precipitation over the UIB.

High warming over the northwestern regions could deplete the already thin glacial cover over these regions (e.g., Immerzeel et al., 2015). Therefore, future water supply from the western tributaries (e.g., Kunhar, Kabul, and Swat rivers) might decrease in the long run (e.g., Bokhari et al., 2018). However, relatively low warming and nearly stable precipitation over the Karakoram region may not endanger its cryosphere. Due to favorable precipitation-temperature changes, the main Indus and its eastern tributaries could increase seasonal flows. Such increased flows could compensate for some water reductions from western catchments.

### 3.6.3 Monsoon changes

Global warming will continue to influence regional precipitation and temperatures during the future monsoon. The ensemble changes showed significantly wet and low-warming conditions over the UIB towards the end of the 21st century. The nighttime temperatures consistently showed less warming with some cooling possibility over the UIB. Since monsoon clusters represented the highest observed altitude (> 4700 m), these inferences cover significant elevations over the basin during the peak melt period. Such climatic changes could substantially increase river flows with a possibility of intact glaciers even under a high warming scenario. However, $T_{max}$-dominated warming over the Lower Indus also suggested a substantially high water demand in the future.

Such summer warming over the UIB may not cause rapid glacier meltings as prevailing temperatures over the glacial surface are always well below the freezing point (e.g., Armastrong, 2010; Hewtt, 2005). Besides, future monsoon strengthening and typical $T_{min}$ changes could increase solid precipitation over HA regions to augment the existing cryosphere. Increased albedo associated with fresh snow and the presence of debris cover (e.g., Kraaijenbrink et al., 2017) could also prevent excessive glacier melting. It can be argued that glaciers melting under debris may increase due to increased absorption of solar radiation. Many regional studies (Scherleret al., 2011, Sakai and Fujita, 2017) have contradicted such a notion due to the greater thickness of the debris cover serving as an insulator. Pre-monsoon warming and increased liquid precipitation in winter may also promote downslides to increase the debris cover, further helping sustain the regional cryosphere (Herreid et al., 2020). Using field measurements, Muhammad et al. (2020) have shown that even thinner debris could prevent meltings over this region. Such low-temperature sensitivity of the regional glaciers is unique, as also endorsed by de Kok and Immerzeel (2019).

Projected monsoon currents may increase aerosol loadings over the UIB by transporting additional salt from the Arabian sea (Wake, 1989) and dust loading associated with pre-monsoon aridity. This research has shown that the Arabian Sea mainly contributes to monsoon precipitation over the UIB, and future

monsoon strengthening could increase sea salt deposits over HA regions. These inorganic aerosols could cluster atmospheric moisture (Coen et al., 2018) to reduce solar irradiance over the UIB. Besides marine and terrestrial aerosols, future infrastructure development may also enhance (mainly inorganic) aerosols over the UIB to support cooling tendencies. Those ensemble members that better resolve aerosol forcing (e.g., Norwegian models) have already projected minimum monsoon warming to support the argument. However, black carbon (organic) aerosols can potentially cause atmospheric warming due to increased absorption of solar radiation (Myhre et al., 2013). Inefficient local and distinct combustion promotes black carbon depositions over the HKH region over the recent periods (Li et al., 2016). Future positive precipitation changes over the HA regions may wash such organic aerosols, which last longer than their inorganic counterparts. However, further dedicated research would be required to explore the impact of aerosols and their nature on regional glaciers. Projected high warming over the Indian subcontinent and Lower Indus may increase future irrigation requirements. Irrigation-related cooling tendencies over the UIB are known (e.g., de Kok et al., 2018) that may also promote future glacial stability.

Bias-corrected downscaling (e.g., Ali et al., 2020, 2015, Khan et al., 2015) has always projected high summer warming and consequent glacial instability over the UIB. Structural GCM (Ashfaq et al., 2017) and RCM limitations (Pritchard et al., 2019), adopting uniform temperature lapse rates (e.g., Immerzeel et al., 2015) without considering regional heterogeneity (e.g., seasonality, glacier, debris cover) (e.g., Muhammad et al., 2020) may promote warm biases in such downscaling studies. Using model experiments, Lin et al. (2021) showed that GCMs overestimate the Himalayans' glacier retreat due to misrepresenting glacial-air interactions at HA regions during the monsoon season. Karki et al. (2019) suggested time-varying lapse rates in central Himalayans to address lapse rate issues. However, it would be sensible to derive lapse rates using both time and space dimensions. Identification of many different precipitation sub-regions in a single season over the UIB further supports such assessments. Availability of the recent HA observations could facilitate lapse rate computation within some clustering frameworks.

In summary, accurate mountain topography and monsoon circulation modeling will remain a scientific challenge for accounting for uncertainty about future hydrology and glacial response. Increased HA monitoring, improvements in the GCMs, and transboundary data sharing would essentially help improve future hydrological simulations.

# 4

# Sources of Uncertainty

This PhD study used an advanced statistical downscaling framework to improve future precipitation and temperature simulations over Pakistan's Indus River basin. Incorporating fresh evidence from nearly two dozen HA observatories and accounting for common uncertainty sources through methodological considerations could improve simulations. Nevertheless, the study findings were based upon certain assumptions. For instance, the altitudes beyond 4730 m and the transboundary UIB regions could not be represented due to data availability issues. Such observational lackings may influence the adequacy of the regionalization process in capturing climate variability over the actual drainage basin.

Curio and Scherer (2016) classified the precipitation over Asian mountain regions using dynamically downscaled High Asia Refined analysis data that also covered the entire elevation and spatial extent of the UIB. They concluded that at least four precipitation classes could adequately capture the mountain precipitation features. Using observations, the present study also averagely identified four different precipitation regions over the UIB. Therefore, the adopted regionalization might explain most precipitation variations over the entire UIB. Spatial inferences beyond observations could then be linearly inferred from surrounding clusters. Since orography mainly controls the regional precipitation that linearly increases with elevations, at least up to the equilibrium line altitude (ELA) (Winiger et al., 2005). Therefore, verticle gap fillings between cluster observations and the ELA using a linear relationship seem logical. The ELA elevation is estimated at 5500 m altitudes in the UIB (e.g., Khan et al., 2014), and any precipitation (temperature) change beyond ELA does not affect the river runoff. Lastly, the same large-scale atmospheric forcing triggers precipitation over the entire UIB; despite differences in precipitation magnitude under localized modulations of the climate forcing, a spatial co-variation remains possible. Some studies (e.g., Archer and Fowler, 2004) have pointed out such linear precipitation variation among the UIB stations in India and Pakistan. Therefore, extending spatial precipitation inferences (horizontally and vertically) beyond observational clusters seems appealing. It should be noted that spatial gap fillings using respective cluster inferences are being proposed rather than generalized linear gap fillings that undermine regional heterogeneity.

The latest ERA5 predictors could not be used for downscaling due to their unavailability at the start of this research during 2016. Since downscaling models used large-scale circulation patterns, the improvements in ERA5 horizontal resolution may not drastically impact downscaling results. The robustness of ERA-Interim predictors was tested against ERA5 counterparts once those were publically available. As expected, a strong predictor matching among two reanalysis datasets justified using ERA-Interim-based regional analysis.

The CMIP5 representativeness of the 8-model ensemble used in the current study could be argued. Apart from the literature review, an exploratory analysis over a sample monsoon region over the UIB was performed to evaluate the regional suitability of the 8-model ensemble. Additional 15 GCMs were selected from the CMIP5 archive that contains precipitation predictors of the sample region. Additional GCMs were selected by avoiding multiple replicas from the same modeling centers. The historical and future uncertainty spread of the 8- and 15-model ensembles were likewise computed against ERA-Interim patterns (i.e., PS) and compared using the box and whisker plots. There was no significant difference between the two GCM ensembles, justifying the CMIP5 representatives of the 8-model ensemble strongly.

The study used monthly time series to infer future precipitation (temperature) changes and their influence on the regional cryosphere. Ideally, sub-daily downscaling models should be developed since the cryosphere is more sensitive towards such temporal resolutions (de Kok et al., 2021). However, the long-term sub-daily observations are not available in the high mountains. The availability issues of modeled predictors may further constrain such fine-scale analysis. Since this study focused on water management at the basin scale rather than extreme event analysis, monthly resolution seems justified.
Spatial temperature inferences using precipitation regionalization may lack reliability. Temperature correlations between the time series of RR stations and regional centroids were computed (separately for each sub-region) to evaluate the efficacy of precipitation regions in explaining temperature variability. Such correlations were consistently high ($> 0.70$) to justify using precipitation clusters for temperature analysis.

Despite some limitations, the study presented an alternative simulation perspective to assess fine-scale climate variability over the significant parts of the effective drainage basin to draw rational inferences about future water balance.

# 5

# Scientific Contributions

The Indus basin's climate response has shown conflicting signals (Bashir et al., 2017, Fowler and Archer, 2006). Observational (Immerzeel et al., 2015) and GCM limitations (Hasson et al., 2019) over the high mountain UIB mainly contribute to such uncertainty. The current PhD study attempted to improve regional climate simulations by accounting for existing data and GCM limitations within a statistical downscaling framework. Quantifying climate uncertainties at finer scales using large-scale atmospheric dynamics was unique in the region and could provide an alternate as well as more reliable simulation perspective. Such a robust statistical framework could influence future climate research in the region and other data-scarce regions with similar simulation challenges.

Firstly, the research showed that climate variables could be mapped using precipitation co-variability to account for high spatiotemporal variability despite issues of observation lackings, variable data lengths, and reliability (e.g., erroneous HA measurements). Such climate mapping could help identify stations offering temporally complete, homogeneous, and historical observations for downscaling to draw meaningful spatial (horizontal and vertical) inferences. Such a framework would significantly reduce downscaling efforts and prevent temporal and quantitative biases associated with shorter data and erroneous precipitation measurements over HA regions.

GCMs have progressively shown better skills in simulating large-scale atmospheric dynamics than corresponding predictands (e.g., precipitation, Trigo et al., 2001). Therefore, using large-scale atmospheric patterns instead of modeled predicatands in the downscaling process could improve simulation quality over complex terrains like the UIB. These atmospheric patterns could also help to quantify climate uncertainties and select better-performing GCMs. Although previous studies (e.g., McSweeney et al., 2015) have rated GCMs using atmospheric circulations, selection based upon atmospheric patterns controlling finer-scale precipitation variability over the mountain regions seems more appropriate as proposed here. GCMs that better represent the large-scale atmospheric forcing may improve precipitation simulations over the regional scales. Still, their usefulness for sub-regional mountainous inferences where orography strongly modulates the large-scale forcing is questionable.

The adopted downscaling framework demonstrated an inclusive GCM approach for future climate analysis by simultaneously considering the complex stochastic nature of the climate system and variable GCM performances. On the contrary, the previous regional studies tend to either exclude poor performing models (e.g., Lutz et al., 2016a) or assign equal weights to GCMs in an ensemble without considering regional suitability (Pallazi et al., 2014). Both ensemble approaches are debatable (e.g., Hasson et al., 2019; Kannuti, 2010). Thus the study contributed to serving scientific interests and

community expectations. Three research articles outlining various aspects of the statistical modeling over the study basin were published in the journals of international repute. Two publications focused only on precipitation modeling due to its complex phenomenon, importance in the hydrological cycle, and its largely unknown nature over the region.

**Article 1** aims to skillfully model the observed precipitation dynamics across the study basin using time-space differentiated analysis and focus on the UIB. Methodological considerations and fresh evidence from more than 20 HA observatories could improve precipitation simulations over the basin. It was demonstrated that i) regional precipitation could be mapped using co-variability to fill spatial gaps despite observational challenges, ii) HA precipitation dynamics could advantageously be represented by the relatively low altitude stations, iii) using large-scale atmospheric patterns instead of GCM simulated precipitation in downscaling could improve simulation quality, and iv) basin-wide downscaling is necessary for integrated water management. It was further shown that v) statistical models showed more predictability over the UIB, vi) trans-Himalayans regions require more complex models, vii) statistical models also explain the underlying physical mechanisms, and viii) such statistically skillful and physically consistent models could provide a sound basis to infer future climate and water balance over the complex, data-scarce, and climate-sensitive river basin.

**Article 2** focused on future precipitation changes under RCP4.5 and RCP8.5 scenarios and their robustness using the precipitation models developed in Article 1. Besides computing future precipitation, it was shown that the predictors could also be used to quantify the reference and GCM level of uncertainties and select better-performing GCMs. It was also demonstrated that i) higher statistical skills and low (reference and GCM) uncertainty during the westerly-dominated seasons could increase the reliability of seasonal projections over the UIB, ii) relatively high reference uncertainty during the monsoon season restricted accurate GCM evaluations, iii) future precipitation would follow elevation-dependent patterns, where the HA regions will receive significantly more precipitation, (iv) the highest precipitation increase would be over the Karakoram region, and v) the intense warming scenario (RCP8.5), better performing GCMs, and signal-to-noise ratios further support positive (negative) changes during the winter and monsoon (pre-monsoon) periods. Future strengthening and increased northward penetrating winter westerlies (monsoon easterlies) could support the regional cryosphere, particularly over the Karakoram region, even under a high warming scenario. The Lower Indus projections indicated monsoon strengthening over the spate-irrigated regions, which could augment future water availability. The winter and pre-monsoon precipitation changes were largely positive.

Since precipitation alone can not close the melt-dominated Indus water balance, the statistical downscaling was extended further to assess future temperatures ($T_{max}$ and $T_{min}$) over the study basin.

**Article 3** used the MLR framework to model observed temperatures skilfully and evaluate future changes. It was demonstrated that i) close similarities among the precipitation and temperatures' predictors could confirm their interdependence, ii) identified predictors successfully represented seasonally varying climatology, iii) climate uncertainty magnitudes were similar to precipitation counterparts, and iv) a combination of high statistical skills and low uncertainties (reference and GCM) over the HA regions could increase confidence in subsequent projections. Future multi-model temperature changes showed that v) despite non-uniform and complex warming patterns, the EDW could not be verified at the basin scale, vi) $T_{min}$ changes would govern the winter warming that was highest among all seasons, vii) $T_{max}$ dominated the pre-monsoon warming, viii) low-warming monsoon conditions could prevail over the UIB, and ix) the Lower Indus would warm significantly more than the UIB during all seasons. Projected strengthening and northward penetrations of the winter westerlies and monsoon circulations, increased HA precipitation and associated negative feedbacks, and intensification of the Tibetan High may explain future warmings in different seasons. The seasonal temperature changes suggested increased water availability from the UIB, a substantial rise in future water demand, and the likelihood of continuing the anomalous UIB response, particularly over the Karakoram region, at the end of the 21st century even under the RCP8.5 forcing.

# 6

# Summary and Conclusions

Pakistan's Indus River basin is one of the world's largest and most complex river basins with a relatively unknown climate response within the cryosphere-dominated UIB. By focusing on the UIB, the present study modeled future precipitation and temperatures over the study basin under selected global warming scenarios to infer future hydrology. Accounting for high climate variability, adopting a more suitable downscaling approach, and taking advantage of the recently established HA monitoring within an advanced statistical downscaling framework could improve simulation quality. The downscaling focused on estimating future climatic changes and associated uncertainties by circumventing GCM simulated predictands that show significant biases over the UIB (e.g., Hasson et al., 2019). Available observations (e.g., Pallazai et al., 2013) may not adequately correct such GCM biases. Instead, large-scale atmospheric dynamics were used in the downscaling process due to relatively improved representation by the modern GCMs.

Firstly, the K-means clustering algorithm was used to characterize the basin into homogeneous precipitation regions to account for high spatial variability on seasonal scales. The clustering process demonstrated how relatively low altitude stations could be used to explain the precipitation dynamics over HA regions. Predictors from the ERA-Interim reanalysis dataset were then used to identify atmospheric drivers of the observed precipitation and temperatures ($T_{max}$ and $T_{min}$) at sub-regional scales. Statistically skillful and physically consistent downscaling models provided a robust platform for climate change analysis, particularly over the UIB. A close similarity among precipitation and temperature predictors confirmed their interdependence. The precipitation (temperature) predictors were compared with corresponding variables from two additional reanalysis datasets and historical CMIP5-GCM simulations to quantify reference and GCM level of uncertainties. In general, various dynamical (thermodynamic) variables governed the basin's GCM (reference) level of uncertainty, which was nearly double the reference level magnitude. A relatively high reference level of uncertainty during the monsoon season restricted accurate GCM evaluations. Although no single GCM successfully captured the full climate variability, the model ranking procedure helped identify models demonstrating significant increases in skill during simulations of past climate over the basin.

GCM predictors under RCP4.5 and RCP8.5 scenarios were used in the downscaling models to assess future precipitation and temperature changes over the study basin. Overall, significantly wet and warmer conditions could dominate the Indus hydrology throughout the 21st century. These signals would intensify under the RCP8.5 scenario and during the 2071-2100 period, which were confirmed by better-performing GCMs and the SNR. Projected precipitation followed elevation-dependent patterns where HA regions would receive more precipitation compared to their counterparts. The winter season would

experience the highest precipitation and ($T_{min}$ dominated) warming. The Karakoram region would experience the highest precipitation increase. A significantly decreased precipitation and ($T_{max}$ dominated) high warming was also estimated during the pre-monsoon. The future monsoon was marked by increased precipitation and strikingly a feature of low-warming conditions over the UIB. The Lower Indus warming was significantly higher compared to the UIB during all seasons, so EDW at the basin scale was not confirmed.

The typical precipitation (temperatures) changes would exert tremendous influence on the basin hydrology. For instance, the liquid precipitation proportion may significantly increase over the UIB due to rising minimum temperatures, particularly during the winter half. A spring season precipitation decrease could partly be compensated by the increased melting (glacial and previously accumulated snow) and more favorable climate changes over the eastern tributaries. Increased winter precipitation could increase base flows, which may cause heavy flooding under the projected monsoon strengthening. Increased minimum temperatures could also trigger avalanches and ice mass redistribution, affecting water resources, infrastructure, and communities.

Favorable precipitation (temperature) changes over the UIB may significantly increase future water availability. Contrary to other downscaling studies, an increase in the water supply may remain possible without a rapid glacial retreat. In particular, the precipitation (temperature) changes over the Karakoram region may continue supporting its anomalous behavior (e.g., Bashir et al., 2017) towards the end of the 21st century under RCP8.5 forcing. Adopting uniform lapse rates without considering topographic, land use (e.g., glacial and debris cover), and seasonal heterogeneity within the UIB (e.g., Muhammad et al., 2021; Smith et al., 2021) may induce warm biases in such studies. Therefore, preserving GCM simulated signals during bias-correction (e.g., Ali et al., 2020) may require precautions in this region where GCMs tend to overestimate glacier retreats (Lin et al., 2021). An alternative could be the bias-corrected perfect prognosis downscaling. However, consistently high warming over the Lower Indus would substantially increase future water demand. Such warming would suggest an early start of the crop growing seasons and readjustments in seasonal water allocations. Better water regulations would help match future water supply with its demand to benefit agricultural and hydropower developments in the basin.

# 7

# Future Research Thrusts

Despite recent advances in regional monitoring, GCM simulations, and statistical frameworks, the uncertainties about future climate simulations would dominate Indus hydrology. The lack of observations over the HA regions has the largest contribution toward future uncertainties. To improve hydrological assessments, systematic monitoring at sub-catchment scales must extend to include ELA estimated between 5500 to 6000 m elevations (e.g., Khan et al., 2014). Besides sub-daily temperature and precipitation, future monitoring should also focus on other meteorological variables (e.g., winds, humidity, solar radiations, cloud covers) to facilitate full energy balance research essential for Indus hydrology. Furthermore, adhering to standardized data collection protocols of the World Meteorological Organization (WMO) can resolve HA precipitation measurement issues and improve data quality. Since Indus is a transboundary River basin, collective and coordinated monitoring efforts with a centralized data sharing facility will benefit scientific research and reduce the financial burdens on individual partners. The Indus River Basin System Authority comprising Pakistan, India, China, and Afghanistan could be established using the Mekong River Commission (https://www.mrcmekong.org/) pattern to oversee, coordinate, and manage transboundary resources more efficiently.

Meanwhile, improved synchronization of the available glacier mass-balance information and the time series of regular monitoring stations would lead to an improved understanding of vertical climate variability over the UIB. However, unlike adopting uniform (and linear) lapse rates (e.g., Immerzeel et al., 2015), such elevation inferences should be derived from space-time considerations to account for multidimensional heterogeneity. Using hierarchical cluster analysis, Smith et al. (2021) recently mapped snow cover-elevation heterogeneity over the UIB. Their findings that instead of elevation, the local topographic factors exert a more profound influence on glacial behavior would also justify time-space varying lapse rates. Future research in this regard can improve elevation-climate inferences over the UIB for better hydrological assessments.

Highly biased GCM and RCM simulations (e.g., Hasson et al., 2019, Mishra, 2015) over the UIB also require structural improvements in modeling frameworks. For instance, improved representation of the regional topography, orographic process, and reducing parametrization could further improve model simulations. Many CMIP5-GCMs did not provide lower-tropospheric predictors over the mountain regions. Despite physical issues, such vertically interpolated (or extrapolated) predictor data is necessary for understanding circulation changes, implementing perfect prognosis downscaling, and inter-model

regional comparison. Future modeling protocols should provide such predictor data. Since High Asia is a climate hotspot that provides freshwater for many large Asian countries (Curio and Scherer, 2016), and GCMs differ substantially in their mountain simulations, it would be of scientific interest to develop a separate coordinated modeling framework for this complex region. That would encourage modeling groups to improve mountain climatology in GCMs and allow robust analysis for assessing future water availability, cryosphere stability, and disaster risk management issues.

Daily downscaling models could assist in extreme event analysis. The climate extremes (e.g., floods, droughts, glacial bursting) pose a significant threat to the region and require proactive regional planning. However, the availability of daily modeled predictors may restrict exploiting the full potential of circulation-based downscaling. Adopting downscaling techniques like Quantile Delta Mapping (Cannon et al., 2015a) that preserve modeled predictand signals should be carefully reviewed over the mountainous areas, where GCM predictands are well-known wrongs (e.g., Lin et al., 2021). Instead, bias-corrected predictors should be used in a perfect prognosis framework over such complex regions. Lastly, the downscaling output should be used in fully distributed hydrological models accounting for full energy balance and glacial processes to quantify future water resources.

# 8

# References


Akhtar, M., Ahmad, N. and Booij, M.J. (2008) The impact of climate changes on the water resources of Hindukush–Karakorum– Himalayaregionunder different glacier coverage scenarios. Journal of Hydrology, 355, 148–163. https://doi.org/10.1016/j. jhydrol.2008.03.015

Ali, S., Kiani, R.S., Reboita, M.S., Dan, L., et al., (2020). Identifying hotspots cities vulnerable to climate change in Pakistan under CMIP5 climate projections. International Journal of Climatology, 41, 559–581. https://doi.org/10.1002/joc.6638.

Ali, S., Li, D., Congbin, F. and Khan, F. (2015) Twenty-first century climatic and hydrological changes over Upper Indus Basin of Himalayan region of Pakistan. Environmental Research Letters, 10, 1–20. https://doi.org/10.1088/1748-9326/10/1/014007

Almazroui, M., Saeed, S., Saeed, F., Islam, MN., Ismail, M. (2020). Projections of Precipitation and Temperature over the South Asian Countries in CMIP6. Earth Syst. Environ. 4, pp. 297–320

Archer, DR., Forsythe, N., Fowler, HJ., Shah, SM. (2010) Sustainability of water resources management in the Indus Basin under changing climatic and socioeconomic conditions. Hydro.Earth Sys.Sci.141669–80

Ashfaq, M., Rastog, D., Mei, R., Toumag, D. et al., (2016). Sources of errors in the simulation of south Asian summer monsoon in the CMIP5 GCMs. Climate Dynamics, 49, 193–223. https://doi.org/10.1007/s00382-016-3337-7

Bashir, F., Zeng, X., Gupta, H., Hazenberg, PA. (2017). Hydrometeorological Perspective on the Karakoram Anomaly Using Unique Valley-Based Synoptic Weather Observations. Geophys. Res. Lett. 44, 10470–10478

Beniston, M. (2005). The risks associated with climatic change in mountain regions. In: Huber, UM., Bugmann, HKM., Reasoner, MA., editors. Global Change in Mountain Regions. An Overview of Current Knowledge. Dordrecht, the Netherlands: Springer, pp 511–519

Bocchiola, D., Diolaiuti, GA., Soncini, A., and Mihalcea, C. (2011) Prediction of future hydrological regimes in poorly gauged high altitude basins: the case study of the upper Indus, Pakistan, Hydrol. Earth System Science, 15(7), 2059–2075. https://doi.org/10.5194/hess-15-2059-2011

Bolch, T., Kulkarni, AV., Kääb, A., and Huggel, C. (2012) The state and fate of Himalayan glaciers. Science, 336(6079), 310–314. https://doi.org/10.1126/science.1215828

Brun, F., Berthier, E., Wagnon, P., Kääb, A., Treichler, D. (2017). A spatially resolved estimate of High Mountain Asia glacier mass balances from 2000 to 2016. Nat. Geosci., 10, 668–673

Cannon, AJ., Sobie, SR., and Murdock, TQ. (2015a). Biase correction of GCM precipitation by Quantile Mapping: How well do methods preserve changes in quantiles and extremes. Journal of Climate, Vol 28. https://doi.org/10.1175/JCLI-D-14-00754.1

Cannon, F., Carvalho, LM., Jones, C., Norris, J. (2015b). Winter westerly disturbance dynamics and precipitation in the western Himalaya and Karakoram: A wave-tracking approach. Theor. Appl. Clim., 125, 27–44. DOI:10.1007/s00704-015-1489-8

Coen, MC., Andrews, E., Aliaga, D., Andrade, M., et al., (2018). Identification of topographic features influencing aerosol observations at high altitude stations. Atmos. Chem. Phys. 2018, 18, 12289–12313. https://doi.org/10.5194/acp-18-12289-2018

Curio J., and Scherer, D. (2016) Seasonality and spatial variability of dynamic precipitation controls on the Tibetan Plateau. Earth Syst Dynam (7): 767–782. https://doi.org/10.5194/esd-7-767-2016

Dahri, ZH., Moors, E., Ludwig, F., Ahmad, S., et al., (2018). Adjustment of measurement errors to reconcile precipitation distribution in the high-altitude Indus basin. Int. J. Clim., 38, 3842–3860. https://doi.org/10.1002/joc.5539

Dars, G.H., Strong, C., Kochanski, AK., Ansari, K., et al., (2020). The Spatiotemporal Variability of Temperature and Precipitation Over the Upper Indus Basin: An Evaluation of 15 Year WRF Simulations. Appl. Sci., 10, 1765. https://doi.org/10.3390/app10051765

de Kok, R.J., and Immerzeel, WW. (2019). The Western Tibetan Vortex as an emergent feature of near-surface temperature variations. Geophysical Research Letters, 46, 14,145–14,152. https://doi.org/10.1029/2019GL085757

de Kok, R.J., Tuinenburg, OA., Bonekamp, PNJ., Immerzeel, WW. (2018). Irrigation as a Potential Driver for Anomalous Glacier Behavior in High Mountain Asia. Geophys. Res. Lett. 45, 2047–2054. https://doi.org/10.1002/2017GL076158

Dee, D.P., Uppala, SM., Simmons, AJ., Berrisford, P., et al., (2011) The ERA-Interim reanalysis: configuration and performance of the data assimilation system. Quarterly Journal of the Royal Meteorological Society, 137, 553–597. https://doi.org/10.1002/qj.828

Dunn, P.K. (2004). Occurrence and quantity of precipitation can be modeled simultaneously. International Journal of Climatology, 24, 1231–1239

Forsythe, N., Hardy, AJ., Fowler, HJ., Blenkinsop, S., et al., (2015). A detailed cloud fraction climatology of the upper Indus basin and its implications for near-surface air temperature. J. Clim., 28, 3537–3556. https://doi.org/10.1175/JCLI-D-14-00505.1

Fowler, H.J., and Archer, DR. (2006). Conflicting signals of climate change in the Upper Indus basin. J. Clim., 19, 4276–4293. https://doi.org/10.1175/JCLI3860.1

Hasson, S.U., Böhner, J., Chishtie, F. (2018). Low fidelity of CORDEX and their driving experiments indicates future climatic uncertainty over Himalayan watersheds of Indus basin. Clim. Dyn. 52, pp. 777–798. https://doi.org/10.1007/s00382-018-4160-0

Heo, K.Y., Ha, KJ., Yun, KS., Lee, SS., Kim, HJ., et al. (2014). Methods for uncertainty assessment of climate models and model predictions over East Asia. International Journal of Climatology, 34, 377–390. https://doi.org/10.1002/joc.3692

Herreid, S., and Pellicciotti, F. (2020). The state of rock debris covering earth's glaciers. Nat. Geosci., 13, 1–7. https://doi.org/10.1038/s41561-020-0615-0

Hersbach, H., Bell, B., Berrisford, P., Hirahara, S., et al., (2020). The ERA5 global reanalysis. QJRMS, 146 (730), 1999–2049. https://doi.org/10.1002/qj.3803

Hertig, E., Merkenschlager, C., Jucundus, J. (2017). Change points in predictors–predictand relationships within the scope of statistical downscaling. Int J Climatol 37, pp. 1619–1633. https://doi.org/10. 1002/joc.4801

Hewitt, K. (2014). Glaciers of the Karakoram Himalaya. Springer, p 363.

Hewitt, K. (2005). The Karakoram anomaly? Glacier expansion and the 'elevation effect, 'Karakoram Himalaya. Mt. Res. Dev. 25, pp. 332–340. https://doi.org/10.1038/s41561-020-0615-0

Hoy, A., Katel, O., Thapa, P., Dendup, N., Matschullat, J. (2016). Climatic changes and their impact on socio-economic sectors in the Bhutan Himalayas: An implementation strategy. Regional Environmental Change 16(5):1401–1415. http://dx.doi.org/10.1007/s10113-015-0868-0

Immerzeel, WW., Van Beek, LP., Bierkens, MF. (2010). Climate change will affect the Asian water towers. Science 328(5984):1382–1385. DOI: 10.1126/science.1183188

Immerzeel, WW., Wanders, N., Lutz, AF., Shea, JM., Bierkens, PFM. (2015). Reconciling high-altitude precipitation in the upper Indus basin with glacier mass balances and runoff. Hydrol. Earth Syst. Sci., (19), pp. 4673–4687. DOI: 10.5194/hess-19-4673-2015

Jain, SK., Agarwal, PK., Singh, VP., Jain, S., Agarwal, P., Singh, V., (2007). Indus Basin. Hydrology and Water Resources of India, Springer Netherlands. 57, pp. 473-511.

Kääb, A., Berthier, E., Christopher, N., Gardelle, J., Arnaud, Y. (2012) Contrasting patterns of early twenty-first-century glacier mass change in the Himalayas. Nature 488(7412):495–498. DOI: 10.1038/nature11324

Karki, R.; Hasson, SU., Gerlitz, L., Talchabhadel, R.; Schickhoff, U., et al. (2020). Rising mean and extreme near-surface air temperature across Nepal. Int. J. Clim. 2020, 40, 2445–2463. https://doi.org/10.1002/joc.6344

Kaspar-Ott, I., Elke, H., Seerin, K., Felix, P., Christoph, R., Heiko, P., Jucunduss, J. (2019). Weights for general circulation models from CIMP3/CIMP5 in a statistical downscaling framework and the impact on future Mediterranean precipitation. *Int. J. Climatol. 2019, 39, PP 3639–3654. DOI: 10.1002/joc.6045*

Khan, AJ., and Koch, M. (2018) Selecting and downscaling a set of climate models for projecting climate change for impact assessment in the upper Indus Basin (UIB). Climate, 6(4), 89. https:// doi.org/10.3390/cli6040089. https://doi.org/10.3390/cli6040089

Khan, F., Pilz, J., Amjad, M. and Wiberg, D. (2015) Climate variability and its impacts on water resources in the Upper Indus Basin under IPCC climate change scenarios. International Journal of Global Warming, 8(1), 46–69. https://doi.org/10.1504/IJGW.2015.071583

Khattak, MS., Babel, MS., and Sharif, M. (2011) Hydro-meteorological trends in the upper Indus River basin in Pakistan. Climate Research, 46, 103–119. https://doi.org/10. 3354/cr00957

Knutti, R. (2010) The end of model democracy? Climatic Change, 102(3–4), 395–404. https://doi.org/10.1007/s10584-010-9800-2

Korner, C. (2013). Alpine ecosystems. In: S.A. Levin (ed.) Encyclopedia of biodiversity, 2nd edition, vol. 1, pp. 148–157. Amsterdam, The Netherlands, Academic Press.

Kraaijenbrink, PDA., Bierkens, MFP., Lutz, AF., Immerzeel, WW. (2017) Impact of a 1.5 °C global temperature rise on Asia's glaciers. Nature 549:257–260. https://doi.org/10.1038/nature23878

Lin, C., Yang, K., Chen, D., Guyennon, N., Balestrini, R.,et al. (2021). Summer afternoon precipitation associated with wind convergence near the Himalayan glacier fronts. Atmospheric Research 259 (2021) 105658. https://doi.org/10.1016/j.atmosres.2021.105658

Lutz, AF., Immerzeel, WW., Kraaijenbrink, PDA., Shrestha, AB. and Bierkens, MFP. (2016b). Climate change impacts on the Upper Indus hydrology: sources, shifts and extremes. PLoS One, 11(11), e0165630. https://doi.org/10.1371/journal.pone.0165630

Lutz, AF., Maat, HWT., Biemans, H., Shrestha, AB., et al., (2016a). Selecting representative climate models for climate change impact studies: an advanced envelope-based selection approach. International Journal of Climatology, 2016(36), 3988–4005. DOI: 10.1002/joc.4608

Mahmood, R. and Babel, MS. (2012). Evaluation of SDSM development by annual and monthly sub-models for downscaling temperature and precipitation in the Jhelum basin, Pakistan, and India. Theoretical and Applied Climatology, 113, 27–44. https://doi.org/10.1007/s00704-012-0765-0

Mc Cullagh, P. and Nelder, JA. (1989) Generalized Linear Models. Monographs on Statistics and Applied Probability, Vol. 37. London: Chapman & Hall

McSweeney, CF., Jones, RG., Lee, RW. and Rowell, DP. (2015) Selecting CIMP5 GCMs for downscaling over multiple regions. Climate Dynamics, 44(11–12), 3237–3260. https://doi.org/10.1007/s00382-014-2418-8

Mishra, V. (2015) Climatic uncertainty in Himalayan water towers. Journal of Geophysical Research: Atmospheres, 120, 2689–2705. https://doi.org/10.1002/2014JD022650

Moberg, A., Jones, P.D., Lister, D., Walther, A., Brunet, M., et al. (2006). Indices for daily temperature and precipitation extremes in Europe analyzed for the. Journal of Geophysical Research: Atmospheres, 111(D22), 1984–2012. https://doi.org/10.1029/2006JD007103

Mueller, B., and Seneviratne, SII. (2014). Systematic land climate and evapotranspiration biases in CMIP5 simulations. Geophysical Research Letters, 41, 128–134. https://doi.org/10.1002/2013GL058055

Muhammad, S., Tian, L., Ali, S., Latif, Y., et al., (2020). Thin debris layers do not enhance melting of the Karakoram glaciers. Sci. Total Environ. 2020, 746, 141119. https://doi.org/10.1016/j.scitotenv.2020.141119

Palazzi, E., von Hardenberg, J., and Provenzale, A. (2013). Precipitation in the Hindu-Kush Karakoram Himalaya: observations and future scenarios. Journal of Geophysical Research: Atmospheres, 118(1), 85–100. https://doi.org/10.1029/2012JD018697

Palazzi, E., von Hardenberg, J., Terzago, S. and Provenzale, A. (2014) Precipitation in the Karakoram-Himalaya: a CMIP5 view. Climate Dynamics, 45, 21–45. https://doi.org/10.1007/ s00382-014-2341-z.
Pepin, N., Bradley, R. *et al.* (2015). Elevation-dependent warming in mountain regions of the world. *Nature Clim Change* **5,** 424–430 (2015). https://doi.org/10.1038/nclimate2563

Philipp, A. (2003). Zirkulationsdynamische Telekonnektivität des Sommerniederschlags im südhemisphärischen Afrika. Disserta- tion, Bayerische Julius-Maximilians-Universität Würzburg.
Preisendorfer, R. (1988). Principal Component Analysis in Meteorology and Oceanography, Vol. 42. Amsterdam: Elsevier

Pritchard, DMW., Forsythe, N., Fowler, HJ., O'Donnell, GM., et al., (2019). Evaluation of Upper Indus Near-Surface Climate Representation by WRF in the High Asia Refined Analysis. J. Hydrometeorol., 20, 467–487. https://doi.org/10.1175/JHM-D-18-0030.1

Sanford, T., Frumhoff, P, C., Luers, A. and Gulledge, J. (2014) The climate policy narrative for a dangerously warming world. Nature Climate Change, 4, 164–166. https://doi.org/10.1038/nclimate2148

Smith, T., Rheinhalt, A., Bookhagen, B. (2021). Topography and Climate in the Upper Indus Basin: Mapping Elevation-Snow Cover Relationships. Science of The Total Environment 786(1):147363. DOI: 10.1016/j.scitotenv.2021.147363

Soncini, A., Bocchiola, D., Confortola, G., Bianchi, AB., Rosso, R., et al. (2015). Future Hydrological Regimes in the Upper Indus Basin: A Case Study from a High-Altitude Glacierized Catchment, J. Hydrometeorol., 16(1), 306–326. https://doi.org/10.1175/JHM-D-14-0043.1

Sperber, KR., Annamalai, H., Kang, IS., Kitoh, A., Moise, A., et al. (2013) The Asian summer monsoon: an intercomparison of CMIP5 vs. CMIP3 simulations of the late 20th century. Clim Dyn 41(9–10):2711–2744. https://doi.org/10.1007/s00382-012-1607-6

Su, B., Huang, J., Gmmer, M., Jian, D., Tao, H., Jiang, T. and Zhao, C. (2016) Statistical downscaling of CMIP5 muli-model ensemble for projected changes of climate in the Indus River Basin. Atmospheric Research, 178-179, 138–149. https://doi.org/10.1016/j.atmosres.2016-03.023

Syed FS., Giorgi, F., Pal, JS., Keay, K. (2010). Regional climate model simulation of winter climate over Central–Southwest Asia, with emphasis on NAO and ENSO effects. Int J Climatol 30:220–235. https://doi.org/10.1002/joc.1887

Tahir, AA., Chevallier, P., Arnaud, Y., Ahmad, B. (2011). Snow cover dynamics and hydrological regime of the Hunza River basin, Karakoram Range. Northern Pakistan Hydrol Earth Syst Sci 15(7):2275–2290. https://doi.org/10.5194/hess-15-2275-2011

Taylor, K.E. (2001) Summarizing multiple aspects of model per- performance in a single diagram. Journal of Geophysical Research, 106(D7), 7183–7192. https://doi.org/10.1029/2000JD900719

Taylor, KE., Stouffer, RJ. and Meehl, GA. (2012) An overview of CMIP5 and the experiment design. Bulletin of the American Meteorological Society, 93, 485–498. https://doi.org/10.1175/BAMS-D-11-00094.1

Trigo, R. and Palutikof, J. (2001) Precipitation scenarios over Ibe- ria: a comparison between direct GCM. Output and different downscaling techniques. Journal of Climate, 14, 4422–4446. https://doi.org/10.1175/1520-0442(2001)014<4422:PSOIAC>2.0.CO;2

UN. (2019). World Population Prospects 2019: Data Booklet. United Nations Department of Economic and Social Affairs. Available at: https://population.un.org/wpp/Publications/Files/WPP2019_DataBooklet.pdf

Wake, CP. (1989). Glaciochemical investigations as a tool for determining the spatial and seasonal variation of snow accumulation in the Central Karakoram, northern Pakistan. Ann. Glaciol., 13, 279–284. DOI: https://doi.org/10.3189/S0260305500008053

WGMS. (2020). Global Glacier Change Bulletin No. 3 (2016–2017). Publication Based on Database Version; World Glacier Monitoring Service: Zurich, Switzerland, p. 274

Wijngaard, JB., Klein, TAMG. and Können, GP. (2003). Homogeneity of 20th-century European daily temperature and precipitation series. International Journal of Climatology, 23, 679–692. https://doi.org/10.1002/joc.906

Wilcoxon, F. Individual Comparisons by Ranking Methods. In Breakthroughs in Statistics; Springer: New York, NY, USA, 1945; Volume 1, p. 80.

Wilks, S. (2006). Statistical methods in the atmospheric sciences. International Geophysical Series, 91.

Winiger, M., Gumpert, M., Yamout, H. (2005). Karakorum–Hindukush– western Himalaya: assessing high-altitude water resources. Hydrol Process 19 (12), pp. 2329–2338. https://doi.org/10.1002/hyp.5887

Wolff, MA., Isaksen, K., Petersen-Øverleir, A., Ødemark, K., et al., (2015). Derivation of a new continuous adjustment function for correcting wind-induced loss of solid precipitation: Results of a Norwegian field study, Hydrology and Earth System Sciences 19 (2): 951-967. https://doi.org/10.5194/hess-19-951-2015

# 9

# Peer-Reviewed Articles

## 9.1 Modeling Regional Precipitation Over The Indus River Basin of Pakistan Using Statistical Downscaling

Muhammad Saleem Pomee[1,2] Moetasim Ashfaq[3], Bashir Ahmad[2], Elke Hertig[1]

[1]Regional Climate Change and Health, Faculty of Medicine, University of Augsburg, Germany

[2]Pakistan Agricultural Research Council (PARC), Islamabad, Pakistan

[3]Computational Sciences and Engineering Division, Oak Ridge National Laboratory, Oak Ridge, TN, USA

This was published as Article in Theoretical and Applied Climatology (https://doi.org/10.1007/s00704-020-03246-9)

## Abstract

Complex processes govern spatiotemporal distribution of precipitation within the high-mountainous headwater regions (commonly known as the upper Indus basin (UIB)) of the Indus River basin of Pakistan. Reliable precipitation simulations, particularly over the UIB, present a major scientific challenge due to regional complexity and inadequate observational coverage. Here, we present a statistical downscaling approach to model observed precipitation of the entire Indus basin, with a focus on UIB within available data constraints. Taking advantage of recent high altitude (HA) observatories, we perform precipitation regionalization using K-means cluster analysis to demonstrate the effectiveness of low-altitude stations to provide useful precipitation inferences over more uncertain and hydrologically important HA of the UIB. We further employ generalized linear models (GLM) with gamma and Tweedie distributions to identify major dynamic and thermodynamic drivers from a reanalysis dataset within a robust cross-validation framework that explains observed spatiotemporal precipitation patterns across the Indus basin. Final statistical models demonstrate higher predictability to resolve precipitation variability over wetter southern Himalayans and different lower Indus regions by mainly using different dynamic predictors. The modeling framework also shows an adequate performance over more complex and uncertain trans-Himalayans and the northwestern regions of the UIB, particularly during the seasons dominated by the westerly circulations. However, the cryosphere-dominated trans-Himalayan regions, which largely govern the basin hydrology, require relatively complex models that contain dynamic and thermodynamic circulations. We also analyzed relevant atmospheric circulations during precipitation anomalies over the UIB to evaluate the physical consistency of the statistical models as an additional measure of reliability. Overall, our results suggest

that such circulation-based statistical downscaling has the potential to improve our understanding towards distinct features of the regional-scale precipitation across the upper and lower Indus basin. Such understanding should help to assess the response of this complex, data-scarce, and climate-sensitive river basin amid future climatic changes to serve communal and scientific interests.

# 1 Introduction

The trans-Himalayan and transboundary Indus River flows approximately 3200 km across its 1.12 million square kilometer basin to ultimately descend into the Arabian Sea (FAO, 2011). The upper Indus basin (UIB), marked by the confluence of the Hindukush, Karakoram, and Himalayans mountain ranges (HKH), contains the largest cryosphere volumes outside the Poles (Soncini et al., 2015; Qiu, 2008). The HKH topography modulates two contrasting synoptic-scale processes: the South Asian Summer Monsoon and Western Disturbances, to determine highly variable patterns of observed precipitation over the UIB (Filippi et al., 2014; Palazzi et al., 2013). Snow and glacial melt within the UIB mainly govern the hydrological regime of the Indus River (e.g., Tahir et al., 2011; Archer and Fowler, 2004), which sustains the livelihood of nearly 215 million downstream inhabitants (Latif et al., 2018; Lutz et al., 2016). In contrast, the lower Indus (LI) primarily has an arid to semi-arid climate and represents large fertile plains, spate irrigation regions, and diverse coastal ecology.

Accurate knowledge of the spatial and temporal distribution of precipitation is largely unknown in the high altitudes (HA) of the UIB (Immerzeel et al., 2015; Hewitt, 2005; Winiger et al., 2005). This lack of certainty in precipitation characteristics stems from an insufficient number of HA meteorological observatories, inaccuracies in available HA measurements (Rasmussen et al., 2012), concerns about the data quality (Hewitt, 2011; Winiger et al., 2005), and serious constraints on transboundary data sharing due to regional politics (Dahri et al., 2016). It should be noted that most of the observatories with long-term records are sparsely located in the low altitudes, while short-term and inconsistent observations of the HA limit our understanding about the regional orography.

Given an elevated susceptibility to climate change and the associated high social-ecological vulnerability (MRI, 2015; Nepal and Shrestha, 2015), a reliable knowledge towards the spatiotemporal organization of regional precipitation is imperative to implement efficient adaptations at the basin level. However, the observational constraints hamper reliable modeling of the processes that govern precipitation distribution within the basin. While different gridded products (e.g., reanalysis, remote sensing, or interpolated station observations) can potentially help to overcome these observational deficiencies (Immerzeel et al., 2015), the scope of such improvements is somewhat limited over the complex and largely snow-covered HA of the UIB (Immerzeel et al., 2015; Huffman et al., 2007; Turner and Annamalai, 2012).

Given the unique observational challenges, different strategies have been adapted to improve the confidence in precipitation simulations over the UIB. However, studies often find contrasting climate change signals over these regions, which range from rapidly retreating glaciers (Kääb et al., 2012, 2015; Wiltshire, 2014; Jacob et al., 2012; Cogley, 2011) to rather glacial expansions in the Karakoram, also known as the Karakoram anomaly (e.g., Bashir et al., 2017; Kapnick et al., 2014; Tahir et al., 2014; Bhambri et al., 2013; Minora et al., 2013). The lack of robustness in the projected change signal and associated glacial response over this region implicates the development of effective policy measures to reduce projected vulnerability over the basin. Therefore, it is imperative to understand the influence of existing observational and modeling challenges on projected climatic changes over this region and to devise strategies for improving spatial inferences of regional precipitation. However, such improvements potentially have to be derived through methodological considerations, as the availability of additional high-quality data is still an ongoing issue.

In this context, the reliability of spatially distributed precipitation estimates may suffer from (i) altitudinal biases, (ii) issues with observational data (homogeneity, time series length, consistency), and/or (iii) the downscaling approaches. We refer to these challenges as the type 1, type 2, and type 3 uncertainties. Many previous studies exhibit the type 1 uncertainty because they rely on the low-altitudinal observations to infer seasonal and annual precipitation statistics over the UIB (e.g., Iqbal and Athar, 2018, Ali et al., 2015; Khan et al., 2015a; Akhtar et al., 2008; Archer and Fowler, 2004, Latif et al., 2018 and Khattak et al., 2011). Estimates in most of these earlier studies neither represent the HA nor provide any quantifiable mechanism for drawing logical inferences between the low and high altitudes and, therefore, may lack reliability. Some of the recent studies (e.g., Immerzeel et al., 2015; Dahri et al., 2016, 2018; Hasson, 2016) have addressed this deficiency either by incorporating the HA perspective using short-term data (e.g., glacial mass balance and or fragmented HA monitoring) or by other assumptions. These studies significantly differ in regional precipitation estimates over the UIB when compared with historically observed estimates recorded by the valley stations. However, although estimates in these studies are derived by maximizing spatial coverage within the UIB, they may suffer from some other shortcomings. For example, the use of a limited number of HA stations, which not only contain short-term observations (e.g., Hasson, 2016) but may also exhibit issues related to homogeneity (e.g., Dahri et al., 2016), measurement errors, and assumption of a linear precipitation gradient along the altitudes (e.g., Immerzeel et al., 2013), and therefore may induce type 2 uncertainties in respective simulations.

The type 3 uncertainty originates from the choice of the adapted statistical downscaling methodology. For instance, bias correction methods, which have been widely used in these previous studies, highly depend on the observations for an appropriate characterization of the region of interest. However, the observation sparsity over the UIB makes the use of bias correction relatively ineffective. Lastly, the current generation of General Circulation Models (GCMs) has persistently failed in the representation

of dynamic and thermodynamic processes that dictate precipitation variability over this region at varying time scales (e.g., Ashfaq et al., 2017; Palazzi et al., 2015; Rastogi et al., 2018). Alternatively, regional climate models (RCMs) generally offer improved regional simulations due to better topographic representation and the flexibility of region-specific tuning of the model parameters. However, an evaluation of the seven fine-scale (0.44°) Coordinated Regional Climate Downscaling Experiment for South Asia (CORDEX-SA) experiments has also shown a limited success over this region since they still derive boundary forcing from the biased GCMs (e.g., Hasson et al., 2019; Mishra, 2015; Syed et al.,2014). The High Asia Refined (HAR) analysis, which is based on dynamical modeling, has shown promising results in reproducing overall regional precipitation climatology and in explaining sub-regional precipitation variability over time (e.g., Maussion et al., 2014; Curio and Scherer 2016). More recently, Pritchard et al. (2019) have evaluated HAR performance specifically over the UIB in terms of precipitation and other important near-surface variables. Although the annual precipitation cycle is reasonably simulated, there exist some biases at seasonal scales, which lead to wetter and colder conditions across the HA areas.

It is clear that further efforts are needed to reduce uncertainties in precipitation estimates over the UIB. For example, incorporating a time series analysis along with careful data quality checks, an avoidance of the direct use of available HA observations, and the adaption of other, potentially better-suited statistical downscaling approaches may help to resolve some of these uncertainties. To this end, perfect prognosis statistical downscaling (Wilks, 2006) is a promising statistical alternative, which offers distinct advantages. However, so far, only a few studies are reported in the region that makes use of this technique (e.g., Kazmi et al., 2016; Mahmood and Babel, 2012). This approach employs large-scale atmospheric circulations within a statistical downscaling framework to resolve the observed precipitation distributions. The use of atmospheric circulations is advantageous as these variables are relatively better modeled in the GCMs (Kaspar-Ott et al., 2019) and can explain the physical mechanisms that govern regional precipitation. Given the observational uncertainty in the UIB, such physical explanations of the downscaled precipitation may further add confidence in the statistical modeling results. Moreover, knowledge towards the large-scale dynamics that influence precipitation distribution over the UIB is relatively robust, as many of the previous studies provide a good overview in this regard that can serve as the basis for comparison. For instance, Syed et al. (2006, 2010), Curio and Scherer (2016), Cannon et al. (2015), Ahmad et al. (2015), and Kazmi et al. (2016) explain different aspects of the precipitation governing circulations over the region.

Considering such advantages and to present a different perspective, we have adapted perfect prognosis downscaling to investigate the observed precipitation dynamics within the Indus basin with a focus on the UIB by accounting for spatiotemporal precipitation variability. Due to the dominant role of synoptic-scale circulations in regional precipitation over the UIB, we assume that despite the differences in magnitudes, distinct linear relationships of temporal precipitation variability between the low and HA

should exist, at least on subregional scales. Such intra-regional signals, if properly identified and captured, can significantly improve the understanding of precipitation variability over the relatively uncertain HA. The availability of the recent HA observations can help to validate this assumption. Especially, this study aims to:

i) Evaluate the effectiveness of low altitude stations in representing HA precipitation dynamics across the UIB without using actual precipitation measurements
ii) Identify precipitation governing circulations within a robust statistical downscaling framework to explain observed spatiotemporal precipitation patterns
iii) Analyze the physical consistency of final statistical models through composites of governing circulations.

Moreover, extending the analysis to the LI further helps to understand the water demand perspective, which is necessary for effective water resources planning at the basin scale.

In Section 2, we provide a brief description of the study area. Data and details of the adapted downscaling framework and the approach for seasonal composites are described in Section 3. This is followed by the description of results and discussion in Section 4 and the details of composite analysis and sources of uncertainty in Section 5. Finally, the conclusions are drawn in Section 6.

## 2 Study Area

The Indus River originates from the southwestern Tibetan Plateau and ultimately descends into the Arabian Sea after traversing through the entirety of Pakistan. The River basin area stretches across four geopolitically complex South Asian countries (i.e., China, India, Afghanistan, and Pakistan) and is ranked 12th in the world in terms of its size (**Figure 1a**). Annual precipitation substantially varies across the basin with a magnitude as low as 150 mm in the south to more than 2000 mm in the northern highlands and follows a nonlinear variation along the altitudes (Archer and Fowler, 2004; Dahri et al., 2016). It should be noted that this study only focuses on the basin area controlled by Pakistan (the largest basin area among all four countries and contains the highest altitudes) due to severe constraints on the availability of data over the rest of the region (**Figure 1b**). Within this study, the UIB outlines the drainage area above the Mangla dam over River Jehlum in Pakistan, as shown in blue color in **Figure 1a**.

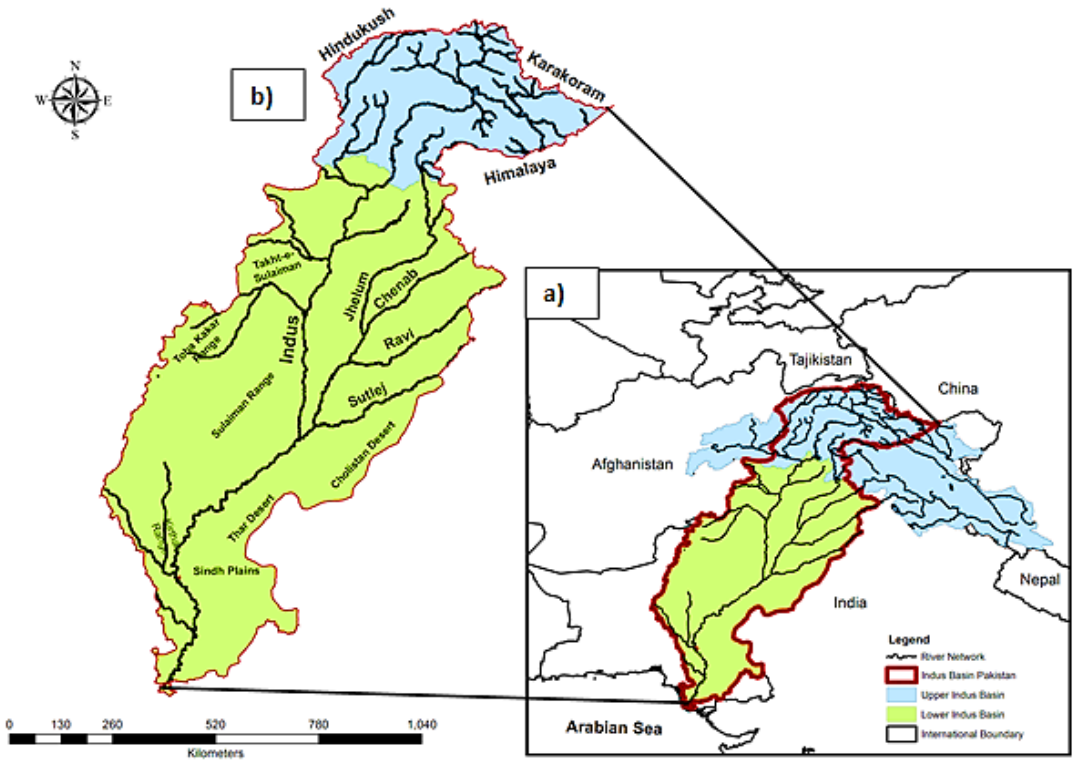


**Figure 1.** **a)** The transboundary Indus River basin, shown as colored regions, along with the major tributary river network. The color scheme differentiates between the upper and lower Indus basin. **b)** The study area (Indus basin of Pakistan) with the same color scheme represents the upper Indus basin (UIB) and lower Indus (LI) basin of Pakistan. The Mountains of the HKH region are also shown around the UIB.

# 3 Data and Methodology

## 3.1 Precipitation: Sources, Homogeneity, and Distributional Considerations

The Pakistan Meteorological Department (PMD) operates the largest monitoring network across Pakistan that also includes the Indus River basin. However, these observatories mostly represent low-altitude regimes (only two stations are located above 2000 m altitude with a maximum of 2394 m). Since the mid1990s, the Water and Power Development Authority (WAPDA) of Pakistan has initiated a systematic monitoring program to represent major sub-catchments within the UIB, and that has significantly improved the spatial and altitudinal coverage. Additionally, the University of Bonn under Cultural Areas Karakoram (CAK) Program has some operational observatories in the HA of Hunza and Gilgit sub-catchments of the UIB.

We obtain precipitation time series of 58 stations (shown in **Figure 2**) from these three sources for further investigations. Out of these 58 stations, 42 stations are located within the UIB to account for its

topographic complexity and significance for the Indus waters. The mean data length of the 35 historical and the 23 recent HA stations is 37 (1979–2015) and 17 (1994–2015) years, respectively. The inclusion of the HA stations has extended the observational coverage of the UIB up to 4730 m (20, 11, and 8 stations are located above 2000, 3000, and 3500 meters, respectively) to understand orographic dynamics, which otherwise is least understood, and govern the basin hydrology. Information about the selected stations is given in **Table 1.**

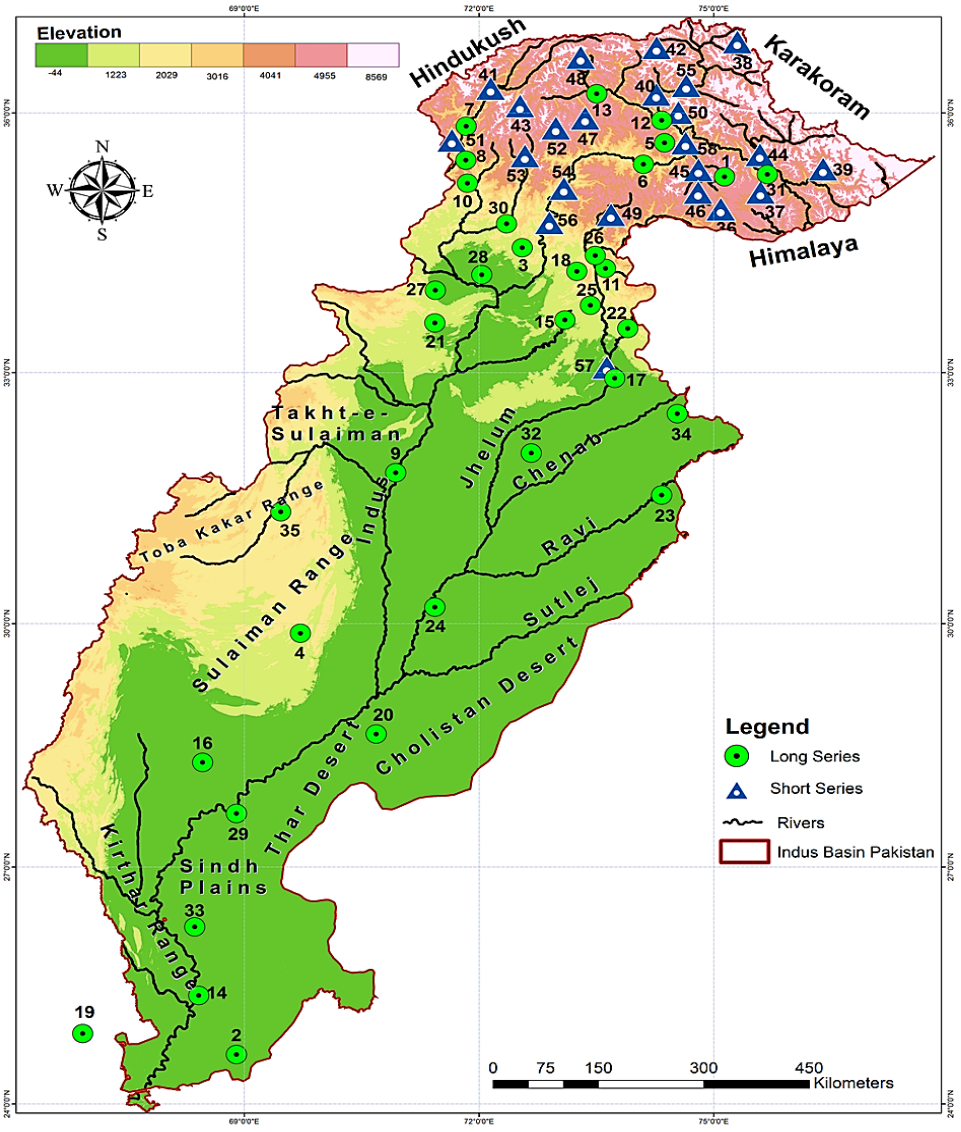


**Figure 2.** Location of the (numbered) study stations over the Indus basin of Pakistan. The green circles represent the locations of historic stations (1979–2015), while triangles show the recent HA installations (1994– 2015) within the UIB. The color scheme here represents the altitudinal perspective across the River basin. The major river network is also shown and named. For information about the numbers, please see **Table 1**.

Based upon station precipitation analysis, we identify three major seasons that cover the winter period spanning from December through March (WS, DJFM), the pre-monsoon spanning from April to June

(PMS, AMJ), and the summer monsoon season that spans from July to September (MS, JAS). These seasons contribute about 34%, 22%, and 36%, respectively, of the annual total of the basin precipitation and provide the basis for further analysis in our study. We group monthly time series in each of the three seasons and check the data for its completeness (Moberg et al., 2006), homogeneity (Wijngaard et al., 2003; Alexandersson, 1986), and underlying data structure. We make use of four different statistical procedures for homogeneity testing to group the stations as "useful" (where at least three tests indicate homogeneity), "doubtful" (where at least two tests indicate inhomogeneity), and "suspect" (where none or only one test indicates homogeneity) after Wijngaard et al. (2003). Although most of the stations appeared as "useful," some seasonal inhomogeneity has also been identified. For example, we find seven stations as "suspect" and seven stations as "doubtful" in the WS, four stations as "suspect" and eight stations as "doubtful" in the PMS, and four stations as "suspect" and nine stations as "doubtful" in the MS. Most of the stations with homogeneity issues are located within the UIB. Therefore, the use of these stations without homogeneity considerations, as has been done in previous studies, can potentially lead to errors in the seasonal precipitation estimates.

We further use several goodness-of-fit measures like the K-S test (Smirnov, 1939), Anderson-Darling Statistics (Anderson and Darling, 1952), and Akaike and Bayesian Information Criterions (Akaike, 1973; Stone, 1979) to identify the underlying distribution for the observed precipitation. Our analysis suggests that gamma distribution is the best statistical representative for nearly all of the study stations. This identification helps to facilitate the choice of an appropriate statistical model, which is described in detail in Section 3.5.

## 3.2 Precipitation Regionalization and Selection of Representative Stations

We assume that large-scale atmospheric circulations drive precipitation variability within the UIB. Therefore, it is expected that despite differences in the magnitudes, commonalities in temporal precipitation variability should exist among the low and HA across the UIB. To test this assumption, we employ a K-means cluster analysis on all 58 stations to identify the precipitation regions with similar covariance, using Spearman correlation as a distance measure (Wilks, 2006). Such a precipitation analysis, which avoids actual precipitation amounts, is advantageous as it can potentially account for the erroneous HA precipitation measurements (e.g., Curio and Scherer, 2016; Tahir et al., 2011). During clustering, the objective function is set to maximize (minimize) correlation within (across) the regions to define sharp regional boundaries. Due to greater uncertainty in precipitation observations within the HA of the UIB, we also performed another regionalization experiment that only covers the HA part of the basin. Subsequently, the cluster centroids are computed and correlated with each of the respective regional members. The regional representative (RR) stations for each region are selected by using multiple considerations, which include a correlation between centroid and station, number of missing values, the level of homogeneity, and the length of the observational record. The time series of these RR

stations serve as predictands during the subsequent modeling process to draw sub-regional precipitation inferences.

**Table 1.** Overview of the meteorological stations used in this study. The Long (Lat) are longitude and latitude measurements, expressed in decimal degrees (dd), and Altitudes represent average station elevation above mean sea level in meters. In the source column, the PMD= Pakistan Meteorological Department, WAPDA= Water and Power Development Authority of Pakistan, CAK= University of Bonn under Cultural Areas Karakoram Program (synthesized from Winiger et al., 2005), respectively.

| Sr. No | Station Name | Long | Lat | Altitude | Time Series | Source | Sr. No | Station Name | Long | Lat | Altitude | Time Series | Source |
|---|---|---|---|---|---|---|---|---|---|---|---|---|---|
| | | (dd) | (dd) | (m) | (length) | | | | (dd) | (dd) | (m) | (length) | |
| 1 | Astore | 74.90 | 35.33 | 2394.00 | 1979-2015 | PMD | 41 | Zaini | 72.15 | 36.28 | 3000.00 | 1994-2015 | WAPDA |
| 2 | Badin | 68.90 | 24.63 | 9.00 | 1979-2015 | PMD | 42 | Ziarat | 74.28 | 36.83 | 3669.00 | 1994-2015 | WAPDA |
| 3 | Balakot | 72.55 | 34.55 | 995.00 | 1979-2015 | PMD | 43 | Schndor | 72.53 | 36.09 | 3719.00 | 1994-2015 | WAPDA |
| 4 | Barkhan | 69.72 | 29.88 | 1097.00 | 1979-2015 | PMD | 44 | Shigar | 75.59 | 35.53 | 2470.00 | 1996-2015 | WAPDA |
| 5 | Bunji | 74.63 | 35.67 | 1372.00 | 1979-2015 | PMD | 45 | Rama | 74.81 | 35.36 | 3140.00 | 1999-2015 | WAPDA |
| 6 | Chilas | 74.10 | 35.42 | 1251.00 | 1979-2015 | PMD | 46 | Rattu | 74.81 | 35.15 | 2920.00 | 1999-2015 | WAPDA |
| 7 | Chitral | 71.83 | 35.85 | 1498.00 | 1979-2015 | PMD | 47 | Ushkore | 73.36 | 36.02 | 3353.00 | 1999-2015 | WAPDA |
| 8 | Darosh | 71.78 | 35.57 | 1464.00 | 1979-2015 | PMD | 48 | Yasin | 73.30 | 36.63 | 3353.00 | 1999-2015 | WAPDA |
| 9 | DI Khan | 70.93 | 31.82 | 172.00 | 1979-2015 | PMD | 49 | SaifulMaluk | 73.69 | 34.84 | 3200.00 | 2000-2015 | PMD |
| 10 | Dir | 71.85 | 35.20 | 1425.00 | 1979-2015 | PMD | 50 | Bagrot | 74.55 | 36.01 | 2310.00 | 1994-2010 | CAK |
| 11 | Ghari Duptta | 73.62 | 34.22 | 814.00 | 1979-2015 | PMD | 51 | Kelash | 71.65 | 35.70 | 2810.00 | 2003-2015 | PMD |
| 12 | Gilgit | 74.33 | 35.92 | 1460.00 | 1979-2015 | PMD | 52 | Kalam | 72.98 | 35.83 | 2744.00 | 1995-2015 | PMD |
| 13 | Gupis | 73.40 | 36.17 | 2156.00 | 1979-2015 | PMD | 53 | Khot | 72.59 | 36.52 | 3505.00 | 1994-2015 | WAPDA |
| 14 | Hyderabad | 68.42 | 25.38 | 28.00 | 1979-2015 | PMD | 54 | Pattan | 73.00 | 35.06 | 752.00 | 2004-2015 | PMD |
| 15 | Islamabad | 73.10 | 33.62 | 508.00 | 1979-2015 | PMD | 55 | Hunza-PMD | 74.65 | 36.32 | 2374.00 | 2007-2015 | PMD |
| 16 | Jacobabad | 68.47 | 28.30 | 35.00 | 1979-2015 | PMD | 56 | Malam Jaba | 72.90 | 34.75 | 2591.00 | 2003-2015 | PMD |
| 17 | Jehlum | 73.73 | 32.93 | 287.00 | 1979-2015 | PMD | 57 | Mangla | 73.60 | 33.10 | 283.00 | 1995-2015 | PMD |
| 18 | Kakul | 73.25 | 34.18 | 1308.00 | 1979-2015 | PMD | 58 | MirKhani | 74.70 | 35.50 | 1250.00 | 2008-2015 | PMD |
| 19 | Karachi-AP | 66.93 | 24.90 | 22.00 | 1979-2015 | PMD | | | | | | | |
| 20 | Khanpur-PBO | 70.68 | 28.65 | 93.00 | 1979-2015 | PMD | | | | | | | |
| 21 | Kohat | 71.43 | 33.58 | 327.00 | 1979-2015 | PMD | | | | | | | |
| 22 | Kotli | 73.90 | 33.52 | 610.00 | 1979-2015 | PMD | | | | | | | |
| 23 | Lahore-PBO | 74.33 | 31.55 | 214.00 | 1979-2015 | PMD | | | | | | | |
| 24 | Multan-PBO | 71.43 | 30.20 | 122.00 | 1979-2015 | PMD | | | | | | | |
| 25 | Muree | 73.40 | 33.90 | 2168.00 | 1979-2015 | PMD | | | | | | | |
| 26 | Muzafarabad | 73.48 | 34.37 | 702.00 | 1979-2015 | PMD | | | | | | | |
| 27 | Peshawer AP | 71.51 | 33.99 | 353.00 | 1979-2015 | PMD | | | | | | | |
| 28 | Risalpur | 71.98 | 34.08 | 308.00 | 1979-2015 | PMD | | | | | | | |
| 29 | Rohri | 68.90 | 27.67 | 66.00 | 1979-2015 | PMD | | | | | | | |
| 30 | Saidu Sharif | 72.35 | 34.73 | 961.00 | 1979-2015 | PMD | | | | | | | |
| 31 | Sakardu-PBO | 75.68 | 35.30 | 2210.00 | 1979-2015 | PMD | | | | | | | |
| 32 | Sargodha | 72.67 | 32.05 | 187.00 | 1979-2015 | PMD | | | | | | | |
| 33 | Shaheed Banazirabad | 68.37 | 26.25 | 37.00 | 1979-2015 | PMD | | | | | | | |
| 34 | Sialkot Cant | 74.53 | 32.52 | 255.00 | 1979-2015 | PMD | | | | | | | |
| 35 | Zhob-PBO | 69.47 | 31.35 | 1405.00 | 1979-2015 | PMD | | | | | | | |
| 36 | Burzil | 75.09 | 34.91 | 4030.00 | 1999-2015 | WAPDA | | | | | | | |
| 37 | Deosai | 75.60 | 35.10 | 3910.00 | 1995-2015 | WAPDA | | | | | | | |
| 38 | Kunjrab | 75.40 | 36.85 | 4730.00 | 1994-2015 | WAPDA | | | | | | | |
| 39 | Hushey | 76.40 | 35.37 | 3010.00 | 1994-2015 | WAPDA | | | | | | | |
| 40 | Naltar | 74.27 | 36.22 | 2810.00 | 1995-2015 | WAPDA | | | | | | | |

## 3.3 Predictor Data

We use variables of ERA-Interim reanalysis (Dee et al., 2011) at a 2º × 2º grid resolution as predictors. Using the understanding established in earlier studies (e.g., Ahmad et al., 2015; Kazmi et al., 2016;

Mahmood and Babel, 2012; Syed et al., 2010), a number of dynamic and thermodynamic variables at different vertical levels have been selected. These include geopotential heights (zg) at three atmospheric levels (200, 500, 700 hPa), meridional and zonal winds (ua and va) at four atmospheric levels (200, 500, 700, 850 hPa), and mean sea level pressure (psl) as dynamic variables, and relative and specific humidity (hur and hus) at two atmospheric levels (1000 and 700 hPa) as thermodynamic predictors. A larger domain was considered for the dynamic variables (10° E to 100° E, 10° N to 60° N) compared with the domain used for thermodynamic variables (64° E to 80° E, 22° N to 40° N) to account for both, the large-scale dynamical and more regional-scale thermodynamic influences.

## 3.4 Principle Component Analysis

We perform s-mode Varimax-rotated PCA separately for each predictor to identify important centers of variation and to reduce the dimensionality of the predictors (see Preisendorfer, 1988). The number of PCs is extracted using a modified dominance criterion (Philipp 2003) with some additional constraints that each retained PC should dominate all other PCs by more than one standard deviation over at least seven grid boxes and explains at least 3 % of the total variance. The PC scores serve as the predictor time series, and the PC loadings define the location of centers of variation.

## 3.5 Generalized Linear Models

We adapt GLM framework (McCullagh and Nelder, 1989) to model the relationships between the atmospheric variables (PC scores) and observed precipitation of the RR stations. We selected the GLM framework due to gamma-distributed monthly precipitation. Within a GLM framework, the maximum likelihood estimation is used to estimate the model parameters for the expected value E of a random variable ($Y_t$) at any given time t:

$$E(Y_t) = \mu_t = g^{-1}(\eta_t) = g^{-1} \sum_1^n X_{tj}\beta_j \qquad (1)$$

Where $\mu_t$ is the mean for the probability density function (PDF) at time t, $\eta_t$ is a combination of linear predictors, g is the canonical link function, $X_{tj}$ is the value of the jth covariate for observation t, n is the total number of covariates, and $\beta_j$ are parameters whose values have to be estimated from the data.

We use the log-canonical link function in this study. For those cases having exact zeros in observed time series of the RR, we use Tweedie exponential dispersion models within a GLM framework due to their ability for simultaneous modeling of discrete and continuous precipitation features (e.g., Dunn, 2004; Hertig and Jacobite, 2015; Hertig et al., 2017). The Tweedie family of distributions has three parameters (i.e., $\mu$, mean, dispersion parameter $\phi > 0$, and the Tweedie index parameter p). The index p defines the particular distribution, and a typical case ($1 < p < 2$) represents Poisson-gamma models, which are suitable for modeling positive continuous data with exact zeros (Hasan and Dunn, 2011). The variance of the distribution is var [Y] = $\phi\mu^p$. The estimation of the index parameter requires sophisticated

numerical computations that have been resolved using the profile maximum likelihood estimate provided in the Tweedie R package (Dunn, 2010). In summary, we use Tweedie models only when exact zeros appear in the predictand time series and otherwise gamma models for regression analysis.

### 3.5.1 Measures of model performance

Mean squared error skill score (MSESS) is a commonly employed metric to judge the accuracy of continuous nonprobabilistic forecasts like precipitation over the long-term climatology (Wilks, 2006). MSESS is defined as:

$$MSESS = 1 - \frac{\text{MSE}_{\text{modeled}}}{MSE_{reference}} \quad X\ 100 \tag{2}$$

Where,

$$MSE\ modeled = \frac{1}{n}\sum_{n=1}^{n}(\text{y}^{*} - \text{y})^2 \tag{3}$$

$$MSE\ reference = \frac{1}{n}\sum_{n=1}^{n}(\bar{\text{y}} - \text{y})^2 \tag{4}$$

and,

MSE = mean squared errors

y* = model prediction

y = observation

$\bar{\text{y}}$ = mean over the observations

n = number of observations

MSESS ranges from 0% (no skill improvement over the reference model, in this case, a long-term climatology) to 100 % (perfect model).

## 3.6 Downscaling Framework: Model Development and Selection

We develop GLM-based regression models to identify the atmospheric variables that exert the strongest influence on precipitation. We use a cross-validation framework by randomly selecting calibration (two-thirds of available time series) and validation periods (remaining one-third) and adapt the following stepwise reduction process, which is randomly repeated 1000 times to identify effective and robust statistical models:

(I) The PC time series of each predictor is individually regressed against each of the RR stations. Initially, the regression models are developed using all PCs of an individual predictor as input. Subsequently, the revised models are developed based on an adjusted PC input (i.e., dropping PCs, one by one), and the corresponding MSE is calculated. We use MSE to rank the significance of the PCs and to identify the most influential PCs of each predictor (i.e., PCs whose absence maximized the errors were considered the most

important). Next, the models containing only the two most influential PCs are developed, and the corresponding errors and MSESS are computed. These 2 PC models are further complemented one by one with the remaining ranked PCs to identify the best PC combination per predictor (i.e., which maximizes MSESS during the calibration and validation phases). We repeat this process for all 15 predictors, and the model that demonstrates maximum predictability over the calibration and validation periods (sum of the MSESS) is termed as the best signal predictor model (SPM).

(II) We further test different predictor combinations to evaluate any performance improvement over the best SPM from step I. For such combinations, the best SPM is complemented one by one with the remaining predictors. If two correlated PCs of different variables (absolute correlation threshold of 0.40) are found, only the more influential PC (showing greater error effect, when removed) was retained for further consideration. Moreover, an addition of a second predictor is only considered if it improves the prediction skills by at least 7% over the best SPM. This arbitrary number effectively demonstrates reasonable validation improvements without overfitting the models. The same procedure is repeated during the combinations of three or more predictor variables to identify better-performing combinations, wherever applicable.

## 3.6 Composite Analysis

Composites can help to identify atmospheric circulations that are associated with different precipitation regimes to evaluate the physical consistency (reliability) of the statistical models. We construct the sample composites where monthly scores of the dominating PC (as identified in the final regression models) exceed or fall below ± 1.5 PC scores to subsample the cases of higher positive and higher negative PC scores. These subsets are evaluated to identify wetter (dryer) precipitation regimes of the predictand and their associated summary statistics such as the number of events, mean precipitation rate per event, and the dominant month. The same thresholds are further used to subsample relevant large-scale seasonal circulations to define climatology over respective subsamples, and the standardized anomalies of these predictors are plotted to investigate precipitation supporting (suppressing) circulation patterns. Similarly, the difference between these contrasting regimes is also plotted to identify the circulation anomalies that support above-normal precipitation.

# 4 Results and Discussion

## 4.1 Precipitation Regionalization

In our analyses, the K-means clustering identifies six WS, seven PMS, and seven MS precipitation regions across the Indus basin to explain adequately the observed precipitation variability under the

basin-wide experiment. The regionalization scheme successfully clusters 57%, 78%, and 48% of the total recent HA stations (23) around the historical observatories within the identified WS (three), PMS (four), and MS (five) precipitation regions in the UIB. The second regionalization experiment identifies four subregions during each of these seasons and further improves the spatial coverage within the UIB by clustering 70%, 83 %, and 83% of the HA stations around different historic stations. **Table 2** presents the statistical performance during both of these regionalization experiments. Both experiments show a good inter-and intra-regional performance in terms of selected statistical attributes with the exception of the MS in the second experiment. Thus, both regionalization experiments validate our assumption of similarities in the precipitation variability between the recent HA and historic stations. Therefore, the historic stations can advantageously be used to infer orographic precipitation over more uncertain HA through these regionalization schemes.

**Figures 3, 4, 5, and 6** describe the outcome of the precipitation regionalization process and identify the RR and those HA stations that could not be clustered around any of the surrounding historic stations during both regionalization experiments. Averagely, four different regions have been identified through both of these experiments to represent the precipitation dynamics of the UIB. These regions represent precipitation variability of the southern Himalayans, northern Himalayans, and the northwestern parts of the UIB and provide an opportunity for a fine-scale analysis. The identification of such distinct precipitation regions further justifies the need for a sub-regional approach, as such heterogeneity may not be properly reflected by considering UIB as a single unit. Similarly, some of the important LI features (e.g., spate irrigation, irrigated plains, and the coastal belt) are also identified during the basin-wide regionalization experiment. These are important reflectors of the water demand and should simultaneously be considered to demonstrate integrated water resources planning at the basin scale.

Overall, the regionalization schemes successfully capture the orographic heterogeneity within the UIB, show a good regional coherence, and significantly cover the altitudinal perspective within the observational profile during all three seasons. Moreover, our regionalization provides a more realistic basis for understanding subregional precipitation characteristics when compared with the previously used hydrological units (Dahri et al., 2016) or the administrative units (Iqbal and Athar, 2018).

## 4.2 Seasonal Precipitation Models

Using the outlined downscaling procedure (Section 3.6), we successfully model observed seasonal precipitation patterns over 29 sub-regions of the study basin under both regionalization experiments. However, we were unable to determine valid models for three smaller regions representing the coastal belt within the basin-wide experiment (R2 in PMS and R2 in WS) and one UIB region (R3 in MS) during the revised regionalization experiment. This issue partly stems from the relatively large number of dry months (84, 80, and 21, respectively) in the observed time series of RR stations for these regions.

**Table 2.** Summary of precipitation regionalization experiments on seasonal scales. Column 1 represents the precipitation seasons, and column 2 defines the number of precipitation regions. Columns 3 and 4 show the sum of squared errors (SSE) within (WI) and between (BW) regions. The total explained variance is shown in column 5. Columns 6 and 7 define the correlation within (WI) and between (BW) the regions, respectively.

| **Basin-wide Regionalization** | | | | | | |
|---|---|---|---|---|---|---|
| **Season (1)** | **Final Regions (2)** | **SSE (WI) (3)** | **SSE (BW) (4)** | **EVar (%) (5)** | **Corr (WI) (6)** | **Corr (BW) (7)** |
| WS ( Dec-Mar) | 6 | 23.44 | 130.11 | 85 | 0.78 | 0.46 |
| PMS ( Apr-Jun) | 7 | 48.2 | 346.54 | 88 | 0.82 | 0.18 |
| MS ( Jul-Sep) | 7 | 38.05 | 139.19 | 78.6 | 0.77 | 0.28 |
| **HA-UIB Regionalization** | | | | | | |
| WS (Dec-Mar) | 4 | 12.84 | 55.86 | 81 | 0.84 | 0.48 |
| PMS (Apr-Jun) | 4 | 22.25 | 121.97 | 84 | 0.82 | 0.36 |
| MS (Jul-Sep) | 4 | 26.93 | 54.17 | 70 | 0.76 | 0.27 |

### 4.2.1 Predictor significance

The final composition of valid seasonal precipitation models **(Table 3)** indicates a dominant influence of wind predictors in basin-scale precipitation distribution (nearly 80% in total). Particularly, the lower tropospheric winds most effectively resolve the basin-wide regional models (50.9%). The influence of upper tropospheric winds is also significant at the basin scale (25.5 %). Among these wind predictors, the meridional wind velocities in the lower (40%) and upper troposphere (25%) are more prominent in these sub-regional models. However, their effectiveness has a stronger seasonality, where a maximum contribution is realized during the MS (va850= 52.5%,va200 = 32.5%). After the wind components, the contribution of thermodynamic predictors is at its maximum at the basin scale (about 15%), which also exhibits strong seasonality with the maximum during the PMS (nearly 26%) and WS (about 15 %) and a minimum during the MS(5%). Among thermodynamic predictors, relative humidity (especially at 1000 hPa level) is the most effective predictor during all precipitation seasons. The lower level dynamic

variables (psl, zg700) form the third important predictor set among regional models (7.6%) and mainly dominate during the WS.

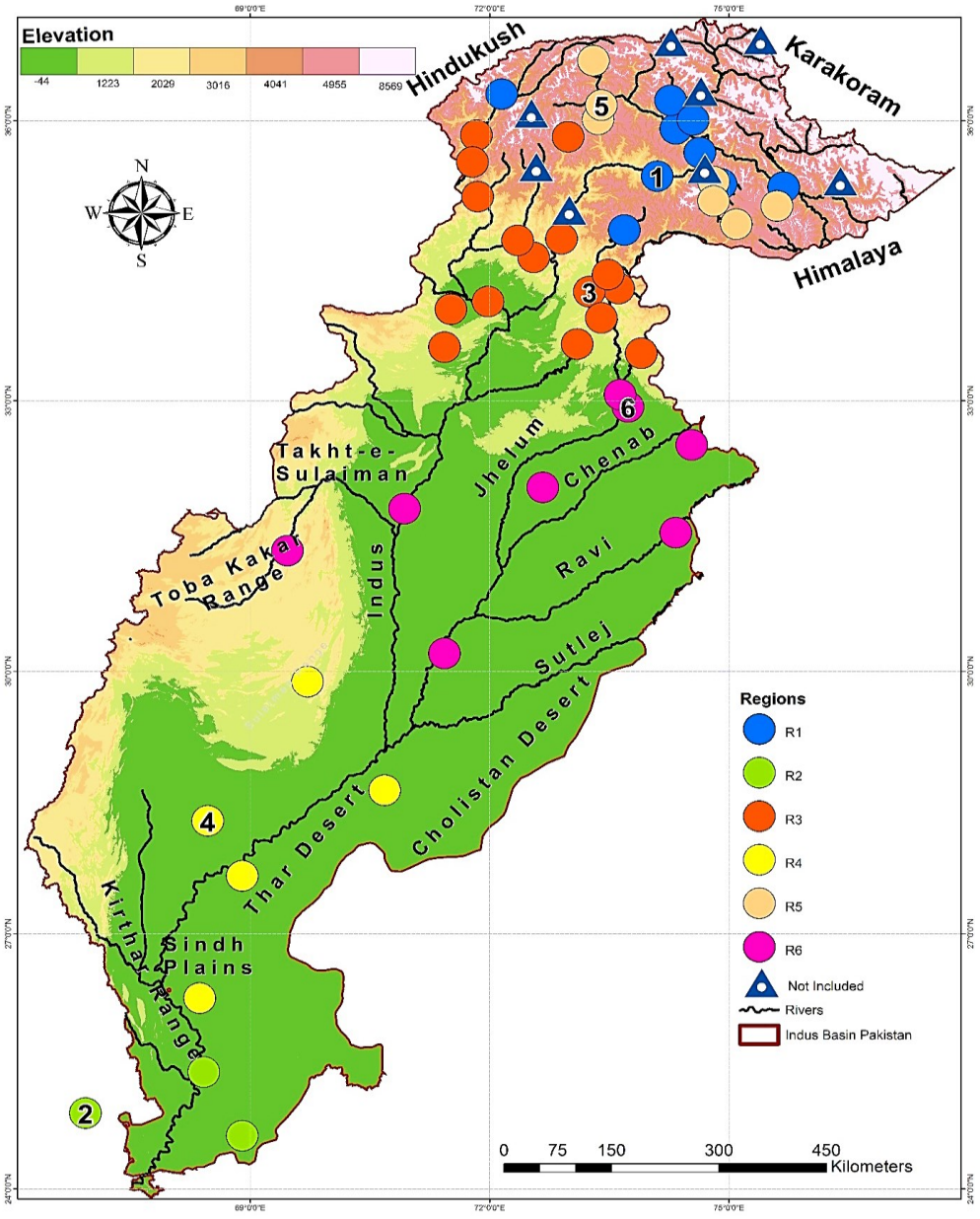


**Figure 3.** The WS (i.e., DJFM) precipitation regionalization under the basin-wide experiment. The colored circles show different precipitation regions with similar co-variability. The numbered circles are the locations of the RR stations in respective precipitation regions. The triangles define those HA stations that could not be grouped with any of the available historic stations within the UIB.

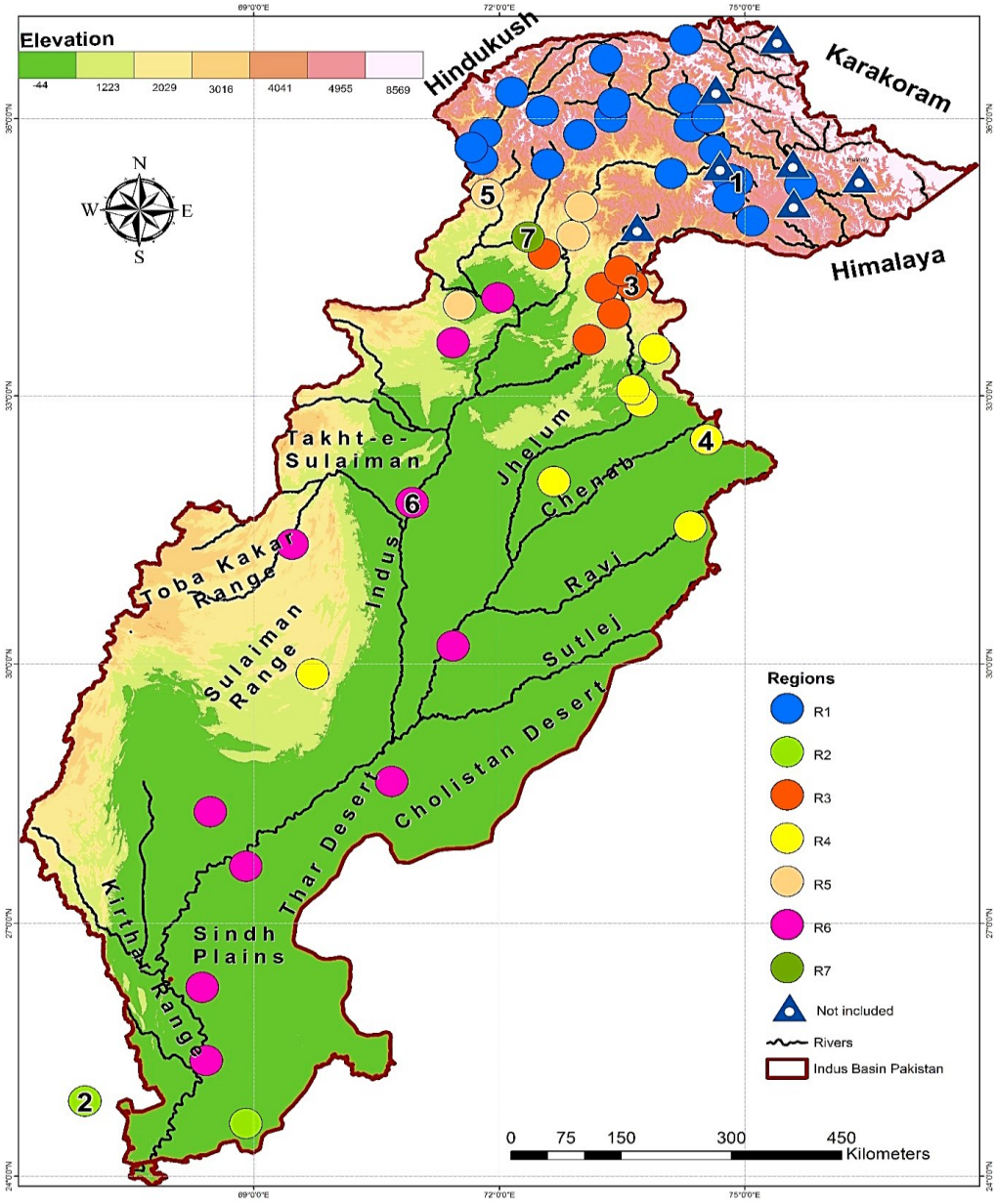


**Figure 4.** Same as **Figure 3** but for the PMS precipitation season (i.e., AMJ)

These final predictors capture the seasonally varying regional climatology to explain observed precipitation patterns. For instance, the thermally induced local Hadley circulations during the MS are adequately represented by the meridional component of tropospheric winds. Similarly, the atmospheric moisture sources from local evapotranspiration within the basin and advection from different remote oceanic and terrestrial sources (e.g., the Arabian, Caspian, and Mediterranean Seas) during the PMS and WS play a crucial role in regional precipitation (e.g., Cannon et al., 2015; Curio and Scherer, 2016; Mei et al., 2015; Syed et al., 2010). Our statistical models represent such moisture influences through the humidity-related predictors, particularly during the PMS, when the strength of dynamic forcing reduces over this region. Thus, the identified predictors are representative of the major physical processes that govern the regional precipitation and therefore enhance the confidence in statistical simulations.

Similarly, explanations are also valid for the predictors of the HA-UIB regionalization experiment due to their close similarity with the basin-wide experiment. More details about the physical explanations of the statistical models will follow in Section 5.

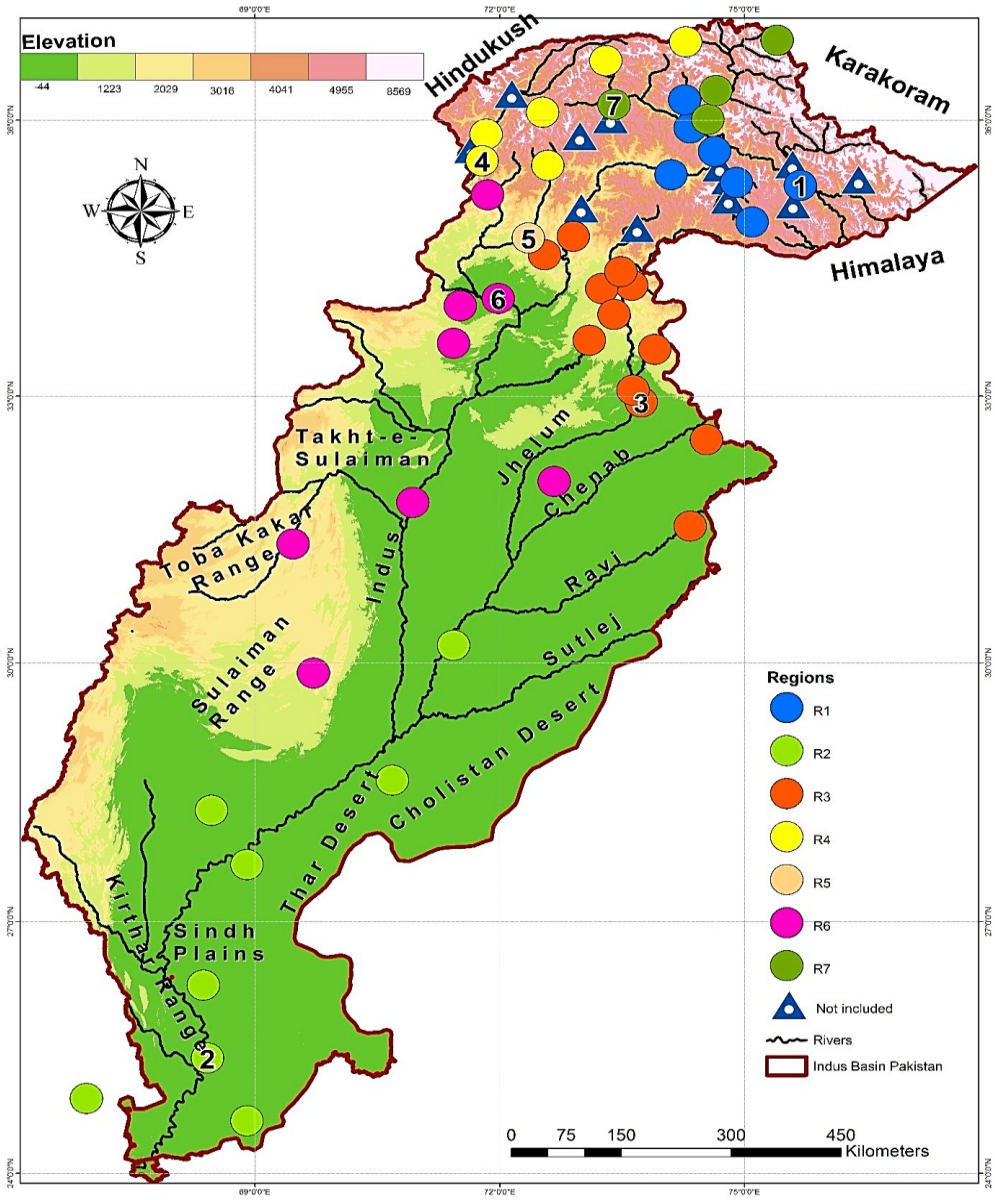


**Figure 5.** Same as **Figure 3** but for the MS precipitation season (i.e., JAS)

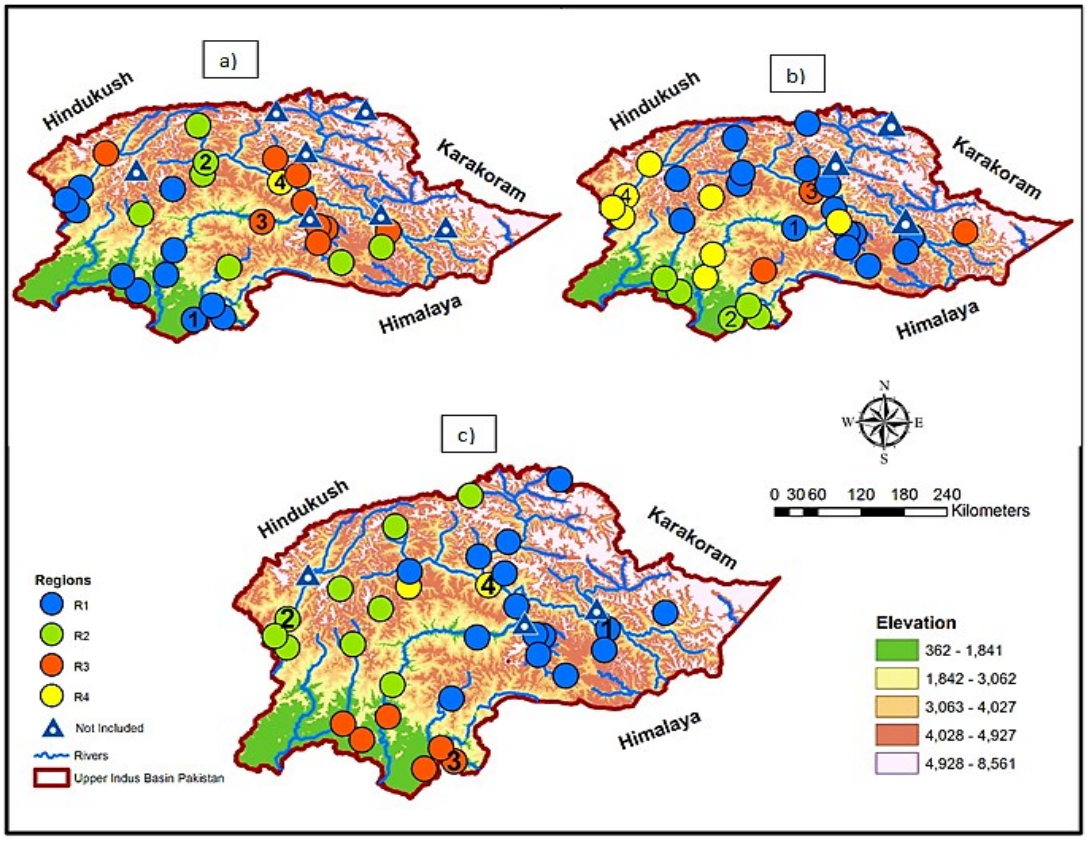


**Figure 6.** Same as **Figure 3** but for the HA-UIB precipitation regionalization. **a)** WS, **b)** PMS, and **c)** MS precipitation regions, respectively.

### 4.2.2 Winter season models

The summary of the seasonal modeling process (**Table 4**) shows that GLM-Tweedie models adequately represent the WS precipitation dynamics across all five precipitation regions of the Indus basin. For information about these regions and the RR stations, please see **Figure 3.** Within its three UIB regions (R1, R2, and R5), the mean calibration (validation) root mean squared error (RMSE) amount to 27.14 mm (27.93 mm) with a corresponding MSESS of 41.60% (34.69%). The R3 region (stretching along the foothills of the southern Himalayans and covering the lower Hindukush areas further northwest) contains 16 study stations, including some of the HA, and receives the highest precipitation amounts (93 mm per month) among all other UIB regions during the WS. Therefore, precipitation (snow and liquid) within this larger region dominates the river flows during the winter and early spring seasons, and its accurate modeling is highly desirable.

**Table 3.** Frequency of the predictors (in percentage) in final seasonal precipitation models for different sub-regions of the Indus basin of Pakistan. Column 1 shows the large-scale predictors used in this study. The number after each predictor reflects the atmospheric level (pressure level in hPa). Columns 2–4 represent the predictor frequencies in the different seasons. The last column shows the average of the seasonal predictor frequencies.

| Predictors (1) | WS (%) (2) | PMS (%) (3) | MS (%) (4) | Basin-Wide (%) (5) |
|---|---|---|---|---|
| va200 | 20 | 19.4 | 32.5 | 24 |
| ua200 | 0 | 0 | 2.5 | 0.8 |
| zg200 | 0 | 0 | 0 | 0 |
| zg500 | 0 | 0 | 0 | 0 |
| zg700 | 20 | 0 | 0 | 6.7 |
| hus700 | 0 | 0 | 2.5 | 0.8 |
| hur 700 | 0 | 9.7 | 0 | 3.2 |
| hur1000 | 8.6 | 16.1 | 2.5 | 9.1 |
| hus1000 | 5.7 | 0 | 0 | 1.9 |
| va500 | 0 | 0 | 2.5 | 0.8 |
| ua500 | 0 | 0.0 | 2.5 | 0.8 |
| ua700 | 14.3 | 0 | 0 | 4.8 |
| va700 | 0 | 22.6 | 0 | 7.5 |
| va850 | 31.4 | 12.9 | 52.5 | 32.3 |
| ua850 | 0 | 19.4 | 0 | 6.5 |
| psl | 0 | 0 | 2.5 | 0.8 |
| *Total* | ***100*** | ***100*** | ***100*** | ***100*** |

The RR station strongly represents precipitation characteristics of this region (correlation = 0.93 with regional centroid) and therefore allows to make reliable inferences over a broad altitudinal range (308 to 2744 m) in this region. A single predictor (va850) effectively models the observed precipitation of this RR with a high validation skill (49.57%). Another large UIB region (R1), which mainly covers the Karakorum and trans-Himalayan valleys of the Hindukush, also exhibits an acceptable validation skill (26.1%) despite a large number of dry months. This is mainly a cryosphere-dominated region, which is also strongly represented by its RR station (correlation = 0.83 with regional centroid) and provides inference over the relatively higher altitudes (1251–3200 m) of more uncertain trans-Himalayas. Zonal winds at 700 hPa level (ua700) and specific humidity at 1000 hPa level (hus1000) effectively model the observed precipitation patterns in this region.

Similarly, another northern Himalayan region (R5) shows a higher predictability skill (28.39%) despite having the largest number of dry months and provides important information for the highest altitudinal bands (2156–4030 m) in our analysis. This region has the largest cryosphere extent, receives mainly

solid precipitation, and, together with R1, helps to regulate the hydrology of the Indus River. Such a skillful statistical representation of the observed WS precipitation that covers the larger spatial-altitudinal scales within theUIB can greatly help in reducing the uncertainty in future projections.

Two LI regions (R4 and R6) also exhibit significant validation skills (25.39 % and 32.89%) for making reliable inferences over diverse conditions of the northeastern rain-fed areas, irrigated plains, and southwestern spate regions. However, precipitation in these regions requires both dynamic and thermodynamic predictors for effective modeling, as shown by the final models (**Table 4**). The relatively higher error rates in some of the WS cases are discussed in Section 5.3.

### 4.2.3 Pre-monsoon season models

During the PMS, the GLM-gamma models provide the best modeling performance with an overall skill score of approximately 50% during calibration and 42% in the validation (**Table 4**). Moreover, the average validation performance (43.90%) and the average ability of the RR stations in describing the spatial perspective (correlation coefficient of 0.92) over four different UIB regions (R1, R3, R5, and R7, see also **Figure 4**) are at its maximum, compared with other precipitation seasons. Within the UIB, the largest northern Himalayan region (R1) contains 21 study stations, including most of the HA observatories, and covers a larger altitudinal band (1251–4030 m). R1 exhibits a validation skill of nearly 50%. Similarly, two northwestern regions (R5 and R7) that exhibit higher monthly precipitation (106 mm and 82 mm) have also been skillfully modeled (50.42% and 46.97%) and allow reliable precipitation inference over an elevation band between 353 and 2591 m. The southern Himalayan UIB region (R3) that receives more than 100 mm of monthly precipitation and represents the lower northeastern elevations (508– 2168 m) also demonstrates a good validation performance (about 29%).

During the PMS simulations over the UIB, relative humidity is an important predictor (see Section 4.2.1) along with lower tropospheric winds to explain the observed spatial variability. Overall, a highly skillful UIB modeling during this transitional season is important for the assessment of seasonal water availability in the future period. Additionally, the PMS modeling performance over the two LI regions (R4 and R6) exhibits higher validation skills (40.11% and 37.64%, respectively) to infer precipitation dynamics over the irrigated plains and lower southwestern spate regions. These conditions are simulated by a set of dynamic and thermodynamic predictors.

### 4.2.4 Monsoon season

Precipitation dynamics are spatially more complex over the UIB during the MS, as it requires five different precipitation regions (R1, R3, R4, R5, and R7, see also **Figure 5**). Moreover, both the GLM-gamma and Tweedie models are required for statistical simulations of observed precipitation variability over the UIB. Nonetheless, a reasonable average validation performance across all of these UIB regions (32.73%) contributes to confidence in resulting spatial inferences. Within the UIB, maximum validation

skill (52.41%) is demonstrated over the wettest southern Himalayan region, R3, which receives monthly precipitation sums of 181 mm over a larger vertical horizon (122 to 2591 m). The RR station for this region exhibits a correlation of 0.84 with the regional centroid. The R3 region mainly receives liquid precipitation, which helps to regulate the downstream reservoir operations (e.g., hydropower and irrigation). The modeling process of the two other UIB regions (R1 and R7) also exhibits reasonable validation skills (28.57% and 23.65%, respectively). These regions reflect the highest observed altitudinal range (1251 to 4030 m and 2156 to 4730 m) over the Karakoram and Hindukush areas. Similarly, two northwestern regions (R5 and R4) also demonstrate reasonable validation skills (20.71% and 39%) and represent an altitudinal range from 962 to 3719 m. A strong dynamic forcing during the MS helped to largely resolve the complex MS processes within the UIB, as shown by various predictors of the statistical models **(Table 4).**

In contrast, the homogenous topography and the strong MS influence across the LI help to relatively better model precipitation over spate and irrigated regions (R4 and R2), with validation skills of 32.06% and 42.32 %, respectively. Spate regions not only provide an abundance of flows during the MS to support diverse livelihood but also cause regular havoc through damage to downstream infrastructure and human lives during extreme events. Therefore, its consideration is important to minimize the socio-economic suffering as well as for enhancing national water availability through effective planning.

## 4.3 HA-UIB modeling

The HA-UIB modeling summary (**Table 5**) shows some performance compromises. For instance, the mean validation skills over four WS regions show a decrease of 3.5% compared with the corresponding skills in the basin-wide modeling (34.69%). However, this performance loss is primarily due to a poor simulation of a single-station region (R4), which exhibits a lower validation skill (18.42 %). The performance for this particular region suffers from a relatively lower precipitation rate (7 mm/month), a higher number of dry months (33), and the presence of some outliers. All other WS regions in the HA-UIB modeling exhibit comparable skills by mainly using different dynamical predictors. However, the trans-Himalayan regions (R2, R4) additionally require specific humidity as a predictor.

Four PMS regions show a very similar average skill (42.62%) compared with the basin-wide modeling (43.90%) despite the presence of some dry months in the time series of some RR stations (R3 and R4). Thermodynamic contributions still largely dominate the PMS precipitation simulations (Table 5), where the lower level relative humidity appears as the most influential predictor (i.e., best SPM) in three out of four sub-regional models. Similarly, the average modeling performance in the MS across its three different precipitation regions also exhibits nearly similar prediction skills (30.60%, ~ 2% less). Still, the dynamic predictors largely dominated these HA-MS simulations, as shown by the final statistical models (**Table 5**). However, the model for the northern Himalayan region (R1) also includes the contribution of specific humidity.

**Table 4.** Statistical performance of the seasonal downscaling models over the Indus Basin of Pakistan. Column 1 outlines the identified precipitation region, column 2 indicates the name of the regional representative (RR) station, and its correlation with the respective regional centroid is given in the parenthesis. Column 3 (Reg. Alt) indicates the mean regional altitude in meters (m) above mean sea level and, in parenthesis, the range of regional altitude. Columns 4, 5, 6, 7, and 8 show the adapted GLM, number of dry months in the time series of RR station, number of final predictors, predictor names, and number of PCs in final regression models, respectively. The mean monthly-observed (modeled) precipitation rates of RR station are shown in column 9 (10), respectively. The calibration (validation) root mean squared errors (RMSE) and mean squared error skill scores (MSESS) are reflected in columns 11 (12) and 13 (14), respectively. The blue (green) color indicates UIB (LI), and the red color shows the average outcome of seasonal models over the entire Indus basin.

| Region | RR (Corr) | Reg. Alt | GLM | Dry Mon | Predictor | | | PCs | Mean Preci (mm/mon) | | RMSE (mm) | | MSESS (%) | |
|---|---|---|---|---|---|---|---|---|---|---|---|---|---|---|
| | | (m) | | (Nos) | (Nos) | (Name) | | (Nos) | Obs | Mod | Cal | Val | Cal | Val |
| **WS Models** | | | | | | | | | | | | | | |
| R1 | Chilas (0.83) | 2223 (1251-3200) | Tweedie | 39 | 2 | va850+zg700 | | 8 | 18 | 17 | 17.60 | 18.10 | 33 | 26.1 |
| R3 | Kakul (0.93) | 1173.5 (308-2744) | Tweedie | 7 | 1 | va850 | | 7 | 93 | 93 | 49.88 | 50.54 | 51.92 | 49.57 |
| R5 | Gupis (0.70) | 3266 (2156-4030) | Tweedie | 56 | 2 | ua700+hus1000 | | 6 | 11 | 12 | 13.95 | 15.15 | 39.87 | 28.39 |
| R4 | Jacobabad (0.80) | 266 (35-1097) | Tweedie | 69 | 2 | va200+hus1000 | | 8 | 7 | 7 | 10.69 | 11.64 | 47.86 | 28.75 |
| R6 | Jehlum (0.89) | 365 (122-1405) | Tweedie | 19 | 2 | hur1000+zg700 | | 6 | 46 | 46 | 37.53 | 37.98 | 41.98 | 36.62 |
| Avg.Basin | | | | 38 | 1.8 | | | 7.0 | 35 | 35 | 25.93 | 26.68 | 42.93 | 33.89 |
| Avg.UIB | | | | 34 | 1.7 | | | 7.0 | 41 | 41 | 27.14 | 27.93 | 41.60 | 34.69 |
| Avg.LI | | | | 44 | 2.0 | | | 7.0 | 27 | 27 | 24.11 | 24.81 | 44.92 | 32.69 |
| **PMS Models** | | | | | | | | | | | | | | |
| R1 | Astore (0.86) | 2627 (1251-4030) | Gamma | 0 | 2 | hur700+va850 | | 7 | 57 | 57 | 32.6 | 34.02 | 55.44 | 49.37 |
| R3 | Ghari Duputta (0.91) | 1327 (508-2168) | Gamma | 0 | 2 | va700 + ua850 | | 8 | 101 | 101 | 44.74 | 48.29 | 41.14 | 28.83 |
| R5 | Dir (0.94) | 1281 (353-2591) | Gamma | 0 | 1 | hur1000 | | 2 | 106 | 104 | 45.62 | 47.63 | 56.68 | 50.42 |
| R7 | Saidu Shairf (1) | 961 (961) | Gamma | 0 | 2 | hur1000+ua850 | | 5 | 82 | 80 | 44.58 | 45.45 | 54.53 | 46.97 |
| R4 | Sialkot (0.84) | 419 (187-1097) | Gamma | 0 | 1 | va200 | | 6 | 43 | 42 | 30.92 | 31.71 | 45.98 | 40.11 |
| R6 | DI Khan (0.74) | 259 (28-1405) | Tweedie | 20 | 2 | hur1000+ua850 | | 3 | 21 | 20 | 17.71 | 18.23 | 44.65 | 37.64 |
| Avg.Basin | | | | 3 | 1.7 | | | 5.2 | 68 | 67 | 36.03 | 37.56 | 49.74 | 42.22 |
| Avg.UIB | | | | 0 | 1.8 | | | 5.5 | 87 | 86 | 41.89 | 43.85 | 51.95 | 43.90 |
| Avg.LI | | | | 10 | 1.5 | | | 4.5 | 32 | 31 | 24.32 | 24.97 | 45.32 | 38.88 |
| **MS Models** | | | | | | | | | | | | | | |
| R1 | Sakardu (0.74) | 2218 (1251-4030) | Tweedie | 16 | 2 | va850+hus700 | | 7 | 13 | 13 | 11.32 | 12.77 | 44.09 | 28.57 |
| R3 | Jehlum (0.84) | 746.25 (122-2591) | Gamma | 0 | 1 | va200 | | 7 | 181 | 180 | 76.73 | 78.63 | 56.92 | 52.41 |
| R4 | Darosh (0.76) | 2868 (1464-3719) | Tweedie | 11 | 1 | va200 | | 6 | 21 | 21 | 16.26 | 16.82 | 28.82 | 20.71 |
| R5 | Saidu.Sharif (1) | 961(961) | Gamma | 0 | 2 | va850+hur1000 | | 11 | 115 | 116 | 54.7 | 60.03 | 52.71 | 38.32 |
| R7 | Gupis (0.69) | 2892 (2156-4730) | Tweedie | 20 | 3 | va850+psl+ua200 | | 8 | 19 | 20 | 18.61 | 20.65 | 41.69 | 23.65 |
| R6 | Risalpur (0.75) | 659 (172-1425) | Gamma | 0 | 2 | va700+ua500 | | 7.0 | 114 | 115 | 74.26 | 76.89 | 41.13 | 32.06 |
| R2 | Hyderabad (0.88) | 52 (9-122) | Tweedie | 45 | 2 | ua700+va500 | | 4.0 | 40 | 40 | 45.16 | 46.58 | 46.58 | 40.32 |
| Avg.Basin | | | | 8 | 1.8 | | | 7.7 | 72 | 72 | 41.96 | 44.27 | 44.23 | 32.62 |
| Avg.UIB | | | | 9 | 1.8 | | | 7.8 | 70 | 70 | 35.52 | 37.78 | 44.85 | 32.73 |
| Avg.LI | | | | 23 | 2.0 | | | 5.5 | 77 | 78 | 59.7 | 61.74 | 43.86 | 36.19 |

Overall, the HA-UIB regionalization significantly improves the spatial-altitudinal representation over the UIB in all seasons without losing much of the predictability power. This increased spatial coverage helps to infer precipitation dynamics over the hydrologically important yet highly uncertain HA regions within the UIB. The resulting inferences can be significantly trusted for the wetter southern Himalayan regions during all seasons and the northwestern Hindukush and the Karakorum regions during the PMS and WS due to the stronger representations by the respective RR stations. However, caution is required during the MS, particularly over the northwestern Hindukush region (R2) and the Karakoram central region (R1), due to relatively poor representation by the respective RR stations. The weaker MS penetration into the northwestern and Karakoram region could be one of the reasons. Overall, thermodynamic contributions increase in the trans-Himalayan regions, which reflect the role of atmospheric moisture buildup around the UIB from different moisture sources, as demonstrated by various centers of variation for humidity-related predictors (not shown).

# 5 Physical Consistency of The Statistical Relationships: Composite Analysis

Composites can help to identify atmospheric conditions during different precipitation regimes to evaluate and explain the physical mechanisms of statistical models. The choice of model(s) to be presented in the following section is based on the relative importance for the season (i.e., the core precipitation seasons), the significance of the regional scale, prediction performance of the statistical models, and distinct domination of a single PC in the final regression models. Using these multiple considerations, we select one MS and one WS region to discuss the atmospheric characteristics underlying the statistical models.

## 5.1 MS Synoptic Analysis Using Composite

During the MS, a larger region (R3) that contains 12 stations and receives a higher amount of precipitation (181 mm/ month) is selected for the composite analysis. We use upper-level meridional winds (va200) to model the precipitation variations at its RR station, which exhibits a high statistical skill during validation (52.41%). We use PC1, which has a correlation (Spearman) of 0.62 with the observations of RR station to construct composites. The positive loading pattern of PC1 (**Figure 7**) stretches over a larger region (from the Bay of Bengal to the East African coast) with its center over the Arabian Sea. Positive PC scores indicate drier conditions and vice versa. We select a threshold of ± 1.5 PC scores, which helps to clearly define these contrasting patterns **(Table 6)** with ten positive cases (average 69 mm per month) and six negative cases (average 344 mm per month).

**Table 5.** Same as **Table 4**, but for HA-UIB regions.

WS Models

| Region | RR (Corr ) | Reg. Alt | GLM | Dry Mon | Predictors | | PCs | Mean Preci (mm/mon) | | MSE (mm) | | MSESS (%) | |
|---|---|---|---|---|---|---|---|---|---|---|---|---|---|
| | | (m) | | (Nos) | (Nos) | (Name) | (Nos) | Obs | Mod | Cal | Val | Cal | Val |
| R1 | Kakul (0.95) | 1174 (308-2744) | Tweedie | 7 | 1 | va850 | 7 | 93 | 93 | 49.88 | 50.54 | 51.92 | 49.57 |
| R2 | Gupis (0.65) | 3201 (2156-4030) | Tweedie | 56 | 2 | ua700+hus1000 | 6 | 12 | 11 | 14.11 | 15.35 | 39.87 | 28.39 |
| R3 | Chilas (0.78) | 2379 (1251-3146) | Tweedie | 39 | 2 | va850+zg700 | 8 | 17 | 18 | 17.67 | 18.21 | 33 | 26.1 |
| R4 | Gilgit (1) | 1460 (1460) | Tweedie | 33 | 2 | va700+hus1000 | 6 | 7 | 7 | 8.79 | 8.81 | 20.85 | 18.42 |
| Avg.UIB | | | | 34 | 1.8 | | 6.8 | 32 | 32 | 22.60 | 23.20 | 36.41 | 31.12 |

PMS Models

| | | | | | | | | | | | | | |
|---|---|---|---|---|---|---|---|---|---|---|---|---|---|
| R1 | Astore (0.78) | 2896 (1251-4030) | Gamma | 0 | 2 | hur700+va850 | 7 | 57 | 57 | 32.6 | 34.02 | 55.44 | 49.37 |
| R2 | Ghari Duputta (0.94) | 956 (702-1308) | Gamma | 0 | 2 | va700 + ua850 | 8 | 101 | 101 | 44.74 | 48.29 | 41.14 | 30.83 |
| R3 | Gilgit (1) | 2874 (1460-3200) | Tweedi | 8 | 2 | hur700+ua200 | 8 | 21 | 21 | 17.21 | 18.59 | 43.66 | 29.54 |
| R4 | Chitral (0.91) | 2014 (752-3000) | Tweedi | 12 | 2 | hur1000+va500 | 6 | 43 | 43 | 23.28 | 23.97 | 68.68 | 63.74 |
| Avg.UIB | | | | 5 | 2 | | 7.3 | 56 | 55 | 29.46 | 31.22 | 52.23 | 43.37 |

MS Models

| | | | | | | | | | | | | | |
|---|---|---|---|---|---|---|---|---|---|---|---|---|---|
| R1 | Sakardu (0.68) | 2788 (1251-4730) | *Tweedie* | 16 | 2 | va850+hus700 | 7 | 13 | 13 | 11.32 | 12.77 | 44.09 | 28.57 |
| R2 | Darosh (0.67) | 2618 (752-3719) | *Tweedie* | 11 | *1* | *va200* | *6* | *21* | *21* | 16.20 | 16.79 | 30.82 | 20.71 |
| R3 | GDP (0.90) | 2218 (1251-4030) | *Gamma* | 5 | 1 | ua500 | 7 | 186 | 186 | 75.31 | 80.19 | 52.06 | 44.72 |
| Avg.UIB | | | | 11 | 1.3 | | 6.7 | 73 | 73 | 34.28 | 36.58 | 42.32 | 30.60 |

The monsoon circulation is characterized by an anticyclone with its center along the southern boundary of the Tibetan Plateau, a tropical easterly jet in the upper troposphere, a westerly jet over the Arabian Sea, and the southwesterly flow over the Bay of Bengal in the lower troposphere (e.g., Krishnamurti,1973; Ashfaq et al., 2009; Duan et al., 2012). More recently, the analysis of extratropical influences on regional MS dynamics has identified an upper level high over west-central Asia (WCA) as a stronger MS precursor (e.g., Kazmi et al., 2016). In our composite analyses, we analyze the relevant dynamical circulations in the upper and lower tropospheres to explain the associated physical mechanisms.

During the wet MS composite of zg200 **(Figure 8a),** a stronger high-pressure anomaly over the WCA and a low-pressure anomaly over the Indian Peninsula reflect amplification of the upper level anticyclone and tropical easterly jet. Strong upper level easterlies **(Figure 8a)** point towards a stronger than normal local Hadley circulation. All of these conditions should favor a stronger than normal cross-equatorial moisture flow. Additionally, the circulation anomalies in **Figure 9a** exhibit stronger than normal westerlies over the Arabian Sea and south-westerlies over the Bay of Bengal. These upper and lower tropospheric anomalies **(Figures 8c and 9c)** in monsoon dynamics point towards a stronger than normal monsoon due to an enhanced moisture supply through oceanic sources and an increased dynamic and orography forcing (Hunt et al., 2018; Ashfaq et al., 2017; Curio and Scherer, 2016; Mei et al., 2015; Saeed et al., 2010).

On the contrary, the composite during dryer MS **(Figure 8b)** exhibits an eastward shift in the upper-level anticyclone and a weakening of the tropical easterly jet. The weakening of the easterly jet **(Figure 8b)** points towards a weaker than normal local Hadley circulation, which reduces the cross-equatorial flow. Similarly, an eastward shift of the anticyclone is linked with drier than normal conditions over western South Asia and the UIB and wetter than normal conditions over eastern South Asia (Ashfaq et al., 2009; Soman and Kumar, 1993). In the lower levels, both westerlies over the Arabian Sea and south-westerlies over the Bay of Bengal exhibit a weakening. It should be noted that the Arabian Sea and Bay of Bengal are important moisture sources for northern and northwestern South Asia (Mei et al., 2015). Therefore, anomalies in the lower level circulations should **(Figure 8c)** lead to a decrease in moisture supply from these two oceanic sources, which, when combined with upper-level circulation anomalies, lead to a decrease in the MS precipitation, particularly over western South Asia that includes the UIB (Wang et al., 2019; Ashfaq et al.m 2016; Ahmad et al., 2012).

The composite differences (**Figure 8c**) reflect the relative strength of upper-level circulations (WCA high, tropical easterly jet) to restrict the interaction of mid-latitude MS currents around UIB and their lower-level dynamical signatures (**Figure 9c**) to produce an excessive MS precipitation around UIB.

## 5.2 WS Synoptic Analysis Using Composite

Similar to the MS, we construct composites for the WS to analyze the circulation characteristics during the wet and dry precipitation regimes over a selected UIB region. We select region R3 in the WS for the construction of composites, which contains 16 stations and receives high regional precipitation (70 mm per month). A single predictor (va850) effectively models the observed precipitation at its RR station with a validation skill of 53%. PC2, which has the highest absolute regression coefficient (0.51) and high co-variability with the RR station (correlation coefficient of 0.65), is used to sub-sample the composites. The higher positive loadings of PC2 extend over a larger region that stretches from southern Pakistan to Africa and is centered over the Arabian Sea off the East African coast (**Figure 10**). Due to

a positive regression coefficient and the loading pattern, the higher positive PC scores (**Table 7**) support above-normal precipitation (12 cases, 187 mm per month), whereas the higher negative PC scores support below-normal precipitation (4 cases, 8 mm per month).

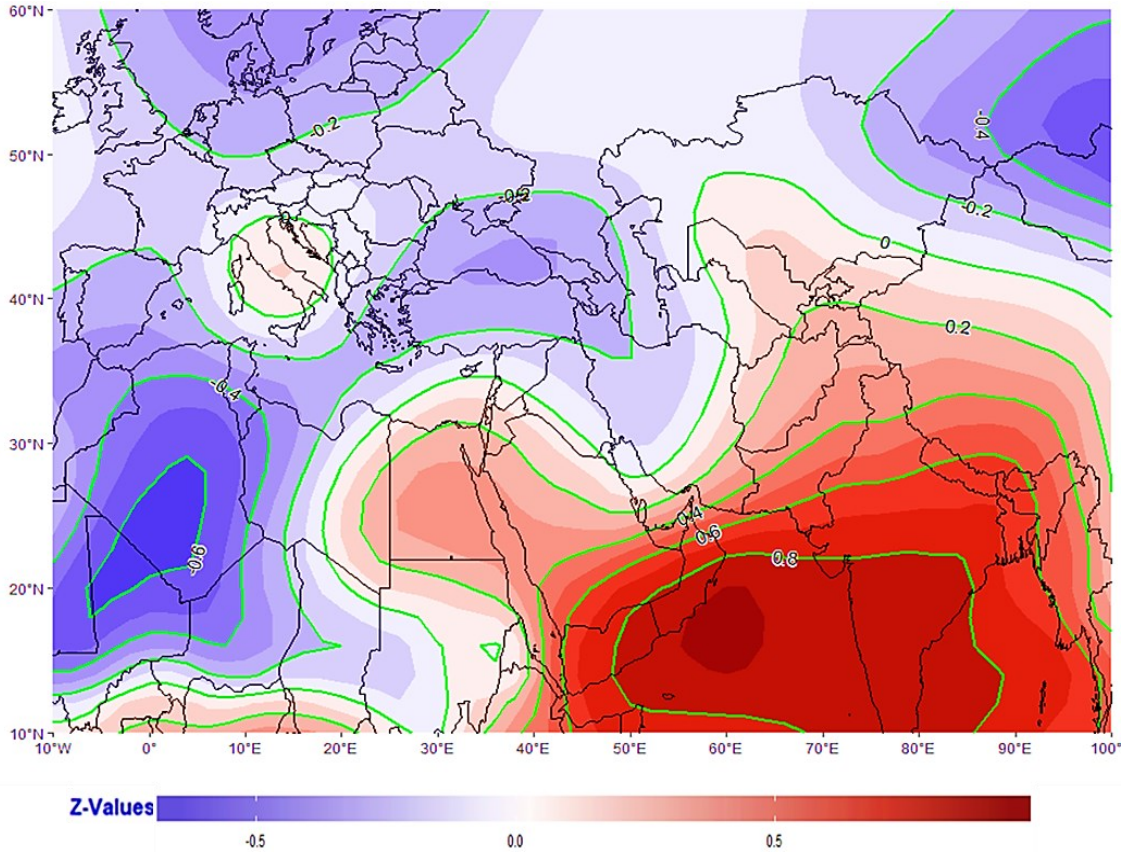


**Figure 7.** Loading pattern of PC1-va200 (most influential PC in the final regression model due to the highest absolute regression coefficient) during the MS season. The green contours show labeled loadings over different regions.

During the WS, the extratropical storms originate mainly at the surface level around the North Atlantic, Europe, and the Mediterranean region and propagate eastward by prevailing westerlies at mid and upper tropospheric levels to produce precipitation over the UIB (e.g., Martyn, 1992; Barlow et al., 2005). Therefore, in the following discussion, we analyze composites of relevant dynamical predictors to describe the anomalous WS precipitation regimes over the UIB.

During a wetter WS, the sea level pressure composites (**Figure 11a**) exhibit a higher pressure anomaly over northern Siberia and Europe and a low-pressure anomaly over northern Africa, which supports a strong eastward propagation of the extratropical cyclones, commonly known as the Western Disturbances (Ridley et al., 2013). Such an anomaly is analogous to the pattern that emerges during the negative phase of the North Atlantic Oscillation (NAO) and facilitates cyclogenesis activities around the Mediterranean, Europe, and the Middle East region. These storm tracks are further intensified over the WCA region due to a low-pressure anomaly (**Figure 11a**), which favors a positive precipitation

anomaly over the UIB and surrounding areas (Syed et al., 2006). Moreover, a low sea level pressure anomaly over the Bay of Bengal, eastern Tibetan Plateau, and a low-pressure anomaly over the southern Arabian Sea also support a stronger moisture transport from the Arabian Sea towards the UIB—a condition well known during the positive or warm phase of the El Niño-Southern Oscillation (ENSO), as shown by Syed et al. (2006, 2010) and Wang and Xu (2018).

**Table 6.** A statistical summary of the MS composite analysis of a selected UIB precipitation region (R3). The table provides information about the association between observed and modeled precipitation, adopted GLM framework to identify governing circulations (predictor), and the regression coefficients of different PCs, including the intercept term. The last column gives the significance level of the estimated model coefficients. The information about the most influential PC, its correlation with observations of the RR, the threshold of PC scores used to subset contrasting precipitation regimes, and their statistical summaries are also provided in the table.

| **Parameters** | **Value/ description** | **Model significance level (alpha, α)** |
|---|---|---|
| Mean observed precipitation rate of the RR (mm/month) | 181 | NA |
| Adapted GLM framework | gamma | |
| Governing predictor | va200 | |
| Mean modeled precipitation rate of the RR (mm/month) | 180 | |
| Correlation between observed and modeled precipitation (Spearman) | 0.80 | |
| Regression coefficient (intercept term) | 5.05 | 0.001 |
| Regression coefficent (PC1**)** | *-0.43* | **0.001** |
| Regression coefficent (PC2) | -0.27 | 0.001 |
| Regression coefficent (PC4) | -0.11 | 0.05 |
| Regression coefficent (PC5) | 0.08 | 1 |
| Regression coefficent (PC7) | -0.10 | 0.1 |
| Regression coefficent (PC9) | -0.09 | 0.1 |
| Regression coefficent (PC10) | 0.14 | 0.001 |
| Most influential PC (maximum absolute regression coefficient) | *PC1* | **NA** |
| Correlation between PC1 and RR observations | 0.62 | |
| PC scoring threshold for composites | 1.50 | |
| No. of Positive Cases (PC scores = > 1.50) | 10 | |
| Mean precipitation per positive event (mm/month) | 69 | |
| Dominant month during positive cases | September | |
| No. of negative cases (PC scores = < -1.50) | 6 | |
| Mean precipitation per negative event (mm/month) | 344 | |
| Dominant month during negative cases | July | |

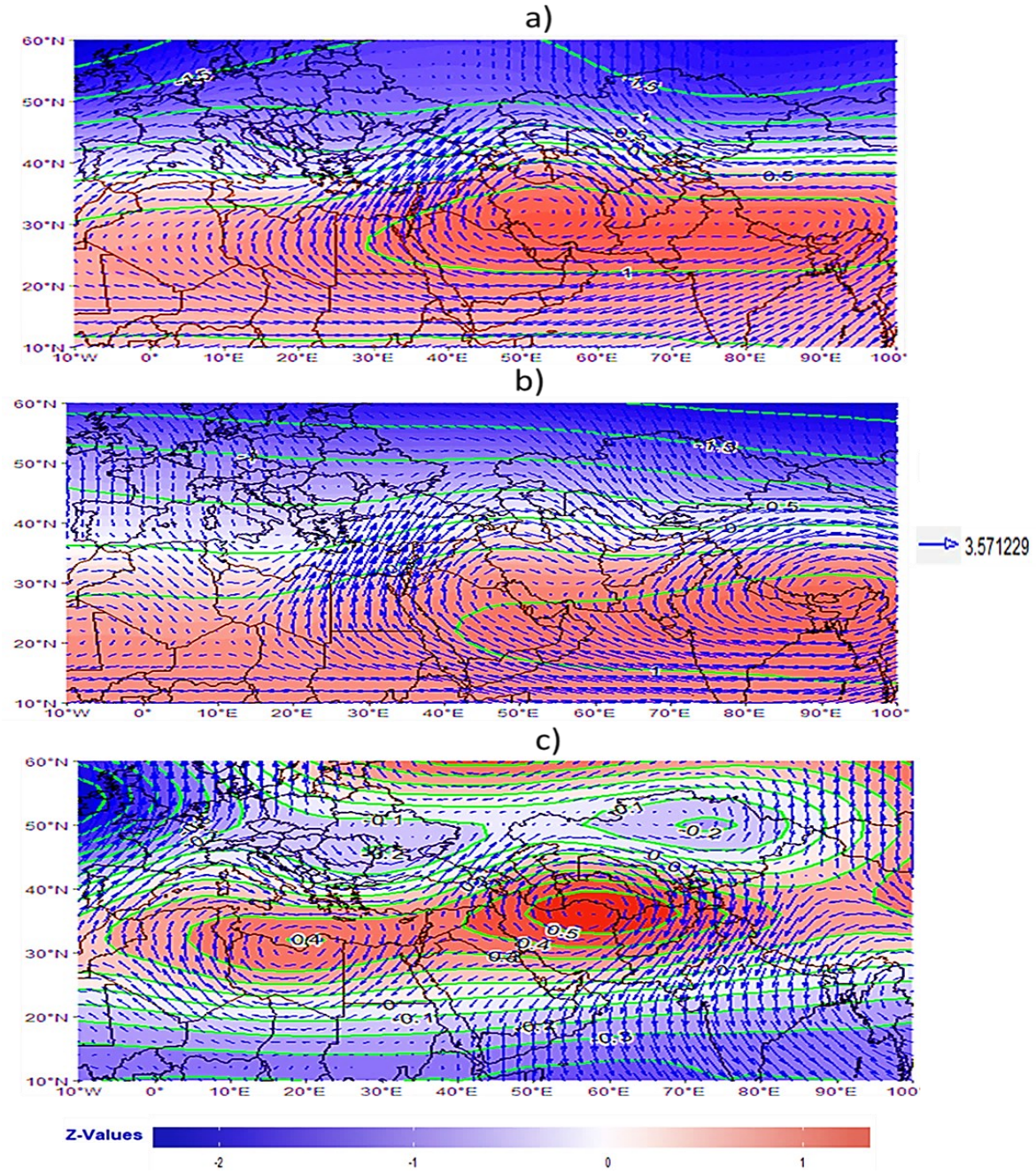


**Figure 8.** Standardized composite means of geopotential heights and atmospheric winds at 200 hPa (wind vector, m/s) during the MS precipitation season for a sample UIB region (R3). Panel **a)** shows the mean state of the large-scale circulations during above-normal precipitation, and **b)** represents the conditions during below-normal precipitation over R3. Panel **c)** reflects the difference between these two circulations (a minus b).

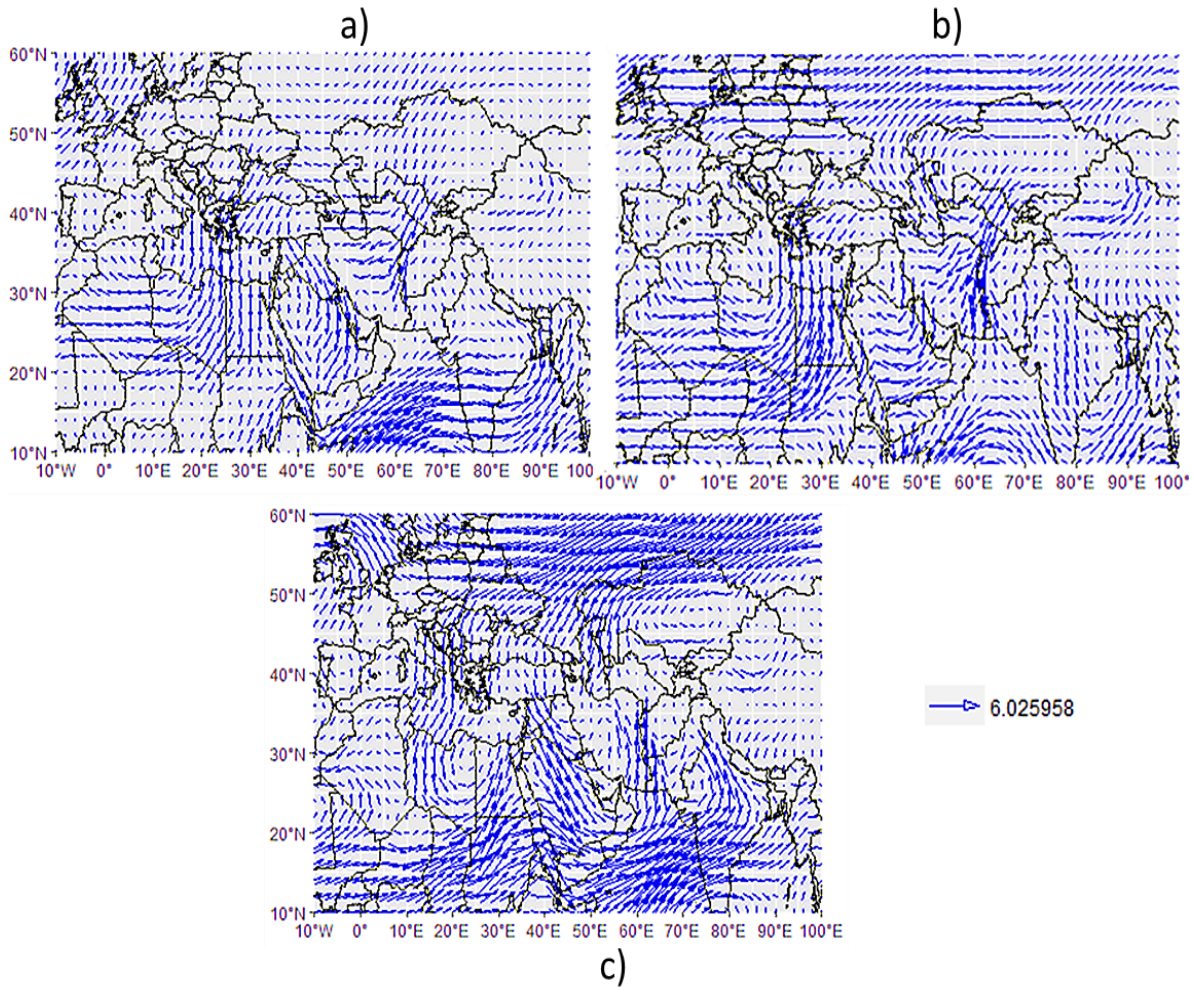


**Figure 9. (a-c).** Same as **Figure 8** but for lower tropospheric wind composites at 850 hPa atmospheric level (wind vector, m/s) during the MS precipitation season.

A cyclonic circulation anomaly in **Figure 12a** and the eastward circulation anomaly over the Mediterranean Sea provide further evidence of excessive precipitation around the UIB. On the other hand, the dryer WS composite **(Figure 11b)** exhibits a southward shift of the Siberian high and produces high sea level pressure anomalies over the UIB, Central Asia, and the Mediterranean, and a low sea level pressure anomaly over northern Europe. These conditions are analogous to the positive phase of the NAO and favor a northward movement of the extratropical cyclones tracks during the WS. Consequently, the lack of cyclogenesis activity reduces the strength and moisture transport towards the UIB. Additionally, the moisture supply from the Arabian Sea also greatly reduces due to the anomalous northerly winds **(Figure 12b),** as also pointed out by Hunt et al. (2018). Wind anomalies over the Mediterranean Sea and land **(Figure 12b)** also favor reduced moisture flow, eventually resulting in lower than normal precipitation over the UIB, as reflected in our corresponding composite. The

difference plots (**Figures 11c, 12c**) reflect the influence of relative dynamical forcing supporting positive precipitation around the UIB.

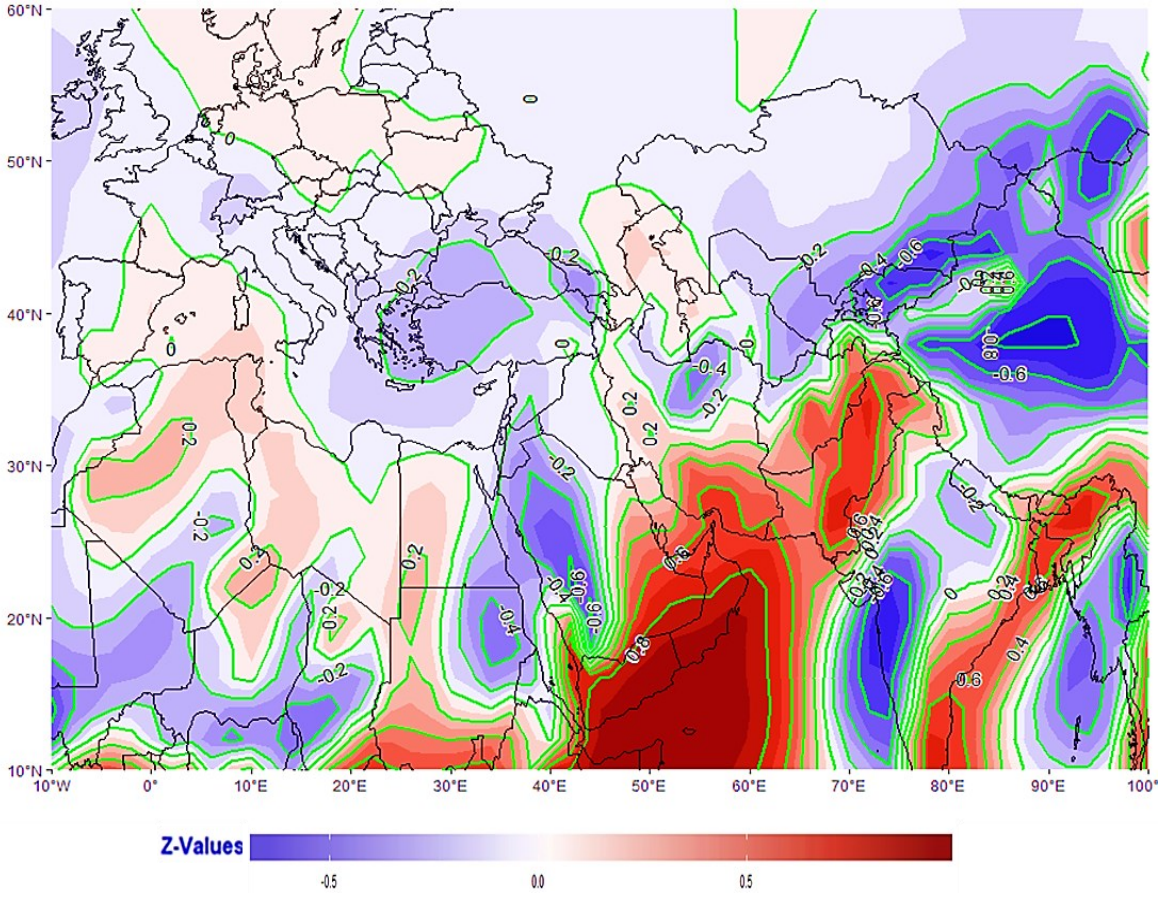


**Figure 10**. Loading pattern of PC2-va850 (most influential PC in the final regional model due to highest absolute regression coefficient) during the WS precipitation. The green contours show labeled loadings over different regions.

We also constructed similar composites for the geopotential heights at 700 hPa, 500 hPa, and 200 hPa atmospheric levels to analyze the corresponding circulations as the low-pressure systems travel at high altitudes towards the UIB (**Figure 13**). The corresponding difference plots (**Figures 13a-c**) confirm the presence of previously described mechanisms and their barotropic nature across the troposphere. It is important to note that some of the earlier studies relate a positive NAO signal with increased winter precipitation over the UIB (e.g., Syed et al., 2010; Ahmad et al., 2015), which is not consistent with our findings. Instead, we see evidence that perhaps the negative NAO supports positive winter precipitation over the UIB. Some other studies, such as Archer and Fowler (2004), also point towards a mixed precipitation response during the positive and negative phases of the NAO. Therefore, further investigation is needed to establish a robust understanding of the NAO influence on winter precipitation variability over the UIB.

# 5 Sources of Uncertainty

In this study, we have attempted to improve seasonal precipitation assessments within the UIB by addressing many of the common uncertainty sources through methodological improvements. Still, our estimates are based on certain assumptions. For instance, despite significantly improving the HA representation in our station ensemble, altitudes beyond 4730 m (**see Table 1**) still have no representation in our analysis due to the unavailability of reliable time series data. This lack of representation of higher altitudes has the potential to influence the regionalization process and reliability of precipitation inferences over the UIB. However, it is worth mentioning that the bulk of the UIB precipitation falls between 3000 and 4500 m altitudes (Hewitt, 2014), and its magnitude starts decreasing rapidly above 5000 m (Hewitt, 2014; Winiger et al., 2005).

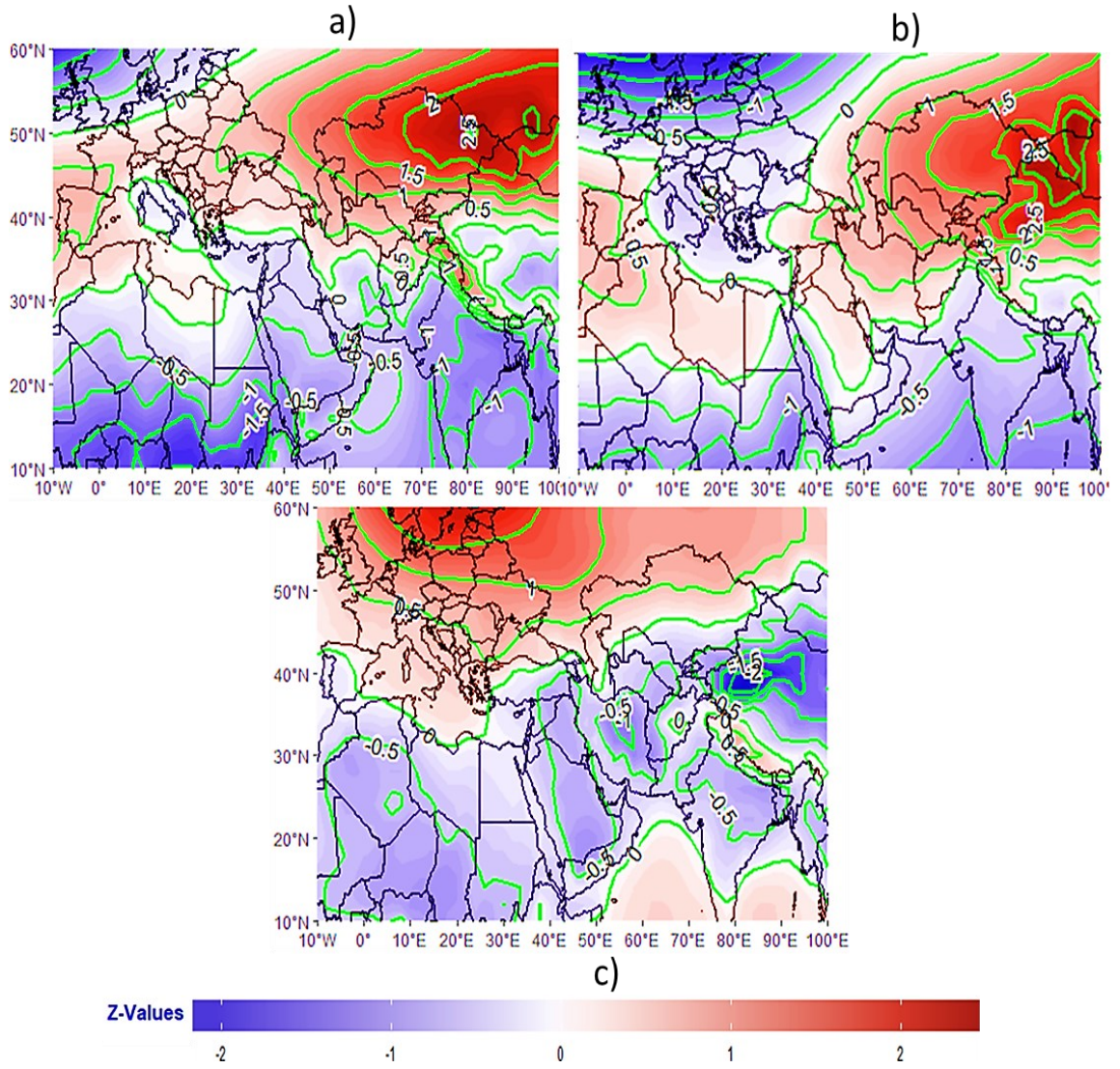


**Figure 11. (a-c).** Same as **Figure 9** but for sea level pressure composites during the WS.

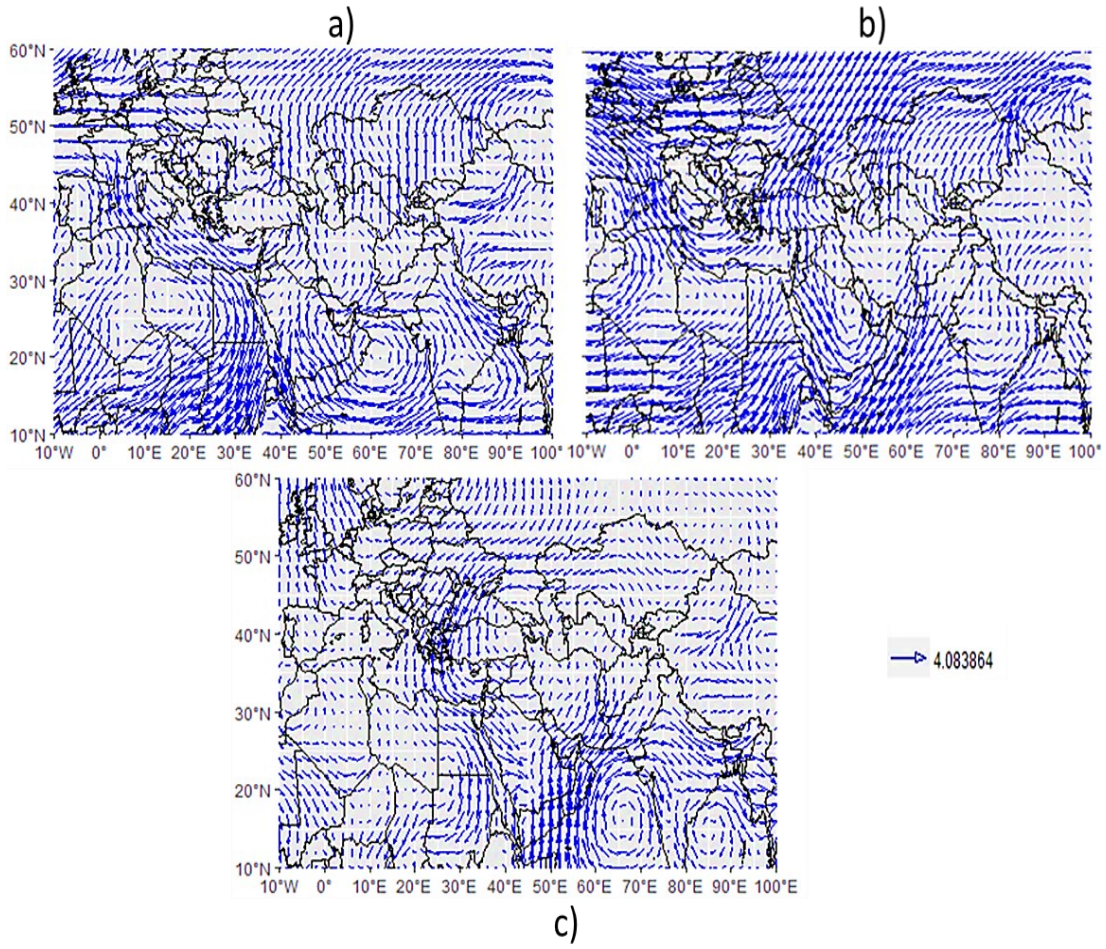


**Figure 12. (a–c).** Same as **Figure 9** but during the WS precipitation

Thus, it is expected that the regions of maximum precipitation are well represented in our station ensemble (see Section 3.1 and Table 1). Moreover, the mean equilibrium line altitude (ELA) is estimated between 4500 and 5500 m (e.g., Khan et al., 2015b) in the UIB, and any precipitation beyond the ELA does not contribute to the runoff. We assume that precipitation variation between 4730 m and the ELA may be represented by our identified UIB regions, and thus, inferences can be extended to fill gaps beyond the available observations. Curio and Scherer (2016) classified the region around the UIB into at least four different precipitation classes to define spatiotemporal precipitation variation using HAR data that covers the entire orography of the UIB. We also identify, on average, four different regions based upon observations, which are in line with their findings and support our assumption regarding the adequacy of our regionalization in explaining effective orography of the entire UIB. Our study is also limited to only those station observations that are located on the Pakistan side of the UIB. While there are some online data sources (e.g., NOAA-NCDC's data available from https://www.ncdc.noaa.gov) that provide observations of a few stations on the Indian side of the UIB; those are mostly located in the low-altitude areas and do not overlap the recent period covered by the HA stations used in this study. Therefore, while it is understandable that additional station observations should improve the spatial coverage of the UIB, substantial effort is needed for the spatiotemporal homogenization of these datasets

for drawing meaningful inferences and particularly to infer orography, which is the focus of our study. We rather assume that precipitation variability explained by our regions may also represent the conditions in the surroundings of the UIB of Pakistan, as the same large-scale forcing governs the regional precipitation. Already some studies (e.g., Archer and Fowler, 2004) have pointed out that some of the Indian stations show stronger covariation with precipitation of adjacent stations of Pakistan.

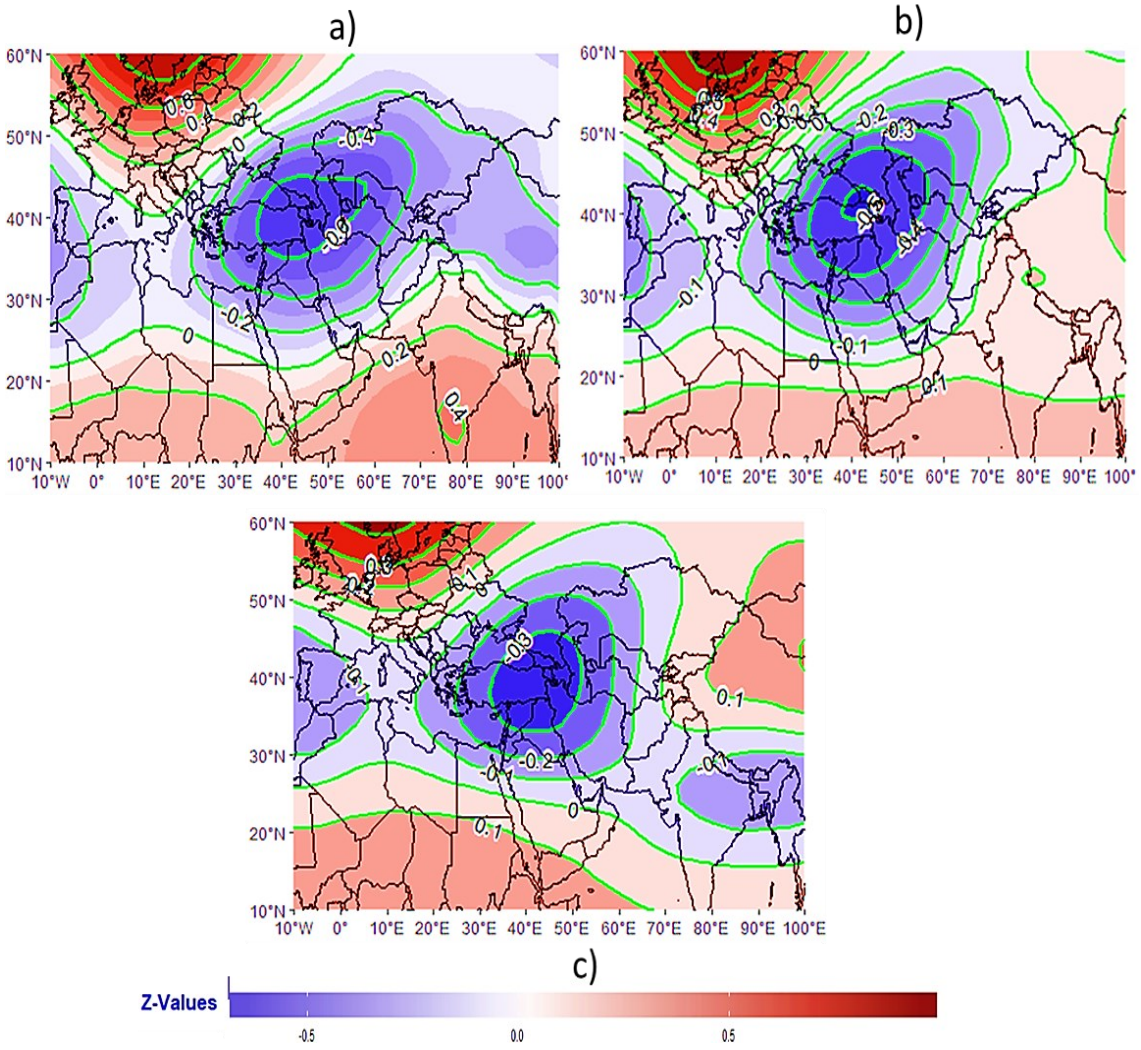


**Figure 13.** Composites of geopotential height differences across the troposphere during WS. **a)** geopotential heights at 700 hPa, **b)** geopotential heights at 500 hPa, and **c)** geopotential heights at 200 hPa

Moreover, we have employed ERA-Interim-based predictors in our study, as the more recent ERA5 (Hersbach et al. 2018) was not publicly available at the time when this study was begun.Since statistical downscaling is based on the use of large-scale circulations, we do not expect that the improvements in the horizontal resolution in ERA5 will have a significant impact on the downscaling results. In any case, we evaluate the robustness of ERA-Interim-based final predictors by performing a similar PCA on ERA5 predictors and use Taylor diagrams (Taylor, 2001) for the comparison of loading patterns (centers

of variation) of the two datasets. We find a high correspondence among dynamical predictors that dominate our final regression models (Section 4.2.1). Thus, the strong correspondence of governing PCs among these different datasets (not shown) provides confidence in the use of ERAInterim as predictors.

**Table 7.** Same as **Table 6** but provide information about a selected UIB region (R3) during the WS

| **Parameters** | **Value/ description** | **Model significance level (alpha, α)** |
|---|---|---|
| Mean observed precipitation rate of the RR (mm/month) | 93 | NA |
| Adapted GLM framework | Tweedie | |
| Governing predictor | Va850 | |
| Mean modeled precipitation rate of the RR (mm/month) | 93 | |
| Correlation between observed and modeled precipitation (Spearman) | 0.78 | |
| Regression coefficient (Intercept term) | 4.33 | 0.001 |
| Regression coefficent (PC2) | 0.51 | 0.001 |
| Regression coefficient (PC6) | -0.21 | 0.001 |
| Regression coefficient (PC7) | -0.16 | 0.01 |
| Regression coefficient (PC9) | 0.23 | 0.001 |
| Regression coefficient (PC10) | 0.18 | 0.001 |
| Regression coefficient (PC13) | -0.12 | 0.05 |
| Regression coefficient (PC15) | -0.11 | 0.05 |
| Most influential PC (maximum absolute regression coefficient) | PC2 | NA |
| Correlation between PC1 and RR observations | 0.64 | |
| PC scoring threshold for composites | 1.50 | |
| No. of Positive Cases (PC scores = > 1.50) | 12 | |
| Mean precipitation per positive event (mm/month) | 187 | |
| Dominant month during positive cases | March | |
| No. of negative cases (PC scores = < -1.50) | 4 | |
| Mean precipitation per negative event (mm/month) | 8 | |
| Dominant month during negative cases | December | |

Another shortcoming is related to the RMSEs in **Tables 4** and **5**, which are sometimes higher than the corresponding precipitation rates. However, the relatively higher RMSEs are associated with a higher number of zeros in the observed time series, which increases the total errors due to the addition of smaller errors in simulating exact zeros in the regression models. In the case of gamma or those Tweedie models that have very few months with zero precipitation, the mean errors are within an acceptable range (e.g., in **Table 4**, PMS-R3 and WSR3). Therefore, despite relatively higher error rates during some (relatively dry) winter cases, the ability of our models to simulate a large fraction of observed seasonal variance is still significant.

Despite some of these uncertainties, our study presents a unique approach to assess and explain fine-scale precipitation variability over large parts of the effective drainage basin using large-scale circulations and carefully selected actual observations. This will serve to meet communal and scientific interests by providing an alternative to analyze the complex, climate-sensitive, and yet data-scarce region within the available observational framework.

# 6 Summary and Conclusions

Complex processes govern spatiotemporal characteristics of regional precipitation over the UIB. An inadequacy of observational coverage within the UIB and regional limitations of various de facto precipitation products further compound the challenge of reliable estimation of precipitation at varying time scales. In this study, we employed atmospheric circulations within a statistical modeling framework to resolve the observed (seasonal) precipitation over the Indus basin of Pakistan with a focus on the UIB. By taking a distinct advantage of data from recent HA observatories, we adapted a K-means cluster analysis to demonstrate the effectiveness of relatively low-altitude stations with historical data to provide precipitation inferences over more uncertain but hydrologically important HA of the UIB. This precipitation regionalization scheme also captured the spatial heterogeneity of precipitation over the UIB by identifying more sub-regions within the UIB when compared with the ones identified over the LI. We argue that the precipitation regionalization is effective in filling out the spatial gaps over the UIB despite the lack of observations at very high altitudes. Furthermore, the RR stations for each of the precipitation regions were carefully identified to serve as predictands. We used different dynamical and thermodynamic variables from the ERA-Interim reanalysis as predictors.

We adapted a GLM framework with gamma and Tweedie distributions to model the typical predictor predictand relationships across the Indus River basin during the major precipitation seasons. The final selection of precipitation models was based on minimizing the MSE (maximizing the MSESS) by duly considering the multicollinearity among different predictors within a robust cross-validation framework. Overall, the precipitation models exhibited a high performance over the wetter southern Himalayans and various LI regions by mainly using different dynamical predictors. The typical modeling framework also demonstrated an adequate performance in resolving the seasonal precipitation of cryosphere-dominated and topographically complex trans-Himalayans regions, which largely govern the hydrological regime of the Indus River system. Knowing that highly localized processes are difficult to model and also govern some part of the mountainous precipitation variability, the modeled skills over different parts of the UIB are quite reasonable to explain the precipitation dynamics using large-scale atmospheric circulations.

Skillful modeling of the trans-Himalayan regions, particularly during the westerly dominated circulations (PMS and WS), which mainly nourish the seasonal snowpacks, should help to improve our

limited understanding about the spatial characteristics of regional precipitation and to assess the future stability of the associated cryosphere. However, relatively complex models containing both dynamic and thermodynamic predictors were required to simulate such cryosphere-dominated trans-Himalayan regions. Moreover, we also separately modeled the HA part of the UIB due to its importance in the basin hydrology and associated greater uncertainty. We also demonstrated the robustness of ERA-Interim circulations against the latest ERA5 reanalysis and the insensitivity of the final precipitation models against different precipitation measurement losses.

Furthermore, we constructed composites for two major wet seasons (MS and WS) to analyze and explain the large-scale atmospheric structures during the wet and dry precipitation anomalies over the UIB. These composites provided additional confidence regarding the reliability of the statistical models by explaining the physical processes that govern precipitation dynamics over the complex UIB. We showed that the strength and location of an upper level high over the WCA (Siberian high) influence the anomalous behavior of UIB precipitation by triggering different dynamical and thermodynamic instabilities during the MS (WS).

We have also simultaneously modeled the precipitation distribution over different LI regions in a similar way to have a coherent perspective about the water supply (UIB) and its demand (LI). Such investigations will further help in devising appropriate strategies for water resources planning at the basin scale. These statistically skillful and physically consistent models also offer an opportunity to investigate the sub-regional response of the Indus basin under different climate scenarios by downscaling relevant circulations from the GCMs. Given that the latest GCMs tend to exhibit a relatively better skill in representing large-scale circulations when compared with their raw precipitation output (e.g., Mueller and Seneviratne 2014), future precipitation changes derived through such predictors may provide more realistic policy feedback to support the regional adaptations.

However, considering the melt-dominated hydrological regime of the Indus basin, the downscaling of precipitation alone cannot fulfill the requirements for understanding the basin hydrology. Therefore, similar efforts are needed to downscale regional temperatures. Thus, we plan to apply similar statistical downscaling techniques on the temperature fields in addition to the use of these models for precipitation projections amid different climate scenarios.

## Acknowledgments

The authors would like to thank PMD and WAPDA for sharing the meteorological data. The authors also acknowledge the ECMWF for the provision of the ERA-Interim and ERA5 datasets. This manuscript has been co-authored by an employee of Oak Ridge National Laboratory, managed by UT Battelle, LLC, under contract DE-AC0500OR22725 with the US Department of Energy. The Himalayan Adaptation, Water and Resilience (HI-AWARE) consortium through PARC under the Collaborative

Adaptation Research Initiative in Africa and Asia (CARIAA) under financial support from UK-ID and IDRC, Canada, mainly funded this work. The DAAD Germany and the University of Augsburg provided additional funding, which also needs due appreciation. M. A. was supported by the National Climate-Computing Research Center, which is located within the National Center for Computational Sciences at the Oak Ridge National Laboratory (ORNL) and supported under a Strategic Partnership Project, 2316-T849-08, between DOE and NOAA. E.H. was supported by the Deutsche Forschungsgemeinschaft (DFG, German Research Foundation) under project number 408057478.Open access funding was provided by the DEAL project.

## References

Ahmad, S., Kazuaki, N., Tamura, T., Ohta, T., et al., (2012). Characteristics of Climatological Troposheric Conditions during Pre- Monsoon and Matured Phases of Pakistan Summer Monsoon. *Ann. J. of Hydraluic Enginnering, JSCE, Vol.56 (4)*, pp. I_157-162. https://doi.org/10.2208/jscejhe.68.I_157.

Ahmad, I., Ambreen, R., Sun, Z., Deng, W. (2015). Winter-spring precipitation variability in Pakistan. Am J Clim 4:115–139. https://doi.org/10.4236/ajcc.2015.41010

Akaike, H. (1973) Information theory as an extension of the maximum likelihood principle. *Second International Symposium on Information Theory, Akademiai Kiado*, pp. 267-281

Akhtar, M., Ahmad, N., Booij, M.J. (2008). The impact of climate changes on the water resources of Hindukush–Karakorum–Himalayaregionunder different glacier coverage scenarios. *J. Hydrol. 355*, pp. 148–163. Retrieved from https://doi.org/10.1016/j.jhydrol.2008.03.015

Alexandersson, H. (1986) A homogeneity test applied to precipitation data .*Int. J. Climatol. 6*, pp. 661–675. Retrieved from https://doi.org/10.1002/joc.3370060607.

Ali, S., Li, D., Congbin, F., Khan, F. (2015) Twenty first century climatic and hydrological changes over Upper Indus Basin of Himalayan region of Pakistan. *Environ. Res. Lett. (10) 014007*, pp. 1-20. https://doi.org/10.1088/1748-9326/10/1/014007.

Anderson, T.W., and Darling, D.A. (1952) Asymptotic theory of certain goodness-of-fit criteria based on stochastic processes. *Ann. Math. Stat., (23)*, pp. 193-212

Archer, D.R., and Fowler, H.J. (2004) Spatial and temporal variations in precipitation in the Upper Indus Basin, global teleconnections and hydrological implications. *Hydrol. Earth Syst. Sci. 8 (1)*, pp. 47–61. https://doi.org/10.5194/hess-8-47-2004.

Ashfaq, M, Shi, Y, Tung, W.W, Trapp, R.J, Gao, X.J, Pal, J.S, Diffenbaugh, N.S (2009) Suppression of south Asian summer monsoon precipitation in the 21st century. *Geophys Res Lett*. https://doi.org/10.1029/2008gl036500.

Ashfaq, M., Rastog, D., Mei, R., Toumag, D., et al., (2016). Sources of errors in the simulation of south Asian summer monsoon in the CMIP5 GCMs. *Clim Dyn (2017) 49*, pp. 49:193–223. https://doi.org/10.1007/s00382-016-3337-7

Barlow, M., Wheeler, M., Lyon, B., Cullen, H. (2005) Modulation of daily precipitation over southwest Asia by the Madden-Julian oscillation. *Mon Weather Rev, 133*, pp. 3579–3594

Bashir, F., Zeng, X., Guptta, H., Hazenberg, P. (2017) A Hydro-Meteorological Perspective on the Karakoram Anomaly using Unique Valley-Based Synoptic Weather Observations. *Geophysical Research Letters 44(20)*, pp. 1-9. https://doi.org/10.1002/2017GL075284.

Bhambri, R., Bolch, T., Kawishwar, P., Dobhal, D.P, Srivastava, D., Pratap, B. (2013) Heterogeneity in glacier response in the upper Shyok valley, northeast Karakoram. *Cryosphere 7*, pp. 1385–1398. https://doi.org/10.5194/tc-7-1385-2013.

Cannon, F., Carvalho, L.M.V., Jones, C., Norris, J. (2015) Winter westerly disturbance dynamics and precipitation in the western Himalaya and Karakoram: a wave-tracking approach. *Theor Appl Climatol*. https://doi.org/10.1007/s00704-015-1489-8.

Cogley, J.G (2011) Present and future states of Himalaya and Karakoram glaciers. *Ann. Glaciol. 52 (59)*, pp. 69–73

Curio, J., and Scherer, D. (2016) Seasonality and spatial variability of dynamic precipitation controls on the Tibetan Plateau. *Earth Syst. Dynam., (7)*, pp. 767–782. https://doi.org/10.5194/esd-7-767-2016

Dahri, Z.H, Moors, E., Ludwig, F., Ahmad, S., Khan, A., Ali, I., Kabat, P. (2018) Adjustment of measurement errors to reconcile precipitation distribution in the high-altitude Indus basin. *Int. J. Climatol. 2018, 38*, pp. 3842–3860. https://doi.org/10.1016/j.scitotenv.2016.01.001

Dahri, Z.H, Ludwig, F., Moors, E., Ahmad, B., and Kabat, P. (2016) An apprisal of precipitation distribution in the high altitude catchments of the Indus basin. *Sci. of the Total Envir. 548-549*, pp. 289-306. Retrieved from https://doi.org/10.1002/joc.553

Dee, D.P, Uppala, S.M., Simmons, A.J., Berrisford, P., Poli, P, Kobayashi, S., Andrae, U., Balmaseda, M.A., Balsamo, G, Bauer, P., Bechtold, P., Beljaars, .AC.M., van de Berg, L., Bidlot, J., Bormann, N., Delsol, C., Dragani, R., Fuentes, M., Geer, A. (2011) The ERA-Interim reanalysis: configuration and performance of the data assimilation system. *Q. J. R. Meteorol. Soc. (137)*, pp. 553–597. https://doi.org/10.1002/qj.828,2011.4757,4759,4775

Duan, A.M., Wu, G.X, Liu, Y.M, Ma, Y.M., Zhao, P. (2012) Weather and climate effects of the Tibetan Plateau. *Adv Atmos Sci (29)*, pp. 978–992

Dunn, P.K. (2004) Occurrence and quantity of precipitation can be modelled simultaneously. *Int. J. of Climatol., (24)*, pp. 1231–1239

Dunn, P.K. (2010) Tweedie: Tweedie exponential family models. R package. *Version 2.0.5*.

FAO (2011) Irrigation in Southern and Eastern Asia in figures – AQUASTAT Survey – 2011. Retrieved from http://www.fao.org/nr/Water/aquastat/basins/indus/indus-CP_eng.pdf

Filippi, L, Palazzi, E, von Hardenberg, J, Provenzale, A (2014) Multidecadal variations in the relationship between the NAO and winter precipitation in the Hindu-Kush Karakoram. *J Clim*. Retrieved from https://doi.org/10.1175/JCLI-D-14-00286.1

Hasan, M.M and Dunn, P.K (2011) Two Tweedie distributions that are near-optimal for modelling monthly rainfall in Australia. *Int. J. Climatol., (31)*, pp. 1389–1397

Hasson, S. (2016) Future water availability from Hindukush-Karakoram-Himalaya upper Indus basin under conflicting climate change signals. *Climate, 4(3) 40*. https://doi.org/10.3390/cli4030040

Hasson, S, Böhner, J, and Chishtie, F (2019) Low fidelity of CORDEX and their driving experiments indicate future climatic uncertainty over Himalayan watersheds of Indus basin. *Climate Dynamics (2019) 52*, pp. 777–798. https://doi.org/10.1007/s00382-018-4160-0

Hersbach, H., de Rosnay, P., Bell, B., Schepers, D., et al., (2018). Operational global reanalysis: progress, future directions and synergies with NWP, ERA-report, Serie 27, https://www.ecmwf.int/node/18765.

Hertig, E and Jacobeit, J. (2015) Considering observed and future nonstationarities in statistical downscaling of Mediterranean precipitation. *Theor. Appl. Climatol., (122)*, pp. 667–683

Hertig, E., Merkenschlager, C., Jucundus, J. (2017) Change points in predictors–predictand relationships within the scope of statistical downscaling. *Int. J. Climatol. 37*, pp. 1619–1633. https://doi.org/10.1002/joc.4801

Hewitt, K. (2005) The Karakoram anomaly? Glacier expansion and the 'elevation effect', Karakoram Himalaya. *Mt. Res. Dev. (25)*, pp. 332–340. Retrieved from https://doi.org/10.1659/02764741(2005)025[0332:TKAGEA]2.0.CO;2

Hewitt, K. (2011) Glacier change, concentration, and elevation effects in the Karakoram Himalaya, Upper Indus Basin. *Mt. Res. Dev. 31 (3)*, pp. 188–200. Retrieved from https://doi.org/10.1659/mrd-journal-d-11-00020.1

Hewitt, K. (2014) Glaciers of the Karakoram Himalaya. Springer, pp. 363

Huffman, G.J, Adler, R.F, Bolvin DT, Gu G, Nelkin EJ, Bowman KP, Hong Y, Stocker EF, Wolff DB (2007) The TRMM Multi-satellite Precipitation Analysis (TMPA): Quasi-Global, Multiyear, Combined-Sensor Precipitation Estimates at Fine Scales, J. Hydrometeorol., 8, 38–55, https://doi.org/10.1175/JHM560.1

Hunt, K.M.R, Turner, A.G, Shaffrey, L.C. (2018) Extreme Daily Rainfall in Pakistan and North India: Scale Interactions, Mechanisms, and Precursors. *Amer. Meteo. Soc., Vol (146)*, pp. 1005-1022. https://doi.org/10.1175/MWR-D-17-0258

Immerzeel, W.W, Pellicciotti, F., and Bierkens, M.F.P. (2013) Rising river flows throughout the twenty-first century in two Himalayan glacierized watersheds, Nat. Geosci., 6, 742–745, https://doi.org/10.1038/NGEO1896

Immerzeel, W.W, Wanders, N., Lutz, A.F, Shea, J.M., et al., (2015). Reconciling high-altitude precipitation in the upper Indus basin with glacier mass balances and runoff. *Hydrol. Earth Syst. Sci., (19)*, pp. 4673–4687. https://doi.org/10.5194/hess-19-4673-2015

Iqbal, M.F., and Athar, H. (2018) Variability, trends, and teleconnections of observed precipitation over Pakistan. *Theor Appl Climatol, 134*, pp. 613–632. https://doi.org/10.1007/s00704-017-2296-1

Jacob, T., Wahr, J., Pfeffer, W.T, Swenson, S. (2012) Recent contributions of glaciers and ice caps to sea-level rise. *Nature 482*, pp. 514–518

Kääb, A., Berthier, E., Christopher, N., Gardelle, J., et al., (2012). Contrasting patterns of early twenty-first-century glacier mass change in the Himalayas. *Nature, 488(7412)*, pp. 495–498

Kääb, A., Treichler, D., Nuth, C., Berthier, E. (2015). Brief Communication: contending estimates of 2003–2008 glacier mass balance over the Pamir–Karakoram–Himalaya. *Cryosphere 9*, pp. 557–564. Retrieved from https://doi.org/10.5194/tc-9-557-2015

Kapnick, S.B., Thomas, L.D., Moetasim, A., Segey, M. (2014). Snowfall less sensitive to warming in Karakoram than in Himalayas due to a unique seasonal cycle, Nat. Geosci., 7(11), 834–840, https://doi.org/10.1038/ngeo2269

Kaspar-Ott, I., Elke, H., Seerin, K., Felix, P. et al., (2019). Weights for general circulation models from CIMP3/CIMP5 in a statistical downscaling framework and the impact on future Mediterranean precipitation. *Int. J. Climatol. 2019, ;39, PP 3639–3654*. https://doi.org/10.1002/joc.6045

Kazmi, D.H., Li, J., Ruan, C., Zaho, S., Sen, Z., et al., (2016). A statistical downscaling model for summer rainfall over Pakistan. Clim. Dyn. 47 (7). https://10.1007/s00382-016-2990-1

Khan, A., Naz, B.S, Bowling, L.C. (2015). Separating snow, clean and debris covered ice in the Upper Indus basin, Hindukush–Karakoram–Himalayas, using Landsat images between 1998 and 2002. Journal of Hydrology, 521(2015), 46–64

Khan, F., Pilz, J., Amjad, M., Wiberg, D. (2015b) Climate variability and its impacts on water resources in the Upper Indus Basin under IPCC climate change scenarios. *Int. J. Global Warming, Vol (8) No. 1*, pp. 46–69. https://doi.org/10.1504/IJGW.2015.071583

Khattak, M.S., Babel, M.S., Sharif, M. (2011). Hydro-meteorological trends in the upper Indus River basin in Pakistan. *Clim.Res., Vol., 46 (103)*, pp. 103–119. https://doi.org/10.3354/cr00957

Krishna, R., Kumar, V., Sugi, S., Yoshimura, J. (2009) Internal Feedbacks from Monsoon–Midlatitude Interactions during Droughts in the Indian Summer Monsoon. *J. Atmos. Sci., (66)*, pp. 553-578. doi:10.1175/2008JAS2723.1

Krishnamurti, T.N. (1973). Tibetan high and upper tropospheric tropical circulation during northern summer. *Bull. Amer. Meteor. Soc. , (54)*, pp. 1234–1249

Latif, Y., Yaoming, M., Yaseen, M. (2018). Spatial analysis of precipitation time series over the Upper Indus basin. *Theor. Appl. Climatol., 131(1-2)*, pp. 761-775. Retrieved from https://doi.org/10.1007/s00704-016-2007-3

Lutz, A.F, Immerzeel, W.W, Kraaijenbrink, P.D.A, Shrestha, A.B., Bierkens, M.F.P. (2016) Climate change impacts on the Upper Indus hydrology: sources, shifts and extremes. *PLoS One, 11(11), e0165630*. https://doi.org/10.1371/journal.pone.0165630

Mahmood, R., and Babel, M.S . (2012). Evaluation of SDSM developed by annual and monthly sub-models for downscaling temperature and precipitation in the Jhelum basin, Pakistan and India. *Theor Appl Climatol*. https://doi.org/10.1007/s00704-012-0765-0

Martyn, D. (1992). Climate of the World. *Elsevier:New York*

Maussion, F., Scherer, D., Mölg, T., Collier, E., Curio, J., Finkelnburg, R. (2014). Precipitation Seasonality and Variability over the Tibetan Plateau Resolved by the High Asia Reanalysis. J Clim,27,1910–1927, https://doi.org/10.1175/JCLI-D-13-00282.1

McCullagh, P., and Nelder, J.A. (1989). Generalized Linear Models. Monographs on Statistics and Applied Probability. *Vol. (37),Chapman & Hall: London*

Mei, R., Ashfaq, M., Rastogi, D., Leung, L.R., et al., (2015). Dominating controls for wetter south Asian summer monsoon in the twenty-first century.. *J Clim 28(8)*, pp. 3400–3419. https://doi.org/

10.1175/JCLI-D-14-00355.1

Minora, U., BocchiolaD, D., Agata, C., Maragno, D., et al., (2013). 2001– 2010 glacier changes in the Central Karakoram National Park: a contribution to evaluate the magnitude and rate of the "Karakoramanomaly." *CryosphereDiscuss.7(3)*, pp. 2891–2941. doi:http://dx.doi.org/10.5194/tcd-7-2891-2013

Mishra, V. (2015). Climatic uncertainty in Himalayan water towers. *Journal of Geophysical Research: Atmospheres, 120*, pp. 2689–2705. https://doi.org/10.1002/2014JD022650

Moberg, A., Jones, P.D., Lister, D., Walther, A., et al., (2006). Indices for daily temperature and precipitation extremes in Europe analyzed for the. *J. Geophys. Res. Atmos. 111 (D22)*. https://doi.org/10.1029/2006JD007103

MRI (2015). Elevation-dependent warming in mountain regions of the world. *Nat. Clim. Chang, 5* , pp. 424–430

Mueller, B., and Seneviratne, S.I. (2014). Systematic land climate and evapotranspiration biases in CMIP5 simulations. *Geophys Res Lett, 41*, pp. 128–134. https://doi.org/10.1002/2013GL058055

Nepal, S., and Shrestha, A.B. (2015) Impact of climate change on the hydrological regime of the Indus, Ganges and Brahmaputra river basins: a review of the literature. *Int. J. Water Resour. Dev., (627)*, pp. 1–18. https://doi.org/10.1080/07900627.2015.1030494

Palazzi, E., von Hardenberg, J., Provenzale, A. (2013) Precipitation in the Hindu-Kush Karakoram Himalaya: observations and future scenarios. *J. Geophys. Res. Atmos. 118 (1)*, pp. 85–100. https://doi.org/10.1029/2012JD018697

Philipp, A. (2003). Zirkulationsdynamische Telekonnektivität des Sommerniederschlags im südhemisphärischen Afrika. Dissertation,. *Bayerische Julius-Maximilians-Universität Würzburg*

Preisendorfer, R. (1988). Principal Component Analysis in Meteorology and Oceanography. *Vol 42, Elsevier, Amsterdam*

Pritchard, D.M., Forsythe, N., Fowler, H.J., O'Donnell, G.M., et al., (2019). Evaluation of Upper Indus Near-Surface Climate Representation by WRF in the High Asia Refined Analysis. J Hydrometeorol. https://doi.org/10.1175/JHM-D-18-0030.1

Qiu, J. (2008). China: The third pole,climate change is coming fast and furious to the Tibetan Plateau. *Nature 454*, pp. 393–396. https://doi.org/10.1038/454393a

Rasmussen, R., Baker, B., Kochendorfer, J., Meyers, T., et al., ( 2012). How well are we measuring snow: the NOAA/FAA/NCAR winter precipitation test bed. Bull. Am. Meteorol. Soc. 93, 811–829. https://doi.org/10.1175/BAMS-D-11-00052.1

Rastogi, D., Ashfaq, M., Leung, L., Ghosh, S., et al., (2018). Characteristics of Bay of Bengal Monsoon Depressions in the 21st Century. *Geophysical Research Letters 45(13), pp. 6637-6645* https://doi.org/10.1029/2018GL078756

Ridley, J., Wiltshire, A., Mathison, C. (2013). More frequent occurrence of westerly disturbances in Karakoram up to 2100. doi:10.1016/j.scitotenv.2013.03.074

Saeed, S., Muller, W.A., Hagemann, S.T., Daniela, J. (2010). Circumglobal wave train and the summer monsoon over northwestern India and Pakistan: the explicit role of the surface heat low. *Clim Dyn*. https://doi.org/10.1016/j.scitotenv.2013.03.074

Smirnov, N. (1939). On the estimation of discrepancy between empirical curves of distribution for two independent samples. *Bulletin Mathematique de 'Universite de Moscou , 2*, pp. 3-14

Soman, M.K., and Kumar, K.K. (1993) Space-Time Evolution of Meteorological Features associated with the Onset of Indian Summer Monsoon. Monthly Weather Review,: 121(4). DOI: 10.1175/1520-0493(1993)121<1177:STEOMF>2.0.CO;2.

Soncini, A., Daniele, B., Gabriele, C., Alberto, B. et al., (2015). Future Hydrological Regimes in the Upper Indus Basin: A Case Study from a High-Altitude Glacierized Catchment, J. Hydrometeorol., 16(1), 306–326, https://doi.org/10.1175/JHM-D-14-0043.1

Stone, M. (1979). Comments on Model Selection Criteria of Akaike and Schwarz. *J. R. Stat. Soc. Ser. B Stat. Methodol. 41*, pp. 276-278

Syed, F., Giorgi, F., Pal, J.S., King, M. (2006). Effect of remote forcings on the winter precipitation of central southwest Asia part 1: observations. *Theoret Appl Climatol 86(1–4)*, pp. 147–160. https://doi.org/10.1002/joc.1887

Syed, F.S., Giorgi, F., Pal, J.S., Keay, K. (2010). Regional climate model simulation of winter climate over Central–Southwest Asia, with emphasis on NAO and ENSO effects. *Int. J. Climatol., (30)* , pp. 220–235. https://doi.org/10.1002/joc.1887

Syed, F.S., Iqbal, W., Syed, A.A.B., Rasul, G. (2014). Uncertainties in the regional climate models simulations of south-asian summer monsoon and climate change. Clim Dyn 42(7–8), pp. 2079–2097 Tahir AA, Chevallier P, Arnaud Y, Ahmad B (2011) Snow cover dynamics and hydrological regime of the Hunza River basin, Karakoram Range, Northern Pakistan. Hydrol. Earth Syst. Sci. 15 (7), pp. 2275–2290

Tahir, A.A., Chevallier, P., Arnaud, Y., Ashraf, M. et al., (2014). Snowcover trend and hydrological characteristics of the Astore River basin (Western Himalayas) and its comparison to the Hunza basin (Karakoram region). *Sci. Total Environ. 505*, pp. 748–761. Retrieved from https://doi.org/10.1016/j.scitotenv.2014.10.065

Taylor, K.E. (2001). Summarizing multiple aspects of model performance in a single diagram. J Geophys Res Atmos 106(D7):7183–7192. https://doi.org/10.1029/2000JD900719. (ISSN 2156-2202)

Turner, A.G., and Annamalai, H. (2012). Climate change and the South Asian summer monsoon. *Nat Clim Chang, 2*, pp. 587–595. https://doi.org/10.1038/nclimate1495

Wang, Y., and Xu, X. (2018). Impact of ENSO on the Thermal Condition over the Tibetan Plateau. *J of the meteo. soc. of Japan, Vol (96) No.3* , pp. 269-281. https://doi.org/10.1038/nclimate1495

Wang, Z.,Yang, S., Duan, A., Hua, W.,et al., (2019). Tibetan Plateau heating as a driver of monsoon rainfall variability in Pakistan. *Climate Dynamics, (52)*, pp. 6121–6130. Retrieved from https://doi.org/10.1007/s00382-018-4507-6

Wijngaard, J.B., Klein, T.A.M.G., Können, G.P. (2003). Homogeneity of 20th century European daily temperature and precipitation series. *Int. J. Climatol. (23)*, pp. 679–692. Retrieved from https://doi.org/10.1002 joc.906

Wilks, S. (2006). Statistical methods in the atmospheric sciences. *International Geophysical Series, Vol. 91*

Wiltshire, A.J. (2014). Climate change implications for the glaciers of the Hindu Kush, Karakoram and Himalayan region. *The Cryosphere, 8*, pp. 941–958. https://doi.org/10.5194/tc-8-941

Winiger, M., Gumpert, M., Yamout, H. (2005). Karakorum–Hindukush–Western Himalaya: assessing high-altitude water resources. *Hydrol. Process. 19 (12)*, pp. 2329–2338. Retrieved from https://doi.org/10.1002/hyp.5887

## 9.2 Precipitation Projections Over The Indus River Basin of Pakistan For the 21st Century Using a Statistical Downscaling Framework

Muhammad Saleem Pomee[1,2] and Elke Hertig[1]

[1]Regional Climate Change and Health, Faculty of Medicine, University of Augsburg, Germany

[2]Pakistan Agricultural Research Council (PARC), Islamabad, Pakistan

This article was published in the International Journal of Climatology
(https://doi.org/10.1002/joc.7244)

### Abstract

We estimate future changes in precipitation over the entire Indus basin of Pakistan with a particular focus on the high-elevation Upper Indus Basin (UIB). A statistical downscaling approach is used. We consider the spatial variability of observed precipitation on seasonal scales. Large-scale atmospheric patterns are employed for general circulation model (GCM) selection and subsequent projections. Firstly, we identify the precipitation governing predictors from ERA-Interim reanalysis. We further quantify the robustness of governing predictors against other reanalysis datasets (ERA5 and NCEP-NCAR-II) to assess future projections' fidelity. We perform S-mode Principal Component Analysis on predictor fields and compare loading patterns using Taylor diagrams to assess predictor correspondence between different reanalysis. Similarly, we compare ERA-Interim variables with model-simulated fields during the historical period to select better-performing GCMs and quantify model uncertainty. The regional suitability of available GCMs in our study is also demonstrated.

Ensemble (median) changes in regional precipitation derived through atmospheric fields show an elevation-dependent response of the UIB at representative concentration pathway (RCP) scenarios RCP4.5 and RCP8.5, where increased precipitation will mostly fall at high elevations. However, the positive signals are more distinct during the winter and monsoon seasons, particularly over the central Karakoram. Meanwhile, a decrease in precipitation is robust during the pre-monsoon period, particularly over the northwestern regions. These signals intensify and become more robust during 2071–2100 under RCP8.5, and the better-performing models and signal-to-noise ratios further support this finding. The spatial patterns of projected changes suggest stronger (weaker) and further northward penetrating westerly systems during the winter (pre-monsoon) season. Increased warming will also strengthen monsoon circulations, and these will penetrate further into the northwestern and trans-Himalayan regions. The Lower Indus shows a mixed seasonal response that is more uncertain. The present analysis

provides an alternative perspective to the ongoing research of assessing climate responses in complex regions.

## Keywords

atmospheric patterns, CMIP5, downscaling, model uncertainty, precipitation, reference uncertainty

# 1 Introduction

The Indus River system originates within the massifs of the Hindukush, Karakoram, and Himalayans (HKH), which contains the largest non-polar cryosphere (e.g., Bocchiola et al., 2011; Soncini et al., 2015). The River system provides water, renewable energy, food security, and other ecological services to sustain millions of downstream populations (Archer and Fowler, 2004). Complex processes involving an interplay of synoptic-scale circulations (i.e., the western disturbances and Indian summer monsoon) with HKH topography largely govern precipitation within the Upper Indus Basin (UIB) that varies in space and time, and with elevation (e.g., Hewitt, 2005; Bolch et al., 2012). In contrast, the Lower Indus (LI) has an arid to semi-arid climate and depends heavily upon the meltwater from the UIB (Immerzeel et al., 2015).

Projected global warming and changes in large-scale circulations will impact the Indus hydrology by altering input precipitation and glacier contributions (e.g., De Souza et al., 2015). An increase in water demand due to a rapidly growing population (UN, 2019) and future environmental conditions will also disrupt the hydrological balance at the basin level (e.g., Lutz et al., 2016b). Therefore, a pragmatic assessment of the basin's climate response towards projected global warming is essential to support integrated water management.

Precipitation projections are fundamental to assess future water availability, cryosphere stability, and irrigation demand across the basin. Presently, such projections can only be derived by downscaling, either statistically or dynamically, the output of general circulation models (GCMs, e.g., Wilby et al., 2000). Both downscaling methods have been adopted within the UIB to estimate future precipitation (e.g., Akhtar et al., 2008; Lutz et al., 2016b; Khan and Koch, 2018). Nonetheless, uncertainty about projected precipitation (signal strength and direction, seasonality, spatial patterns, temporal evolution, and cryosphere stability) remains high (e.g., Gebre and Ludwig, 2014; Ali et al., 2015; Khan et al., 2015; Hasson, 2016; Su et al., 2016). Such uncertain scientific feedback can undermine the policy response to minimize the projected vulnerability of a large population.

Most uncertainty in downscaling studies stems from the choice of models (e.g., Heo et al., 2014), how precipitation is derived from these models (Pomee et al., 2020), and adopted observations (e.g., Palazzi et al., 2013). For example, the latest GCMs in the Coupled Model Intercomparison Project Phase 5-

CMIP5 (Taylor et al., 2012) still show major limitations in representing critical dynamic and thermodynamic processes over this complex region (e.g., Sperber et al., 2013; Ashfaq et al., 2017). Regional Climate Models (RCMs) often provide improved simulations, but the evaluation of the CORDEX-SA experiments (e.g., Kulkarni et al., 2013; Mishra, 2015; Hasson et al., 2019) has shown only limited success over this region. Therefore, using an arbitrarily selected single model to simulate precipitation over topographically heterogeneous UIB (e.g., Akhtar et al., 2008; Mahmood and Babel, 2012; Khan et al., 2015) may lack fidelity for regional adaptations.

Model ensembles encompassing a broader uncertainty (e.g., Gleckler et al., 2008; Sperber et al., 2013) are more useful for such complex regions. Nevertheless, the selection of representative models is a challenge due to rapidly growing climate models. For example, the CMIP3 (Meehl et al., 2007) contains 25 GCMs, whereas more than 60 GCMs are available in the CMIP5 archive. Different model ranking metrics are available for ensemble selections. For instance, the past performance criterion identifies models demonstrating better skills in reproducing past climate (e.g., Christensen et al., 2010; Biemans et al., 2013). The so-called envelope approach only considers the range of projected changes in the variable(s) of interest during ensemble selections (e.g., Sorg et al., 2014; Warszawski et al., 2014). Some- times both approaches are combined to select models that better simulate the observations and encompass broader future evolutions (e.g., Giorgi and Mearns, 2002; McSweeney et al., 2015). Issues like subjective decisions during the model rankings, the choice and effectiveness of performance metrics, and inter-model similarities can still induce uncertainty in these ensembles (e.g., Knutti et al., 2017). Therefore, a thoughtful model selection to better serve the intended objectives is still an ongoing research challenge.

Within the UIB, some studies used ensemble approaches by either using the past performance (e.g., Hasson, 2016) or a combination of future spread and past simulations (e.g., Immerzeel et al., 2013; Lutz et al., 2016a; Khan and Koch, 2018). However, using precipitation for model ranking and subsequent projections remains common, which may induce significant uncertainties since even the latest GCMs do not reliably simulate precipitation due to complex generating mechanisms and high spatiotemporal variability (Trigo and Palutikof, 2001; Mueller and Seneviratne, 2014). Such model deficiencies further manifest over high-mountain regions like the UIB, where orography causes additional precipitation variability. Without long-term, reliable, and consistent observations to account for regional orography of the UIB (e.g., Immerzeel et al., 2015; Pomee et al., 2020), even the bias-corrected model precipitation may lack reliability.

While additional data availability is still an ongoing issue, the methodological considerations can reduce some uncertainties. For instance, using large-scale atmospheric fields instead of precipitation to develop downscaling models offers one such promising alternative. The latest GCMs show better skills in simulating these patterns than raw precipitation output (e.g., Kaspar-Ott et al., 2019). We used such

atmospheric variables for precipitation analysis over the entire Indus basin by focusing on the UIB. Firstly, we identify precipitation-governing variables from ERA-Interim reanalysis within a robust statistical downscaling framework by accounting for seasonality and spatial variability of the observed precipitation. For GCM ranking, we quantify the correspondence between ERA-Interim predictors and corresponding CMIP5- simulations during the historical period using Taylor diagrams (Taylor, 2001). During GCM selection, we also consider predictor influence on precipitation by weighing the GCM predictors with downscaling models' regression coefficients. The sub-regional approach further helps to evaluate model performance over multiple regions. Given the regional complexity, we also evaluate ERA-Interim predictors' robustness against two additional reanalysis datasets (NCEP-NCAR-II and ERA5) to quantify the reference uncertainty. Finally, we use governing predictors to derive ensemble precipitation changes over the study basin for selected radiative-forcing scenarios. We also evaluate the robustness of the change signals by using a signal-to-noise ratio (SNR). The extension of analysis further to the LI helps to analyze the supply-demand perspective for water management at the basin scale.

In summary, we consider predictor (multiple reanalyses), predictand (homogeneous and long time series stations), and GCM (ensemble) levels to provide a more realistic precipitation assessment for the Indus basin during the 21st century. To our knowledge, such fine-scale analysis has never been performed in this region, and hence a different simulation perspective is provided. Our methodology can also facilitate climate assessment studies elsewhere.

## 2 Study Area

The present study focuses on the Indus basin of Pakistan, covering an area of 1.31 million $km^2$ (FAO, 2011), which ultimately drains into the Arabian Sea (**Figure 1a**). Although the Indus River system originating within high-mountains of the HKH region also shares its UIB ($4.03 \times 10^5$ $km^2$, Dahri et al., 2018) with China, India, and Afghanistan (**Figure 1b**), we could not include these regions in our analysis due to constraints on updated data availability. The Indian summer monsoon, western disturbances, and the Tibetan anticyclone (e.g., Wake, 1989) largely govern the basin-wide precipitation that varies significantly over the UIB. Besides, moisture recycling within the Indian subcontinent and HKH region also plays a significant role in annual precipitation (e.g., Curio and Scherer, 2016). The LI (0.72 million $km^2$) depends heavily on seasonal water supplies from the UIB.

## 3 Data and Methodology

This study builds on previous work (Pomee et al., 2020), where predictor-predictand relationships are used to model observed precipitation at sub-regional scales over the study basin. The present study concentrates on quantifying reference uncertainties, GCM ranking, and precipitation downscaling results under future climate change constraints using previously identified predictors and seasonal precipitation characterization of the basin. In the following sections, we provide a brief description of

the data, the adapted regionalization scheme, and the model development process to give the necessary background. More detailed information can be found in Pomee et al. (2020).

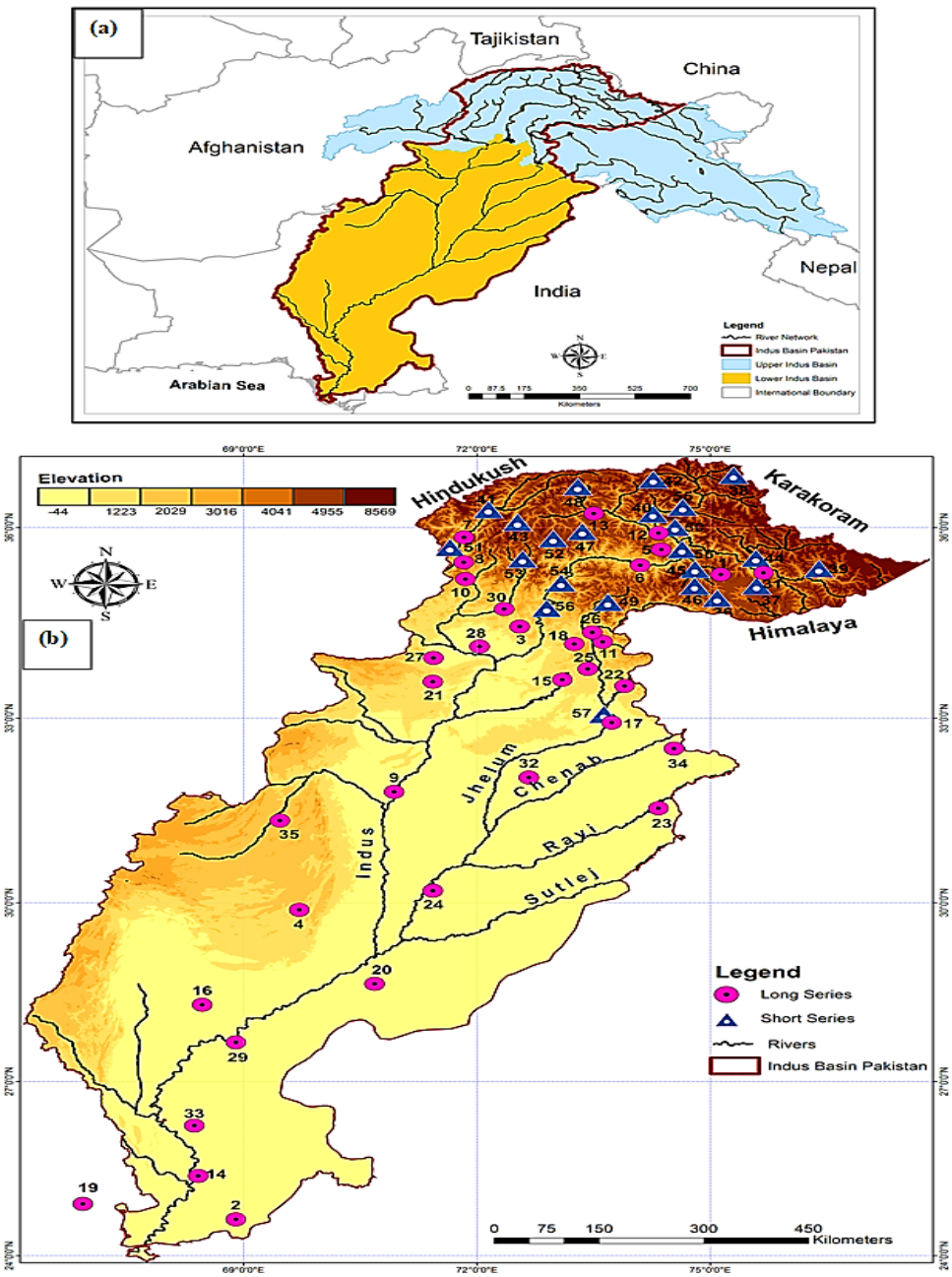


Source: Adapted from Pomee et al. (2020)

**Figure 1. (a).** The Transboundary Indus River basin and demarcation of the study area, where the shading differentiates between the Upper Indus Basin and Lower Indus regions. **(b)** The locations of the meteorological stations (numbered) used in our study. The circles represent the long time series (1979-2015), and triangles show the recent high-altitude stations with shorter series (1994-2015). Note that the shading scheme in **(b)** represents the altitudinal variations (elevations above mean sea level) within the study basin. **Table 1** of the **Supporting Information** provides more information about these stations.

## 3.1 Precipitation: Data and Regionalization

We use monthly precipitation time series of 58 meteorological stations located across the study basin (**Figure 1b**). These stations provide historical (35 stations, 1979–2015) and relatively short-term data (23 stations, 1994–2015) over the lower-elevation and high-elevation (HA) regions of the UIB, respectively. The HA stations (average data length of 17 years) have considerably expanded spatial-altitudinal coverage within the UIB to provide valuable insights about regional orography that governs the basin hydrology. Most study stations are located in the UIB to account for topographic complexity and its significance for Indus flows. More information about the study stations is available in **Table S1**.

Based on observations, we identify three major precipitation seasons for further analysis. These include the winter season-WS (DJFM), pre-monsoon-PMS (AMJ), and monsoon season-MS (JAS), respectively. We group the time series of study stations into these seasons and check data for completeness (Moberg et al., 2006). We use four different statistical procedures to test the homogeneity of the time series after Wijngaard et al. (2003).

We employ K-means cluster analysis on all 58 stations to identify precipitation regions with similar covariance using Spearman correlation as a distance measure (Wilks, 2006). We set the objective function during clustering to maximize (minimize) correlation within (across) the regions to define sharp regional boundaries. Considering more uncertainty over the HA, we perform another regionalization experiment covering only elevated parts of the UIB. Our regionalization schemes identify, on average, four precipitation clusters within the UIB, accounting for the high spatial variability. These regions represent precipitation dynamics in the southern Himalayans, trans-Himalayans (including the Karakoram), and northwestern parts of the UIB during each season. Besides, on average, two regions describe LI precipitation variability. Regional representative (RR) stations for each precipitation cluster are selected through multiple considerations (including homogeneity) and serve as predictands. The seasonal precipitation regionalizations for both experiments are shown in **Figures 2 and 3.**

## 3.2 Predictors: Data and Principal Component Analysis (PCA)

We use variables from ERA-Interim reanalysis (Dee et al., 2011) at different pressure levels to identify major dynamic and thermodynamic drivers of regional precipitation. We consider a larger domain for circulation-dynamic variables (10–100° E, 10–60° N, spatial resolution (2° × 2°) compared to the domain for thermodynamic fields (64–80° E, 22–40° N) to account for large-scale dynamical and more localized thermodynamic influences on precipitation. We did not use ERA5, as its data was not publically available at the beginning of our research in early 2016.

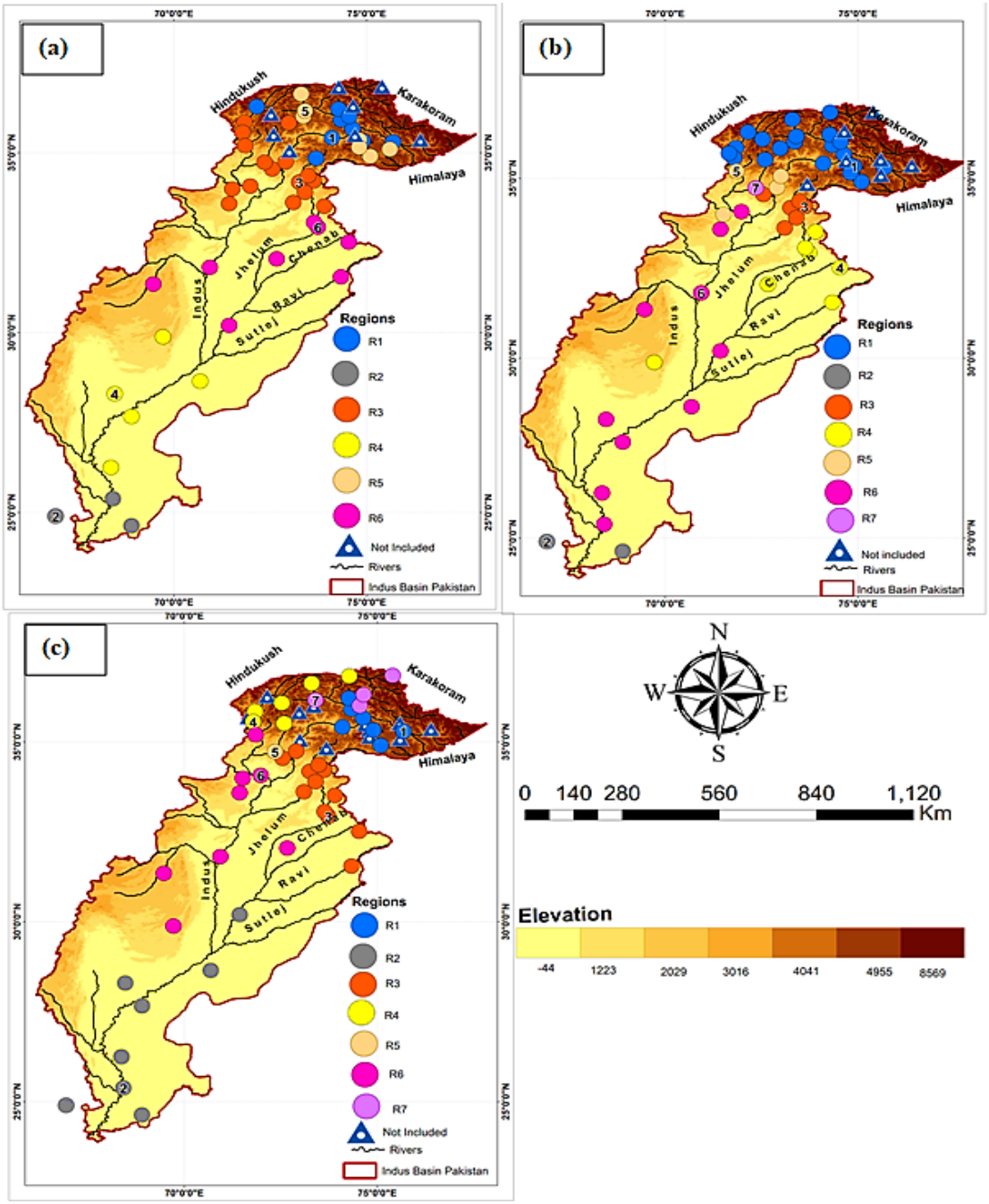


Source: Adapted from Pomee et al. (2020)

**Figure 2.** Precipitation regionalization of the entire Indus Basin of Pakistan using K-means cluster analysis on seasonal scales. Different colors represent the identified regions. The circles with the same color show similar precipitation variability and thus belong to one precipitation region. The numbered circles indicate the location of regional representative (RR) stations of the respective precipitation regions. Triangles represent those stations that could not be clustered to any of the identified precipitation regions. The WS **(a),** PMS **(b),** and MS (c) regionalization.

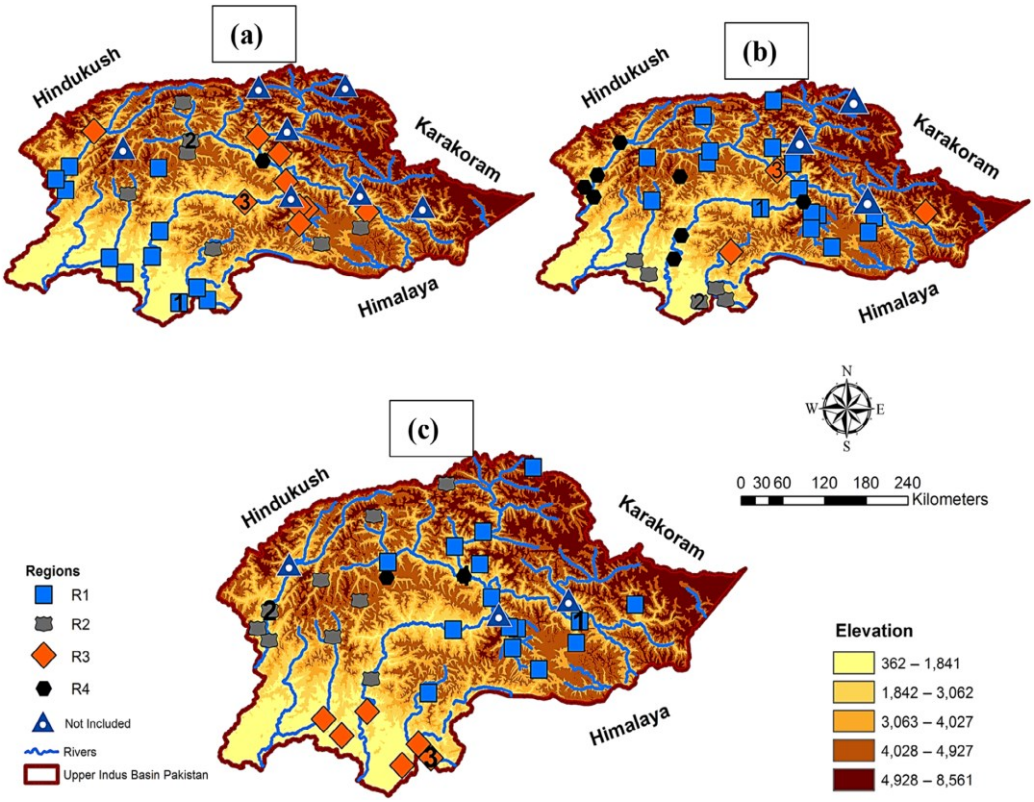


Source: Adapted from Pomee et al. (2020)

**Figure 3.** Same as **Figure** 2 but showing the seasonal precipitation regions identified under the HA-UIB regionalization experiment.

We perform S-mode Varimax-rotated Principal Component Analysis (S-mode PCA) on each predictor field for dimension reduction (e.g., Preisendorfer, 1988). Following the modified dominance criterion (Philipp, 2003) with some additional constraints (Pomee et al., 2020), we retain a maximum of 20 PCs to explain the predictor variance adequately. The resulting PC scores serve as predictor time series, and corresponding PC loadings define the centers of predictor variations.

## 3.3 Generalized Linear Models and Statistical Downscaling Framework

We adopt a generalized linear model (GLM) framework (McCullagh and Nelder, 1989) to model predictor-predictand relationships within a robust cross-validation setting. For those predictand cases containing exact zeros in their time series, Tweedie exponential dispersion models (e.g., Dunn, 2004) and otherwise GLM gamma models are used. We use mean squared error skills scores (MSESS) as a performance criterion (Wilks, 2006) and consider multicollinearity among predictors to identify predictor combinations that best resolve the observed precipitation. The information about identified governing predictors and the regression models' statistical performance is provided in **Tables 1, S2, and S3**, respectively. **Appendix S1** provides details of the downscaling framework after Pomee et al. (2020).

## 3.4 GCMs: Data and Precipitation Downscaling

We first consider all CMIP5 GCMs (Taylor et al., 2012). However, the availability of governing predictors (Table 1) in the historical period restricts this number to 29. Due to high mountains in our study domain, only eight of those 29 GCMs could provide complete spatial coverage of the required predictors. Many GCMs do not provide spatially complete lower-tropospheric predictors over the high mountains due to the intersection of pressure coordinates with mountain elevations. These spatial inconsistencies may emerge as many modeling centers avoid employing any vertical interpolation (or extrapolation) algorithms over the mountain regions when transforming data from the model to pressure levels. These data gaps are too large to be effectively filled with an interpolation scheme at the end-user level and restrict the computation of spatially consistent historical and future predictor PCAs. Therefore, we could only analyze the output of eight models during the historical (1976–2005) and two future time periods, covering the mid (2041–2070) and end-of-the 21$^{st}$ century (2071–2100) for precipitation downscaling. We could not consider model independence (e.g., Sanderson and Wehner, 2017) in detail due to the smaller ensemble but investigated its influence over a sample region in Section 4.3.

We consider RCP4.5 and RCP8.5 scenarios for precipitation projections. RCP4.5 portrays a future where technological advancements will help stabilize greenhouse gas emissions after 2,100. Conversely, RCP8.5 depicts a populous world without abatement efforts where radiative forcing reaches a maximum of 8.5 watts/m2 in 2100 (Van Vuuren et al., 2011). These RCPs cover a plausible range of radiative forcing (Sanford et al., 2014) to support adaptations and comparison with previous studies. We only consider the first realization ('r1i1p1') of these GCMs during the historical and future periods. **Table 2** provides information on the CMIP5 models used in our study. Before downscaling, the GCM data is conservatively re-gridded ($2^o \times 2^o$) to match the adopted ERA-Interim resolution. The modeled predictors are standardized over the historical and future time-slices (separately for each scenario) and then projected onto the corresponding loading patterns of the ERA-Interim variables to generate new predictor time series (more details on this method are available in Von Storch and Zwiers, 1999). These new predictor time series are used in the regression models (**Tables S2 and S3**) to derive downscaled historical and projected precipitation totals. The difference between downscaled precipitation during the historical and two future time-slices (separately for each RCP and time slice) is used to compute median precipitation changes across the basin.

We further evaluate the robustness of projected change signals in light of observational uncertainty by computing a signal-to-noise ratio (SNR). The ratio uses median precipitation changes (signal) simulated by the individual models and their ensembles and corresponding standard deviations of the historical period (noise). SNR >1 indicates that the change signal exceeds the internal climate variability.

**Table 1.** The predictor frequency (in %) in final seasonal precipitation models for different sub-regions of Pakistan's Indus Basin. Column 1 provides the list of large-scale predictors used in this study where zg, va, ua, hur, hus, and psl denote geopotential heights, meridional wind, zonal wind, relative humidity, specific humidity and, mean sea level pressure fields, respectively. The number after each predictor reflects the atmospheric level (pressure level in hPa). Columns 2–4 represent the seasonal frequencies of different predictors chosen to resolve observed precipitation dynamics over the study basin. The last column shows the average predictor frequencies over different seasons.

| **Predictors**<br><br>**(1)** | **WS (%)**<br><br>**(2)** | **PMS (%)**<br><br>**(3)** | **MS (%)**<br><br>**(4)** | **Basin-Wide Seasonal Average (%)**<br>**(5)** |
|---|---|---|---|---|
| **va200** | 20.0 | 19.4 | 32.5 | 24 |
| **ua200** | 0.0 | 0.0 | 2.5 | 0.8 |
| **zg200** | 0.0 | 0.0 | 0.0 | 0.0 |
| **zg500** | 0.0 | 0.0 | 0.0 | 0.0 |
| **zg700** | 20.0 | 0.0 | 0.0 | 6.7 |
| **hus700** | 0.0 | 0.0 | 2.5 | 0.8 |
| **hur 700** | 0.0 | 9.7 | 0.0 | 3.2 |
| **hur1000** | 8.6 | 16.1 | 2.5 | 9.1 |
| **hus1000** | 5.7 | 0.0 | 0.0 | 1.9 |
| **va500** | 0.0 | 0.0 | 2.5 | 0.8 |
| **ua500** | 0.0 | 0.0 | 2.5 | 0.8 |
| **ua700** | 14.3 | 0.0 | 0.0 | 4.8 |
| **va700** | 0.0 | 22.6 | 0.0 | 7.5 |
| **va850** | 31.4 | 12.9 | 52.5 | 32.3 |
| **ua850** | 0.0 | 19.4 | 0.0 | 6.5 |
| **psl** | 0.0 | 0.0 | 2.5 | 0.8 |
| **Total** | **100** | **100** | **100** | **100** |

Source: Pomee et al. (2020).

**Table 2.** The CMIPP5-GCMs used for precipitation analysis in this study

| No. | Model ID | Horizontal Resolution (Lon x Lat) in degrees | Modeling Centre | Key Reference |
|---|---|---|---|---|
| *1* | CMCC-CMS | 1.875 x 1.875 | CMCC | Davini et al. (2013) |
| *2* | CMCC-CM | 0.75 x 0.75 | CMCC | Scoccimarro et al. (2011) |
| *3* | CNRM-CM5 | 1.40625 × 1.40625 | CNRM-CERFACS | Voldoire et al. (2013) |
| *4* | Can-ESM2 | 2.8125 × 2.8125 | CCCMA | Arora et al. (2011) |
| *5* | MPI-ESM-LR | 1.875 × 1.875 | MPI-M | Giorgetta et al. (2013) |
| *6* | MPI-ESM-MR | 1.875 × 1.875 | MPI-M | Giorgetta et al. (2013) |
| *7* | Nor-ESM-ME | 2.5 × 1.9 | NCC | Bentsen et al. (2013) |
| *8* | Nor-ESM-M | 2.5 × 1.9 | NCC | Bentsen et al. (2013) |

## 3.5 GCM Ranking Process

A stepwise procedure is used to rank the GCMs according to their ability to simulate precipitation-governing variables of the ERA-Interim reanalysis during the historical period. ERA-Interim reanalysis provides simulations from 1979 onwards; hence, we could only compare the reference-model predictors during the overlapping historical period (1979–2005).

(I) Initially, S-mode PCA is performed (Section 3.2) for every governing predictor (Table 1) of each individual GCMs to extract the same number of PCs as from ERA-Interim.

(II) Subsequently, the model PC loadings are compared with corresponding ERA-Interim loadings (separately for each GCM) using Taylor diagrams. A simple performance score (PS) derived using two of the three summary statistics of Taylor diagrams is computed to quantify the predictor correspondence. Mathematically, the PS is:

$$PS = |CR| - |NSD - 1| \qquad (1)$$

Where,

PS = performance score. For a perfect predictor agreement, PS = 1. CR = pattern correlation between the reference (ERA-Interim) and model (GCM) loadings. For a perfect phase match, CR = 1.
NSD = normalized ratio of variance (standard deviation of the reference and model loadings). Ideally, the NSD should also take the value 1.

Under ideal conditions, the PS will attain its highest unit value due to maximization of the phase correspondence (i.e., CR = 1), and the same magnitude of predictor spread (i.e., the term NSD – 1) becomes zero) between the reference and model simulations. Similarly, a smaller PS value will show a weaker predictor correspondence. The PS magnitude will also intuitively influence the third summary statistics (i.e., standardized RMSE), where its maximum value (PS = 1) will ensure zero error. Conversely, the smaller values (PS <1) will reflect higher errors, though not following a clear linear trend due to the typical relationship among these three summary statistics (see Taylor, 2001). Thus, the PS contains useful information about the strength of correspondence between the reference and model-simulated fields and can be used to identify the best-matching pairs for every governing predictor.

(III) We draw two separate sets of Taylor diagrams for each precipitation region and season. In the first set of diagrams, a given reference PC is compared with all modeled PCs (separately for each GCM) to compute the corresponding PS. The reference-model pair demonstrating the maximum PS among all PCs of a GCM is selected as the best GCM-PC for that particular reference. Thus, each GCM has one best corresponding PC for a given reference. This process is repeated for all other PCs and predictors of the regression models. Subsequently, all best-matching (individual) PCs of different predictors are grouped into the second set of Taylor diagrams (separately for each GCM) to assess the ability of individual GCMs in representing ERA-Interim precipitation-governing predictors over a region. The summary statistics of the second Taylor diagrams are used to compute the average unweighted PS for each GCM. The PS is termed unweighted due to equal PC weighting in the computation.

(IV) Given that each PC has a different influence in a regression model, we further adopted (absolute) regression coefficients of the PCs as weights and computed the weighted PS. Thus, a model with the highest (lowest) weighted PS score can be identified as the best (worst) GCM due to its improved (poor) simulations for more important predictors. This process (Step I–IV) is repeated for all sub-regions to identify the best regional GCM in different seasons.

(V) Finally, we consider GCM performance over multiple regions to identify models that show superior simulations over the whole spatial scales of the UIB and LI, respectively. We prefer a GCM demonstrating better simulations over multiple sub-regions. Spatial consideration is

important since an outlier may strongly influence a model's overall PS (e.g., very high PS just over one sub-region).

### 3.5.1 GCM ranking: an example

We demonstrate the above procedure over a sample WS region (R6). Six PCs from two different predictors (hur1000 and zg700) were selected to skillfully resolve observed precipitation over this region **(Table S2).** We represent these as reanalysis predictors 1 (R1) and 2 (R2), respectively, and construct three different sets of Taylor diagrams to illustrate each selection step. Firstly, the Taylor diagrams (**Figure 4**) visually outline the best-matching pairs of the reanalysis PC1 of the first predictor, that is, hur1000 ('R1.1'), and modeled PCs of this predictor for every GCM. We use these Taylor diagrams' statistics to identify the best PC match (for every GCM) using the PS and plot them through the second set of Taylor diagrams (**Figure 5**). We repeat this process for the remaining five PCs to identify the best-matching pairs for each GCM (not shown). Subsequently, we group all six best-matching pairs of each GCM into a third set of Taylor diagrams (**Figure 6**). Finally, we compute the weighted PS (from the statistics of **Figure 6**) using regression coefficients (absolute) as weights to identify the best-performing model. In this example, CMCC-CM appears as the best model due to its highest average PS of 0.78 (see **Table 3**).

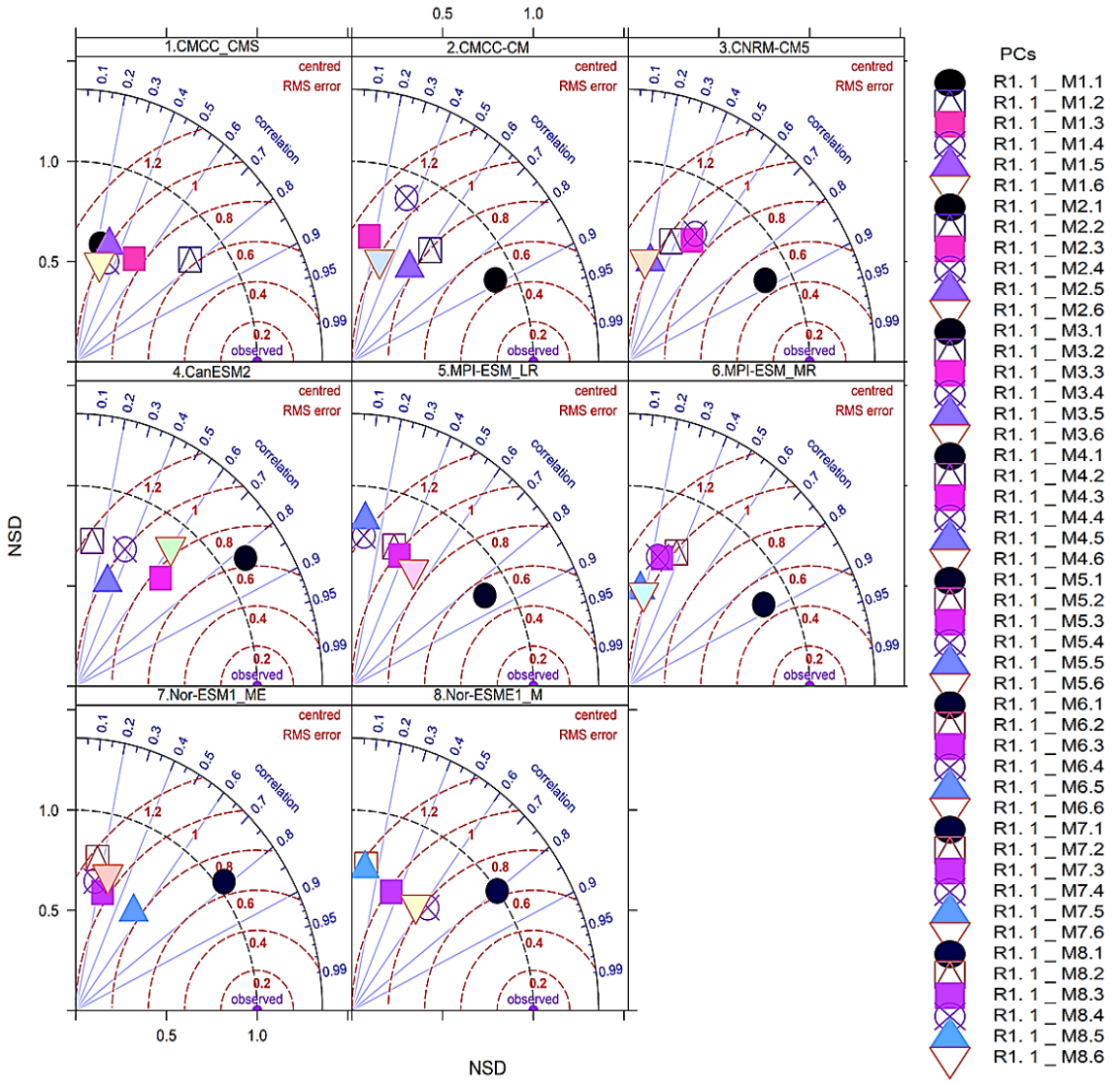


**Figure 4.** Identification of the best-matching pairs of the reference (ERA-Interim) and model (GCMs) simulated PCs of a given predictor using Taylor diagrams. Each Taylor diagram elaborates the PC matching process separately for each GCM by comparing all modeled PCs of a predictor field with a given reference PC. In this example, we use reanalysis PC1 of hur1000 to identify the best matching PC of hur1000 as simulated by different GCMs. The letter R (M) and associated numbers represent the reference (model) related PC information for a given predictor field in the legend key. For instance, in the text 'R1.1', the letter 'R1' stands for the first reference predictor (i.e., hur1000), and the following number ('.1') reveals the identification of its PC (i.e., PC1 of hur1000). Similarly, in the text 'M1.1', the letter 'M1' and the following number ('.1') show the first GCM (CMCC_CM) and the identification of its simulated PC (i.e., PC1) of the predictor field (i.e., hur1000), respectively. Likewise, The letter 'M2.6' shows the second GCM (CMCC_CMS) and its simulated PC (i.e., PC6). Thus, identifying the modeled PC that best corresponds to PC1 of the reanalysis predictor (hur1000) can be seen in each of

the above Taylor diagrams. In the case of GCM4 (CanESM2), among all six modeled PCs, its first PC (M4.1) better corresponded to the given reanalysis PC (R1.1)

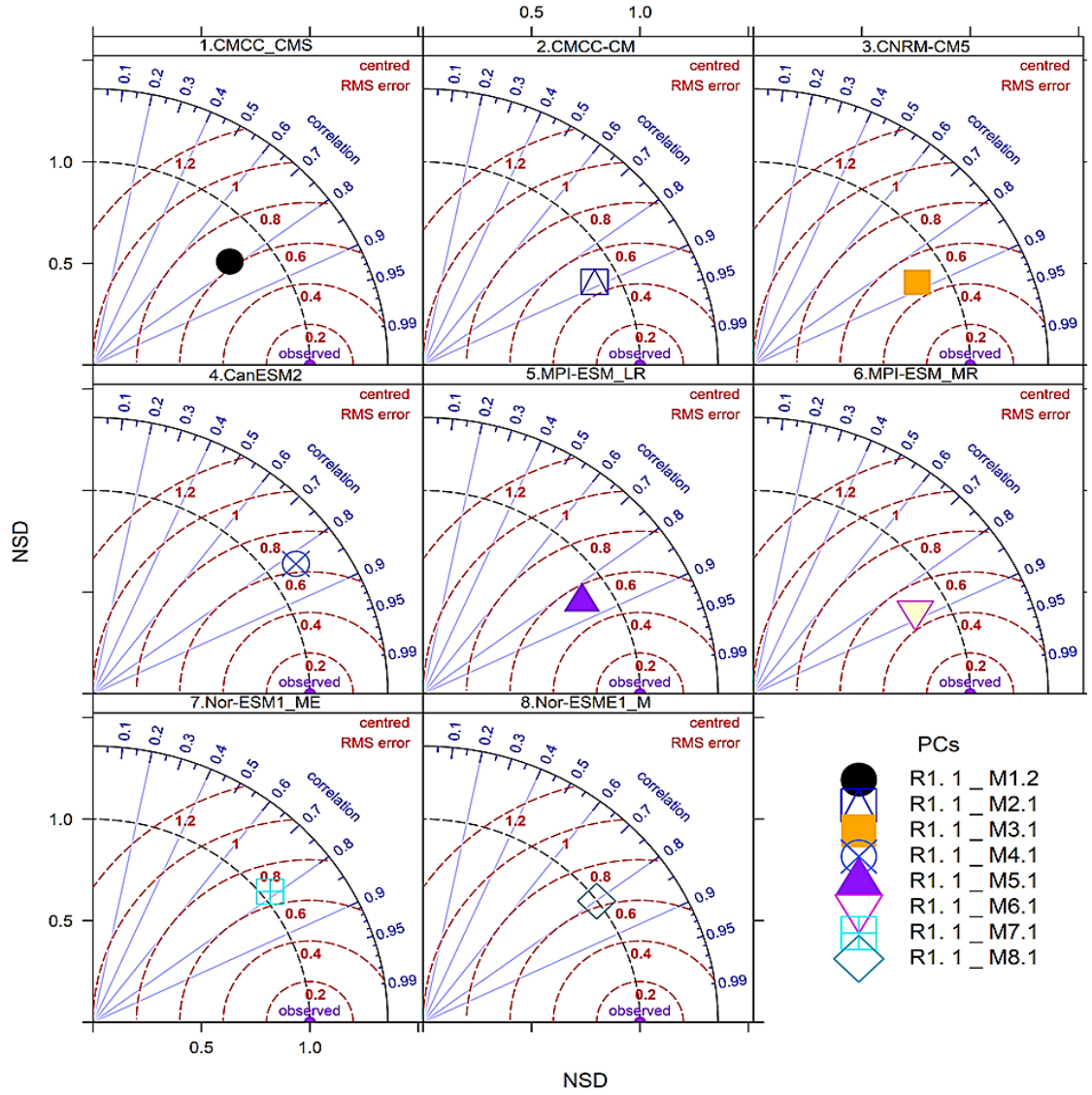


**Figure 5**. Effectiveness of the PS in identifying the best reference-model PC combinations of **Figure 4.** The other details are the same as **in Figure 4**. The statistics of **Figure 4** are used to compute the PS for all modeled PCs (separately for each GCM). The model simulated PC that shows the maximum PS is identified and plotted through separate Taylor diagrams of **Figure 5**. As the best PCs in **Figures, 4 and 5** are precisely the same; therefore, the PS can be used to identify such pairs numerically.

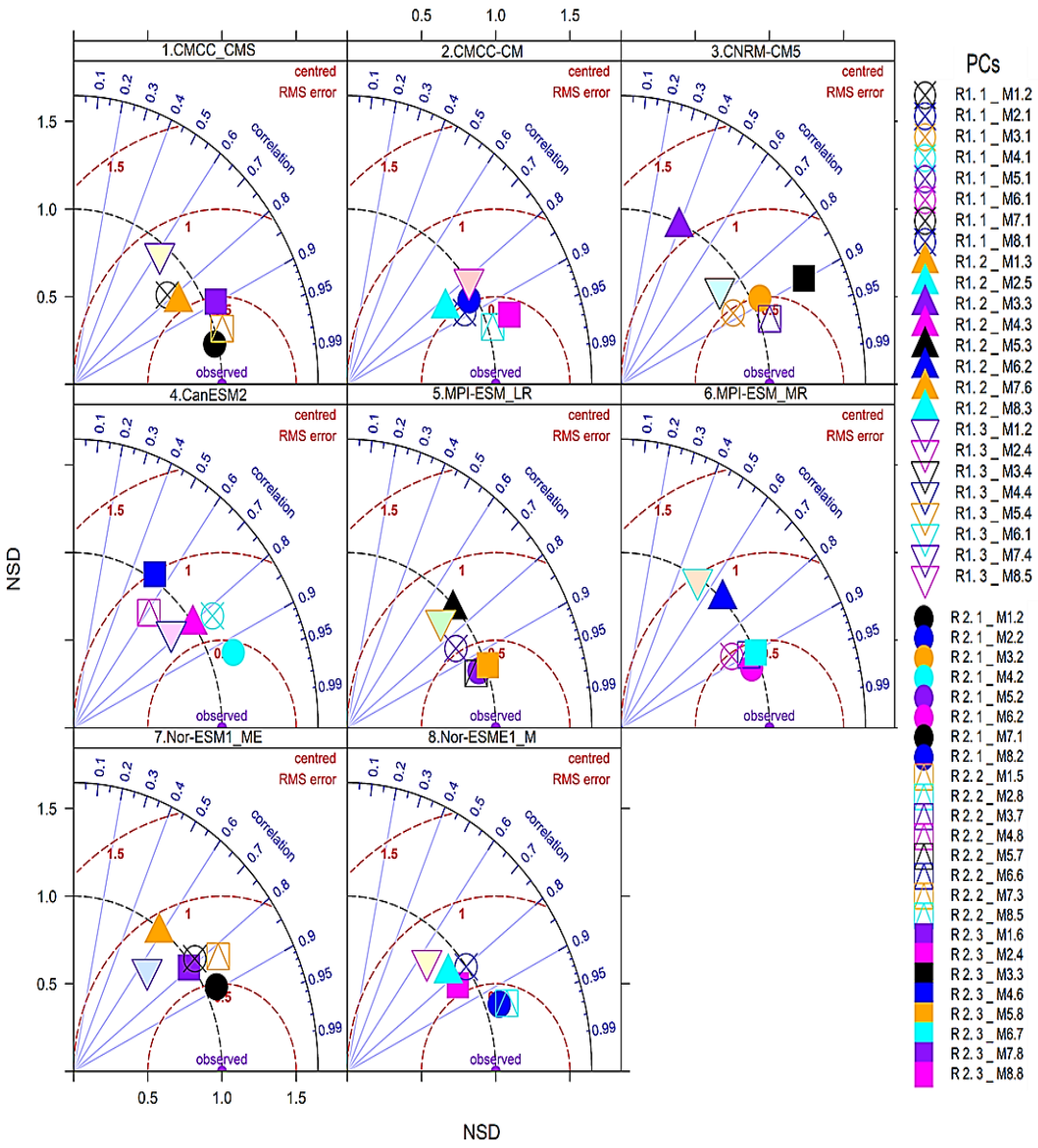


**Figure 6.** Final Taylor diagrams representing all six modeled PCs (separately for each GCM) of the two governing predictors (i.e., R1 = hur1000 and R2 = zg700) that show maximum correspondence with ERA-interim simulated PCs. The statistics of these Taylor diagrams are used to compute the PS, and the model that shows the maximum weighted PS (across all six PCs) can be identified as the best model. In this example, GCM2 (CMCC-CM) shows the highest PS (see Table 3) and is hence selected as the best GCM for this particular WS region. Visual inspection of these Taylor diagrams also confirms this selection, where its modeled PCs show higher correspondence with reanalysis data than other GCMs.

## 3.6 Quantification of Reference Uncertainty

We further consider governing predictors **(Table 1)** from the latest ERA5 (Hersbach et al., 2020) and from NCEP- NCAR-II (Kalnay et al., 1996) reanalysis datasets to evaluate the usefulness of ERA-

Interim for precipitation modeling. After re-griding to a common spatial resolution ($2^o \times 2^o$), the predictors from these additional reanalysis datasets were subjected to a similar S-mode PCA. The resulting PC loadings are compared (separately for each reanalysis) with ERA-Interim using the procedure described in Section 3.5 (without Step V). Thus, the weighted PS of these other two reanalyses can define the range and average magnitude of reference uncertainty.

# 4 Results and Discussion

## 4.1 Reference Uncertainty

**Table 3** quantifies the strength of ERA-Interim predictors' correspondence with the other two reanalysis datasets (ERA5 and NCEP-NCAR-II) and each available GCM in different precipitation seasons. The regions are grouped into the UIB and LI scales to estimate ERA-Interim predictors' spatial effectiveness (uncertainty) against each dataset by computing average PS over these two regions.

First, we use the output of **Table 3** to quantify reference uncertainty. Generally, the three reanalysis datasets indicate more robust simulations of the various dynamic drivers compared to the thermodynamic drivers of regional precipitation (**Table 1**). The reliability of ERA-Interim predictors varies with season, reanalysis, and over the regions. For example, ERA-Interim predictors show more robust correspondence with ERA5 (NCEP- NCAR-II) over five different UIB regions during the MS, as indicated by a higher average PS of 0.84 (0.72). Considering the mountainous terrain and MS complexity, represented by a set of diverse predictors located across the troposphere (see Table S1), the strong predictor correspondence justifies ERA-Interim use for precipitation modeling over the UIB. Similar predictor robustness is noticed over two LI regions (ERA5 = 0.81 and NCEP-NCAR-II = 0.70) and demonstrates the ERA-Interim predictors' reliability for the basin-wide MS precipitation analysis.

ERA-Interim also shows strong predictor similarities with ERA5 and NCEP-NCAR-II during the WS (0.83 and 0.74) and PMS (0.76 and 0.71) over multiple UIB regions. A similar predictor correspondence over different LI regions during these two seasons further highlights the effectiveness of ERA-Interim for westerly-dominated regimes. Although governing predictors are robust among different reanalyses datasets, still some interesting patterns emerge. For example, free atmospheric predictors that largely dominate the seasonal precipitation models (e.g., MS-R3, PMS-R1, and WS-R1 in **Table S2**) show more similarities among reanalysis datasets, partly because the atmospheric boundary layer exerts lesser influence over these predictors, and most of the predictor PCs are located outside the mountain region (not shown). Therefore, their simulations are more robust across different numerical models. Conversely, the simulations of near-surface predictors (notably hur1000) show larger differences (e.g., PMS-R6 and WS-R6), which may arise due to the stronger influence of the atmospheric boundary layer.

**Table 3.** Quantification of the reference and model predictor correspondence on seasonal scales across the Indus Basin of Pakistan using weighted PS. The reference correspondence is estimated by comparing ERA-Interim patterns with ERA5 and NCEP-NCAR-II reanalysis datasets separately to evaluate their effectiveness for precipitation modeling. Columns 1 and 2 give the sub-regions of the basin for each season. Avg. PS, UIB (Avg. PS, LI) shows the average PS across all individual regions within the UIB (LI) in different seasons. Similarly, Avg. Uncer., UIB (Avg.Uncer., LI) outlines the magnitude of predictor uncertainties ((1 − weighted PS) *100) in percentage over the UIB (LI) scales, respectively. The blue (bold), brown (italic bold), and yellow (italic) shades represent the best, second best, and worst models with respect to their predictor correspondence with ERA-Interim.

| Seasons | Regions | Reanalysis | | GCMs | | | | | | | |
|---|---|---|---|---|---|---|---|---|---|---|---|
| | | ERA5 | NCEP-NCAR II | CMCC-CMS | CMCC-CM | CNRM-CM5 | Can-ESM2 | MPI-ESM-LR | MPI-ESM-MR | Nor-ESM1-ME | Nor-ESM1-M |
| MS | UIB | | | | | | | | | | |
| | R1 | 0.76 | 0.59 | **0.40** | 0.30 | ***0.37*** | 0.33 | 0.31 | *0.13* | 0.36 | 0.20 |
| | R3 | 0.96 | 0.82 | **0.70** | 0.56 | 0.58 | 0.40 | *0.38* | 0.54 | ***0.66*** | 0.62 |
| | R4 | 0.91 | 0.76 | ***0.53*** | 0.52 | 0.45 | 0.41 | 0.36 | 0.51 | *0.36* | **0.58** |
| | R5 | 0.77 | 0.67 | 0.41 | **0.53** | 0.45 | 0.38 | ***0.46*** | 0.39 | 0.41 | *0.37* |
| | R7 | 0.81 | 0.74 | 0.48 | ***0.52*** | **0.55** | 0.43 | 0.40 | 0.45 | *0.35* | 0.42 |
| | *Avg. PS, UIB* | ***0.84*** | ***0.72*** | **0.50** | ***0.49*** | 0.48 | 0.39 | *0.38* | 0.40 | 0.43 | 0.44 |
| | *Avg. Uncer., UIB (%)* | ***16*** | ***28*** | ***50*** | ***51*** | ***52*** | ***61*** | ***62*** | ***60*** | ***57*** | ***56*** |
| | LI | | | | | | | | | | |
| | R2 | 0.87 | 0.79 | 0.50 | 0.42 | ***0.62*** | 0.33 | **0.69** | 0.56 | 0.45 | *0.30* |
| | R6 | 0.75 | 0.60 | ***0.37*** | **0.41** | 0.36 | *0.26* | 0.34 | 0.36 | **0.41** | 0.40 |
| | *Avg. PS, LI* | ***0.81*** | ***0.70*** | ***0.44*** | ***0.42*** | ***0.49*** | ***0.30*** | ***0.52*** | ***0.46*** | ***0.43*** | ***0.35*** |
| | *Avg. Uncer., LI (%)* | ***19*** | ***31*** | ***57*** | ***59*** | ***51*** | ***71*** | ***49*** | ***54*** | ***57*** | ***65*** |
| PMS | UIB | | | | | | | | | | |
| | R1 | 0.88 | 0.74 | ***0.53*** | 0.52 | 0.54 | **0.57** | 0.51 | 0.43 | *0.41* | 0.44 |
| | R3 | 0.84 | 0.69 | 0.28 | 0.4 | ***0.41*** | **0.45** | 0.35 | 0.39 | 0.35 | *0.24* |
| | R5 | 0.69 | 0.71 | 0.69 | 0.73 | **0.78** | *0.47* | ***0.75*** | 0.71 | 0.49 | 0.57 |
| | R7 | 0.64 | 0.70 | ***0.72*** | 0.71 | 0.71 | *0.46* | **0.75** | 0.69 | 0.48 | 0.6 |
| | *Avg. PS, UIB* | ***0.76*** | ***0.71*** | ***0.56*** | ***0.59*** | ***0.61*** | ***0.49*** | ***0.59*** | ***0.56*** | ***0.43*** | ***0.46*** |
| | *Avg. Uncer., UIB (%)* | ***24*** | ***29*** | ***45*** | ***41*** | ***39*** | ***51*** | ***41*** | ***45*** | ***57*** | ***54*** |
| | *LI* | | | | | | | | | | |
| | R4 | 0.92 | 0.89 | 0.59 | 0.61 | **0.5** | **0.72** | *0.59* | 0.61 | 0.58 | ***0.64*** |
| | R6 | 0.60 | 0.61 | ***0.66*** | 0.64 | 0.63 | 0.38 | **0.72** | 0.63 | *0.36* | 0.49 |
| | *Avg. PS, LI* | ***0.76*** | ***0.75*** | ***0.63*** | ***0.63*** | *0.57* | *0.55* | ***0.66*** | ***0.62*** | ***0.47*** | *0.57* |
| | *Avg. Uncer., LI (%)* | ***24*** | ***25*** | ***38*** | ***38*** | ***44*** | ***45*** | ***35*** | ***38*** | ***53*** | ***44*** |
| WS | UIB | | | | | | | | | | |
| | R1 | 0.89 | 0.72 | 0.58 | 0.60 | ***0.62*** | 0.48 | **0.69** | 0.46 | 0.51 | *0.42* |
| | *R3* | 0.84 | 0.73 | 0.56 | **0.67** | 0.46 | 0.48 | ***0.64*** | 0.45 | 0.31 | *0.30* |
| | R5 | 0.77 | 0.77 | 0.55 | 0.57 | 0.59 | *0.47* | **0.68** | 0.56 | 0.59 | ***0.66*** |
| | *Avg. PS, UIB* | **0.83** | **0.74** | **0.56** | ***0.61*** | **0.56** | **0.48** | **0.67** | **0.49** | **0.47** | **0.46** |
| | *Avg. Uncer., UIB (%)* | **17** | **26** | **44** | **39** | **44** | **52** | **33** | **51** | **53** | **54** |
| | *LI* | | | | | | | | | | |
| | R4 | 0.94 | 0.91 | 0.58 | 0.62 | **0.71** | 0.58 | *0.43* | 0.61 | ***0.67*** | 0.60 |
| | R6 | 0.51 | 0.72 | 0.72 | **0.78** | 0.63 | 0.66 | ***0.76*** | 0.72 | *0.60* | 0.66 |
| | *Avg. PS, LI* | ***0.73*** | ***0.82*** | ***0.65*** | ***0.70*** | ***0.67*** | ***0.62*** | ***0.60*** | ***0.67*** | ***0.64*** | ***0.63*** |
| | *Avg. Uncer., LI (%)* | ***27*** | ***19*** | ***35*** | ***30*** | ***33*** | ***38*** | ***41*** | ***34*** | ***37*** | ***37*** |

Note that all thermodynamic PCs are located over and in the surrounding of high mountains due to a reduced predictor domain for these variables. Differences in the numerical models and interpolation issues for the near-surface variables over the mountains (e.g., Palazzi et al., 2013) may further add to

such simulation disparities. The contribution of hur1000 in precipitation models is low, and the weaker correspondence is mainly limited to some LI regions, particularly during the PMS and WS. Such region-specific discrepancies may not substantially influence the overall regional suitability of ERA-Interim, particularly over the UIB that controls river flows during all seasons.

Another pattern relates to the seasonal out-performance (higher PS) of ERA5 over NCEP-NCAR- II (except the WS-LI regions due to more differences in simulations of hur1000). That seems logical as both ERA-Interim and ERA5 are ECMWF reanalysis and share more similarities in their simulation schemes. However, we purposefully select NCEP-NCAR-II that shares the same temporal resolution with ERA-Interim (from 1979 onward), maximizes the use of post-70s satellite measurements, and provides the opportunity to assess ERA-Interim variables more independently.

The difference between a perfect predictor match (PS = 1) and actual correspondence among reanalysis data can define the reference uncertainty range. ERA5 mostly defines the lower, and NCEP-NCAR-II outlines the upper bound of such uncertainty. Table 3 provides reference uncertainty during the MS (16–28%), PMS (24– 29%), and WS (17–26%) over the UIB. The corresponding LI uncertainty ranges from 19% to 30%, 24% to 25%, and 18% to 27%, respectively. Considering regional heterogeneity, such strong predictor correspondence (low uncertainty) of ERA-Interim with different reanalysis datasets fully justifies its use for constructing downscaling models.

## 4.2 GCM Ranking

Similarly, we identify better-performing GCMs using weighted PS. During the MS, all GCMs show relatively low correspondence with ERA-Interim predictors over different UIB regions **(Table 3)**. Such poor predictor similarities (except for R3) highlight the MS complexity and its highly uncertain representation in most GCMs (e.g., Ashfaq et al., 2017). Among available models, CMCC-CMS turns up as the best single model (PS = 0.50 over five UIB regions). This model outperforms over two larger sub-regions (R1 and R3; see Figure 3c for regional identification) and appears the second-best model for the northwestern region (R4). Moreover, its performance over the remaining two UIB regions (R5 and R7) is comparable with other GCMs. Therefore, its use for MS projections over the entire UIB seems more justified among available models. Although this model only shows 50% predictor correspondence, a high reference uncertainty (up to 28%) also needs to be considered for judging its true fidelity. In contrast, Can-ESM2 and MPI-ESM-LR show the least predictor correspondence over the UIB. The MS predictors for two LI regions are better simulated by MPI-ESM-LR (PS = 0.52).

All GCMs showed relatively high predictor correspondence with ERA-Interim during the PMS. However, CNRM-CM5 offers more consistent performance over four UIB regions (PS = 0.61). In contrast, MPI-ESM-LR better represents the LI predictors. Both models provide improved simulations of hur1000, a primary predictor to simulate precipitation over R5 and R6 regions (**Tables S2 and S3**).

Consequently, the basin-wide compatibility of these models with ERA-Interim predictors improves significantly.

During the WS, most ensemble members demonstrate the highest PS. Among these, MPI-ESM-LR shows maximum predictor correspondence over the UIB (PS = 0.67) by outperforming predictor simulations over the two large and cryosphere-dominated regions in trans- Himalayans (R1 and R5). It also shows comparable performance with other GCMs over the third UIB region (R3). As before, a different model (CMCC-CM) provides better simulations of the governing predictors over two LI regions.

In summary, no single model can effectively simulate precipitation dynamics at the basin level without making significant compromises. However, our model ranking process can identify models demonstrating spatially consistent performance over the UIB (LI) with tolerable uncertainties. Significantly improved representation of the westerly circulations in our ensemble may increase our understanding and confidence about projected cryosphere dynamics that largely influence basin sustainability.

It is important to note that our model rankings only rely on predictor correspondence during the historical period and require a stationarity assumption for their future validity (e.g., Lanzante et al., 2018). The stationarity considerations may induce some additional uncertainties, as the predictor-predictand relationships and the models' ability for their simulations may alter in the future (e.g., Hertig et al., 2017). Stationarity violation may particularly happen in high-mountain regions, where numerous feedback mechanisms exert influence on regional climate, and their future evolution may substantially differ from the observations.

## 4.3 Diversity of the GCM Ensemble

Only eight GCMs in our study may not adequately represent the entire CMIP5 simulation diversity. Using literature review and exploratory quantitative analysis, we evaluate our ensemble's regional efficacy. For instance, Khan and Koch (2018) assess the entire CMIP5 dataset under RCP4.5 and RCP8.5 scenarios to shortlist the GCMs defining a so-called full spectrum of future climate over the UIB. Their final models explaining Warm-Wet (Can-ESM2), Dry-Cold (MPI-ESM-LR), and mean climate (Nor-ESM1-ME) are available in our ensemble. Besides, our ensemble also includes their secondary considerations for Dry-Warm (CMCC-CMS) and Wet-Cold (CNRM-CM5) regional future (see **Table 2**). Similarly, the 14-model CMIP5 ensemble of Ali et al. (2020) also contains almost all our models. Such ensemble similarities justify the regional relevance of our models, despite its smaller sample size.

We further performed an additional analysis over a sample MS-UIB region (R3) whose precipitation predictor (va200) was available in most CMIP5 GCMs. We selected 15 GCMs belonging to 13 different modeling centers **(Table 4)** to cover most of the remaining institutional spread in the CMIP5. The historical uncertainties of these additional GCMs were similarly computed (see Section 3.5) and compared with the 8-model ensemble using the box and whisker plots (**Figure 7**). The ensemble comparison shows that nearly all 15 GCMs lie within the uncertainty spectrum defined by the 8-models; the medians are similar, and the best GCM (lower outlier of the 8-model ensemble) remains the same. The reduced uncertainty among the new GCM ensemble suggests close similarities between these models for MS simulations instead of providing a significantly different perspective. Therefore, both literature review and sample analysis demonstrate the regional suitability of our 8-model ensemble.

We also investigate the influence of model uniqueness (Sanderson et al., 2017) over the sample MS region. We computed historical uncertainties using 23 GCMs (model democracy) and compared them with18 GCMs belonging to different modeling centers (model independence; see **Tables 1 and 4**). Using the box and whisker plots (not shown), we could not find significant differences in the two distributions. Besides, similar uncertainty estimates of the independent models and the 8-model ensemble over the sample region also induce confidence in our ensemble simulations.

## 4.4 Downscaled Future Precipitation Changes

We use available GCMs to compute the median precipitation changes for two future periods (2041–2071 and 2071–2100) relative to the historical period (1976–2005) under RCP4.5 and RCP8.5. **Figure 8** shows sub-regional multi-model ensemble (MME) and individual GCM simulated precipitation changes during the end of the 21st century (2071–2100) under both RCPs. The inter-model spread defines the range of uncertainty around MME signals. The corresponding changes during 2041–2071 are quantitatively different but show similar spatial patterns (not shown).

### 4.4.1 WS projections

The WS projections under both RCPs (**Figure 8a,b**) show considerable positive changes (MME) over large parts of the UIB, covering mainly the HA regions of the trans- Himalayan and northwestern Hindukush (R5, R1; refer to **Figure 2a** for regional location). The positive signals are robust (all models project positive changes) and much stronger over the central Karakoram (R1) than the north-western and eastern regions (R5) under both scenarios. Some precipitation decrease appears along the lower elevations of the northwestern and southern Himalayans (R3) under RCP4.5 (**Figure 8a**), but it will eventually stabilize under RCP8.5 forcing. The precipitation changes suggest that increased warming (RCP8.5) will promote an elevation-dependent response in the UIB, where HA regions will receive more precipitation. The best seasonal model (MPI-ESM-LR) demonstrating high predictor correspondence during the historical period further supports these ensemble signals, particularly for

RCP8.5. The likelihood of decreasing precipitation over the UIB remains low, as mainly negative signals are projected by two Norwegian models that demonstrate the lowest historical performance (**Table 3**). The large inter-model spread reflects a highly uncertain future over the UIB.

**Table 4.** Details of the additional GCMs used to evaluate the CMIP5 representativeness of the 8-model ensemble (Table 2) in our study. Like in **Table 3**, the PS and uncertainty estimates are computed and denote the strength of reference-model predictor correspondence over the sample MS region (R3) during the overlapping historical period.

| No. | Model ID | Horizontal Resolution (Lon X Lat) in degrees | Modeling Centre | PS | Uncertainty (%) |
|---|---|---|---|---|---|
| 1 | ACCESS1-0 | 1.875 x 1.25 | CSIRO-BOM | 0.54 | 46 |
| 2 | ACCESS1-3 | 1.875 x 1.25 | CSIRO-BOM | 0.56 | 44 |
| 3 | BCC-CSM1-1 | 2.8125 × 2.8125 | BCC | 0.64 | 36 |
| 4 | BNU-ESM | 2.8125 x 2.7906 | BNU | 0.53 | 47 |
| 5 | CCSM4 | 1.25 × 0.9 | NCAR | 0.55 | 45 |
| 6 | FGOALS-g2 | 2.8125 × 2.8125 | LASG-CESS | 0.49 | 51 |
| 7 | GFDL-ESM2G | 2.5 × 2 | GFDL | 0.46 | 54 |
| 8 | GISS-E2-H | 2 x 2.5 | NASA | 0.54 | 56 |
| 9 | *HadCM3 | 2.5 x 3.5 | MOHC | 0.60 | 40 |
| 10 | HadGEM2-AO | 1.875 × 1.24 | MOHC | 0.65 | 35 |
| 11 | INM-CM4 | 2 × 1.5 | INM | 0.49 | 51 |
| 12 | IPSL-CM5A-MR | 2.5 × 1.2587 | IPSL | 0.36 | 64 |
| 13 | MIROC5 | 1.40625 × 1.40625 | MIROC | 0.54 | 46 |
| 14 | MRI-CGCM3 | 1.125 x 1.12148 | MRI | 0.55 | 45 |
| 15 | CSIRO-Mk3-6-0 | 1.875 × 1.875 | CSIRO-QCCCE | 0.63 | 37 |

*Future predictors from this model are not available.

The westerlies approaching the UIB bifurcate into northern and southern branches along the Himalayans (e.g., Pang et al., 2014). Increased strength and more north-ward penetrating westerlies at the end of the 21st century may increase dynamic forcing over the UIB to explain the typical spatial changes under warming scenarios. Note that circulation-dynamic predictors (**Table S1**) mainly govern the regional precipitation. The strong and northward located westerlies may continue to support the regional cryosphere and anomalous behavior of the Karakoram. Conversely, the precipitation changes are subtler

over the two LI regions (R6 and R4) under both RCPs. For instance, the MME change over the upper irrigated plains (R6) shows some robust decrease (many models show negative signals), which confirms the weakening of the southern westerly limb. Meanwhile, the lower irrigated plains (R4) indicate strongly positive and robust changes under both RCPs. Local feedback mechanisms may strongly influence the future precipitation changes over this region. Overall, some decrease in LI precipitation seems plausible (though with more uncertainty) due to quantitatively more negative changes over a large region (R6) than the positive signals over R4.

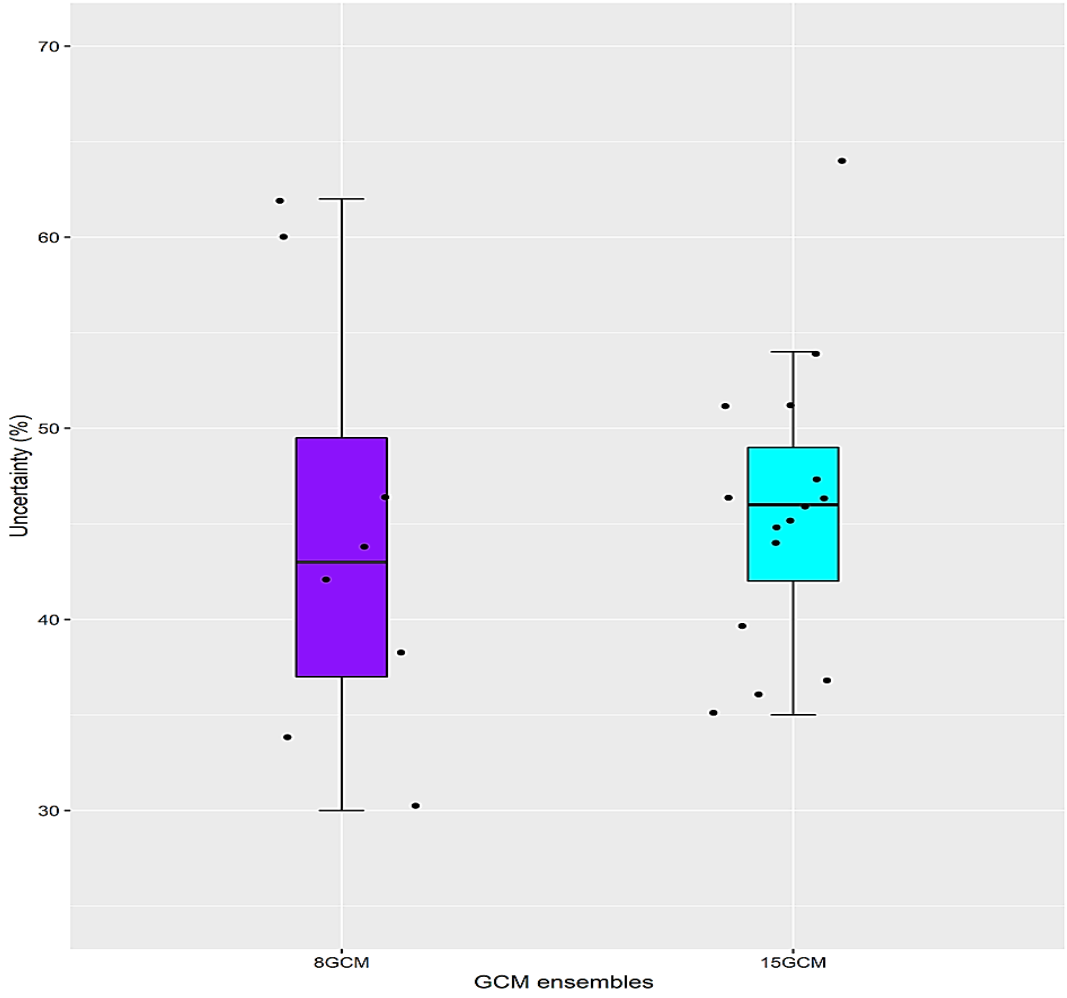


**Figure 7.** Comparison of the two GCM ensembles for simulating precipitation predictors (seven PCs of va200) over a sample MS region (R3) during the overlapping historical period (1979–2005). The uncertainties along the y-axis reflect the degree of mismatch between the ERA-Interim reanalysis's predictor and corresponding simulations of every available GCM (black dots) in the two ensembles. The GCM uncertainty is computed using the mathematical relationship (1 − PS)*100

### 4.4.2 PMS projections

PMS changes (MME) show a decrease in precipitation over all four UIB regions (R1, R5, R3, R7; see also **Figure 3b**) that further intensify with increased warming (**Figure 8c,d**). These changes exhibit

spatial variability, and strongly negative signals (up to 25%) are noticeable in the lower northwestern regions (R5 and R7). Most individual models also project negative changes for these regions except Can-ESM2, but it shows the lowest predictor correspondence in the historical period. However, a large HA part of the trans-Himalayans region (R1) indicates a lesser decrease and more uncertainty (some models even project similar positive signals) under both scenarios. Moreover, a wetter northeastern region (R3) shows nearly neutral changes, and the best seasonal model (CNRM-CM5) instead projects a slight increase in regional precipitation. Generally, a precipitation decrease is more robust over the UIB, though its intensity and reliability reduce with elevation and over eastern parts. The decreasing trend is also visible over large parts of the southwestern highlands and the LI plains (R6). In contrast, the upper irrigated plains and northeastern rainfed regions (R4) show some precipitation increase that becomes stronger under RCP8.5. Generally, a smaller inter-model spread suggests more robustness of the sub-regional signals during the PMS.

Weaker and more northward-oriented westerlies may reduce the moisture advection to reduce future precipitation, particularly over the lower northwestern regions, where relative humidity has a strong impact (**Table S2**). Alternatively, the projected seasonal warming (e.g., Ashfaq et al., 2020) may reduce the saturated atmospheric moisture content (i.e., relative humidity) to delay precipitation onset.

### 4.4.3 MS projections

We assess an overall precipitation increase over the entire Indus basin under both RCPs (**Figure 8e,f)**. Most individual models, including the best seasonal models, further support these sub-regional trends that intensify further under RCP8.5. However, the change signals significantly vary over different UIB regions (R7, R6, R1, R3, R5; see **Figure 3c**). For example, the highest elevations towards the Karakoram–West (R7) show some consistent decrease (MME = approx. −8%). In contrast, a northwestern region (R4) and a larger area around the central Karakoram (R1) depict an up to 12% increase in future precipitation. Similarly, a large and the wettest part along the southern Himalayans (R3) also show increased precipitation (MME = ~ 4%) in both scenarios. Another northwestern region representing the lower elevation of the Hindukush (R5) also indicates some positive signals (up to 2%). These distinct precipitation changes (predominantly positive) support the monsoon system's strengthening and further penetration into the Northwestern and trans-Himalayans regions under increased warming scenarios. Such intense MS circulations may continue to support the regional cryosphere and downstream water needs in the future. More uncertainty over the magnitude and the direction of precipitation signals highlights the complex interplay between the MS currents and UIB topography.

Similarly, two LI regions (R6 and R2), covering spate irrigation in the southwestern mountains, irrigated plains, and coastal areas, mainly project positive changes under both RCPs. Therefore, increased water

development potential in spate regions and a slight decrease in net irrigation over the plains are likely under future warming. Compared to the UIB, the inter-model agreement over the LI precipitation changes is high.

## 4.5. Impact of Model Weighting on Ensemble Changes

**Figure 9** shows the impact of model weighting (**Table 3**) on sub-regional ensemble changes during 2071–2100 under both RCPs. Generally, better-performing models (models with higher weights) have a relatively small impact on change signals due to the adopted weighting scheme (maximum value of 1) and intermodel similarities in our ensemble. Still, the weighting has demonstrated refinement of the change signals by altering magnitude in many cases. For instance, the model weighting shows maximum influence during the MS season (**Figure 9c**) by mainly strengthening positive changes over the UIB under RCP8.5. A considerable increase in precipitation over the central Karakoram and northwestern HA, including the wettest part (R3) in the UIB, is apparent. This pattern also continues into the southern highlands (R6) and irrigated plains (R2) in the LI. The strengthening of MS circulations appears more in better-performing models under the intense warming (RCP8.5) than RCP4.5 forcing, where a mixed response mostly prevails.

In contrast, the model weighting increases PMS dryness over most of the UIB for both scenarios (**Figure 9b**). Thus, the weakening of the westerly system during PMS is more consistent among better-performing GCMs, particularly under RCP8.5. During the WS, the model weighting has mainly enhanced the positive signals over the UIB (**Figure 9a**) to indicate a slight strengthening of the westerly circulations in better-performing models. Since HA regions receive much higher precipitation (e.g., Immerzeel et al., 2015; Pomee et al., 2020), even a slight increase in precipitation signals during the main seasons (MS and WS) can substantially increase the actual precipitation over the UIB under RCP8.5.

Using model weights in an ensemble setting can explain additional insights about projected changes in complex regions to assess confidence in projected signals despite the lesser impact.

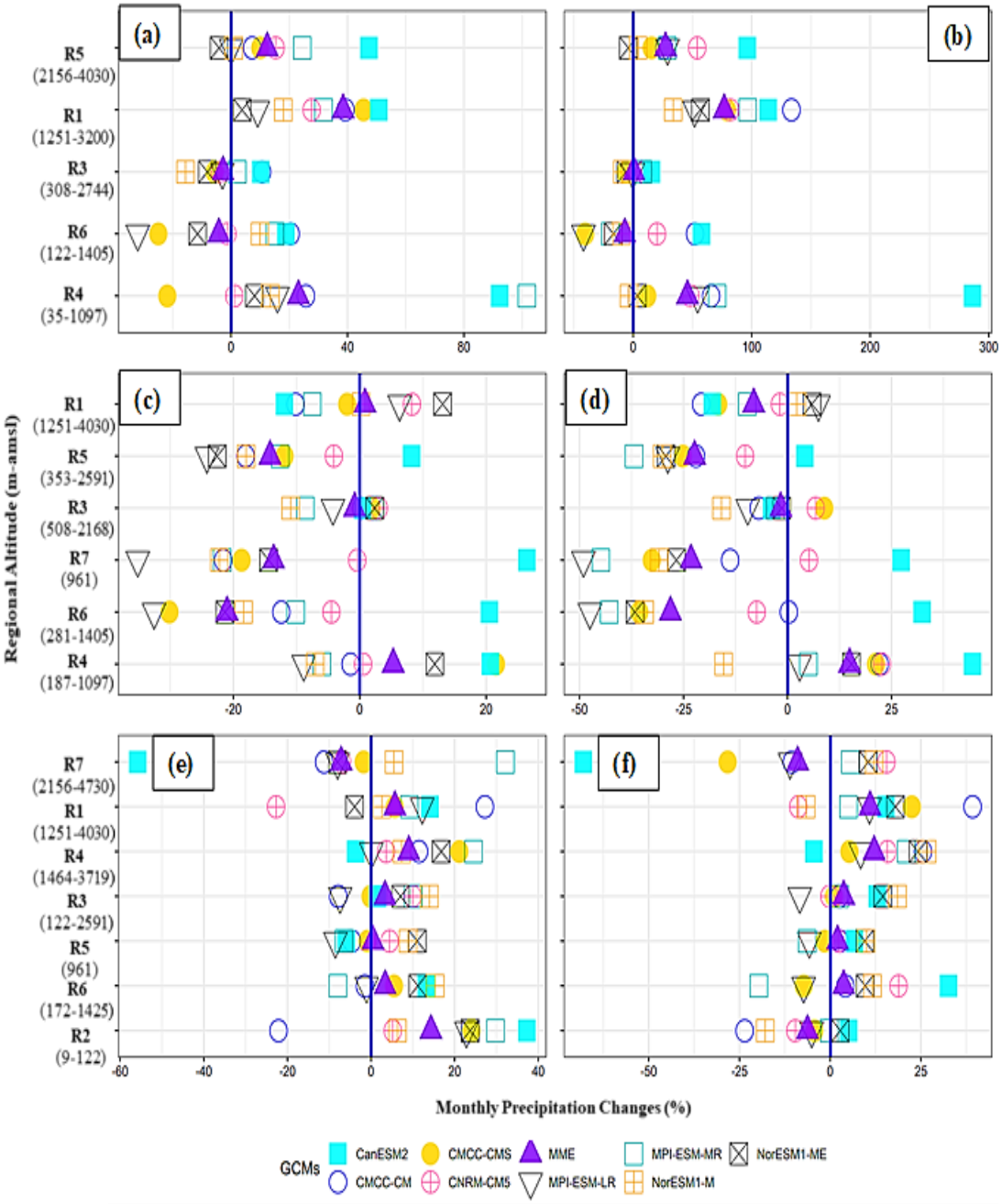


**Figure 8.** Downscaled unweighted seasonal precipitation changes in % over the Indus Basin of Pakistan during the future period (2071–2100) relative to the historical period (1976–2005) under RCP4.5 and RCP8.5. The y-axis shows the identified precipitation regions and the corresponding range of regional altitudes that decreases from top to bottom. The regional altitudes are expressed as the elevations above mean sea level (m-amsl). The WS, PMS, and MS precipitation changes under RCP4.5 and RCP8.5 scenarios are shown by the subplots (a,b), (c,d), and (e,f), respectively. The coloured circles (triangles) show the individual GCM (MME) simulated precipitation changes. The solid blue line indicates no change compared to the historical period. Note that the range of the x-axis (i.e., precipitation changes) is different in these panels

## 4.6 Robustness of the Change Signals

We use SNR to evaluate the strength of projected signals over the observational uncertainty, which remains very high over this complex region. **Figure 10** shows the WS distribution of SNR as a function of regional elevations during 2071–2100 under RCP scenarios. Generally, the sub-regional ratios are higher under the RCP8.5 forcing than under the RCP4.5 scenario, confirming the positive role of increased warming on regional precipitation changes. These ratios also demonstrate elevation dependency of future changes by depicting positive (strong) signals over HA regions compared to negative (weak) values over low elevations. The spatial patterns of SNR further support future strengthening and the northward-oriented westerly regimes that will induce distinct positive changes over the HA-UIB. The other seasons also show similar patterns for both RCPs (not shown).

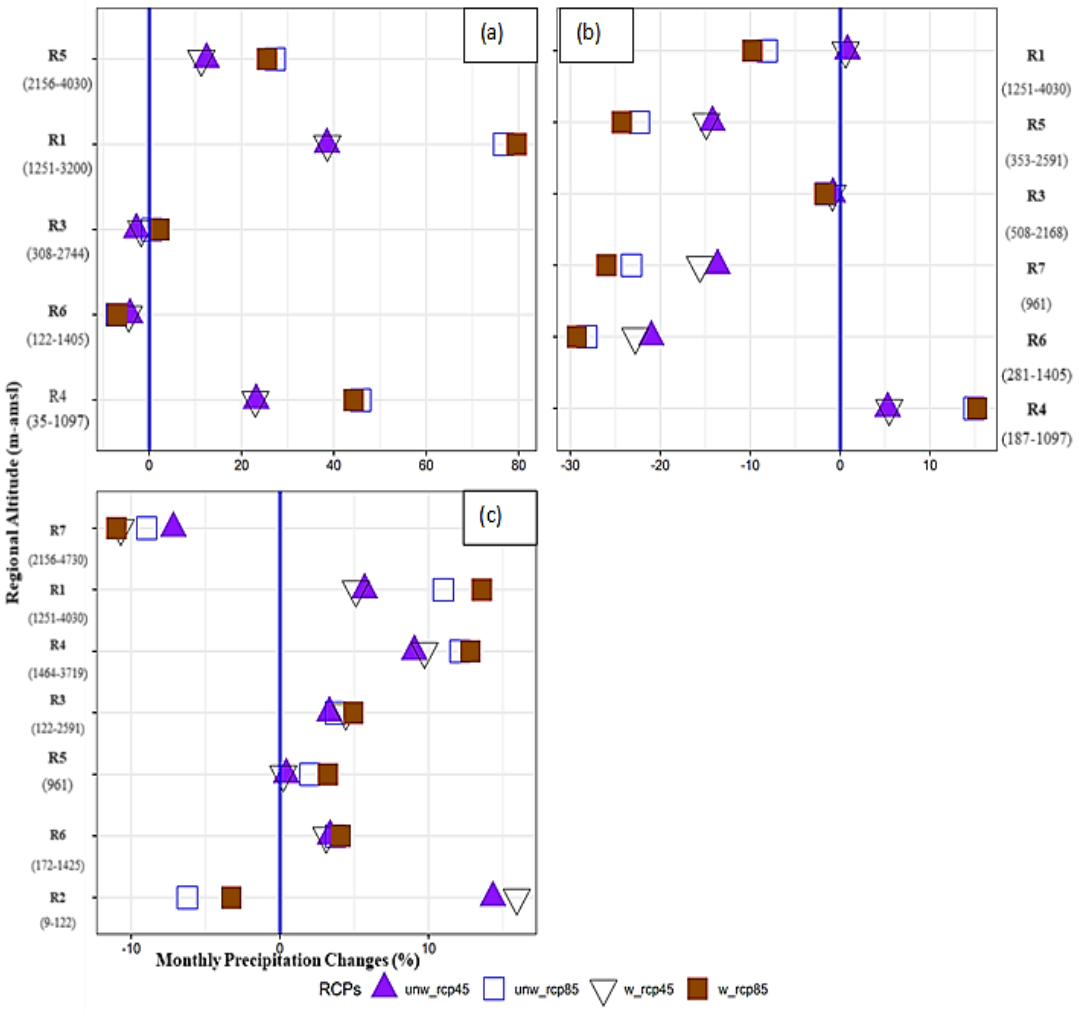


**Figure 9.** Impact of the model weighting on ensemble precipitation changes (i.e., MME) during 2071–2100 under RCP4.5 and RCP8.5 scenarios. **(a)** The WS, **(b)** the PMS, and **(c)** the MS sub-regional changes under both RCPs. In the legend, the 'unw' stands for unweighted, and 'w' represents the weighted ensemble changes for each RCP simulation

## 4.7 Downscaled Precipitation: HA-UIB Regionalization Scenario

We also separately compute precipitation changes, model weighting, and SNR over HA regions of the UIB. **Figure 11** only shows the precipitation changes during 2071–2100 under RCP8.5. These seasonal changes further confirm our previous findings (Section 4.7) about the strengthing and northward penetrating westerlies during the WS and easterlies during the MS to promote positive precipitation changes over the high-elevation UIB. The PMS dryness over large parts of the UIB is also verified, indicating a future weakening of the westerly circulations during this season. The magnitude of changes differs, but the spatial patterns are similar for RCP4.5 (not shown).

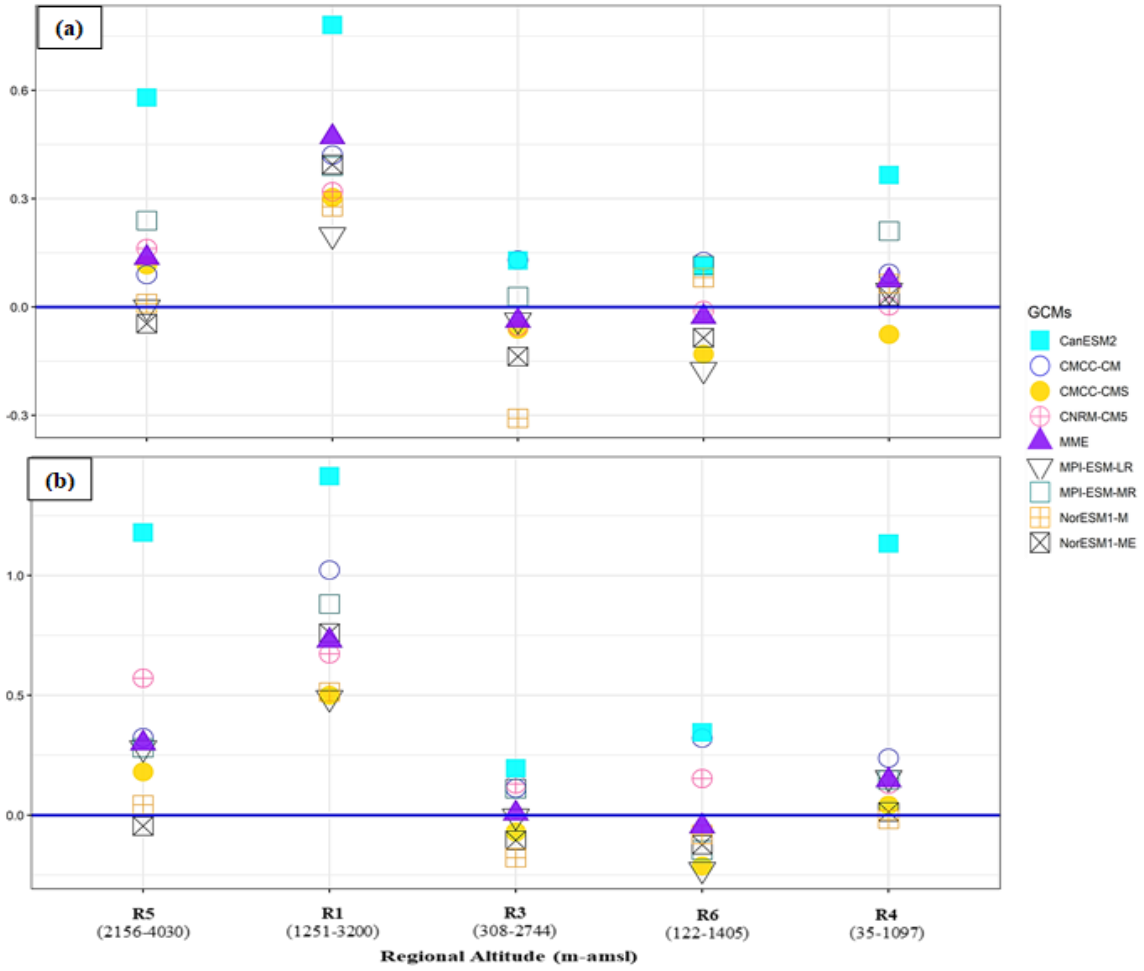


**Figure 10.** WS distribution of the SNR to evaluate the robustness of projected precipitation changes under RCP4.5 **(a)** and RCP8.5 **(b)** scenarios over Pakistan's Indus Basin. The ratios are computed by dividing median changes (signal) during 2071–2100 with standard deviations (noise) of the historical period (1976–2005). The absolute value of the SNR along the Y-axis indicates the magnitude of signal strength. The blue horizontal line serves as a reference and indicates no strength of the projected signal. The precipitation regions are shown along the x-axis and arranged in decreasing altitudes from left to right.

## 4.8 Further Discussions

Our main findings support the results of some earlier studies. For example, Ali et al. (2015) and Khan and Koch (2018) also reported elevation-dependent precipitation changes over the UIB. Similarly, Lutz et al. (2016b) concluded a drying (increased precipitation) during the PMS (MS and WS) months. Although their changes were different in detail, the spatial patterns of increasing precipitation from west to east confirm our findings. Bokhari et al. (2018) also estimated a reduction in future precipitation over the Kabul river basin, located in the northwestern UIB. Studies by Archer and Fowler (2004), Khattak et al. (2011), and Forsythe et al. (2014) also projected increased precipitation during the main seasons.

However, our findings contrast with Palazzi et al. (2013, 2014), who found insignificant WS changes over the UIB. Using direct GCM precipitation, which contains significant wet biases over the region, in these studies may reduce signal strength. A bias-corrected analysis, despite some criticism (e.g., Ehret et al., 2012; Mezghani et al., 2017), may sharpen or even reverse the signal direction (e.g., Hagemann et al., 2011; Navarro-Racines et al., 2020). Similarly, the intensity of drying (Khan and Koch, 2018) and a remarkable increase of projected precipitation over the UIB, particularly during PMS months, as shown by Hasson (2016) under RCP8.5, are not in agreement with our analysis. Surprisingly, both studies used the output of CORDEX-SA experiments but concluded a contrasting regional outlook, mainly due to differences in the reference datasets. For example, Hasson (2016) only used three short-term HA stations located along the Karakoram for scaling, which might induce a wet bias. In contrast, the adopted climatology of Khan and Koch (2018) could produce a dry tendency, as some recent studies (e.g., Immerzeel et al., 2015; Dahri et al., 2018) showed much higher precipitation over the UIB compared to the precipitation amounts used in their study.

Using the so-called model democracy (e.g., Knutti, 2010) and appreciating the complexity and future uncertainty of the climate system, some studies criticize model rankings (e.g., Chiew et al., 2009; Hasson et al., 2019). We argue that some known model performances may reduce future climate uncertainties. We also analyzed future precipitation changes over the sample MS region (R3) during 2071–2100 under selected RCPs using the 8- and 14 model ensembles **(Table 4).** The two ensembles showed strong similarities (not shown). Outliers in the 14-model ensemble were mostly those GCMs that demonstrated the lowest historical performance (e.g., IPSL-CM5A-MR, GFDL-ESM2, FGOALS-g2, and INMCM4). These models are known for their poor MS simulations over the study region (e.g., McSweeney et al., 2015) and could have been eliminated during the model ranking process. In summary, the 8-model ensemble adequately captures the future simulated by a larger CMIP ensemble and stands useful for precipitation analysis over the region for practical purposes. Model-uniqueness influence on future precipitation signals over the sample region also remains negligible (not shown).

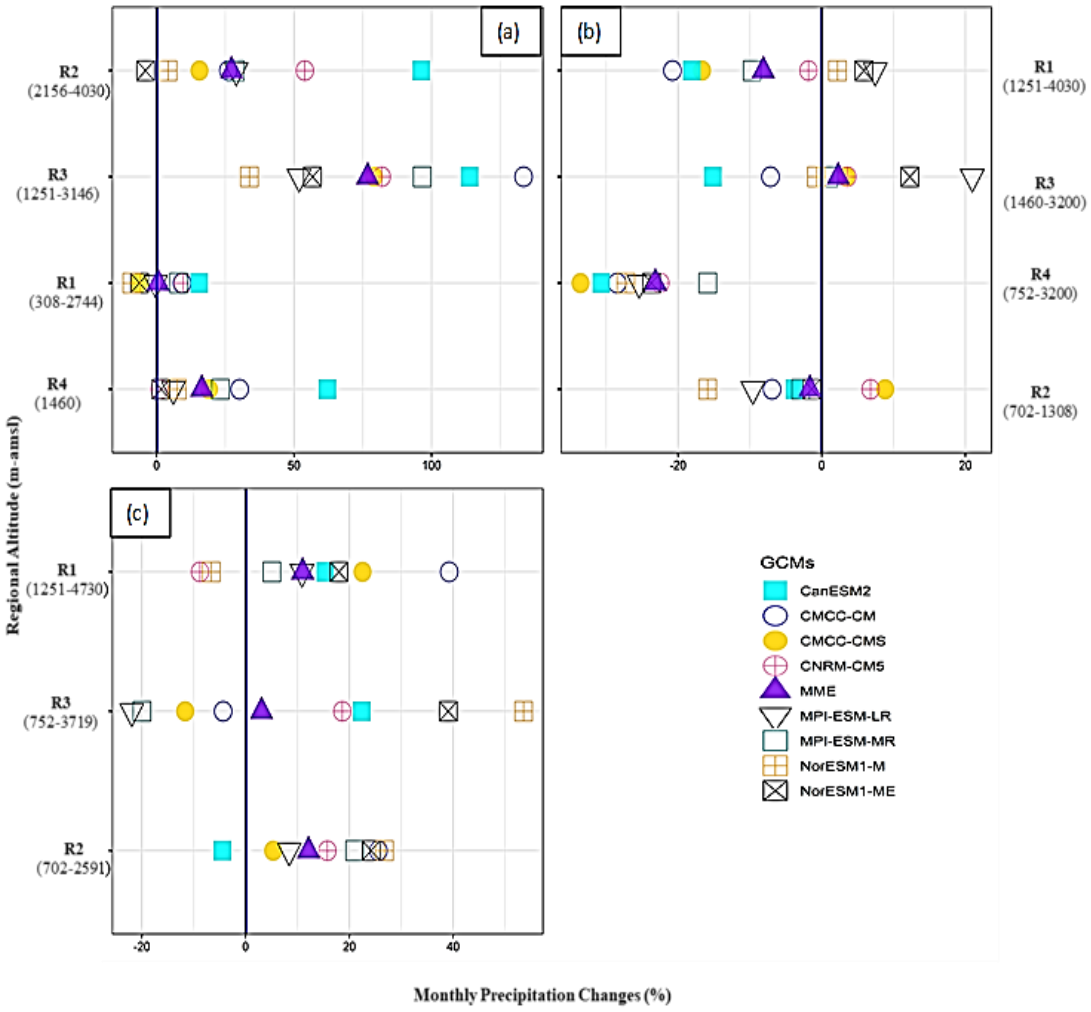


**Figure 11.** Downscaled unweighted precipitation changes from 1976–2005 to 2071–2100, using the HA-UIB regionalization experiment's output under RCP8.5. Subplots **(a), (b)**, and **(c)** represent sub-regional precipitation changes over the UIB during the WS, PMS, and MS, respectively.

## 5 Summary and Conclusions

We assessed future precipitation changes over Pakistan's Indus basin that primarily derives runoff from cryosphere-dominated watersheds in the UIB. Large-scale atmospheric patterns were used as predictors for constructing downscaling models, uncertainty quantification, GCM selection, and subsequent projections, as raw precipitation of the GCMs still lacks reliability. Such GCM limitations manifest over high-mountain regions like the UIB, where complex processes govern precipitation variation at sub-grid levels.

Firstly, we identify precipitation-governing predictors from ERA-Interim reanalysis within a robust statistical downscaling by accounting for spatial variability of the observed precipitation on seasonal scales. K-means cluster analysis was used for basin characterization. We further evaluated ERA-Interim

predictors' robustness against two other reanalysis datasets (ERA5 and NCEP- NCAR-II) to demonstrate their usefulness for precipitation modeling.

We also identified better-performing GCMs by comparing model-simulated predictors with ERA-Interim variables during the overlapping historical period. On a seasonal scale, the MS governing predictors were more diverse, indicating their poor representation by most GCMs. Some earlier studies (e.g., Ashfaq et al., 2017) also reported major shortcomings of the GCMs in simulating MS dynamics over this region. We argue that a high reference uncertainty may restrict an accurate model assessment during the MS. In contrast, the available GCMs better simulated westerly-dominated seasons that account for more than two-thirds of the HA precipitation (Hewitt et al., 1989). Our analysis further showed that no single model could effectively simulate the basin-wide precipitation during different seasons. However, within a season, our model ranking process could identify models that provide improved simulations for influential predictors over multiple sub-regions. Such better-performing models can also guide the selection of driving GCMs in the scope of dynamic downscaling in this region.

Concerning future changes, the ensemble medians showed an elevation-dependent response of the UIB towards projected warming, where HA regions will mostly receive more precipitation. These positive signals were distinct during the main precipitation seasons (i.e., WS and MS), particularly over the central Karakoram. A decreasing precipitation pattern also emerged during the PMS, particularly towards the north-western regions. These positive and negative signals further intensified under RCP8.5 at the end of the 21st century.

The projected spatial changes suggest a strengthening (weakening) and further northward penetration of the westerly system during the WS (PMS). Similarly, the future MS circulations will also intensify and penetrate further into the northwestern and trans-Himalayan regions. However, the LI regions showed a mixed seasonal response, where MS precipitation will primarily increase. We also evaluated the impact of model weighting on ensemble signals, which generally was small and more prominent during the MS. In many cases, the model weighting refined the change signals by assigning more importance to better-performing models. For example, the weighting indicated a further strengthening of the WS westerlies and MS circulations and increased dryness during the PMS under RCP8.5. As the GCMs that perform better during the historical period may also provide reliable projections (e.g., Shukla et al., 2006), using historical weights in an ensemble setting can be advantageous (e.g., Kaspar-Ott et al., 2019).

We used SNR to assess the robustness of change signals and demonstrated the significance of positive changes over observational uncertainty, particularly at HA regions. The HA-UIB analysis further supported elevation-dependent precipitation changes. Our precipitation projections support augmentation of the existing cryosphere and continuing anomalous behavior of the Karakoram (e.g., Bashir et al., 2017) even under the extreme warming scenario during the end of the 21st century.

Although we used predictor, predictand, and model level considerations to improve the quality of projected precipitation, some issues may still affect our analysis. For example, the absence of a large number of CMIP5 models and the existence of inter-model similarities in our ensemble may induce additional uncertainties. Although we demonstrated the usefulness of our 8-model ensemble through literature review and sample analysis, additional GCMs may differently model other precipitation predictors. Stationarity assumption may induce uncertainties not estimated in our analysis. Quantifying such uncertainties is difficult, but some studies (e.g., Merkenschlager et al., 2017) suggested mechanisms of non-stationarity considerations in statistical downscaling. Such analysis is, however, beyond the scope of the present work. We also assume our regionalization scheme's effectiveness to extend precipitation inferences beyond the observations and draw conclusions over the transboundary basin regions not covered in our analysis (Pomee et al., 2020). Since our projection patterns are primarily in line with those studies that employ glacial and transboundary information (e.g., Lutz et al., 2016b), our assumptions regarding inferences beyond the observations seem justified.

Despite some limitations, our study presented an alternative and realistic perspective to assess precipitation changes over a complex, highly uncertain, and yet enormously important river basin. Our approach will open new avenues of regional research and has the potential for replication in other regions. However, for the correct assessment of future water availability and cryosphere stability, temperature modeling is similarly required.

## Acknowledgment

PARC mainly supported our research work through the Himalayan Adaptation, Water, and Resilience (HI-AWARE) project, funded by the CARIAA consortium. The German Research Foundation supported EH under project number 408057478, and DAAD through Augsburg University provided valuable financial support for Muhammad Saleem Pomee. The authors also acknowledge the World Climate Research Programmer's Working group on the Coupled Modelling, ECMWF, and NOAA-ESRL Physical Sciences Division for publically sharing CMIP5 and reanalysis datasets. Open access funding enabled and organized by the Projekt DEAL.

## References

Akhtar, M., Ahmad, N. and Booij, M.J. (2008) The impact of climate changes on the water resources of Hindukush–Karakorum– Himalayaregionunder different glacier coverage scenarios. Journal of Hydrology, 355, 148–163. https://doi.org/10.1016/j. jhydrol.2008.03.015

Ali, S., Kiani, R.S., Reboita, M.S., Dan, L., Eum, H.I., Cho, J., Dairaku, K., Khan, F., and Shreshta, M.L. (2020) Identifying hotspots cities vulnerable to climate change in Pakistan under CMIP5 climate projections. International Journal of Climatology, 41, 559–581. https://doi.org/10.1002/joc.6638

Ali, S., Li, D., Congbin, F. and Khan, F. (2015) Twenty first century climatic and hydrological changes over upper Indus Basin of Himalayan region of Pakistan. Environmental Research Letters, 10, 1–20. https://doi.org/10.1088/1748-9326/10/1/014007

Archer, D. and Fowler, H.J. (2004) Spatial and temporal variations in precipitation in the upper Indus Basin, global teleconnections and hydrological implications. Hydrology and Earth System Sciences, 8(1), 47–61. https://doi.org/10. 5194/hess-8-47-2004

Arora, V.K., Scinocca, J.F., Boer, G.J., Christian, J.R., Denman, K. L., Flato, G.M., Kharin, V.V., Lee, W.G. and Merryfield, W.J. (2011) Carbon emission limits required to satisfy future representative concentration pathways of greenhouse gases. Geo physical Research Letters, 38, L05805. https://doi.org/10.1029/2010GL046270

Ashfaq, M., Cavazos, T., Rebolta, M.S., Torres-Alavez, J.A., Im, E-S., Olusegun, C.F., Alves, L., Key, K., Adeniyi, M.O., Tall, M., Sylla, M.B., Mehmood, S., Zafar, Q., Das, S., Diallo, I., Coppola, E., and Giorgi, F. (2020) Robust late twenty-first century shift in the regional monsoons in RegCM-CORDEX simulations. Climate Dynamics. https://doi.org/10.1007/s00382-020- 05306-2

Ashfaq, M., Rastog, D., Mei, R., Toumag, D. and Leung, L.R. (2017) Sources of errors in the simulation of south Asian summer monsoon in the CMIP5 GCMs. Climate Dynamics, 49, 193–223. https://doi.org/10.1007/s00382-016-3337-7

Bashir, F., Zeng, X., Guptta, H. and Hazenberg, P. (2017) A hydrometeorological perspective on the Karakoram anomaly using unique valley-based synoptic weather observations. Geophysical Research Letters, 44(20), 1–9. https://doi.org/10.1002/2017GL075284

Bentsen, M., Bethke, I., Debernard, J.B., Iversen, T., Kirkevåg, A., Seland, Ø., Drange, H., Roelandt, C., Seierstad, I.A., Hoose, C. and Kristj ansson, J.E. (2013) The Norwegian earth system model, NorESM1-M-part 1: description and basic evaluation of the physical climate. Geoscientific Model Development, 6, 687– 720. https://doi.org/10.5194/gmd-6-687-2013

Biemans, H., Speelman, L.H., Ludwig, F., Moors, E.J., Wiltshire, A. J., Kumar, P., Gerten, D. and Kabat, P. (2013) Future water resources for food production in five south Asian river basins and potential for adaptation—a modeling study. Science of the Total Environment, 2013(468), S117–S131

Bocchiola, D., Diolaiuti, G.A., Soncini, A. and Mihalcea, C. (2011) Prediction of future hydrological regimes in poorly gauged high altitude basins: the case study of the upper Indus, Pakistan, Hydrol. Earth System Science, 15(7), 2059–2075. https://doi.org/10.5194/hess-15-2059-2011

Bokhari, S.A.A., Ahmad, B., Ali, J., Ahmad, S., Mushtaq, H., and Rasul, G. (2018) Future climate change projections of the Kabul River basin using a multi-model ensemble of high-resolution statistically downscaled data. Earth Systems and Environment, 2, 477–497. https://doi.org/10.1007/s41748-018-0061-y

Bolch, T., Kulkarni, A.V., Kääb, A., and Huggel, C. (2012) The state and fate of Himalayan glaciers. Science, 336(6079), 310–314. https://doi.org/10.1126/science.1215828

Chiew, F., Teng, J., Vaze, J. and Kirono, D. (2009) Influence of global climate model selection on runoff impact assessment. Journal of Hydrology, 379(1), 172–180

Christensen, J.H., Kjellström, E., Giorgi, F., Lenderink, G. and Rummukainen, M. (2010) Weight assignment in regional cli mate models. Climate Research, 44, 179–194

Curio, J. and Scherer, D. (2016) Seasonality and spatial variability of dynamic precipitation controls on the Tibetan Plateau. Earth System Dynamics, 7(7), 767–782. https://doi.org/10.5194/esd-7-767-2016

Dahri, Z.H., Moors, E., Ludwig, F., Ahmad, S., Khan, A., Ali, I., and Kabat, P. (2018) Adjustment of measurement errors to reconcile precipitation distribution in the high-altitude Indus basin. International Journal of Climatology, 2018(38), 3842–3860. https://doi.org/10.1002/joc.553

Davini, P., Cagnazzo, C., Fogli, P.G., Manzini, E., Gualdi, S. and Navarra, A. (2013) European blocking and Atlantic jet stream variability in the NCEP/NCAR reanalysis and the CMCC-CMS climate model. Climate Dynamics, 43, 71–85. https://doi.org/10.1007/s00382-013-1873-y

De Souza, K., Kituyi, E., Blane, H., Michele, L., Kallur, S.M. and James, D.F. (2015) Vulnerability to climate change in three hot spots in Africa and Asia: key issues for policy-relevant adaptation and resilience-building research. Regional Environmental Change, 15, 747–753. https://doi.org/10.1007/s10113-015-0755-8

Dee, D.P., Uppala, S.M., Simmons, A.J., Berrisford, P., Poli, P., Kobayashi, S., Andrae, U., Balmaseda, M.A., Balsamo, G., Bauer, P., Bechtold, P., Beljaars, A.C.M., van de Berg, L., Bidlot, J., Bormann, N., Delsol, C., Dragani, R., Fuentes, M. and Geer, A. (2011) The ERA-Interim reanalysis: configuration and performance of the data assimilation system. Quarterly Journal of the Royal Meteorological Society, 137, 553–597. https://doi.org/10.1002/qj.828

Dunn, P.K. (2004) Occurrence and quantity of precipitation can be modelled simultaneously. International Journal of Climatology, 24, 1231–1239. Ehret, U., Zehe, E., Wulfmeyer, V., Warrach-Sagi, K. and Liebert, J. (2012) HESS opinions "should we apply bias correction to global and regional climate model data?". Hydrology and Earth System Sciences, 16, 3391–3404. https://doi.org/10.5194/hess-16-3391-2012

FAO (2011) Irrigation in Southern and Eastern Asia in figures –AQUASTAT Survey – 2011. Available at: http://www.fao.org/nr/Water/aquastat/basins/indus/indus-CP_eng.pdf.

Forsythe, N., Fowler, H.J., Blenkinsop, S., Burton, A., Kilsby, C.G., Archer, D.R., Harpham, C. and Hashmi, M.Z. (2014) Application of a stochastic weather generator to assess climate change impacts in a semi-arid climate: The Upper Indus Basin. J Hydrol. Elsevier B.V, 517, 1019–1034. https://doi.org/10.1016/j.jhydrol.2014.06.031

Gebre, S.L. and Ludwig, F. (2014) Spatial and temporal variations of impacts of climate change on the hydrometeorology of Indus River Basin using R.C.P.s scenarios, South East Asia. Journal of Earth Science and Climatic Change, 5, 241. https://doi.org/10.4172/2157-7617.1000241

Giorgetta, M.A., Jungclaus, J., Reick, C., et al. (2013) Climate and carbon cycle changes from 1850 to 2100 in MPI-ESM simulations for the coupled model intercomparison project phase 5. Journal of Advances in Modeling Earth Systems, 5, 572–597. https://doi.org/10.1002/jame.20038

Giorgi, F. and Mearns, L. (2002) Calculation of average, uncertainty range, and reliability of regional climate changes from AOGCM. Simulations via the "reliability ensemble averaging" (REA) method. Journal of Climate, 15, 1141–1158. https://doi.org/10.1175/1520-0442(2002)015<1141:COAURA>2.0.CO;2

Gleckler, P.J., Taylor, K.E. and Doutriaux, C. (2008) Performance metrics for climate models. Journal of Geophysical Research, 113, D06104. https://doi.org/10.1029/2007JD008972

Hagemann, S., Chen, C., Haerter, J.O., Heinke, J., Gerten, D. and Piani, C. (2011) Impact of a statistical bias correction on the projected hydrological changes obtained from three GCMs and two hydrology models. Journal of Hydrometeorology, 12, 556– 578. https://doi.org/10.1175/2011jhm1336.1

Hasson, S. (2016) Future water availability from Hinukush- Karakoram-Himalaya upper Indus basin under conflicting climate change signals. Climate, 4(3), 40. https://doi.org/10.3390/cli4030040

Hasson, S., Böhner, J. and Chishtie, F. (2019) Low fidelity of CORDEX and their driving experiments indicate future climatic uncertainty over Himalayan watersheds of Indus basin. Climate Dynamics, 52, 777–798. https://doi.org/10.1007/s00382-018- 4160-0.

Heo, K.Y., Ha, K.J., Yun, K.S., Lee, S.S., Kim, H.J. and Wang, B. (2014) Methods for uncertainty assessment of climate models and model predictions over East Asia. International Journal of Climatology, 34, 377–390. https://doi.org/10.1002/joc.3692

Hersbach, H., Bell, B., Berrisford, P., Hirahara, S., Hor_anyi, A., Muñoz-Sabater, J., Nicolas, J., Peubey, C., Radu, R., Schepers, D., Simmons, A., Soci, C., Abdalla, S., Abellan, X., Balsamo, G., Bechtold, P., Biavati, G., Bidlot, J., Bonavita, M., Chiara, G., Dahlgren, P., Dee, D., Diamantakis, M., Dragani, R., Flemming, J., Forbes, R., Fuentes, M., Geer, A., Haimberger, L., Healy, S., Hogan, R.J., H_olm, E., Janiskov_a, M., Keeley, S., Laloyaux, P., Lopez, P., Lupu, C., Radnoti, G., Rosnay, P., Rozum, I., Vamborg, F., Villaume, S. and Thépaut, J.N. (2020) The ERA5 global reanalysis. QJRMS, 146 (730), 1999–2049. https://doi.org/10.1002/qj.3803

Hertig, E., Merkenschlager, C. and Jucundus, J. (2017) Change points in predictors–predictand relationships within the scope of statistical downscaling. International Journal of Climatology, 37, 16191633. https://doi.org/10.1002/joc.4801

Hewitt, K. (2005) The Karakoram anomaly? Glacier expansion and the 'elevation effect,' Karakoram Himalaya. Mountain Research and Development, 25, 332–340. https://doi.org/10.1659/0276-4741(2005)025[0332:TKAGEA]2.0.CO;2

Hewitt, K., Wake, C., Young, G.J. and David, C. (1989) Hydrological investigations at Biafo glacier, Karakoram Himalaya, Pakistan: an important source of water for the Indus River. Annals of Glaciology, 13, 103–108

Immerzeel, W.W., Pellicciotti, F. and Bierkens, M.F.P. (2013) Rising river flows throughout the twenty-first centImmerzeel. Nature Geoscience, 6, 742–745. https://doi.org/10.1038/ngeo1896

Immerzeel, W.W., Wanders, N., Lutz, A.F., Shea, J.M. and Bierkens, P.F.M. (2015) Reconciling high-altitude precipitation in the upper Indus basin with glacier mass balances and runoff. Hydrology and Earth System Sciences, 19, 4673–4687. https://doi.org/10.5194/hess-19-4673-2015

Kalnay, E., Kanamitsu, M., Kistler, R., et al. (1996) The NCEP/NCAR 40-year reanalysis project. Bulletin of the American Meteorological Society, 77, 437–471. https://doi.org/10.1175/1520-0477(1996)077<0437:TNYRP>2.0.CO;2

Kaspar-Ott, I., Elke, H., Seerin, K., Felix, P., Christoph, R., Heiko, P. and Jucunduss, J. (2019) Weights for general circulation models from CIMP3/CIMP5 in a statistical downscaling framework and the impact on future Mediterranean precipitation. International Journal of Climatology, 39, 3639–3654.

https://doi.org/10.1002/joc.6045

Khan, A.J. and Koch, M. (2018) Selecting and downscaling a set of climate models for projecting climate change for impact assessment in the upper Indus Basin (UIB). Climate, 6(4), 89. https://doi.org/10.3390/cli6040089

Khan, F., Pilz, J., Amjad, M. and Wiberg, D. (2015) Climate variability and its impacts on water resources in the Upper Indus Basin under IPCC climate change scenarios. International Journal of Global

Warming, 8(1), 46–69. https://doi.org/10.1504/IJGW.2015.071583

Khattak, M.S., Babel, M.S. and Sharif, M. (2011) Hydrometeorological trends in the upper Indus River basin in Pakistan. Climate Research, 46, 103–119. https://doi.org/10.3354/cr00957

Knutti, R. (2010) The end of model democracy? Climatic Change, 102(3–4), 395–404. https://doi.org/10.1007/s10584-010-9800-2

Knutti, R., Sedl_acek, J., Sanderson, B., Lorenz, R., Fischer, E.M. and Eyring, V. (2017) A climate model projection weighting scheme accounting for performance and interdependence. Geophysical Research Letters, 44, 1909–1918. https://doi.org/10.1002/2016GL072012

Kulkarni, A., Patwardhan, S., Kumar, K.K., Ashok, K. and Krishnan, R. (2013) Projected climate change in the hindukush-himalayan region by using the high-resolution regional climate model precis. Mountain Research and Development, 33(2), 142–151

Lanzante, J.R., Dixon, K.W., Nath, M.J., Whitlock, C.E., and Adams- Smith, D. (2018) Some pitfalls in statistical downscaling of future climate. Bulletin of the American Meteorological Society, 99(4), 791–803. https://doi.org/10.1175/BAMS-D-17-0046.1

Lutz, A.F., Immerzeel, W.W., Kraaijenbrink, P.D.A., Shrestha, A.B. and Bierkens, M.F.P. (2016b) Climate change impacts on the Upper Indus hydrology: sources, shifts and extremes. PLoS One, 11(11), e0165630. https://doi.org/10.1371/journal.pone.0165630

Lutz, A.F., Maat, H.W.T., Biemans, H., Shrestha, A.B., Wester, P. and Immerzeel, W.W. (2016a) Selecting representative climate models for climate change impact studies: an advanced envelope-based selection approach. International Journal of Climatology, 2016(36), 3988–4005

Mahmood, R. and Babel, M.S. (2012) Evaluation of SDSM developed by annual and monthly sub-models for downscaling temperature and precipitation in the Jhelum basin, Pakistan and India. Theoretical and Applied Climatology, 113, 27–44. https://doi.org/10.1007/s00704-012-0765-0

McCullagh, P. and Nelder, J.A. (1989) Generalized Linear Models. Monographs on Statistics and Applied Probability, Vol. 37. London: Chapman & Hall.

McSweeney, C.F., Jones, R.G., Lee, R.W. and Rowell, D.P. (2015) Selecting CIMP5 GCMs for downscaling over multiple regions. Climate Dynamics, 44(11–12), 3237–3260. https://doi.org/10.1007/s00382-014-2418-8

Meehl, G.A., Covey, C., Delworth, T., Latif, M., McAvaney, B., Mitchell, J.F.B., Stouffer, R.J. and Taylor, K.E. (2007) The WCRP CMIP3 multi-model dataset: a new era in climate change research. Bulletin of the American Meteorological Society, 88, 1383–1394.

Merkenschlager, C., Hertig, E. and Jacobeit, J. (2017) Nonstationarities in the relationships of heavy precipitation events in the Mediterranean area and the large-scale circulation in the second half of the 20th century. Global and Planetary Change, 151, 108–121. https://doi.org/10.1016/j.gloplacha.2016

Mishra, V. (2015) Climatic uncertainty in Himalayan water towers. Journal of Geophysical Research: Atmospheres, 120, 2689–2705. https://doi.org/10.1002/2014JD022650

Moberg, A., Jones, P.D., Lister, D., Walther, A., Brunet, M., Jacobeit, J., Alexander, L. V., Della-Marta, P. M., Luterbacher, J., Yiou, P., Chen, D., Klein Tank, A. M. G., Saladié, O., Sigr_o, J., Aguilar, E., Alexandersson, H., Almarza, C., Auer, I., Barriendos, M., Begert, M., Bergström, H., Böhm, R., Butler, C. J., Caesar, J., Drebs, A., Founda, D., Gerstengarbe, F.-W.,Micela, G., Maugeri, M., Österle, H., Pandzic, K., Petrakis, M., Srnec, L., Tolasz, R., Tuomenvirta, H., Werner, P. C., Linderholm, H., Philipp, A., Wanner, H. and Xoplaki, E. (2006) Indices for daily temperature and precipitation extremes in Europe analyzed for the. Journal of Geophysical Research: Atmospheres, 111(D22), 1984–2012. https://doi.org/10.1029/ 2006JD007103

Mueller, B. and Seneviratne, S.I.I. (2014) Systematic land climate and evapotranspiration biases in CMIP5 simulations. Geophysical Research Letters, 41, 128–134. https://doi.org/10.1002/2013GL058055

Navarro-Racines, C., Tarapues, J., Thornton, P., Jarvis, A. and Ramirez-Villegas, J. (2020) High-resolution and bias-corrected CMIP5 projections for climate change impact assessments. Scientific Data, 7, 7.

Palazzi, E., von Hardenberg, J. and Provenzale, A. (2013) Precipitation in the Hindu-Kush Karakoram Himalaya: observations and future scenarios. Journal of Geophysical Research: Atmospheres, 118(1), 85–100. https://doi.org/10.1029/2012JD018697

Palazzi, E., von Hardenberg, J., Terzago, S. and Provenzale, A. (2014) Precipitation in the Karakoram-Himalaya: a CMIP5 view. Climate Dynamics, 45, 21–45. https://doi.org/10.1007/s00382-014-2341-z

Philipp, A. (2003). Zirkulationsdynamische Telekonnektivität des Sommerniederschlags im südhemisphärischen Afrika. Dissertation, Bayerische Julius-Maximilians-Universität Würzburg

Pomee, M.S., Ashfaq, M., Ahmad, B. and Hertig, E. (2020) Modeling regional precipitation over the Indus River Basin of Pakistan using statistical downscaling. Theoretical and Applied Climatology,142, 29–57. https://doi.org/10.1007/s00704-020-03246-9

Preisendorfer, R. (1988) Principal Component Analysis in Meteorology and Oceanography, Vol. 42. Amsterdam: Elsevier.

Sanderson, B.M., Wehner, M. and Knutti, R. (2017) Skill and independence weighting for multi-model assessments. Geoscientific Model Development, 10(6), 2379–2395.

Sanderson, B.M. and Wehner, M.F. (2017) Model weighting strategy. In: Wuebbles, D.J., Fahey, D.W., Hibbard, K.A., Dokken, D.J., Stewart, B.C. and Maycock, T.K. (Eds.) Climate Science Special Report: Fourth National Climate Assessment, Vol. I. Washington, DC: US Global Change Research Program, pp. 436–442. https://doi.org/10.7930/J06T0JS3

Sanford, T., Frumhoff, P.C., Luers, A. and Gulledge, J. (2014) The climate policy narrative for a dangerously warming world. Nature Climate Change, 4, 164–166.

Shukla, J., DelSole, T., Fennessy, M., Kinter, J. and Paolino, D. (2006) Climate model fidelity and projections of climate change. Geophysical Research Letters, 33, L07702. https://doi.org/10.1029/2005GL025579

Soncini, A., Daniele, B., Gabriele, C., et al. (2015) Future hydrological regimes in the Upper Indus Basin: a case study from a high-altitude glacierized catchment. Journal of Hydrometeorology, 16(1), 306–326. https://doi.org/10.1175/JHM-D-14-0043.1

Sorg, A., Huss, M., Rohrer, M. and Stoffel, M. (2014) The days of plenty might soon be over in glacierized Central Asian catchments. Environmental Research Letters, 9(10), 1–8. https://doi.org/10.1088/1748-9326/9/10/104018

Sperber, K.R., Annamalai, H., Kang, I.S., Kitoh, A., Moise, A., Turner, A., Wang, B. and Zhou, T. (2013) The Asian summer monsoon: an intercomparison of CMIP5 vs. CMIP3 simulations of the late 20th century. Climate Dynamics, 41, 2711–2744. https://doi.org/10.1007/s00382-012-1607-6

Su, B., Huang, J., Gmmer, M., Jian, D., Tao, H., Jiang, T. and Zhao, C. (2016) Statistical downscaling of CMIP5 muli-model ensemble for projected changes of climate in the Indus River Basin. Atmospheric Research, 178-179, 138–149. https://doi.org/10.1016/j.atmosres.2016-03.023

Taylor, K.E. (2001) Summarizing multiple aspects of model performance in a single diagram. Journal of Geophysical Research, 106(D7), 7183–7192. https://doi.org/10.1029/2000JD900719

Taylor, K.E., Stouffer, R.J. and Meehl, G.A. (2012) An overview of CMIP5 and the experiment design. Bulletin of the American Meteorological Society, 93, 485–498

Trigo, R. and Palutikof, J. (2001) Precipitation scenarios over Iberia: a comparison between direct GCM. Output and different downscaling techniques. Journal of Climate, 14, 4422–4446.https://doi.org/10.1175/1520-0442(2001)014<4422:PSOIAC>20.CO;2

UN (2019). World Population Prospects 2019: Data Booklet. United Nations Department of Economic and Social Affair. Available at: https://population.un.org/wpp/Publications/Files/WPP2019_DataBooklet.pdf

Van Vuuren, D.P., Edmonds, J., Kainuma, M., Riahi, K., Thomson, A., Hibbard, K., Hurtt, G., Kram, T., Krey, V., Lamarque, J-F., Masui, T., Meinshausen, M., Nakicenovic, N., Smith, S.J. and Rose, S.K. (2011) The representative concentration pathways: an overview. Climatic Change, 2011(109), 5–31. https://doi.org/10.1007/s10584-011-0148-z

Voldoire, A., Sanchez-Gomez, E., Salas y Mélia, D., et al. (2013) The CNRM-CM5.1 global climate model: description and basic evaluation.Climate Dynamics, 40, 2091–2121. https://doi.org/10.1007/s00382-011-1259-y

Von Storch, H. and Zwiers, F.W. (1999) Statistical Analysis in Climate Research. Cambridge, UK: Cambridge University Press, p. 484. Warszawski, L., Frieler, K., Huber, V., Piontek, F., Serdeczny, O. and Schewe, J. (2014) The inter-sectoral impact model intercomparison project (ISI-MIP): project framework. Proceedings of the National Academy of Sciences of the United States of America, 111(9), 3228–3232. https://doi.org/10.1073/pnas.1312330110

Wijngaard, J.B., Klein, T.A.M.G. and Können, G.P. (2003) Homogeneity of 20th-century European daily temperature and precipitation series. International Journal of Climatology, 23, 679–692. https://doi.org/10.1002/joc.906

Wilby, R.L., Hay, L.E., Gutowski, W.J., Arritt, R.W., Takle, E.S., Pan, Z., Leavesley, G.H. and Martyn, P.C. (2000) Hydrological responses to dynamically and statistically downscaled climate model output. Geophysical Research Letters, 27(8), 1199–1202. https://doi.org/10.1029/1999GL006078

Wilks, S. (2006) Statistical methods in the atmospheric sciences. International Geophysical Series, 91.

## Supporting Information

**Table S1.** Overview of Study Stations……(Same as **Table 1** in article 1 of this thesis).

**Table S2.** Sub-Regional Precipitation Models….(Same as **Table 4** in article 1 of this thesis).

**Table S3.** HA-UIB precipitation Models ……(Same as **Table 5** in Article 1 of this thesis).

**Appendix S1.** The model development process …….(Same as **Section 3.6** in article 1 of this thesis).

## 9.3 Temperature Projections Over The Indus River Basin of Pakistan Using Statistical Downscaling

Muhammad Saleem Pomee[1,2] and Elke Hertig[1]

[1]Regional Climate Change and Health, Faculty of Medicine, University of Augsburg, Germany

[2]Pakistan Agricultural Research Council (PARC), Islamabad, Pakistan

This article was published in the atmosphere (https://doi.org/10.3390/atmos12020195)

## Abstract

We assessed maximum ($T_{max}$) and minimum ($T_{min}$) temperatures over Pakistan's Indus basin during the 21st century using statistical downscaling. A particular focus was given to spatiotemporal heterogeneity, reference and General Circulation Model (GCM) uncertainties, and statistical skills of regression models using an observational profile that could significantly be improved by recent high-altitude observatories. First, we characterized the basin into homogeneous climate regions using K-means clustering. Predictors from ERA-Interim reanalysis were then used to model observed temperatures skillfully and quantify reference and GCM uncertainties. Thermodynamical (dynamical) variables mainly governed reference (GCM) uncertainties. The GCM predictors under RCP4.5 and RCP8.5 scenarios were used as "new" predictors in statistical models to project ensemble temperature changes. Our analysis projected non-uniform warming but could not validate elevation-dependent warming (EDW) at the basin scale. We obtained more significant warming during the westerly-dominated seasons, with maximum heating during the winter season through $T_{min}$ changes. The most striking feature is a low-warming monsoon (with the possibility of no change to slight cooling) over the Upper Indus Basin (UIB). Therefore, the likelihood of continuing the anomalous UIB behavior during the primary melt season may not entirely be ruled out at the end of the 21st century under RCP8.5.

## Keywords

Statistical downscaling; multiple linear regression; predictor uncertainty; model weighting; elevation-dependent warming

## 1 Introduction

Anthropogenic activities are estimated to have caused approximately 1 °C global warming over pre-industrial levels (IPCC, 2018). The projected increase is likely between 2 °C to 5 °C by the end of the 21st century under different emission scenarios (IPCC, 2013). Warming has already and will continue to interact with the global climate system and the water cycle (e.g., Giorgi et al., 2019, Su et al., 2016) by triggering important feedbacks such as cloud radiative effects, snow, and surface albedo. It is also

projected that different regions will demonstrate variable climatic sensitivities to global warming. Generally, the Northern Hemisphere's high-latitudes and the mountain regions will show more warming than their counterparts (Karmalkar et al., 2017, Sutton et al., 2007, Pepin et al., 2015).

High mountains of the Hindukush–Karakorum–Himalayans contain large volumes of glaciers that are periodically replenished by precipitation from the Western Disturbances and South Asian Summer Monsoon (e.g., Kumar et al., 2019, Bolch et al., 2012, Azam et al., 2016]. Many large rivers originate from these mountains to meet the water needs of nearly a billion people in South Asia (e.g., Immerzeel et al., 2013). In addition to seasonal precipitation, the regional cryosphere serves as a dynamic control to regulate year-round flows in these rivers (Pritchard et al., 2017, Bolch et al., 2017).

The Indus River system depends heavily on the glacier and seasonal snow melting within these high-mountain regions (e.g., Lutz et al., 2014). Considering the climate hotspot nature (De Souza et al., 2015) of the Upper Indus Basin (UIB), an accurate assessment of its climatic response towards projected warming is highly desirable for supporting regional adaptations through scientific evidence. Notably, the temperature projections in the UIB are crucial as they influence future water availability and cryosphere stability. However, the UIB has shown a somewhat different response to global warming during recent periods (e.g., de Kok et al., 2018). For instance, in contrast to the global retreat of glaciers and ice fields (WGMS, 2020, Zemp et al., 2019), some evidence of glacial surging or at least stability has often been reported, particularly around the Karakoram—the so-called Karakoram anomaly ( e.g., Brun et al., 2017, Hewitt, 2005, Sakai and Fujita et al., 2017). Such glacial responses also contradict the adjacent eastern Himalayans and the Tibetan Plateau, where retreat seems more robust (Bolch et al., 2012, Azam et al., 2018). Moreover, an increasing diurnal temperature range (DTR) (e.g., Fowler and Archer, 2006) and a greater increase in maximum temperatures (e.g., Shrestha et al., 1999, Kattel et al., 2013, Nayava et al., 2017) over the UIB are different patterns than the globally decreasing DTR (e.g., Karl et al., 1993, Jones et al., 1999) and prominent warming of minimum temperatures over adjacent China and Tibetan Plateau (e.g., Tong et al., 2019, Panda et al., 2014). Additionally, elevation-dependent warming (EDW) is well accepted globally (e.g., Pepin et al., 2015, Miller et al., 2012), but some recent studies have argued its relevance within the UIB (e.g., Latif et al., 2019, Yaseen et al., 2020).

Apart from these observational anomalies, there are more contradictions about future temperature patterns over the UIB. For example, Latif et al. (2019) have concluded a year-round cooling that is stronger in the winter period, which is in stark contrast with many earlier studies (e.g., Fowler et al., 2006, Hasson et al., 2017, Khattak et al., 2011, Bashir et al., 2017). While most trend analysis studies have predicted a summer cooling (e.g., Fowler and Archer, 2006, Hasson et al., 2017, Bashir et al., 2017), almost all downscaling studies (Lutz et al., 2016, Ali et al., 2015) have projected consistent warming on seasonal and annual scales. Moreover, the magnitude of projected warming differs significantly among different studies. For instance, a recent study projected about 6 ºC warmer UIB (Ali

et al., 2021), but nearly half of this warming is reported by (Khan et al., 2017) under similar radiative forcing. Considering greater sensitivities of the Indus flows towards warming magnitude, where 1 $^{o}$C rise in the mean temperature can increase up to 16% glacial flows (Archer, 2003), such warming discrepancies can seriously implicate the adaptation planning.

Compared to precipitation, the regional temperatures result from relatively more straightforward processes, show less spatial variability, and the actual high-altitude measurements are more reliable (reduced wind drift influence). Still, regional studies show more contradictions with respect to temperature than precipitation signals over the UIB, as discussed earlier. For instance, increased (decreased) precipitation during the monsoon and winter seasons (pre-monsoon) over the UIB is robust among many studies (e.g., Khattak et al., 2011, Hasson et al., 2017, Bashir et al., 2017, Lutz et al., 2016) yielding at least consensus on the seasonal direction of future precipitation changes. It should also be noted that some precipitation observations exist over very high-altitude regions through periodic mass balance campaigns (e.g., Hewitt, 2005) to improve our understanding of regional precipitation variability. However, comparable temperature measurements are not available, and spatial inferences, which are mainly drawn through low-altitude observations, may increase temperature uncertainty among studies.

Such contradictions certainly warrant further scientific efforts to improve the quality of temperature projections. New observational sites, particularly within the UIB, should help in this regard, but it is still an ongoing process. Meanwhile, exploiting the available observational profile complemented significantly by the recent high-altitude observatories within the UIB can offer new simulation advantages (Pomee et al., 2020). Following a sub-regional analysis, adopting a suitable statistical downscaling approach, uncertainty quantification, and implementing a model ensemble are some options that may improve temperature simulations in this region. Pomee et al. (2020) argue that the basin characterization using climate patterns rather than arbitrarily defined sub-regions (e.g., Hasson et al., 2017, Ali et al., 2021) can support a more realistic climate analysis.

Previous studies highlighted large cold biases over the UIB in different GCM simulations (e.g., Ashfaq et al., 2017, Sperber et al., 2013, Cherchi et al., 2014). Model experiments (Ashfaq et al., 2017) further showed that regional GCM limitations are systematic and irrespective of the model horizontal resolution. The evaluation of high resolution (0.44$^{o}$) RCMs under the Coordinated Regional Climate Downscaling Experiments over the South Asian domain (Hasson et al., 2019, Mishra, 2015) and fine-scale (up to 4 km resolution) WRF simulations also yielded cold biases over the UIB (e.g., Dars et al., 2020, Pritchard et al., 2019). As biases in different GCMs/RCMs are systematic, statistical treatments like bias corrections are necessary for realistic climate change analysis (e.g., Ali et al., 2020, Khan and Koch, 2018, Akhtar et al., 2008). However, inadequate observational profile (e.g., Pomee et al., 2020, Palazzi et al., 2013) and unreliable observational proxies (e.g., Immerzeel et al., 2015) may not accurately

correct such systematic biases, particularly over high-altitude regions. Similarly, the uncertainty analysis using GCM simulated temperatures and insufficient observations may lack fidelity (Ali et al., 20121). In contrast, the GCMs' ability to simulate atmospheric circulation dynamics has considerably improved over time (e.g., Trigo et al., 2001, Kaspar-Ott et al., 2019). These atmospheric patterns can be used to construct downscaling models to infer more reliable temperature distributions. Despite these advantages, only a few studies (Mahmood et al., 2013) have used such predictor-driven temperature downscaling in our region. To provide a different and reliable simulation perspective, we used atmospheric predictors for (i) temperature downscaling, (ii) climate uncertainty quantification, and (iii) GCM selections to assess fine-scale temperature changes using a model ensemble over the UIB. Such temperature modeling has not been implemented in this region yet and holds the potential for further improvements.

We adopted large-scale atmospheric patterns from a reanalysis dataset to model ob- served maximum and minimum temperatures (hereafter Tmax and $T_{min}$, respectively) over the entire basin by following a robust statistical downscaling framework. We incorporated recent but hydrologically critical high-altitude observatories to improve spatial and EDW inferences over the basin. K-means clustering was employed beforehand to identify homogeneous climate sub-regions for fine-scale analysis. We further quantified the reference and model level uncertainties by comparing temperature governing predictors with two other reanalysis datasets and the historical simulations of the GCMs of the Coupled Model Intercomparison Project 5 (CMIP5) (Taylor et al., 2012). The principal drivers of the reference and GCM uncertainty were also identified. The predictor output of RCP4.5 and RCP8.5 scenarios was used to derive ensemble temperature changes during the 21st century. The Lower Indus considerations can estimate future water demand to support basin-level water management.

## 2 Study Area

The transboundary Indus River system of Pakistan (**Figure 1a**) derives runoff from high mountains of the Hindukush–Karakorum–Himalayans that also include K2 and ultimately descends into the Arabian Sea. In the UIB, covering approximately 4.03 $10^5$ $km^2$ (Dahri et al., 2018), the summer extent of glacial and perennial snow is estimated at 13%, and the regional cryosphere exceeds 70% of the UIB during the winter period (Hewitt, 1988). The summer freezing-line elevation within the UIB ranges from 3550 m to 5500 m above mean sea level (Khan et al., 2015). The western disturbances, Indian summer monsoon, and Tibeaten-high regulate year-round moisture and energy fluxes into the basin. A combination of the glacial, nival, and pluvial regimes, whose relative contributions vary further with hypsometry and dominant modes of the large and regional scale circulations, regulate the runoff from UIB (e.g., Hewitt, 2005, Pritchard et al., 2019). In contrast, the Lower Indus has an arid to semi-arid climate and depends heavily on water melting from the UIB.

Global warming has a twin menace for the basin sustainability: changes in large-scale circulations and alterations of the melt contributions. Full energy balance studies alongside precipitation analysis are required to assess the basin's future hydrological response precisely. Among others, Archer (2003) successfully demonstrated the effectiveness of different temperature measurements to assess seasonal water availability from the UIB. We only focused on Pakistan's basin area **(Figure 1b)** due to data availability constraints from other countries. The study area represents the largest and the highest fraction of the basin and is regarded here as a representative for the whole basin.

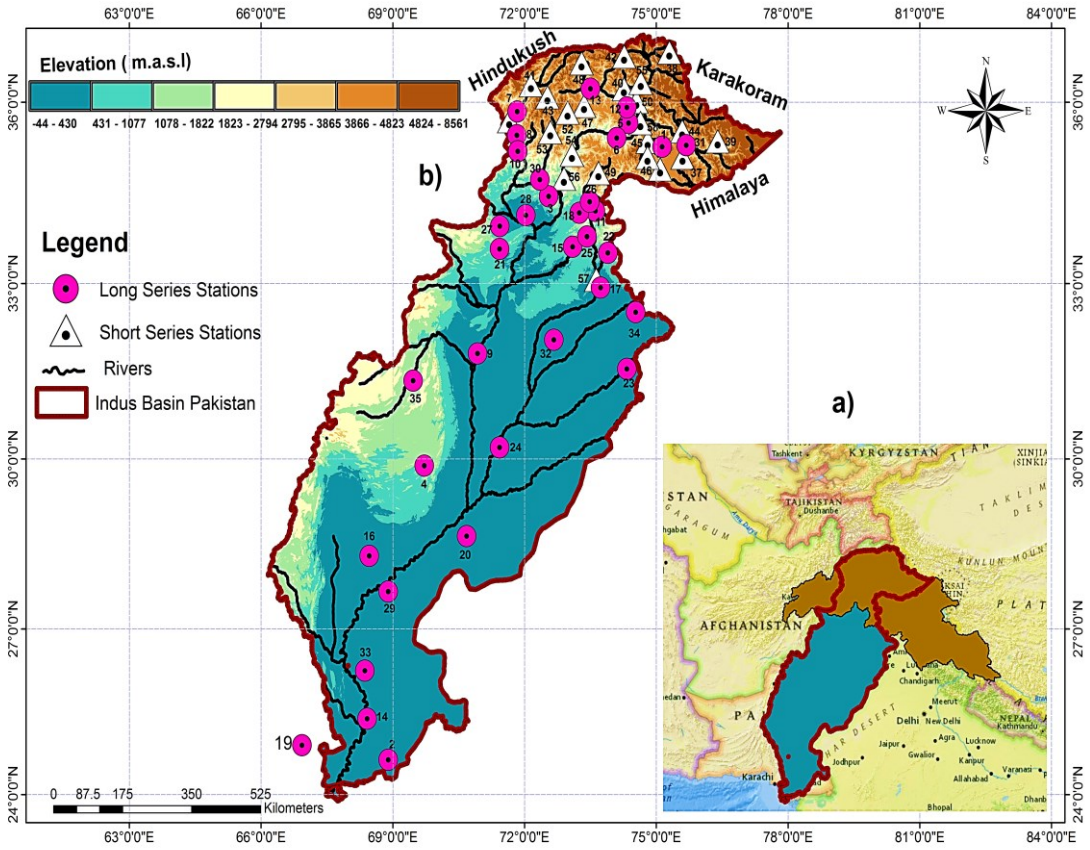


Source: Adapted from Pomee et al. (2020).

**Figure 1.** (**a).** The transboundary Indus River Basin, indicating Upper Indus Basin (brown), Lower Indus (blue), and demarcation of the study area (red boundary). **b)** Locations of the meteorological stations used in the study. Pink circles show the longer time series (1979–2015), and triangles indicate high-altitude stations with shorter time series (1994–2015). Note that the color scheme in **(b)** represents the elevation variation in the study area. The study stations' geographic details are given after the numbers shown in **b)** in Supplementary Information as **Table S1**.

## 3. Data and Methodology

This study is a part of the regional project that aims to support climate adaptations across the study basin by analyzing key hydrological variables. Pomee et al. (2020) have modeled the observed

precipitation dynamics using predictor-predictand relationships by accounting for observed spatial variability on seasonal scales. Pomee and Hertig (2021) further used precipitation governing predictors to model future precipitation response and associated uncertainties amid selected radiative forcing scenarios.

Here, we further extend our analysis to identify $T_{max}$ and $T_{min}$ governing (atmospheric) patterns within a statistical downscaling framework, quantification of the reference and GCM level uncertainties, and predictor-driven future temperature changes over fine scales. We used the Indus Basin's climate characterization of Pomee et al. (2020) to provide a consistent and coherent perspective about projected precipitation and temperature changes that simultaneously govern the regional hydrology. We briefly provide details of the adapted regionalization scheme, downscaling model development, and GCM ranking processes in the following to give the necessary background for the current work. More details are available in Pomee et al. (2020) and Pomee and Hertig (2021).

## 3.1 Predictand Data

We used a monthly temperature ($T_{max}$ and $T_{min}$) time series of 58 observatories located across the study basin (**Figure 1b**) that simultaneously provide historic (low altitude) and more recent high-altitude climate structures within the UIB. The high-altitude considerations with 23 stations despite shorter time series (average of 17 years) provided a unique opportunity to assess EDW and stability of the regional cryosphere in the light of observations. **Table S1** of the Supporting Information provides more details about the study stations.

Pomee et al. (2020) identified three major precipitation seasons across the Indus basin. These include the winter season (WS) (December to March), pre-monsoon season (PMS) (April to May), and monsoon season (MS) (July to September). K-Means clustering (Wilks, 2006) using Spearman correlation as a distance measure was used to identify sub-regions with similar precipitation variability. During regionalization, the objective was to maximize (minimize) the correlation within (across) regions to define sharp regional boundaries. The cluster members of a region exhibit similar climate characteristics. Two different regionalization experiments were performed to analyze precipitation dynamics over the entire basin and separately over the high-altitude UIB. The regionally representative stations (RR) were identified through multiple considerations, such as station homogeneity, length of time series, and correlation with regional centroids. The time series of RR served as predictands for downscaling models. The output of two regionalization experiments is shown in **Figures 2 and 3**, respectively. For more details, see Pomee et al. (2020).

We adapted the precipitation regions and associated RR to downscale $T_{max}$ and $T_{min}$ distributions to provide consistent feedback on key hydrological variables across the basin. The identified regions cover the southern Himalayans, trans-Himalayans (including the Karakoram), and northwestern (Hindukush) parts of the UIB that mainly regulate the water supply. In addition, a significant clustering of recent high-altitude observatories in these regions can also facilitate inferences about EDW. Similarly, the projections over the irrigated plains primarily represent the seasonal water demand in the Lower Indus. Thus, our adapted regionalization framework provides realistic grounds for a comprehensive water supply-demand analysis over the basin. We also tested RR for homogeneity by following (Wijngaard et al., 2003) .

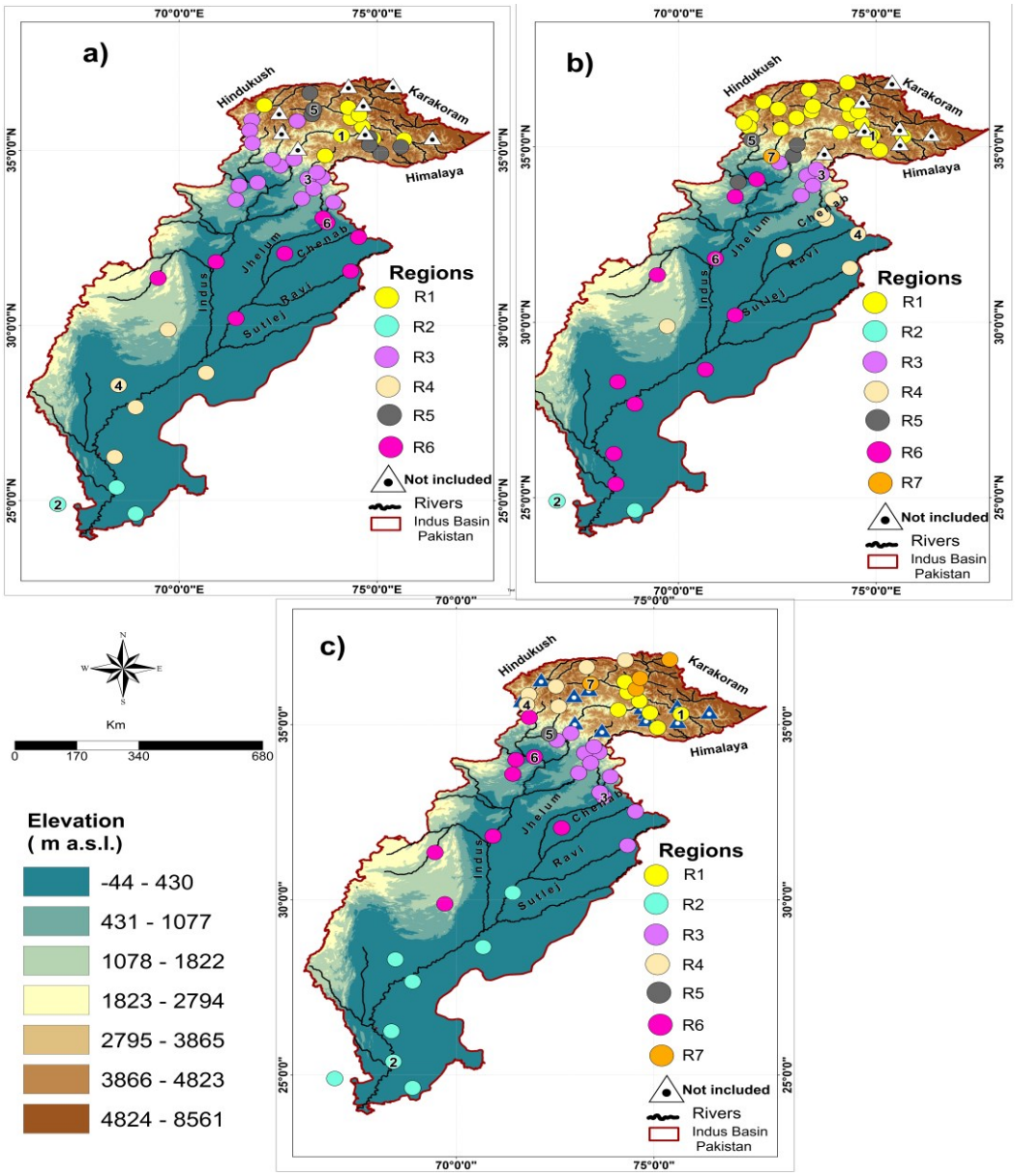


Source: Adapted from Pomee et al. (2020)

**Figure 2.** The climate characterization of the Indus Basin of Pakistan using K-means cluster analysis. Different colored circles represent the identified regions. In the legend Regions, R stands

for the region, and the following number indicates its number (i.e., R1 is region 1, and so on). The circles with the same color indicate the members of a given region that show similar co-variability. The circles with numbers define the location of regional representative stations (RR). For example, a circle with the number 2 indicates the representative station's (RR) location of the second region (i.e., R2). Triangles represent those stations, which could not be assigned to any of the identified regions. The WS **(a),** PMS **(b),** and MS **(c)** regionalization.

## 3.2 Predictor Data

We used ERA-Interim reanalysis data (Dee et al., 2012) to identify governing predictors of the observed $T_{max}$ and $T_{min}$ patterns over the basin. We did not use ERA5 (Hersbach et al., 2018) as it was not publically available in 2016 when our research began. Existing regional studies (e.g., Pomee et al., 2020, Mahmood and Babel, 2013) were consulted for initial predictor selection. The variables (**Table 1**) include different circulation dynamics (geopotential heights, sea level pressure, meridional, and zonal winds), thermo-dynamic (relative and specific humidity), and thermal parameters (air temperature) across the troposphere. Predictors were re-gridded to $2^o$ x $2^o$ spatial resolution. The monthly averages of each available predictor were grouped into the seasons to correspond with the RR time series of the temperature predictand.

A larger domain ($10^o$ E to $100^o$ E, $10^o$ N to $60^o$ N) was used for circulation-dynamic and thermal variables compared to thermodynamic predictors ($64^o$ E to $80^o$ E, $22^o$ N to $40^o$ N) to account for both large-scale and more localized forcing on regional temperatures. We performed S-mode Varimax-rotated principal component analysis (PCA) (Preisendorfer, 1988) separately on each predictor field for dimension reduction. Using a modified dominance criterion (Philipp, 2003) with some additional constraints (Pomee et al., 2020), we retained PCs that sufficiently explain predictor variance (**Table S2**). The resulting PC scores (loadings) served as predictor time series (locations of the centers of variation) for downscaling models.

## 3.3 Statistical Modeling Framework

We selected the multiple linear regression framework to model predictor-predictand relationships in the observations since the time series of nearly all RR follow the normal distribution (e.g., Shapiro–Wilk test). To identify robust atmospheric drivers of the regional temperatures ($T_{max}$ and $T_{min}$) from the chosen predictors (**Table 1**), we adapted the downscaling framework of Pomee et al. (2020). The typical downscaling framework uses the mean squared error skill score (MSESS) as a performance criterion (Wilks, 2006) within cross-validation through 1000 random calibration-validation

iterations. In addition, multi-collinearity among predictors was also considered during the modeling process.

The models that showed maximum MSESS during the calibration and validation process using independent predictors were selected for downscaling. We also calculated root mean square errors (RMSE) and coefficient of determination (R2) to evaluate the statistical performance. The final models were further tested for their error distributions and heteroscedasticity (Breusch–Pagan test) to meet other multiple linear regression requirements. We constructed downscaling models for the RR of each region to infer mean temperature variations in the respective regions

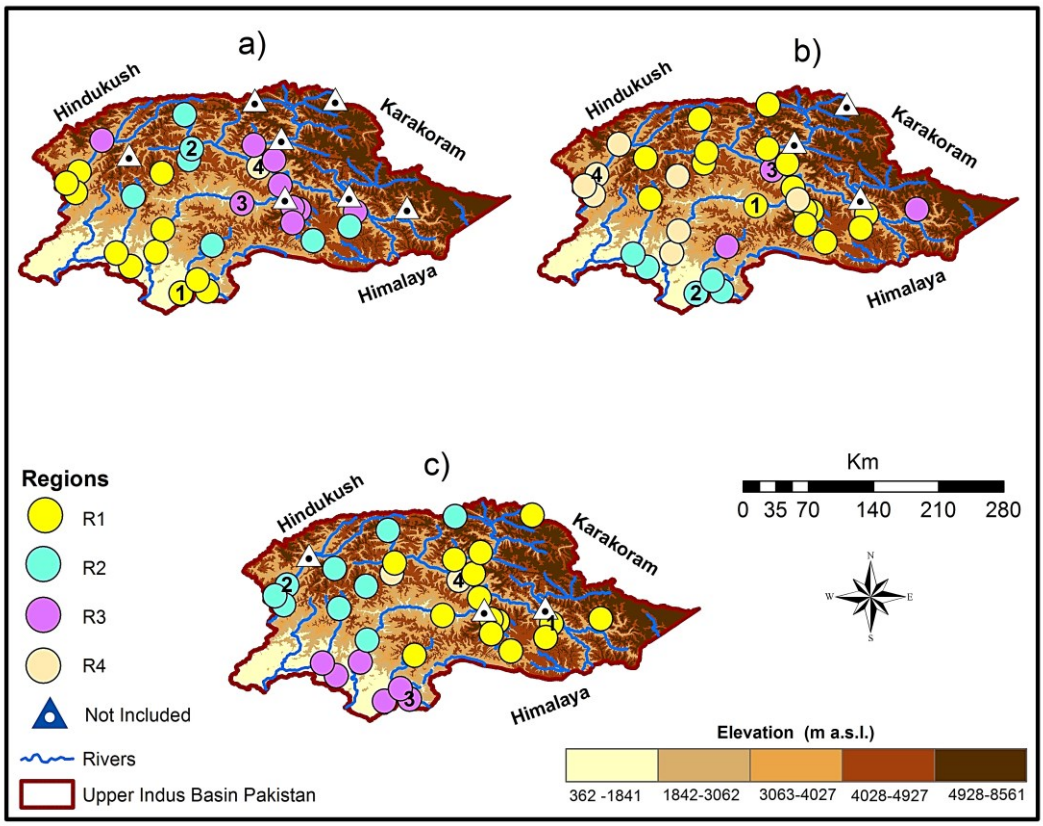


...Source: Adapted from Pomee et al., (2020)

**Figure 3.** It is the same as **Figure 2** but shows regions under the high-altitude Upper Indus Basin (UIB) regionalization experiment.

## 3.4 GCMs: Predictor-Based Downscaling

Initially, we considered more than 60 CMIP5-GCMs. However, the availability of governing predictors (**Table 1**) and their complete spatial coverage over the study domain restricted this number to only eight. Many GCMs have large simulation gaps over the high mountains for lower-tropospheric predictors due to the intersection of pressure coordinates with regional elevations. These simulation gaps can not be filled with interpolation schemes (Pomee et al., 2021) and restrict

the computation of spatially consistent PCA during the historical period. Therefore, we could only use the output of these eight models during the historical (1976–2005) and two future time-slices (2041–2070 and 2071–2100). We considered governing predictors from two scenarios (RCP4.5 and RCP8.5) for temperature projections. These RCPs represent the managed (RCP4.5) and unabated (RCP8.5) societal response throughout the 21st century and are considered suitable for supporting regional adaptations (Sanford et al., 2014). Further, we only considered the first realization ("r1i1p1") of these GCMs for downscaling. **Table S3** provides information about the CMIP5 models used in our study.

Before downscaling, the GCM predictors were also conservatively re-gridded to $2^o$ x $2^o$ to match with ERA-Interim predictor resolution. The model predictors were standardized over the historical and future time-slices (separately for each scenario). These standardized modeled variables were projected onto the corresponding PC loadings of ERA-Interim to generate new predictor time series (more details on this method in Von Storch and Zeiers, 1984). The new predictor time series were used in the ERA-Interim-based regression models to derive downscaled historical and future Tmax and $T_{min}$ distributions. The difference between downscaled historical and two future time slices (separately for each RCP and time slice) was then used to compute median temperature changes over the basin.

We also used the signal-to-noise ratio (SNR) to evaluate the robustness of projected warming (signals) against the observational uncertainty (noise) at the individual model and ensemble levels. This typical variate of the SNR can be computed by dividing median changes with historical standard deviations, and an SNR > 1 indicates the robustness of change signals compared to observational uncertainty.

## 3.5 GCM Ranking for Uncertainty Quantification

Pomee and Hertig (2021) developed a stepwise procedure to rank GCMs based on their ability to simulate precipitation-governing predictors in the historical period. They compared loading patterns of the S-mode PCA of governing predictors from a reanalysis dataset with corresponding GCM-simulated variables to evaluate such reference-model correspondence. A simple performance score (PS) was computed using two of the three summary statistics of the Taylor diagram (Taylor, 2001) to quantify the predictor correspondence. Regression coefficients were used as weights during the model evaluation process to identify GCMs that better simulate more influential predictors in a given regression model. Lastly, the consideration of model performance over multiple regions helped to select a GCM with simulation advantages over spatial scales.

We also used this model ranking process to evaluate the GCMs' performance in representing temperature governing predictors (**Table 1**) during the overlapping historical period (1979–2005). Note that ERA-Interim only offers data from 1979 onwards. Based on predictor-simulation similarities (i.e., PS), we further quantified the model (and ensemble) level uncertainties ((1 PS) x 100) to assess the reliability of subsequent projections at different spatiotemporal scales. **Appendix A** provides more details on this procedure.

## 3.6 Reference Uncertainty

We further consider temperature governing predictors (**Table 1**) from ERA5 (Hersbach et al., 2018) and NCEP-NCAR-II (Kalnay et al., 1996) reanalysis datasets to evaluate the regional robustness of ERA-Interim predictors. The weighted PS of these two additional reanalysis datasets (computed separately) was used to quantify the range of reference uncertainty and define the usefulness of ERA-Interim for temperature projections over the study basin.

# 4 Results and Discussion

## 4.1 Governing Predictors

**Table 1** shows the relative frequency of predictors that govern regional temperatures and identified through regression models. Different lower-tropospheric conditions overwhelmingly dominated by the wind components mostly resolved the basin-wide seasonal distributions of both temperatures. However, near-surface humidity (hur1000, hus1000) also played an important role, particularly during the westerly-dominated seasons (i.e., WS and PMS). Our downscaling framework also recognized the complexities of the MS dynamics by identifying relatively more complex models (containing more predictors and atmospheric levels) compared to other seasons.

However, the predictors exhibited a stronger seasonality within and across the temperature fields. For example, the role of va850 (~ 61%) and ta850 (~ 30%) was maximum in the WS simulations of $T_{max}$, but their importance as predictors reduced significantly during the warmer periods and reached the lowest levels during the MS (~ 10% and 9%, respectively). In contrast, va850 showed maximum contribution (~40%) during the MS to resolve $T_{min}$ simulations, but this predictor (along with ta850) could not influence $T_{min}$ patterns during the westerly-dominated seasons. For predictor symbols, please refer to **Table 1**.

Similarly, hur1000 showed maximum contributions (~ 35%) for modeling $T_{max}$ distributions during the PMS but remained ineffective in the WS. On the other hand, hus1000 (~ 27%) appeared as the most important predictor in resolving seasonal $T_{min}$ patterns, with the highest contributions during

**Table 1.** Seasonal contributions of different predictors (in %) that helped to resolve observed temperatures ($T_{max}$ and $T_{min}$) over the Indus basin of Pakistan. Multiple linear regression models were used to identify these temperature-governing predictors. Column 2 provides the list of large-scale atmospheric predictors used in this study, where the symbols zg, va, ua, hur, hus, ta, and psl denote the geopotential heights, meridional winds, zonal winds, relative humidity, specific humidity, air temperature, and mean sea level pressure fields, respectively. The number after each predictor symbol reflects the atmospheric level (pressure level in hPa). The last column shows average predictor frequencies over all three seasons.

| **$T_{max}$** | | | | | |
|---|---|---|---|---|---|
| | **Predictors** | **WS** | **PMS** | **MS** | **All Seasons** |
| 1 | va200 | 0 | 0 | 0 | 0 |
| 2 | ua200 | 0 | 0 | 0 | 0 |
| 3 | zg200 | 2.4 | 0 | 1.3 | 1.4 |
| 4 | zg500 | 0 | 0 | 0 | 0 |
| 5 | zg700 | 0 | 0 | 0 | 0 |
| 6 | hus700 | 0 | 0 | 0 | 0 |
| 7 | hur 700 | 0 | 0 | 0 | 0 |
| 8 | hur1000 | 0 | 34.6 | 15.2 | 14.4 |
| 9 | hus1000 | 7.3 | 7.7 | 0 | 3.4 |
| 10 | va500 | 0 | 0 | 45.6 | 24.7 |
| 11 | ua500 | 0 | 0 | 19 | 10.3 |
| 12 | ua700 | 0 | 0 | 0 | 0 |
| 13 | va700 | 0 | 0 | 0 | 0 |
| 14 | va850 | 61 | 42.3 | 10.1 | 30.1 |
| 15 | ua850 | 0 | 0 | 0 | 0 |
| 16 | ta850 | 29.3 | 15.4 | 8.9 | 15.8 |
| 17 | psl | 0 | 0 | 0 | 0 |
| Total | | 100 | 100 | 100 | 100 |
| **$T_{min}$** | | | | | |
| 1 | va200 | 0 | 0 | 0 | 0 |
| 2 | ua200 | 0 | 0 | 0 | 0 |
| 3 | zg200 | 0 | 0 | 0 | 0 |
| 4 | zg500 | 0 | 0 | 0 | 0 |
| 5 | zg700 | 0 | 0 | 0 | 0 |
| 6 | hus700 | 0 | 0 | 0 | 0 |
| 7 | hur 700 | 0 | 0 | 0 | 0 |
| 8 | hur1000 | 0 | 0 | 0 | 0 |
| 9 | hus1000 | 100 | 34.4 | 8.2 | 26.7 |
| 10 | va500 | 0 | 0 | 44.3 | 25.7 |
| 11 | ua500 | 0 | 21.9 | 0 | 6.7 |
| 12 | ua700 | 0 | 0 | 0 | 0 |
| 13 | va700 | 0 | 25 | 0 | 7.6 |
| 14 | va850 | 0 | 0 | 39.3 | 22.9 |
| 15 | ua850 | 0 | 18.8 | 8.2 | 10.5 |
| 16 | ta850 | 0 | 0 | 0 | 0 |
| 17 | psl | 0 | 0 | 0 | 0 |
| Total | | 100 | 100 | 100 | 100 |

the WS (100%). Different zonal wind PCs also played a significant role in explaining $T_{min}$ distribution, particularly during the PMS. Similarly, strong seasonality was also apparent for the mid-tropospheric winds (va500 and ua500). Statistically identified governing predictors can also explain the essential features of regional climatology. For example, the dominance of dynamic forcing (winds) during the MS and WS represent the strength of the easterly and westerly circulations that shape the regional climate during these periods (e.g., Pomee et al., 2020, Cannon et

al., 2015). Similarly, the increased role of atmospheric humidity in the PMS simulations may represent regional convection due to seasonal warming. The specific humidity PCs that primarily explain the $T_{min}$ seasonal distributions may be connected to cloud radiative feedbacks.

## 4.2 Statistical Performance of Downscaling Models

Our downscaling framework, despite significant spatial variability in the basin, skillfully modeled the day ($T_{max}$) and night ($T_{min}$) time temperatures during all three seasons, as shown by the validation performance metric (i.e., MSESS, RMSE, R2) in **Table 2** and **Table S4**. Validation performance reflects a downscaling model's ability to transfer statistical relationships to other (unknown) periods and strongly influences the projection reliability. However, the performance metric showed seasonality, varied with spatial scales and between the temperature variables. For instance, the PMS simulations ($T_{max}$ and $T_{min}$), dominated by various thermodynamic predictors, showed very high validation skills (average MSESS >88%) over the four UIB and two Lower Indus regions. Similarly, the WS models containing mostly the circulation-dynamic and thermodynamic predictors also demonstrated high simulation performance over the three UIB (MSESS ~ 80%) and two LI regions (MSESS > 83%). Therefore, the downscaling models showed high statistical skills for simulating observed temperatures during the westerly-dominated seasons that mainly regulate the regional cryosphere. Such skillful observational models also provide more reliable future inferences about cryosphere dynamics in these seasons.

However, the downscaling models showed relatively low MS performance, particularly for the $T_{max}$ simulations over the five UIB regions (MSESS ~70%). The statistical skills reduced further over the two Lower Indus regions. Interestingly, the validation skills lacked over those regions that show high temperatures (e.g., R3, R6, and R2). In these particular cases, the climatological reference showed a higher performance due to lesser inter-seasonal variation, and therefore the relative improvements of the downscaling models were reduced. Relatively high R2 and low RMSE values for these regions further supported this argument. The MS regional complexity (e.g., Ashfaq et al., 2017) may also contribute to the relatively low model performances. Still, the MS skills over the UIB were high enough to reliably infer cryosphere response during the main melt season.

In general, the $T_{min}$ models were simpler (fewer predictors were required) compared to $T_{max}$ and showed high statistical performance during all three seasons. Comparing seasons, the MS models were relatively more complicated for both temperatures. Interestingly, the HA regions were modeled with greater statistical skills during all three seasons, improving our understanding of projected temperature changes over these hydrologically sensitive regions. These skillful models may also help to assess seasonal water supply (UIB) and demand (Lower Indus) perspectives simultaneously to support integrated water management amid climate change scenarios.

**Table 2.** Information about the identified sub-regions, regionally representative stations (RR), governing predictors, and the $T_{max}$ downscaling models' statistical performance during all three seasons under the basin-wide regionalization experiment. The blue (violet) and black colors differentiate among the UIB (Lower Indus) regions and the entire basin. In the table, Reg. Alt is the altitudinal range (elevations in m above mean sea level) for a given region, Mean Obs. Temp indicates the mean observed $T_{max}$ at RR. Predictors (PCs) show the explaining variables (number of PCs). RMSE, MSESS, and $R^2$ are the root mean square errors, mean squared error skill scores, and coefficient of determination during the calibration (Cal) and validation (Val) periods, respectively. Additionally shown are the average statistical performances over the UIB (Avg. UIB), Lower Indus (Avg. Lower Indus), and across the entire basin (Avg. basin).

| Region | Reg.Alt (m-amsl) | RR | Mean Obs. $T_{max}$ (C°) | Predictors (Name) | PCs (Nos) | RMSE (C°) Cal | RMSE (C°) Val | MSESS (%) Cal | MSESS (%) Val | $R^2$ Cal | $R^2$ Val |
|---|---|---|---|---|---|---|---|---|---|---|---|
| **WS Models** | | | | | | | | | | | |
| R1 | 2223 (1251-3200) | Chilas | 15.16 | va850 | 11 | 1.29 | 1.43 | 84.34 | 80.00 | 0.84 | 0.86 |
| R3 | 1173.5 (308-2744) | Kakul | 15.23 | va850 | 14 | 1.20 | 1.37 | 81.47 | 75.31 | 0.82 | 0.83 |
| R5 | 3266 (2156-4030) | Gupis | 7.79 | temp850 | 6 | 1.36 | 1.46 | 83.78 | 80.75 | 0.84 | 0.85 |
| R4 | 266 (35-1097) | Jacobabad | *25.85* | *hus1000* | *3* | 1.25 | 1.30 | 87.62 | 86.32 | 0.88 | 0.89 |
| R6 | 365 (122-1405) | Jehlum | 22.44 | temp850+zg200 | 7 | 1.35 | 1.50 | 83.27 | 78.39 | 0.83 | 0.86 |
| Avg. Basin | | | 17.29 | | 8 | 1.29 | 1.41 | 84.10 | 80.15 | 0.84 | 0.86 |
| Avg. UIB | | | 12.73 | | 10 | 1.28 | 1.42 | 83.20 | 78.69 | 0.83 | 0.85 |
| Avg. Lower Indus | | | 24.15 | | 5 | 1.30 | 1.40 | 85.45 | 82.36 | 0.86 | 0.88 |
| **PMS Models** | | | | | | | | | | | |
| R1 | 2627 (1251-4030) | Astore | 19.97 | va850 | 7 | 1.27 | 1.38 | 90.39 | 88.36 | 0.90 | 0.92 |
| R3 | 1327 (508-2168) | Ghari Duputta | 31.91 | hur1000+hus1000 | 3 | 1.29 | 1.37 | 91.04 | 89.62 | 0.91 | 0.91 |
| R5 | 1281 (353-2591) | Dir | 27.99 | hur1000 | 3 | 1.36 | 1.41 | 90.00 | 88.83 | 0.90 | 0.91 |
| R7 | 961 (961) | Saidu Sharif | 31.75 | hur1000 | 2 | 1.41 | 1.46 | 89.88 | 88.83 | 0.90 | 0.91 |
| R4 | 419 (187-1097) | Sialkot | 36.64 | temp850+va850 | 8 | 1.13 | 1.26 | 89.23 | 86.17 | 0.89 | 0.90 |
| R6 | 259 (28-1405) | DI Khan | 38.06 | hur1000+hus1000 | 3 | 0.98 | 1.05 | 92.75 | 91.40 | 0.93 | 0.93 |
| Avg. Basin | | | 31.05 | | 4 | 1.24 | 1.32 | 90.55 | 88.87 | 0.91 | 0.91 |
| Avg. UIB | | | 27.91 | | 4 | 1.33 | 1.41 | 90.33 | 88.91 | 0.90 | 0.91 |
| Avg. Lower Indus | | | 37.35 | | 6 | 1.06 | 1.16 | 90.99 | 88.79 | 0.91 | 0.92 |
| **MS Models** | | | | | | | | | | | |
| R1 | 2218 (1251-4030) | Sakardu | 30.17 | va500 | 13 | 1.16 | 1.33 | 80.10 | 72.47 | 0.80 | 0.82 |
| R3 | 746.25 (122-2591) | Jehlum | 35.08 | hur1000+va500+zg200 | 13 | 0.74 | 0.87 | 70.26 | 55.26 | 0.70 | 0.76 |
| R4 | 2868 (1464-3719 | Darosh | *35.27* | *ua500* | *10* | 0.94 | 1.08 | 79.83 | 72.42 | 0.80 | 0.82 |
| R5 | *961 (961)* | Saidu Sharif | 33.19 | va500 | 11 | 0.78 | 0.90 | 72.08 | 62.05 | 0.72 | 0.77 |
| R7 | 2892.5 (2156-4730) | Gupis | *29.52* | *va850+ua500* | *11* | 1.10 | 1.24 | 84.16 | 79.41 | 0.85 | 0.85 |
| R6 | 659 (172-1425) | Risapur | 36.50 | Temp850+hur1000+va850 | 10 | 0.94 | 1.05 | 73.34 | 65.68 | 0.73 | 0.78 |
| R2 | 52 (9-122) | Hyderabad | 36.51 | temp850+va500 | 11 | 0.67 | 0.74 | 68.33 | 58.81 | 0.68 | 0.72 |
| Avg. Basin | | | 33.75 | | 11 | 0.90 | 1.03 | 75.44 | 66.59 | 0.75 | 0.80 |
| Avg. UIB | | | 32.65 | | 12 | 0.94 | 1.08 | 77.29 | 68.32 | 0.77 | 0.80 |
| Avg. Lower Indus | | | 36.51 | | 11 | 0.81 | 0.90 | 70.84 | 62.25 | 0.71 | 0.75 |

## 4.3 Quantifying Uncertainties

### 4.3.1 Reference uncertainty

We used the weighted PS (**Table 3**) of ERA-Interim predictors to quantify reference uncertainty. The PS represents the simulation robustness of ERA-Interim predictors against two other reanalysis datasets. Generally, a high PS strongly verified the ERA-Interim usefulness for regional temperature ($T_{max}$ and $T_{min}$) modeling.

However, the reliability of ERA-Interim predictors varied over the seasons. For instance, the WS predictor correspondence among three reanalysis datasets was maximum for both temperatures. The MS and PMS predictor agreement followed this. From the perspective of temperature variables, the simulations of $T_{max}$ predictors were more robust than $T_{min}$. Among reanalysis datasets, the ERA-Interim predictors showed greater correspondence with ERA5 during the WS and MS. However, the NCEP-NCAR-II better simulated the PMS governing patterns. Such predictor matching suggests ERA-Interim simulations' robustness against at least one of the two additional reanalysis data during all seasons. If both additional datasets had shown poor correspondence, the fidelity of ERA-Interim predictors would have certainly decreased. Therefore, using ERA-Interim predictors for seasonal temperatures was justified.

A striking feature relates to the substantial agreement among multiple datasets for $T_{max}$ predictors over high-altitude regions in all three seasons (e.g., MS-R4, R7, WS-R5, and PMS-R1). These are hydrologically the most critical regions where $T_{max}$ regulates seasonal melting. Therefore, their robust simulations during the observations can also provide better inferences about projected cryosphere response and water availability under global warming scenarios.

Among predictors, the thermodynamic variables (hus1000 and hus1000) largely controlled the magnitude of reference uncertainty. For example, the simulations of hus1000 in NCEP-NCAR-II were significantly different from ERA-Interim (lower PS) during the WS. As this predictor alone resolved the basin-wide $T_{min}$ distributions (**Table 1**); therefore, the associated uncertainty increased (up to 31%). Similarly, hur1000 helped to model the $T_{max}$ patterns over multiple sub-regions during the PMS (i.e., R1, R3, R5, and R6). However, ERA5 showed more differences in its simulation, which increased the seasonal uncertainty. Likewise, one influential PC of hur1000 (i.e., high regression coefficient) helped to resolve MS-$T_{max}$ conditions over the two regions (R3 and R6). However, both additional datasets showed more differences in the representation of hur1000, which increases uncertainty over these particular regions.

Such differences in thermodynamic variables may stem from variations in simulation models and parameterization schemes representing regional convection that strongly influence local climate.

The variable resolutions of the reanalysis datasets (e.g., Pomee et al., 2020) may also contribute to the simulation differences. Further analysis revealed that the spread of humidity predictor variables mainly reduced the PS, despite higher inter-reference correlations (~ 0.50) in many of these cases. Although the uncertainty magnitude can be reduced by not including predictor spread during uncertainty quantification, we argue that predictor variance considerations are essential due to their importance for climate change analysis. However, the simulations of various dynamic and thermal predictors, which largely govern the basin-wide temperature distributions, are quite robust among these datasets. Therefore, considering regional complexity and the variety of governing predictors, such finer-scale inter-reference robustness provides strong confidence in using ERA-Interim for temperature modeling.

### 4.3.2 Model uncertainty

We similarly used the weighted PS to identify better-performing GCMs for both temperatures. **Table 4** shows the performance of individual models and their ensemble in reproducing ERA-Interim simulated $T_{max}$ predictors. Generally, most GCMs showed a stronger inter and intra-region correspondence with ERA-Interim variables during the WS and PMS. Due to the MS complexities, the GCMs showed relatively smaller PS (more uncertainty).

Interestingly, the model ensemble showed high skills in representing the governing patterns over most high-altitude regions during all three seasons (e.g., WS-R5, PMS-R1, PMS-R5, MS-R4, and MS-R7). In addition, the model ensemble showed nearly similar performance (averaged) over the UIB and Lower Indus regions, except for the WS. The model ranking also helped to distinguish the most suitable model(s). For example, during the WS, CMCC-CM showed the maximum predictor correspondence (average PS = 0.72) over three UIB regions (R1, R3, and R5). The predictors from this particular GCM best simulated the $T_{max}$ predictors over the two larger regions located on either side of the Himalayans divide (R1 and R3). The model also showed comparable performance over the third high-altitude region (R5). The particular model even more strongly represented the predictors (average PS = 0.81) over Lower Indus regions (R4 and R6). Even though only the skill during the historical period (and not in the scenario period) was assessed, its use for basin-wide temperature projections appears favorable.

During the PMS, all GCMs showed a high PS over the entire basin predominately due to better agreement of the hur1000 simulations with ERA-Interim. However, MPI-ESM-LR demonstrated very high and consistent performance (average PS = 0.76) across the four UIB regions and two LI regions (average PS = 0.81), which justifies its selection for projections over the entire basin. All GCMs struggled to model the MS governing patterns effectively, but MPI-ESM-LR showed a

relatively better correspondence with reference reanalysis over the five UIB regions (average PS ~50%). In addition, a different model (Nor-ESM1-M)demonstrated simulation advantages over the two LI regions.

**Table 3.** Quantification of the reference uncertainty for temperature ($T_{max}$ and $T_{min}$) simulations over the study basin using the weighted PS of ERA-Interim predictors. The PS was computed by separately comparing ERA-Interim predictors against the variables of ERA5 and NCEP-NCAR-II reanalysis datasets and shows the strength of predictor correspondence among different datasets. The regions are grouped into the UIB, and Lower Indus scales to assess spatial predictor correspondence between these reanalysis datasets during each season. The last two columns show the range of reference uncertainties in percentage ((1-PS) × 100).

| Seasons | Regions | $T_{max}$ | | $T_{min}$ | | Reference uncertainty (in %) | | | | | |
|---|---|---|---|---|---|---|---|---|---|---|---|
| | | ERA5 | NCEP-II | ERA5 | NCEP-II | $T_{max}$ | | $T_{min}$ | | $T_{max}$ | $T_{min}$ |
| WS | UIB | | | | | ERA5 | NCEP-II | ERA5 | NCEP-II | Range | Range |
| | R1 | 0.83 | 0.66 | 0.95 | 0.69 | 17 | 34 | 5 | 31 | 17-34 | 5-31 |
| | R3 | 0.83 | 0.65 | 0.95 | 0.69 | 17 | 35 | 5 | 31 | 17-37 | 5-31 |
| | R5 | 0.98 | 0.95 | 0.95 | 0.68 | 2 | 5 | 5 | 32 | 2-5 | 5-32 |
| | Avg. over UIB | 0.88 | 0.75 | 0.95 | 0.69 | 12 | 24.67 | 5 | 31.33 | 12-25 | 5-31 |
| | LI | | | | | | | | | | |
| | R4 | 0.94 | 0.68 | 0.94 | 0.69 | 6 | 32 | 6 | 31 | 6-32 | 6-31 |
| | R6 | 0.98 | 0.96 | 0.94 | 0.68 | 2 | 4 | 6 | 32 | 2-4 | 6-32 |
| | Avg. over LI | 0.96 | 0.82 | 0.94 | 0.69 | 4 | 18 | 6 | 31.5 | 4-18 | 6-32 |
| PMS | UIB | | | | | | | | | | |
| | R1 | 0.85 | 0.88 | 0.74 | 0.63 | 15 | 12 | 26 | 37 | 12-15 | 26-42 |
| | R3 | 0.63 | 0.99 | 0.54 | 0.91 | 37 | 1 | 46 | 9 | 1-39 | 9-48 |
| | R5 | 0.60 | 0.88 | 0.57 | 0.60 | 40 | 12 | 43 | 40 | 12-42 | 42-45 |
| | R7 | 0.59 | 0.59 | 0.53 | 0.59 | 41 | 41 | 47 | 41 | 43-43 | 43-49 |
| | Avg. over UIB | 0.67 | 0.84 | 0.60 | 0.68 | 33.25 | 16.5 | 40.5 | 31.75 | 17-35 | 34-42 |
| | LI | | | | | | | | | | |
| | R4 | 0.93 | 0.87 | 0.84 | 0.78 | 7 | 13 | 16 | 22 | 7-13 | 16-22 |
| | R6 | 0.62 | 0.88 | 0.55 | 0.57 | 38 | 12 | 45 | 43 | 12-40 | 45-47 |
| | Avg. over LI | 0.78 | 0.88 | 0.7 | 0.68 | 22.5 | 12.5 | 30.5 | 32.5 | 13-24 | 32-34 |
| MS | UIB | | | | | | | | | | |
| | R1 | 0.78 | 0.64 | 0.83 | 0.77 | 22 | 36 | 17 | 23 | 22-36 | 17-23 |
| | R3 | 0.66 | 0.59 | 0.73 | 0.64 | 34 | 41 | 27 | 36 | 34-43 | 27-36 |
| | R4 | 0.91 | 0.81 | 0.76 | 0.60 | 9 | 19 | 24 | 40 | 9-19 | 24-40 |
| | R5 | 0.74 | 0.64 | 0.79 | 0.58 | 26 | 36 | 21 | 42 | 26-38 | 21-42 |
| | R7 | 0.89 | *0.69* | 0.78 | *0.56* | 11 | 31 | 22 | 44 | *11-31* | 22-44 |
| | Avg. over UIB | 0.80 | 0.67 | 0.78 | 0.63 | 20.40 | 32.6 | 22.2 | 37 | 20-33 | 22-37 |
| | LI | | | | | | | | | | |
| | R2 | 0.80 | 0.66 | 0.80 | 0.58 | 20 | 34 | 20 | 42 | 20-36 | 20-42 |
| | R6 | 0.71 | 0.62 | 0.72 | 0.65 | 29 | 38 | 28 | 0.35 | 29-40 | 28-35 |
| | Avg. over LI | 0.76 | 0.64 | 0.76 | 0.62 | 24.5 | 36 | 23.05 | 21.18 | 25-38 | 23-39 |

Similarly, we evaluated the available GCMs for $T_{min}$ predictor simulations (**Table S5**). Overall, these models showed relatively higher PS over different regions but with a similar seasonality (i.e., higher

correspondence during the westerly periods than the MS). CNRM-CM5 (MPI-ESM-LR) showed the highest and consistent correspondence with the reference reanalysis over multiple regions in the basin during the WS and PMS (MS).

**Table 4.** Same as **Table 3**, but showing General Circulation Model (GCM) uncertainties for $T_{max}$ predictors. Here the ERA-Interim predictors were individually compared with the corresponding GCM simulated predictors during the overlapping historical period 1979–2005 to compute weighted PS. The last column shows the ensemble performance over various scales. Blue (orange) marks indicate the best (worst) GCM according to the highest (lowest) weighted PS.

| Seasons | Regions | CMCC-CMS | CMCC-CM | CNRM-CM5 | Can-ESM2 | MPI-ESM-LR | MPI-ESM-MR | Nor-ESM1-ME | Nor-ESM1-M | Model Ensemble |
|---|---|---|---|---|---|---|---|---|---|---|
| WS | **UIB** | | | | | | | | | |
| | R1 | 0.50 | 0.64 | 0.59 | 0.49 | 0.58 | 0.48 | 0.37 | 0.38 | 0.50 |
| | R3 | 0.52 | 0.62 | 0.54 | 0.48 | 0.57 | 0.52 | 0.36 | 0.33 | 0.49 |
| | R5 | 0.80 | 0.90 | 0.83 | 0.84 | 0.91 | 0.90 | 0.81 | 0.76 | 0.84 |
| | Avg. over UIB | 0.61 | 0.72 | 0.65 | 0.60 | 0.69 | 0.63 | 0.51 | 0.49 | 0.61 |
| | UIB Uncertainity (in %) | 39.33 | 28 | 34.67 | 39.67 | 31.33 | 36.67 | 48.67 | 51 | 38.67 |
| | **Lower Indus** | | | | | | | | | |
| | R4 | 0.71 | 0.76 | 0.81 | 0.72 | 0.63 | 0.64 | 0.62 | 0.65 | 0.69 |
| | R6 | 0.78 | 0.88 | 0.79 | 0.84 | 0.88 | 0.89 | 0.79 | 0.75 | 0.83 |
| | Avg. over Lower Indus | 0.75 | 0.82 | 0.80 | 0.78 | 0.76 | 0.77 | 0.71 | 0.70 | 0.76 |
| | Lower Indus Uncertainity (in %) | 25.50 | 18 | 20 | 22 | 24.5 | 23.50 | 29.5 | 30 | 24.13 |
| PMS | **UIB** | | | | | | | | | |
| | R1 | 0.59 | 0.62 | 0.56 | 0.60 | 0.65 | 0.61 | 0.53 | 0.59 | 0.59 |
| | R3 | 0.65 | 0.74 | 0.77 | 0.43 | 0.76 | 0.65 | 0.50 | 0.48 | 0.62 |
| | R5 | 0.66 | 0.76 | 0.78 | 0.45 | 0.82 | 0.66 | 0.53 | 0.52 | 0.65 |
| | R7 | 0.65 | 0.73 | 0.79 | 0.43 | 0.82 | 0.67 | 0.53 | 0.53 | 0.64 |
| | Avg. over UIB | 0.64 | 0.71 | 0.73 | 0.48 | 0.76 | 0.65 | 0.52 | 0.53 | 0.63 |
| | UIB Uncertainity (in %) | 36.25 | 28.75 | 27.5 | 52.25 | 23.75 | 35.25 | 47.75 | 47 | 37.31 |
| | **Lower Indus** | | | | | | | | | |
| | R4 | 0.58 | 0.64 | 0.69 | 0.65 | 0.66 | 0.72 | 0.58 | 0.63 | 0.64 |
| | R6 | 0.62 | 0.70 | 0.75 | 0.38 | 0.75 | 0.63 | 0.47 | 0.46 | 0.60 |
| | Avg. over Lower Indus | 0.60 | 0.67 | 0.72 | 0.52 | 0.71 | 0.68 | 0.53 | 0.55 | 0.62 |
| | Lower Indus Uncertainity (in %) | 40 | 33 | 28 | 48.5 | 29.5 | 32.5 | 47.5 | 45.5 | 38.06 |
| MS | **UIB** | | | | | | | | | |
| | R1 | 0.38 | 0.39 | 0.40 | 0.34 | 0.43 | 0.39 | 0.35 | 0.29 | 0.37 |
| | R3 | 0.49 | 0.50 | 0.53 | 0.51 | 0.53 | 0.56 | 0.45 | 0.54 | 0.51 |
| | R4 | 0.61 | 0.55 | 0.46 | 0.48 | 0.62 | 0.60 | 0.57 | 0.54 | 0.55 |
| | R5 | 0.39 | 0.41 | 0.41 | 0.40 | 0.46 | 0.43 | 0.42 | 0.36 | 0.41 |
| | R7 | 0.60 | 0.58 | 0.51 | 0.50 | 0.61 | 0.55 | 0.44 | 0.43 | 0.53 |
| | Avg. over UIB | 0.49 | 0.49 | 0.46 | 0.45 | 0.53 | 0.51 | 0.45 | 0.43 | 0.48 |
| | UIB Uncertainity (in %) | 50.60 | 51.40 | 53.80 | 55.40 | 47 | 49.40 | 55.40 | 56.8 | 52.48 |
| | **Lower Indus** | | | | | | | | | |
| | R2 | 0.41 | 0.46 | 0.45 | 0.43 | 0.42 | 0.42 | 0.44 | 0.43 | 0.43 |
| | R6 | 0.37 | 0.44 | 0.51 | 0.58 | 0.48 | 0.47 | 0.55 | 0.65 | 0.51 |
| | Avg. over Lower Indus | 0.39 | *0.45* | *0.48* | *0.51* | *0.45* | *0.45* | *0.50* | 0.54 | 0.47 |
| | Lower Indus Uncertainity (in %) | 61 | 55 | 52 | 49.50 | 55.0 | 55.50 | 50.50 | 46.0 | 53.06 |

**Figure 4,** presents the summary of the reference (model) uncertainty for both temperatures (averaged) over the UIB and LI regions. Generally, the magnitude of (seasonal) reference uncertainty remained lower than the GCM ensemble for both temperatures. Moreover, the best seasonal models showed significant simulation improvements over the model ensembles. Similarly, the range between the worst and best models was quite large and represented the ensemble diversity. While the reference uncertainty was mostly high during the PMS, the model uncertainties were maximum during the MS.

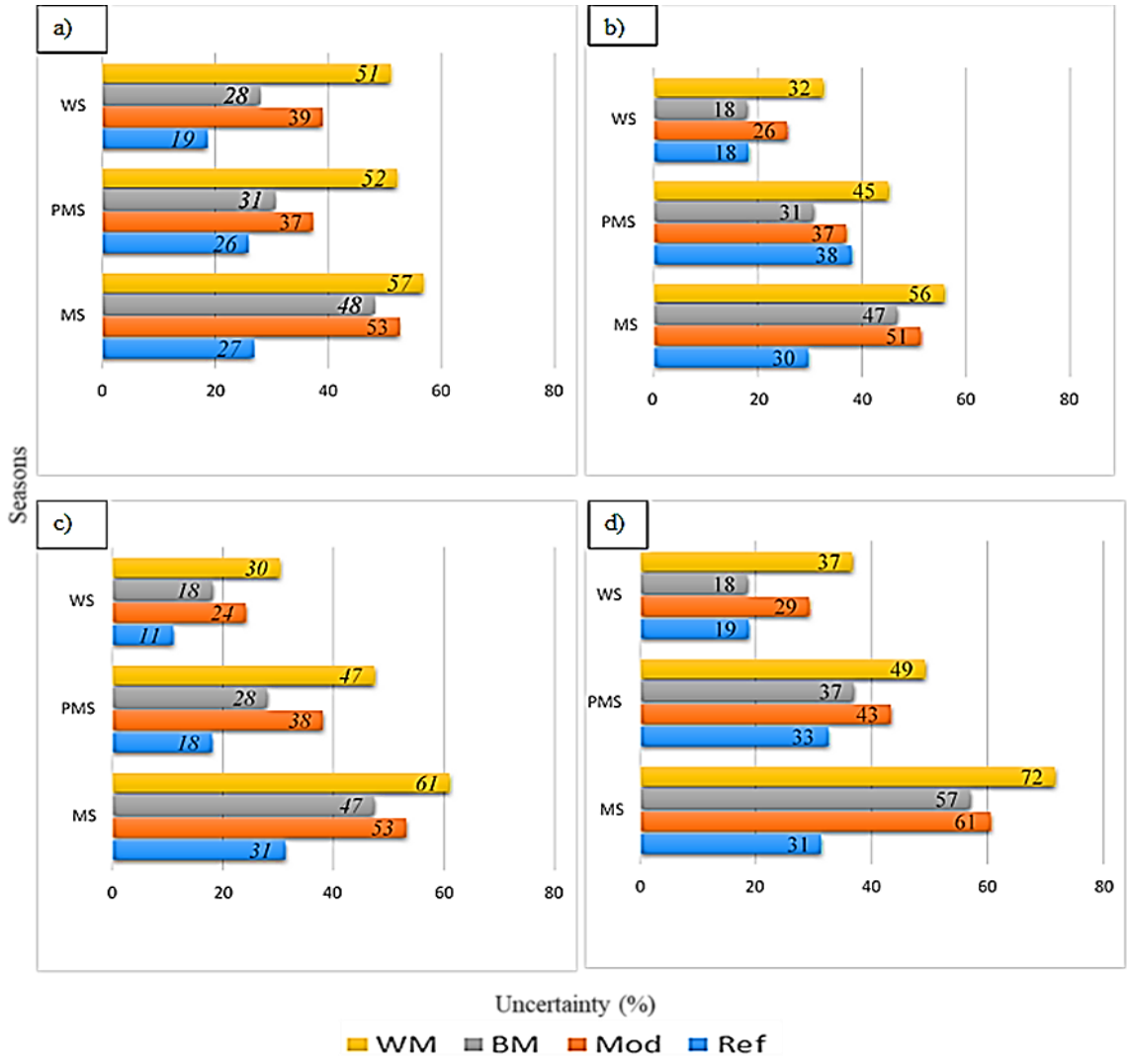


**Figure 4.** Seasonal quantification of the reference and GCM level uncertainties in representing temperature governing predictors over Pakistan's Indus Basin. The seasons (uncertainty) are arranged along the y-axis (x-axis). In the legend, WM, BM, Mod, and Ref refer to the worst model, best model, model ensemble, and the average reference, respectively. **a)** $T_{max}$ predictor uncertainty averaged over UIB regions, **c)** $T_{max}$ uncertainty averaged over Lower Indus regions. The panels **b)** and **d)** show corresponding $T_{min}$ uncertainties.

## 4.4 Future Temperature Changes

We used the GCM-simulated predictors under RCP4.5 and RCP8.5 scenarios to assess seasonal $T_{max}$ and $T_{min}$ median changes during the two future periods (2041–2071, 2071– 2100) relative to the historical period (1976–2005). **Figure 5** presents the temperature changes during 2071–2100 under the RCP8.5 scenario. The multi-model ensembles -MMEs (triangles) and the individual GCM results (colored circles) show the average magnitude of change signals and the associated uncertainty. Results are ordered across the y-axis as a function of regional altitudes to analyze EDW over the basin. The corresponding changes under RCP4.5 and change signals during 2041–2071 under both RCPs showed less warming but similar spatial patterns in most cases (not shown). Note that the x-axis range (i.e., monthly temperature changes) varies in these panels.

### 4.4.1 WS projections

The entire basin will experience warming through both temperature variables during the WS (**Figure 5a,b**). However, the magnitude and reliability of the MMEs differed significantly between the $T_{max}$ and $T_{min}$ and along regional altitudes. For instance, the $T_{min}$ projections always showed more substantial warming (MME ranged from 6.74 ºC to > 11 ºC) than corresponding $T_{max}$ changes (MME range of 0.24 ºC to ~7 ºC). However, the larger intermodel spread in $T_{min}$ projections also highlights the higher uncertainty about warming magnitudes. Another striking feature was related to high warming (in both temperatures), though with more uncertainty (large inter-model spread) over the lower-elevation regions than the HA. Therefore, the model ensemble did not show EDW over the whole basin. However, the EDW became prominent when changes only over the UIB were analyzed. Within the UIB, the highest $T_{max}$ warming (MME ~7 ºC) was projected over the highest (represented) altitudes of the northwestern and northeastern regions (R5). However, the future $T_{max}$ warming reduced significantly over the lower elevations of the northern (R1, MME 0.38 ºC) and southern Himalayans (R3, MME 0.24 ºC) regions. Generally, the $T_{min}$ changes showed mixed patterns with regional altitudes in the UIB. The EDW became distinct when considering the average temperature (mean of $T_{max}$ and $T_{min}$) within the UIB. We also compared MME signals with projections of the best-performing individual GCMs. For example, the best $T_{max}$ model (CMCC-CM) and $T_{min}$ model (CNRM- CM5) always (mostly) showed greater (lesser) $T_{max}$ ($T_{min}$) warming over the basin (mainly in lower elevations). Thus, the best seasonal models projected enhanced warming over the UIB compared to MME signals. A combination of increased surface albedo (Pepin et al., 2015), cloud radiative forcing (e.g., Forsythe et al., 2015)**,** and soil moisture feedback can (at least partly) explain a more significant $T_{min}$ warming within the UIB. A projected increase in WS precipitation, which is robust across many studies (e.g., Ali et al., 2021, Pomee and Hertig, 2021; Almazroui et al., 2020), further supports such feedback. Since the WS precipitation mostly falls as snow, increased albedo

from the fresh snow surface (and associated cloud covers) may largely explain a smaller increase in $T_{max.}$ Similarly, enhanced convection that starts during March (e.g., Cannon et al., 2015) may also reduce insolation over the UIB. Under cloudy conditions, increased soil moisture (due to increased precipitation and melting in the UIB) may also exert positive feedback to increase $T_{min}$.

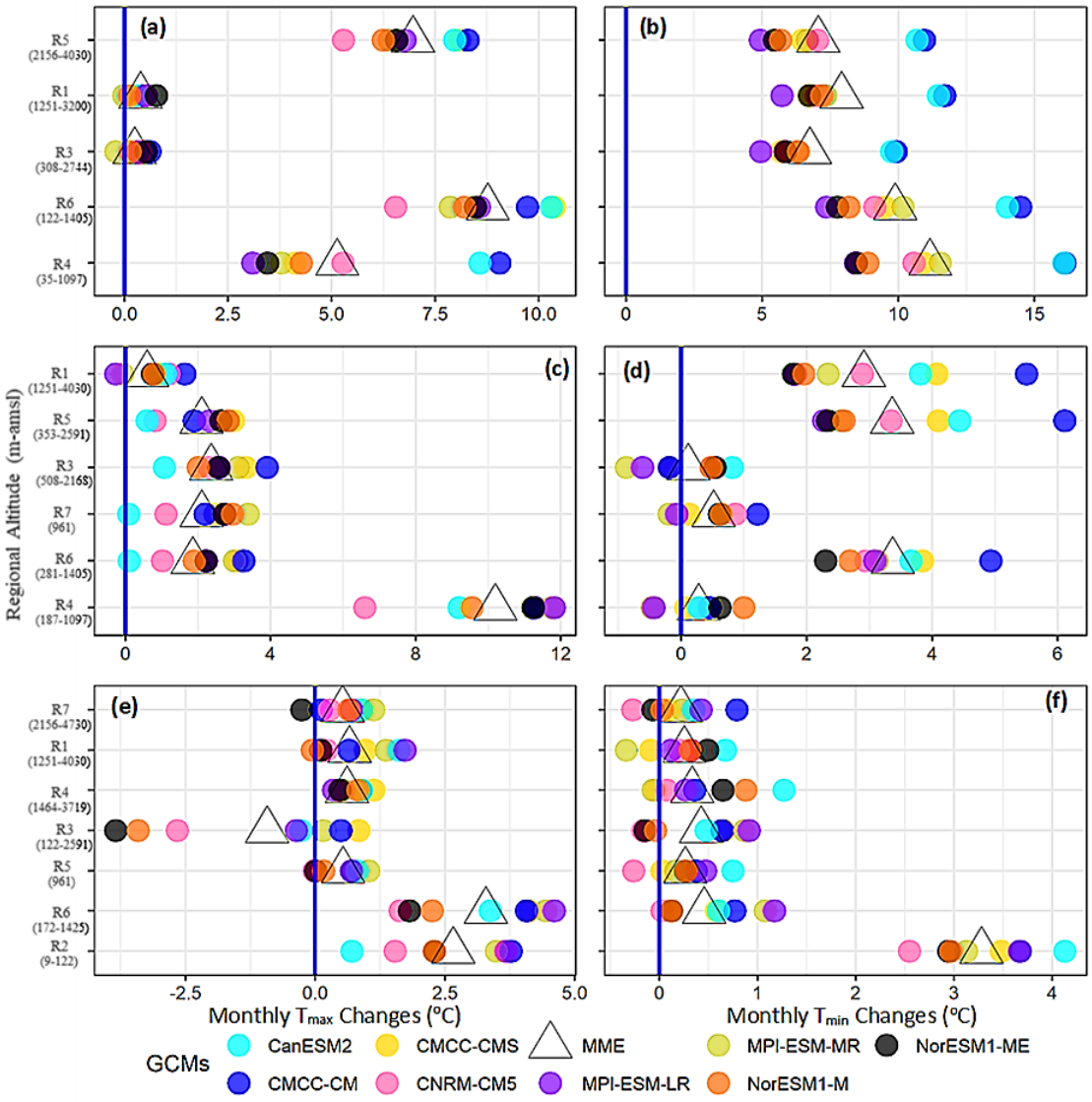


**Figure 5.** Downscaled (unweighted) seasonal temperature changes (°C /month) during 2071–2100 compared to 1976–2005 under the RCP8.5 scenario during the basin-wide regionalization experiment. **(a,b)** show the WS changes for $T_{max}$ and $T_{min}$, respectively. The PMS $T_{max}$ and $T_{min}$ changes are represented by **(c,d),** and corresponding MS changes are shown by panels **(e,f),** respectively. The Y-axis shows the different sub-regions arranged in decreasing altitudinal order from top to bottom and the range of regional altitudes given in parenthesis. The colored circles (triangles) show the individual GCM (MME) median temperature changes. The solid blue line indicates no change.

A high WS warming over the UIB is in line with earlier studies (e.g., Ali et al., 2021, Almazroui et al., 2021). While downscaling studies projected positive $T_{min}$ changes (e.g., Ali et al., 2021), most trend analysis studies instead concluded seasonal warming through $T_{max}$ changes (e.g., Khattak et al., 2011, Bashir et al., 2017). Considering increased future precipitation and associated positive feedbacks, we argue that WS warming through $T_{min}$ changes over the UIB seems more logical.

However, our results (and almost all earlier studies) are in stark contrast with the finding of Latif et al. (2020), where a WS cooling was reported. Using a smaller number of stations with short time series compared to our study and methodological differences (particularly homogeneity treatment) might be responsible for the seasonal discrepancies. In addition, claiming future UIB cooling based on stations depicting a cooling tendency in observations may also be misleading. Therefore, analysis using climate variability and atmospheric dynamics might provide more realistic temperature variations in this topographically challenging region, as shown in our study. A combination of decreased precipitation (Almazroui et al., 2021), an increase in dry periods (Ali et al., 2019), and enhanced evapotranspiration over the irrigated plains due to rising $T_{max}$ may largely explain the patterns of Lower Indus warming (R4 and R6).

### 4.4.2 PMS projections

Warming of the basin was also assessed during the PMS (**Figure 5c,d**). Contrary to the WS, the $T_{max}$ changes were more positive (MMEs range from ~0.60 ºC to >10 ºC) compared to $T_{min}$ warming (MMEs range of 0.11 ºC to 3.7 ºC). The projected uncertainty (about the magnitude and signal direction) mostly remained high for $T_{min}$ projections. Although the $T_{max}$ and $T_{min}$ changes showed significant spatial variability, they did not follow EDW at the basin or the UIB scales. Instead, our analysis suggested a sort of west-east warming pattern that intensifies over the lower elevations.

The regional PMS warming and drying, particularly over the UIB, is a robust feature (Hasson et al., 2017, Ashfaq et al., 2020) and may be linked to clear-sky conditions under the influence of West Tibetan high. The strengthening of the Tibetan high may explain a more increase in regional $T_{max}$. A greater increase in $T_{max}$, particularly over the northwestern regions (R5 and R7) and along the foothills of the southern Himalayans (R3) compared to changes over a larger trans-Himalayan region (R1), may be linked with the weakening and further northward penetration of the westerlies under RCP8.5 (Pomee and Hertig, 2021). However, decreasing precipitation may not adequately explain $T_{min}$ warming over the UIB. We argue that increased precipitation and consistent warming during the WS may enhance melting and soil moisture. Increased soil moisture may be evaporated by daytime heating during the PMS to promote afternoon cloudiness, which can justify the rising $T_{min}$ through radiative feedback. Bashir et al. (2017) used five decades of synoptic observations to show

an increasing trend in the afternoon cloudiness over the UIB. We believe that such a pattern will intensify under the RCP8.5 scenario during the PMS. Note that the humidity predictors dominate the PMS regression models (**Table 4**), and, therefore, future changes in atmospheric humidity will strongly influence the regional temperatures. Previous studies ( e.g., Yaseen et al., 2020, Hasson et al., 2017, Ali et al., 2015) also projected PMS warming over the UIB through $T_{max}$ changes.

The northwestern warming of the UIB will further continue in the lower elevations (R6) with a similar magnitude. However, the upper irrigated plains in the northeastern sides (R4) showed a maximum (smaller) increase of $T_{max}$ ($T_{min}$) though with higher uncertainty. A combination of increased heat advection and reduced convection may regulate such $T_{max}$ changes. The nature of $T_{max}$ predictors ta850 (all PCs are located well outside the region) and va850 indicate the role of heat advection into the region. In contrast, the PMS drying (e.g., Ashfaq et al., 2020) may reduce regional convection (and cloud cover) to justify smaller $T_{min}$ changes.

### 4.4.3 MS projections

The projected warming significantly reduced in the MS (**Figure 5e,f**). In addition, there was a remarkable inter-model consensus about a low-warming future within the mountainous UIB (R7, R1, R4, R3, and R5). Like in other seasons, the basin will experience more (less) warming over Lower Indus (UIB) regions with higher uncertainty. However, a general pattern of EDW for projected $T_{max}$ changes was realized only at the UIB scale. The $T_{max}$ changes mostly dominated the basin-wide seasonal warming (**Figure 5f**).

Within the UIB, the most striking feature relates to a significant $T_{max}$ cooling (MME = 0.93 $^{o}$C) over a relatively low-altitude region along the foothills of southern Himalayans (R3). However, the reliability of regional cooling was relatively weak. For instance, both Norwegian models (Nor-ESM-ME and Nor-ESM-M), which projected maximum cooling (> 2.5 $^{o}$C), showed the lowest historical (predictor) correspondence (**Table 4**). In addition, many GCMs, including the best model (MPI-ESM-LR), instead showed warming (up to ~1 $^{o}$C) over this region. All other UIB regions covering HA of the northwestern and trans-Himalayans showed $T_{max}$ warming that was maximum (MME ~0.70 $^{o}$C) over a trans-Himalayans region also covering central Karakoram (R1). Again, the best seasonal GCM **(Table 4)** mostly projected enhanced warming ($T_{max}$ ~1 $^{o}$C) compared to MMEs over the UIB. The $T_{min}$ ensemble changes also showed consistent warming (of low magnitude) over the entire UIB with maximum warming (MME = 0.43 $^{o}$C) over the lower elevations (R3). However, the likelihood of $T_{min}$ cooling cannot be ruled out in the UIB.

Some earlier studies (Mahmood et al., 2013, 2015) also projected low-warming MS conditions during the 2080s over a region that largely overlaps with our R3 and covers the adjacent Indian part (with a possibility of $T_{min}$ cooling) by using a single GCM. Our model ensemble also covers a similar magnitude of regional warming. Therefore, a low-warming MS in the UIB at the end of the 21st century is possible and may further extend into the high-altitude regions under the same MS forcing. Many earlier studies (e.g., Latif et al., 2019, Yaseen et al., 2020, Khattak et al., 2011, Bashir et al. (2017) have shown MS cooling tendencies. Although our model ensemble did not show MS cooling except over one region, some individual models projected some cooling. Overall a low-warming future (under RCP8.5 forcing) may also resemble the findings of those studies. Increasing MS precipitation (e.g., Hasson et al., 2017, Cook et al., 2003), reduced insolation (e.g., Bashir et al., 2017, Pritchard et al., 2019), the influence of large-scale circulations Fowler and Archer, 2006), internal climatic variability (e.g., Nath et al., 2018), and regional snow dynamics (Kumar et al., 2020) may govern such MS cooling.

Pomee at al.(2020) showed the role of dynamic and thermodynamic forcing on the MS precipitation over the UIB and their strengthening under RCP8.5 to transport additional moisture (Pomee and Hertig, 2021). For instance, they projected a quantitatively large precipitation increase over R3 (MME >7 mm/month) under RCP8.5, which may cause a low-warming or even regional cooling. A close similarity of the precipitation (Pomee et al., 2020) and temperature predictors (**Table 4**) further supports these dynamic interactions. The projected intensification of irrigation practices under future warming over the Indian landmass may promote convection to increase daytime cloudiness (e.g., Bashir et al., 2017). The buildup of such atmospheric moisture may move into the UIB under stronger MS currents to reduce insolation. de Kok et al. (2018) simulated such negative feedback of the regional irrigation to explain glacial expansions in the adjacent high mountains. Some studies (e.g., Saeed et al., 2009, Han and Yang, 2013) also highlighted the role of irrigation practices in shaping regional temperatures.

In contrast, some studies (e.g., Ali et al., 2021, Almazroui et al., 2020) assessed an extensive MS warming over the UIB. Perhaps analysis without high-altitude stations, disregarding regional heterogeneity (treating UIB as a single unit), the variable definition of the MS season, and ignoring homogeneity considerations may induce artificial trends in some of those studies (e.g., Ali et al. 2015, 2021). However, we believe that interpolation issues of the near-surface variables in high mountains and adapting uniform lapse rates may also exert a strong influence in regional studies (Palazzi et al., 2013). The lapse rate variation becomes prominent in the warmer seasons, where a sharper vertical temperature gradient may lead to such MS discrepancies. The usefulness of time-varying lapse rates in the central Himalayans region has already been demonstrated by (Karki et al., 2020). We suggest that lapse rates using regionalization schemes may provide a more realistic basis

for assessing vertical temperature distributions in the complex UIB terrains. The recent high-altitude observations can help in this regard.

However, the average warming over different Lower Indus regions (R6 and R2) is similar to the findings of previous studies (Su et al., 2016, Ali et al., 2021) and attributed to a general decrease in seasonal precipitation (e.g., Almazroui et al., 2020). Ease of topography (lesser interpolation challenges) and the absence of lapse rate requirements may also explain the MS warming similarities among studies.

## 4.5 Model Weighting Influence on Ensemble Signals

We identified the best performing GCMs at sub-regional scales by comparing observation-based reanalysis predictors with historical simulations of the available GCMs. However, the application of different models for different regions would have introduced inconsistencies. Conversely, using a single GCM for the whole basin would require significant simulation compromises and might not suffice for such a complex region. Using a weighted ensemble can offer one alternative to this issue, whereby GCM performance during the observations is used as specific weights for projections. Thus better-performing models get higher weights in the resulting (weighted) ensemble based on justifiable reasons.

We evaluated the impact of such model weighting (**Table 4 and S5**) on ensemble signals by comparing unweighted and weighted temperature changes during 2071–2100 under both RCPs (**Figure 6**). Overall, the model weighting did not significantly modify the ensemble signals, partly due to a small magnitude of the weights, intermodel similarities, and because most GCMs demonstrated similar temperature-simulation skills. Still, the model weighting showed more influence over different Lower Indus regions and for $T_{min}$ changes. During the westerly-dominated seasons, the better performing models projected slightly more warming over the UIB (up to 10%), dominated by the $T_{min}$ changes, particularly under RCP8.5. On the contrary, most models showed similar skills for representing MS dynamics over the UIB, so the seasonal weighting was less effective. However, the GCMs differed more over topographically simpler Lower Indus regions during all three seasons, and hence the weighting was more prominent. We also analyzed the relative impact of model weighting on the median signals and standard deviations under both RCPs (**Figure 7**). The weighting has a smaller but intricate pattern of impact. Generally, the spread (magnitude) of the change signal increases under the RCP8.5 (RCP4.5) scenario and highlights a more uncertain future under intense warming conditions. While the WS weighting mostly increased the basin warming under both RCPs, the MS response was cumbersome. Mostly high-altitude regions during the main seasons (MS and WS) showed more warming than Lower Indus regions. Thus it appears

that better-performing models project a warmer UIB but with increased uncertainty, and the opposite is true for most Lower Indus cases.

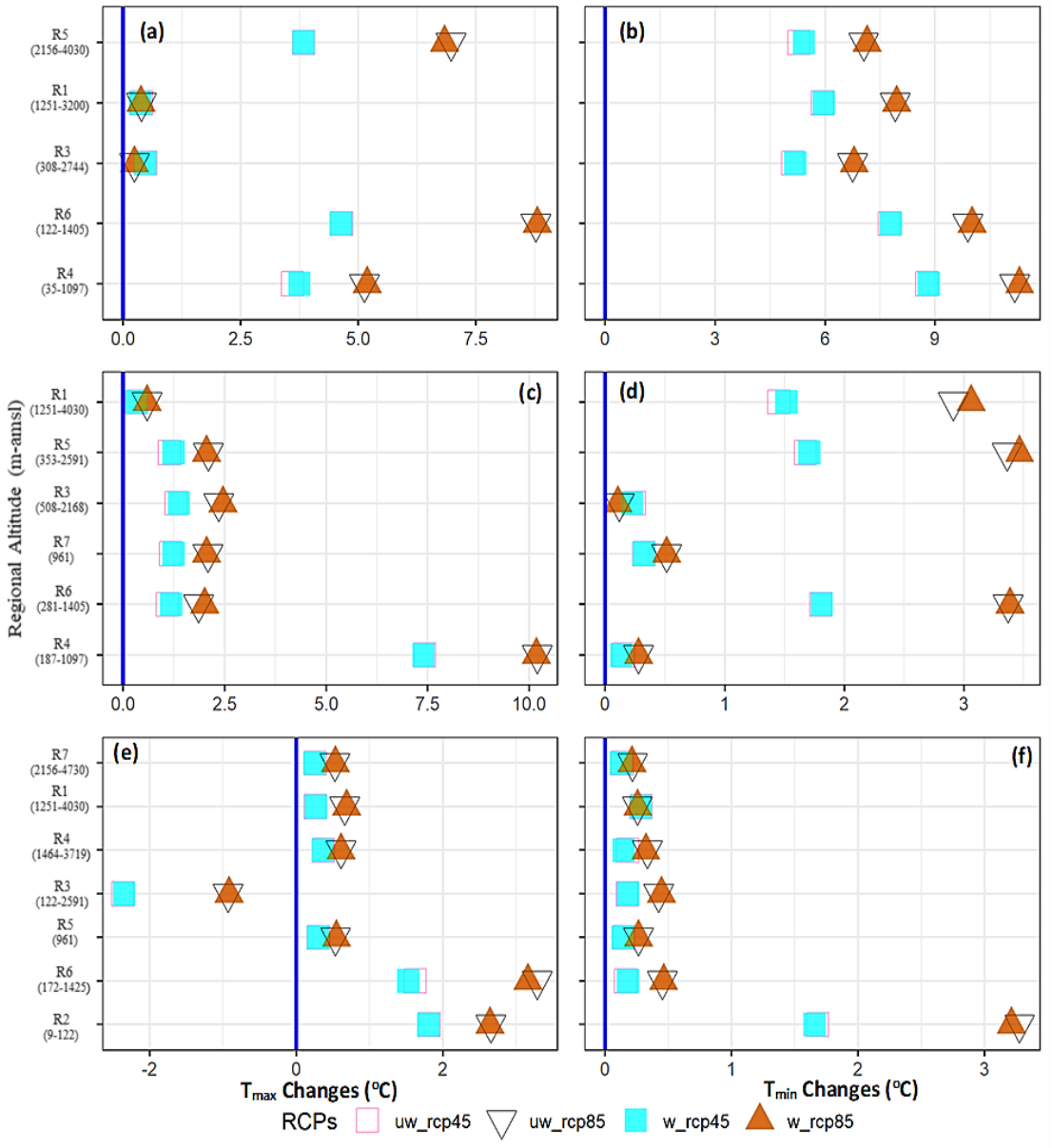


**Figure 6.** Impact of the model weighting on ensemble changes (MMEs) during 2071–2100 under both RCPs. **(a,b)** show weighting impact during the WS for $T_{max}$ and $T_{min}$, respectively. Similarly, the PMS **(c,d)** and the MS **(e,f)** weighting impacts are also shown. In the legend, "unw_" stands for the unweighted, and "w_" shows weighted changes for both RCP scenarios.

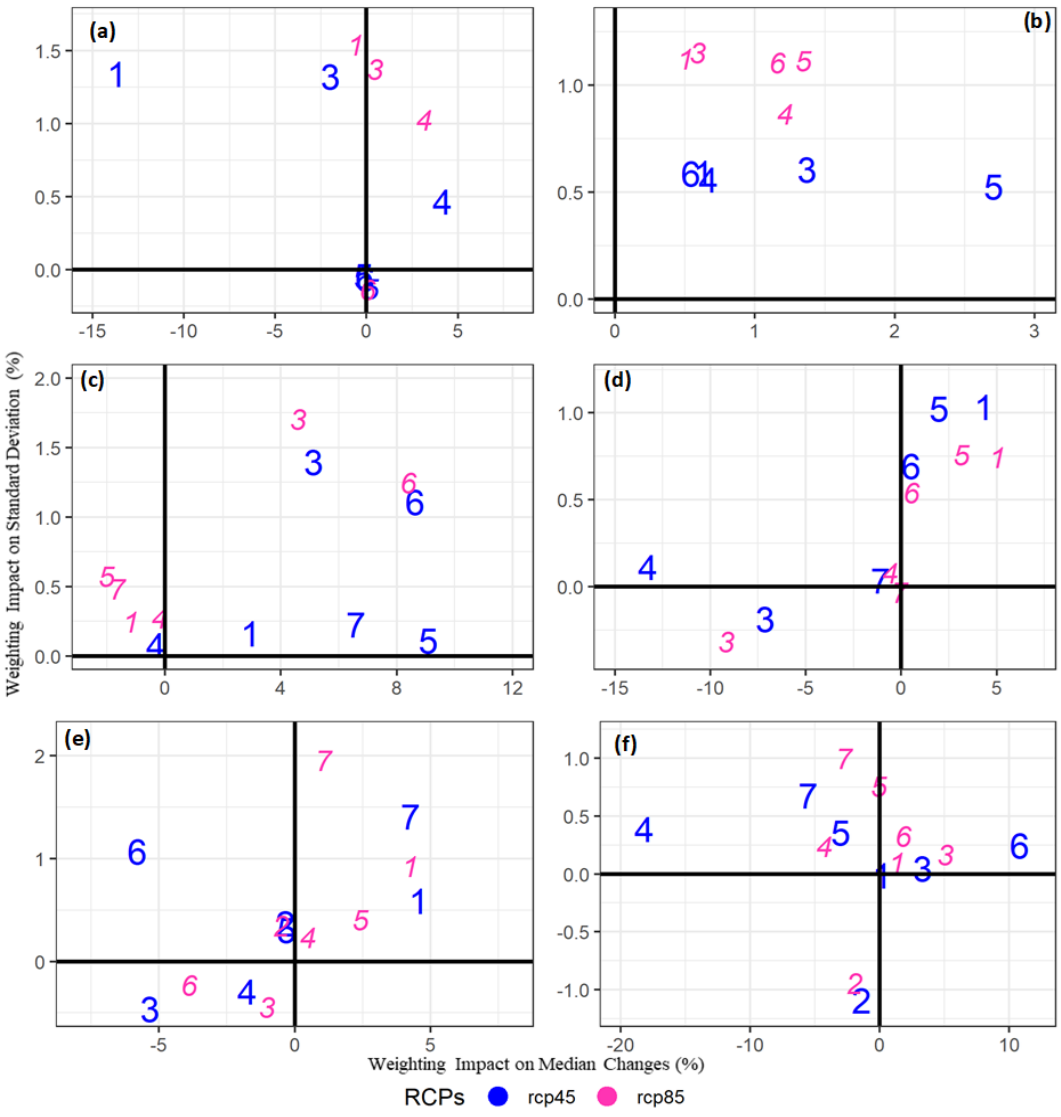


**Figure 7.** Impact of model weighting on ensemble medians (along the x-axis) and standard deviations (along the y-axis) during 2071–2100 under RCP4.5 and RCP8.5 scenarios. The horizontal (verticle) black line reflects no weighting influence on the median (standard deviation) signals. $T_{max}$ weighting impacts during the WS, PMS, and MS are shown by **(a,c,e).** While the corresponding $T_{min}$ changes are shown by **(b,d,f),** respectively. The numbers in these panels represent the identification of seasonal sub-regions through K-means clustering (see **Figure 2** for a description of these regions).

## 4.6 Projected Change Signals: Robustness

We further computed SNRs to evaluate the robustness of projected temperature changes against the observational uncertainty under both RCPs. **Figure 8** shows the results under the RCP8.5 scenario during 2071–2100. Almost all MMEs showed positive ratios, suggesting distinctness of the projected warming over the entire basin. However, there were certain patterns in the distribution of

these SNRs. For instance, the Lower Indus regions mostly showed higher (positive) ratios for both temperatures. Reduced observational variability over the Lower Indus (prolonged dry conditions) compared to heterogeneous UIB can partly explain such altitudinal variations of these ratios.

Similarly, the $T_{min}$ warming was more robust during the westerly-dominated seasons (WS and PMS), particularly at high altitudes, and the opposite was true for the MS. Thus, the future water availability and liquid proportion of the precipitation may increase in the UIB to support rising water demand in the Lower Indus regions. Based upon SNR analysis, the EDW notion at the UIB scale could only be stated for the WS ($T_{max}$) and PMS ($T_{min}$). A combination of weaker signals and high observational uncertainty hampered such an assessment during the MS.

We also used a non-parametric Wilcoxon signed-rank test (Wilcoxon, 1945) to evaluate the statistical significance of ensemble temperature (medians) changes during 2071–2100 compared to 1976–2005 under both RCP scenarios (**Table S6**). The p-values suggest that the statistical significance of future changes increases with RCP8.5 forcing during all three seasons. In particular, the $T_{max}$ changes over all spatial scales were significant. Interestingly most of the MS signals over the UIB were statistically significant despite smaller magnitudes. However, some $T_{min}$ changes over the basin were also non-significant under RCP8.5 during the PMS and MS.

## 4.7 Downscaling over the HA-UIB

We similarly analyzed the seasonal temperature changes, model weighting, and SNRs using the high-altitude UIB regionalization experiment (Section 3.3). **Figure 9** depicts $T_{max}$ and $T_{min}$ changes during 2071–2100 under the RCP8.5 scenario. The previously identified seasonal warming patterns (higher warming during the WS and PMS compared to MS) further persisted over large parts of the high-altitude regions. For instance, a northwestern region during the WS (R4) further verified increased warming over these regions. Similarly, the $T_{max}$ cooling over the southern Himalayans (R3) was also visible during the MS, though its magnitude decreased. In addition, R3 projections also validated weaker $T_{min}$ warming during the MS. Meanwhile, projections over the two new high-altitude regions (R4 and R3) in the northwestern UIB also confirmed PMS warming with elevation inversion. Increased northward deflection of the future westerlies and associated moisture fluxes may support such typical PMS warming patterns over the UIB.

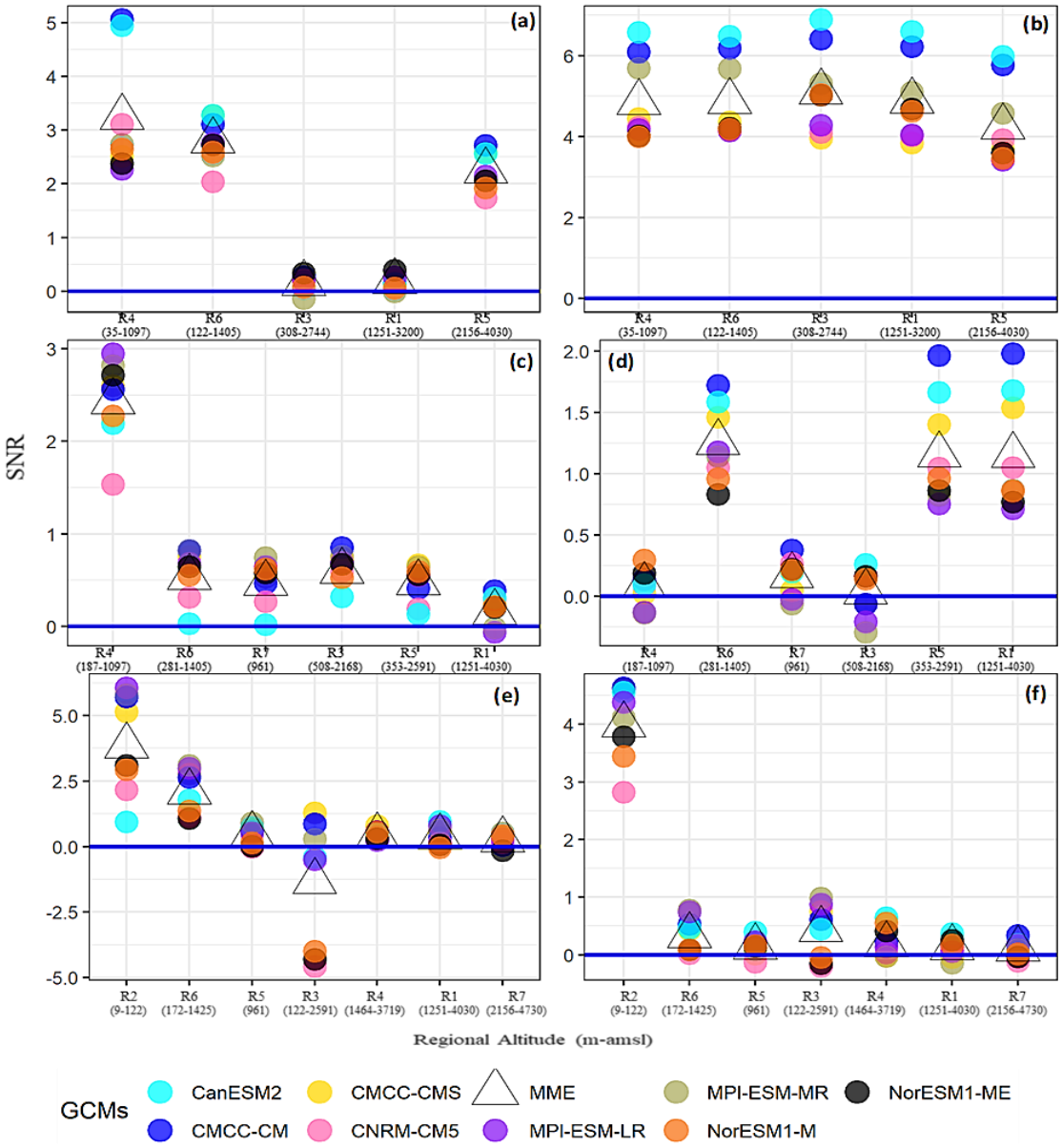


**Figure 8.** Same as **Figure 5**, showing the basin-wide distribution of the signal to noise ratios (SNRs) for both temperatures during 2071–2100 under RCP8.5. The blue horizontal solid line here depicts no strength of the change signal (i.e., median) compared to the historical standard deviation (i.e., noise). Sub-regions with their altitudinal bands are shown along the x-axis, where the elevation increases from left to right. Note that WS $T_{max}$ and $T_{min}$ changes are shown as **(a,b).** Corresponding PMS and MS temperature changes are shown by **(c,d)** and **(e,f),** respectively.

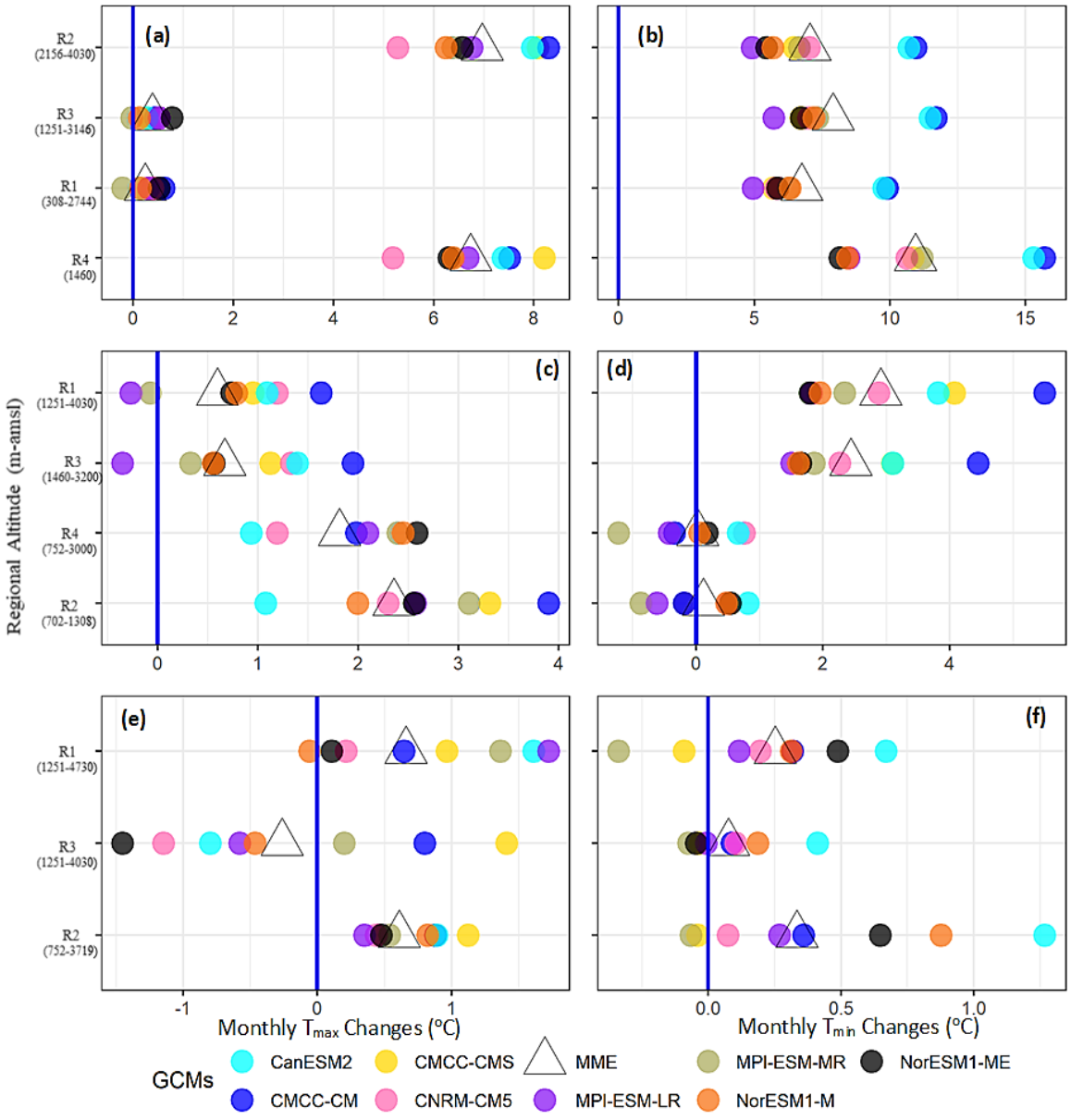


**Figure 9.** Same as **Figure 5** but defining seasonal temperature changes during 2071–2100 under RCP8.5 using the high-altitude UIB regionalization experiment **(a–f).**

## 5 Further Discussion and Conclusions

Temperatures within the UIB are connected with the hydrological regime of the Indus River system through their dynamic influence on the regional cryosphere. In addition, the Lower Indus water demand also depends on temperature. We considered spatiotemporal heterogeneity, reference and GCM level uncertainties, and station-based regression models' skills to statistically project

temperature ($T_{max}$ and $T_{min}$) seasonal patterns over the entire basin. We also used recent high-altitude observations within the UIB to infer EDW characteristics over the basin.

First, the basin was clustered into homogeneous regions of similar climate variability using K-means clustering. Atmospheric predictors from ERA-Interim reanalysis were then used in a cross-validation framework to model observed temperatures skillfully. We compared ERA-Interim temperature-governing predictors with two other reanalysis datasets (ERA5 and NCEP-NCAR-II) and the GCM-simulated variables during the historical period to quantify reference and model level uncertainties, respectively. Inter-reference predictor correspondence was maximum during the accumulation (WS) and melting seasons (MS) at high-altitude regions, particularly for the $T_{max}$. Thermodynamic (dynamic) predictors mainly determined the reference (GCM) level uncertainties. The available GCMs consistently showed high predictor correspondence during the westerly-dominated seasons (WS and PMS). However, consistent with other studies (e.g., Ashfaq et al., 2017) all GCMs struggled to represent MS patterns over the basin.

The GCM predictors under RCP4.5 and RCP8.5 scenarios were used in the regression models to assess median temperature changes during the mid and end of the 21st century. Seasonal projections are summarized as follows;

- The entire basin will non-uniformly (space-time scales) warm during the 21st century under both RCPs. The projected warming is strong under RCP8.5 forcing and during 2071–2100 but follows complex patterns.
- The WS showed maximum warming dominated by $T_{min}$ changes. The changes suggested an EDW (only for $T_{max}$) and a significant reduction in DTR over the UIB. However, high-altitude regions showed a stable DTR.
- PMS warming was spatially more uniform and instead dominated by $T_{max}$ changes. Projected patterns within the UIB suggested a decreasing (increasing) DTR over high-altitudes (low-altitudes) through $T_{min}$ ($T_{max}$) changes.
- A remarkable low-warming (inter-model) consensus, particularly over the UIB, appeared during the MS. The projected changes suggested a small increase in seasonal TDR over the UIB, driven mainly by the $T_{max}$ changes.
- Over the seasons, a strong (weak) warming appeared over the northwestern high-altitude (lower elevations of the southern Himalayans) regions. In addition, the increased warming during the westerly-dominated seasons seems to mask low-warming MS patterns over the UIB. Thus, the UIB will experience substantial warming for mean temperature that follows EDW- a pattern consistent with earlier studies (Lutz et al., 2016). High warming during

the post-monsoon period (e.g., Ali et al., 2021) may further increase year-round heating (MS masking) over the UIB.

- Increased intermodel spread within the UIB indicated more uncertainty about ensemble warming and the possibility of even greater PMS (up to 4 $^{o}$C) and MS (up to 1 $^{o}$C) warming for both temperatures. Better performing GCMs further confirmed higher warming compared to MMEs signals. Such uncertainties highlight the terrain complexities and observational lackings.
- Contrary to the UIB, the projected warming over different Lower Indus regions (with more uncertainty) was in line with those studies that implemented basin-wide analysis (e.g., Su et al., 2016, Almazroui et al., 2020). A combination of simplified topography (lesser interpolation errors) and reduced need for lapse rates may govern such warming similarities. These regions have a stronger mesoscale land-atmosphere coupling (Saeed et al., 2009), which CMIP5 models may not adequately represent due to coarser resolution. Hence more uncertainty prevails over the Lower Indus. The projected precipitation decrease (e.g., Almazroui et al., 2020, Pomee et al., 2021), strengthening of future land-atmosphere coupling, and more decisive influence of the warming oceans in the southwestern and southern regions may largely explain the warming patterns and uncertainty in Lower Indus regions.

Future warming will substantially increase water demand in the Lower Indus. A combination of increased melting, favorable precipitation projections over the UIB (Ali et al., 2021, Pomee et al., 2020), and efficient regulations (Khan et al., 2017) may support such rising water demands in the future. Increased liquid precipitation during the WS and PMS will significantly increase the river flows (Yaseen et al., 2020) before the primary rainy season. When combined with projected MS extremes (Ali et al., 2019), such high river flows may also increase flooding risk in the region.

The prevailing temperature over the cryosphere-dominated HA regions remains well below the freezing point (Hewitt, 2005). Therefore, smaller $T_{max}$ warming during the primary melt season (MS) may not drastically influence glacial stability even under RCP8.5. Projected precipitation increase over high-altitude regions (Kumar et al., 2019, Hasson et al., 2017) may further support glaciers through cloud and albedo feedbacks along with moisture nourishment. In addition, higher warming during the WS and PMS may promote the downslide of debris (Herreid and Pellicciotti, 2020), which, together with favorable energy-moisture input during the MS (Hasson et al., 2017), may also support regional glaciers. Thus unlike other studies (e.g., Immerzeel et al., 2013), increased future water availability in the basin remains possible without rapid glacial retreats.

The aerosol forcing also reduces MS warming (Nath et al., 2018). We argue that future aerosol loadings may increase (e.g., Coen et al., 2018, Zaho et al., 2019), particularly over the high mountains. Increased Arabian Sea contributions during the projected MS precipitation over these mountains (Pomee et al., 2020) and increased aridity over the Indian plains under drying PMS may increase salt (e.g., Wake, 1989) and dust loads over the UIB, respectively. Increased evapotranspiration during the PMS and WS may also enhance atmospheric moistures to create cooling tendencies over the UIB through direct (cloud shading) and indirect aerosol influences (cloud albedo) (e.g., Myhre et al., 2013). Landuse changes in favor of infrastructure developments may also enhance future inorganic aerosols. Both Norwegian models that better represent aerosol dynamics (Bentsen et al., 2013) mostly projected the least MS warming to support our argument. The WS smog over the plains in recent observations may move into the UIB to increase shading and partly justify the rising $T_{min}$. Therefore, analyzing future aerosol contributions may reveal crucial insights for explaining the actual climate response of the UIB under future scenarios. However, understanding the complex glacial dynamics, where heat advection, black carbon depositions, and rapid land-use changes also exert influences, a rapid retreat may also be possible. Further high-altitude observations would be required to precisely model the cryosphere response.

Our analysis has some limitations. For example, a relatively small GCM-ensemble, inter-model similarities (e.g., Knutti et al., 2017), stationarity assumption for future projections (e.g., Lanzamte et al., 2018), and using precipitation regions for temperature downscaling may influence the validity of our analysis. Pomee and Hertig (2021) discussed the regional relevance of our GCM-ensemble despite its smaller size. We checked the RR's effectiveness for temperature analysis and found a very high correlation (> 0.75) with regional centroids in almost all cases. Therefore, using precipitation regions was justified and rather advantageous to have a consistent moisture-energy perspective on the same fine scales to simultaneously assess their influence on regional hydrology. Pomee et al. (2020) discussed the possibility of extending projections beyond the observations and over the transboundary regions. The average statistical downscaling error of about 1 $^{o}$C (**Table 2**) may further reduce the projection reliability in different seasons. We aimed to minimize these errors through multiple considerations in our cross-validation framework, taking into account the high climate variability in the basin and the observational constraints to train the models. However, these errors have to be kept in mind when evaluating the magnitude of the climate change signals derived from the models.

Still, further research efforts are needed to analyze this highly complex region, e.g., by advancing the high-altitude observation network for model development and validation and using the latest CMIP6 dataset that may offer more (independent) models with complete predictor data. Ideally, an ensemble of good and bad models may provide interesting insights (e.g., Knutti et al., 2017, Palazzi

et al., 2014) about future climate changes. We also suggest lapse rates derived through regionalization schemes may provide more realistic inferences of glacial stability as the glacial response depends on climatic and geographical factors (e.g., relief, orientation, and debris cover) that vary widely in the region (e.g., Muhammad et al., 2020). Such space-time differentiated lapse rates will provide a more realistic and differentiated climate perspective in the region for supporting regional adaptations.

## Acknowledgments

The authors are indebted to Pakistan Meteorological Department (PMD), Water and Power Development Authority (WAPDA), and the University of Bonn for sharing the station data, without which this research was not possible. We also acknowledge the World Climate Research Programmer's Working group on the Coupled Modeling, ECMWF, and NOAA-ESRL Physical Sciences Division for publically providing the model and reanalysis dataset. PARC-Pakistan and the German Research Foundation mainly supported our research through the Himalayan Adaptation, Water and Resilience (HI-AWARE) and project number 408057478, respectively. In addition, DAAD funding for foreign PhD students through the University of Augsburg to support MSP is highly appreciated.

## References

Akhtar, M., Ahmad, N. and Booij, M.J. (2008) The impact of climate changes on the water resources of Hindukush–Karakorum– Himalayaregionunder different glacier coverage scenarios. Journal of Hydrology, 355, 148–163. https://doi.org/10.1016/j. jhydrol.2008.03.015

Ali, S., Eum, H.I., Cho, J., Dan, L., Khan, F., et al. (2019). Assessment of climate extremes in future projections downscaled by multiple statistical downscaling methods over Pakistan. Atmos. Res. 2019, 222, 114–133. https://doi.org/10.1016/j.atmosres.2019.02.009

Ali, S.; Kiani, R.S.; Reboita, M.S.; Dan, L.; Eum, H.; Cho, J.; Dairaku, K.; Khan, F.; Shreshta, M.L. Identifying hotspots cities vulnerable to climate change in Pakistan under CMIP5 climate projections. Int. J. Clim. 2021, 41, 559–581.

Ali, S.; Li, D.; Congbin, F.; Khan, F. Twenty first century climatic and hydrological changes over Upper Indus Basin of Himalayan region of Pakistan. Environ. Res. Lett., 10, 014007. https://doi.org/10.1002/joc.6638

Almazroui, M., Saeed, S., Saeed, F.; Islam, M.N., Ismail, M. (2020). Projections of Precipitation and Temperature over the South Asian Countries in CMIP6. Earth Syst. Environ. 2020, 4, 297–320. https://doi.org/10.1007/s41748-020-00157-7

Archer, D. (2003). Contrasting hydrological regimes in the upper Indus Basin. J. Hydrol., 274, 198–210. https://doi.org/10.1016/S0022-1694(02)00414-6

Ashfaq, M., Cavazos, T., Reboita, M.S., Torres-Alavez, J.A., Im, E.S. et al. (2020). Robust late twenty-first century shift in the regional monsoons in RegCM-CORDEX simulations. Clim. Dyn., 1–26. 10.1007/s00382-020-05306-2

Ashfaq, M., Rastogi, D., Mei, R., Touma, D., et al., (2017). Sources of errors in the simulation of south Asian summer monsoon in the CMIP5 GCMs. Clim. Dyn. 2016, 49, 193–223. https://doi.org/10.1007/s00382-016-3337-7

Azam, M.F. Ramanathan, A., Wagnon, P., Vincent, C., et al., (2016). Meteorological conditions, seasonal and annual mass balances of Chhota Shigri Glacier, western Himalaya, India. Ann. Glaciol., 57, 328–338. https://doi.org/10.3189/2016AoG71A570

Azam, M.F., Wagnon, P., Berthier, E., Vincent, C., et al., (2018). Review of the status and mass changes of Himalayan-Karakoram glaciers. J. Glaciol., 64, 61–74. https://doi.org/10.1017/jog.2017.86

Bashir, F.; Zeng, X.; Gupta, H.; Hazenberg, P. (2017). A Hydrometeorological Perspective on the Karakoram Anomaly Using Unique Valley-Based Synoptic Weather Observations. Geophys. Res. Lett., 44, 10470–10478. https://doi.org/10.1002/2017GL075284

Bentsen, M., Bethke, I., Debernard, J.B., Iversen, T., et al., (2013). The Norwegian Earth System Model, NorESM1-M—Part 1: Description and basic evaluation of the physical climate. Geosci. Model. Dev. 2013, 6, 687–720. https://doi.org/10.5194/gmd-6-687-2013

Bolch, T., Kulkarni, A., Kääb, A., Huggel, C., et al. (2012). The State and Fate of Himalayan Glaciers. Science 2012, 336, 310–314. 10.1126/science.1215828

Bolch, T., Pieczonka, T., Mukherjee, K., Shea, J.M. (2017). Brief communication: Glaciers in the Hunza catchment (Karakoram) have been nearly in balance since the 1970s. Cryosphere, 11, 531–539. https://doi.org/10.5194/tc-11-531-2017

Brun, F., Berthier, E., Wagnon, P., Kääb, A., et al. (2017). A spatially resolved estimate of High Mountain Asia glacier mass balances from 2000 to 2016. Nat. Geosci., 10, 668–673. https://doi.org/10.1038/ngeo2999

Cannon, F., Carvalho, L.M.V, Jones C, Norris, J. (2015) Winter westerly disturbance dynamics and precipitation in the western Himalaya and Karakoram: a wave-tracking approach. *Theor Appl Climatol*. https://doi.org/10.1007/s00704-015-1489-8.

Cherchi, A., Annamalai, H., Masina, S.; Navarra, A. (2014). South Asian Summer Monsoon and the Eastern Mediterranean Climate: The Monsoon–Desert Mechanism in CMIP5 Simulations. J. Clim. 2014, 27, 6877–6903. 10.1175/JCLI-D-13-00530.1

Coen, M.C., Andrews, E., Aliaga, D., Andrade, M., et al. (2018). Identification of topographic features influencing aerosol observations at high altitude stations. Atmos. Chem. Phys., 18, 12289–12313. https://doi.org/10.5194/acp-18-12289-2018

Cook, E.R., Krusic, P.J., Jones, P.D. (2003). Dendroclimatic signals in long tree-ring chronologies from the Himalayas of Nepal. Int. J. Clim., 23, 707–732. https://doi.org/10.1002/joc.911

Dahri, Z.H., Moors, E., Ludwig, F., Ahmad, S., et al. (2018). Adjustment of measurement errors to reconcile precipitation distribution in the high-altitude Indus basin. Int. J. Clim., 38, 3842–3860. https://doi.org/10.1002/joc.5539

Dars, G.H., Strong, C., Kochanski, A.K., Ansari, K., et al. (2020). The Spatiotemporal Variability of Temperature and Precipitation Over the Upper Indus Basin: An Evaluation of 15 Year WRF Simulations. Appl. Sci., 10, 1765. https://doi.org/10.3390/app10051765

de Kok, R.J., Tuinenburg, O.A., Bonekamp, P.N.J., Immerzeel, W.W. (2018). Irrigation as a Potential Driver for Anomalous Glacier Behavior in High Mountain Asia. Geophys. Res. Lett., 45, 2047–2054. https://doi.org/10.1002/2017GL076158

De Souza, K., Kituyi, E., Harvey, B., Leone, M., et al., (2015). Vulnerability to climate change in three hot spots in Africa and Asia: Key issues for policy-relevant adaptation and resilience-building research. Reg. Environ. Chang., 15, 747–753. https://doi.org/10.1007/s10113-015-0755-8

Dee, D.P., Uppala, S.M., Simmons, A.J, Berrisford, P., et al., (2011). The ERA-Interim reanalysis: configuration and performance of the data assimilation system. *Q. J. R. Meteorol. Soc. (137)*, pp. 553–597. https://doi.org/10.1002/qj.828,2011.4757,4759,4775

Forsythe, N., Hardy, A.J., Fowler, H.J., Blenkinsop, S., et al. (2015). A detailed cloud fraction climatology of the Upper Indus Basin and its implications for near-surface air temperature. J. Clim. 2015, 28, 3537–3556. https://doi.org/10.1175/JCLI-D-14-00505.1

Fowler, H.J., and Archer, D.R. (2006). Conflicting signals of climate change in the Upper Indus Basin. J. Clim., 19, 4276–4293. https://doi.org/10.1175/JCLI3860.1

Giorgi, F., Raffaele, F., Coppola, E. (2019). The response of precipitation characteristics to global warming from climate projections. Earth Syst. Dyn., 10, 73–89. https://doi.org/10.5194/esd-10-73-2019

Han, S., Yang, Z. (2013). Cooling effect of agricultural irrigation over Xinjiang, Northwest China from 1959 to 2006. Environ. Res. Lett., 8, 024039. 10.1088/1748-9326/8/2/024039

Hasson, S.U. (2016). Future Water Availability from Hindukush-Karakoram-Himalaya upper Indus Basin under Conflicting Climate Change Scenarios. Climate, 4, 40. 10.3390/cli4030040

Hasson, S.U., Böhner, J., Chishtie, F. (2019). Low fidelity of CORDEX and their driving experiments indicates future climatic uncertainty over Himalayan watersheds of Indus basin. Clim. Dyn., 52, 777–798. https://doi.org/10.1007/s00382-018-4160-0

Hasson, S.U., Böhner, J., Lucarini, V. (2017). Prevailing climatic trends and runoff response from Hindukush–Karakoram–Himalaya, upper Indus Basin. Earth Syst. Dyn. 2017, 8, 337–355. https://doi.org/10.5194/esd-8-337-2017

Herreid, S.,and Pellicciotti, F. (2020). The state of rock debris covering Earth's glaciers. Nat. Geosci., 13, 1–7.

Hersbach, H., de Rosnay, P., Bell, B., Schepers, D., et al. (2018). Operational global reanalysis: progress, future directions and Synergies with NWP, ERA-Report. https://www.ecmwf.int/node/18765.

Hewitt, K. (2005). The Karakoram anomaly? Glacier expansion and the 'elevation effect,' Karakoram Himalaya. Mt. Res. Dev., 25, 332–340.

Hewitt, K. (1988). The Snow and Ice Hydrology Project: Research and training for water resource development in the Upper Indus Basin. J. Can. Pak. Coop., 2, 63–72.

Immerzeel, W.W., Pellicciotti, F., Bierkens, M.F.P. (2013). Rising river flows throughout the twenty-first century in two Himalayan glacierized watersheds. Nat. Geosci. 2013, 6, 742–745. https://doi.org/10.1038/NGEO1896

Immerzeel, W.W., Wanders, N., Lutz, A., Shea, J.M., et al., (2015). Reconciling high-altitude precipitation in the upper Indus basin with glacier mass balances and runoff. Hydrol. Earth Syst. Sci. 2015, 19, 4673–4687. . https://doi.org/10.5194/hess-19-4673-2015

IPCC. Climate Change 2013: The Physical Science Basis. In Contribution of Working Group I to the Fifth Assessment Report of the Intergovernmental Panel on Climate Change; Stocker, T.F., Qin, D.,

Plattner, G.-K., Tignor, M., Allen, S.K., Boschung, J., Nauels, A., Xia, Y., Bex, V., Midgley, P.M., Eds.; Cambridge University Press: Cambridge, UK; New York, NY, USA, p. 1535

IPCC. (2018). Summary for Policymakers. In Global Warming of 1.5 ºC. An IPCC Special Report on the Impacts of Global Warming of 1.5 _C above Pre-industrial Levels and Related Global Greenhouse Gas Emission Pathways, in the Context of Strengthening the Global Response to the Threat of Climate Change, Sustainable Development, and Efforts to Eradicate Poverty; World Meteorological Organization: Geneva, Switzerland, p. 32

Jones, P.D., New, M., Parker, D.E., Martin, S.; Rigor, I.G. (1999). Surface air temperature and its changes over the past 150 years. Rev.Geophys. 1999, 37, 173–199. https://doi.org/10.1029/1999RG900002

Kalnay, E., Kanamitsu, M., Kistler, R., Collins,W., et al., (1996). The NCEP/NCAR 40-year reanalysis project. Bull. Am. Meteorol. Soc. 1996, 77, 437–471. https://doi.org/10.1175/1520-0477(1996)077<0437:TNYRP>2.0.CO;2

Karki, R., Hasson, S.U., Gerlitz, L., Talchabhadel, R., et al. (2020). Rising mean and extreme near-surface air temperature across Nepal. Int. J. Clim. 2020, 40, 2445–2463. https://doi.org/10.1002/joc.6344

Karl, T.R., Jones, P.D., Knight, R.W., Kukla, G., et al. (1993). A new perspective on recent global warming—Asymmetric trends of daily maximum and minimum temperature. Bull. Am. Meteorol. Soc., 74, 1007–1023. https://doi.org/10.1175/1520-0477(1993)074<1007:ANPORG>2.0.CO;2

Karmalkar, A.V., and Bradley, R.S. (2017). Consequences of GlobalWarming of 1.5 ºC and 2 ºC for Regional Temperature and Precipitation Changes in the Contiguous United States. PLoS ONE 2017, 12, e0168697. https://doi.org/10.1371/journal.pone.0168697

Kaspar-Ott, I., Hertig, E., Kaspar, S., Pollinger, F., et al. (2019). Weights for general circulation models from CMIP3/CMIP5 in a statistical downscaling framework and the impact on future Mediterranean precipitation. Int. J. Clim. 2019, 39, 3639–3654. *DOI : 10.1002/joc.6045*

Kattel, D.B., Yao, T., Yang, K., Tian, L., et al. (2013). Temperature lapse rate in complex mountain terrain on the southern slope of the Central Himalayas. Theor. Appl. Climatol., 113, 671–682. https://doi.org/10.1007/s00704-012-0816-6

Khan, A., Naz, B.S., Bowling, L.C. (2015). Separating snow, clean and debris covered ice in the Upper Indus Basin, Hindukush-Karakoram-Himalayas, using Landsat images between 1998 and 2002. J. Hydrol., 521, 46–64. https://doi.org/10.1016/j.jhydrol.2014.11.048

Khan, A.J., and Koch, M. (2018). Selecting and Downscaling a Set of Climate Models for Projecting Climatic Change for Impact Assessment in the Upper Indus Basin (UIB). Climate 2018, 6, 89. https://doi.org/10.3390/cli6040089

Khan, F., Pilz, J., Ali, S. (2017). Improved hydrological projections and reservoir management in the Upper Indus Basin under the changing climate. Water Environ. J. 2017, 31, 235–244. DOI:10.1111/WEJ.12237

Khattak, M., Babel, M., Sharif, M. (2011). Hydro-meteorological trends in the upper Indus River basin in Pakistan. Clim. Res., 46, 103–119. DOI :10.3354/cr00957

Knutti, R., Sedlá˘cek, J., Sanderson, B.M., Lorenz, R., et al. (2017). A climate model projection weighting scheme accounting for performance and interdependence. Geophys. Res. Lett. 2017, 44, 1909–1918. https://doi.org/10.1002/2016GL072012

Kumar, P., Saharwardi, S., Banerjee, A., Azam, M.F., et al., (2019). Snowfall Variability Dictates Glacier Mass Balance Variability in Himalaya-Karakoram. Sci. Rep., 9, 18192. https://doi.org/10.1038/s41598-019-54553-9

Lanzante, J.R., Dixon, K.W., Nath, M.J., Whitlock, C.E., et al. (2018). Some Pitfalls in Statistical Downscaling of Future Climate. Bull. Am. Meteorol. Soc. 2018, 99, 791–803. https://doi.org/10.1175/BAMS-D-17-0046.1

Latif, Y., Yao, M., Yaseen, M., Muhammad, S., et al. (2020). Spatial analysis of temperature time series over the Upper Indus Basin (UIB) Pakistan. Theor. Appl. Clim. 2019, 139, 741–758. 10.1007/s00704-019-02993-8

Lutz, A., Immerzeel,W.W., Kraaijenbrink, P.D.A., Shrestha, A.B., et al. (2016). Climate Change Impacts on the Upper Indus Hydrology: Sources, Shifts and Extremes. PloS ONE 2016, 11, e0165630. https://doi.org/10.1371/journal.pone.0165630

Lutz, A.F., Immerzeel,W.W., Shrestha, A.B., Bierkens, M.F.P. (2014). Consistent increase in high Asia's runoff due to increasing glacier melt and precipitation. Nat. Clim. Chang. 2014, 4, 587–592. https://doi.org/10.1371/journal.pone.0165630

Mahmood, R., Babel, M.S. (2012). Evaluation of SDSM developed by annual and monthly sub-models for downscaling temperature and precipitation in the Jhelum basin, Pakistan and India. Theor. Appl. Clim., 113, 27–44. 10.1007/s00704-012-0765-0

Mahmood, R., Mukand, S.B., Shaofeng, J.I.A. (2015). Assessment of temporal and spatial changes of future climate in the Jhelum river basin, Pakistan and India. Weather Clim. Extrem., 10, 40–55. https://doi.org/10.1016/j.wace.2015.07.002

Miller, J.D., Immerzeel, W.W., Rees, G. (2012). Climate change impacts on glacier hydrology and river discharge in the Hindukush-Himalayas. Mt. Res. Dev., 32, 461–467. https ://doi.org/10.1659/MRD-JOURNAL-D-12-00027.1

Mishra, V. (2015). Climatic uncertainty in Himalayan water towers. J. Geophys. Res. Atmos. 2015, 120, 2689–2705. https ://doi.org/10.1002/2014JD022650

Muhammad, S., Tian, L., Ali, S., Latif, Y., et al., (2020). Thin debris layers do not enhance melting of the Karakoram glaciers. Sci. Total Environ. 2020, 746, 141119. 10.1016/j.scitotenv.2020.141119

Myhre, G., Myhre, C.E.L., Samset, B.H., Storelvmo, T. (2013). Aerosols and their Relation to Global Climate and Climate Sensitivity. Nat. Educ. Knowl. 2013, 4, 7.

Nath, R., Luo, Y., Chen, W., Cui, X. (2018). On the contribution of internal variability and external forcing factors to the Cooling trend over the Humid Subtropical Indo-Gangetic Plain in India. Sci. Rep., 8, 18047. https://doi.org/10.1038/s41598-018-36311-5

Nayava, J.L., Adhikary, S., Bajracharya, O.R. (2017). Spatial and temporal variation of surface air temperature at different altitude zone in recent 30 years over Nepal. Mausam, 683, 417–428. https://doi.org/10.54302/mausam.v68i3.649

Palazzi, E., Von Hardenberg, J., Provenzale, A. (2013). Precipitation in the Hindu-Kush Karakoram Himalaya: Observations and future scenarios. J. Geophys. Res. Atmos. 2013, 118, 85–100. https://doi.org/10.1029/2012JD018697

Palazzi, E., Von Hardenberg, J., Terzago, S., Provenzale, A. (2014). Precipitation in the Karakoram-Himalaya: A CMIP5 view. Clim. Dyn. 2014, 45, 21–45. https ://doi.org/10.1007/s00382-014-2341-z

Panda, D.K., Mishra, A., Kumar, A., Mandal, K., et al. (2014). Spatiotemporal patterns in the mean and extreme temperature indices of India, 1971-2005. Int. J. Clim. 2014, 34, 3585–3603. https://hdl.handle.net/10568/58382

Pepin, N., Bradley, R.S., Diaz, H.F., Baraer, M., et al. (2015). Elevation-dependent warming in mountain regions of the world. Nat. Clim. Chang., 5, 424–430. https://doi.org/10.1038/nclimate2563

Philipp, A. (2003). Zirkulationsdynamische Telekonnektivität des Sommerniederschlags im Südhemisphärischen Afrika. Ph.D. Thesis, Bayerische Julius-Maximilians-Universität Würzburg, Würzburg, Germany.

Pomee, M.S., Ashfaq, M., Ahmad, B., Hertig, E. (2020). Modeling regional precipitation over the Indus River basin of Pakistan using statistical downscaling. Theor. Appl. Clim. 2020, 142, 29–57. https://doi.org/10.1007/s00704-020-03246-9

Pomee, M.S., and Hertig, E. (2021). Precipitation Projections over the Indus River Basin of Pakistan for the 21st century using a statistical downscaling framework. Int. J. Climatol. https://doi.org/10.1002/joc.7244

Preisendorfer, R. (1988). Principal Component Analysis in Meteorology and Oceanography; Elsevier: Amsterdam, The Netherlands;p. 42.

Pritchard, D.M.W., Forsythe, N., Fowler, H.J., O'Donnell, G.M., et al., (2019). Evaluation of Upper Indus Near-Surface Climate Representation by WRF in the High Asia Refined Analysis. J. Hydrometeorol. 2019, 20, 467–487. https://doi.org/10.1175/JHM-D-18-0030.1

Pritchard, H.D. (2017). Asia's glaciers are a regionally important buffer against drought. Nat. Cell Biol. 2017, 545, 169–174. DOI: 10.1038/nature25779

Rajbhandari, R., Shrestha, A.B., Kulkarni, A., Patwardhan, S.K., et al., (2014). Projected changes in climate over the Indus river basin using a high resolution regional climate model (PRECIS). Clim. Dyn. 2014, 44, 339–357. https://doi.org/10.1007/s00382-014-2183-8

Saeed, F., Hagemann, S., Jacob, D.J. (2009). Impact of irrigation on the South Asian summer monsoon. Geophys. Res. Lett., 36, 040625. https://doi.org/10.1029/2009GL040625

Sakai, A., and Fujita, K. (2017). Contrasting glacier responses to recent climate change in high-mountain Asia. Sci. Rep. 2017, 7, 13717. https://doi.org/10.1038/s41598-017-14256-5

Sanford, T.J., Frumhoff, P.C., Luers, A., Gulledge, J. (2014). The climate policy narrative for a dangerously warming world. Nat. Clim.Chang. 2014, 4, 164–166. DOI:10.1038/nclimate2148

Shrestha, A.B., Wake, C., Mayewski, P.A., Dibb, J.E. (1999). Maximum temperature trends in the Himalaya and its vicinity: Analysis based on temperature records from Nepal for the period 1971–1994. J. Clim. 1999, 12, 2276–2286.

Sperber, K.R., Annamalai, H., Kang, I.S.; Kitoh, A., et al., (2013). The Asian summer monsoon: An intercomparison of CMIP5 vs. CMIP3 simulations of the late 20th century. Clim. Dyn. 2013, 41, 2711–2744. https://doi.org/10.1007/s00382-012-1607-6

Su, B., Huang, J., Gmmer, M.; Jian, D., et al., (2016). Statistical downscaling of CMIP5 multi-model en-semble for projected changes of climate in the Indus River Basin. Atmos. Res., 178, 138–149. 10.1016/j.atmosres.2016.03.023

Sutton, R.T., Dong, B., Gregory, J.M. (2007). Land/sea warming ratio in response to climate change: IPCC AR4 model results and comparison with observations. Geophys. Res. Lett. 2007, 34, 02701. https://doi.org/10.1029/2006GL028164

Taylor, K.E. (2001). Summarizing multiple aspects of model performance in a single diagram. J. Geophys. Res. Atmos., 106, 7183–7192. DOI: 10.1029/2000JD900719

Taylor, K.E., Stouffer, R.J., Meehl, G.A. (2012). An Overview of CMIP5 and the Experiment Design. Bull. Am. Meteorol. Soc. 2012, 93, 485–498. https://doi.org/10.1175/BAMS-D-11-00094.1

Tong, S., Li, X., Zhang, J., Bao, Y., et al., (2019). Spatial and temporal variability in extreme temperature and precipitation events in Inner Mongolia (China) during 1960–2017. Sci. Total Environ. 2019, 649, 75–89. DOI: 10.1016/j.scitotenv.2018.08.262

Trigo, R.M., and Palutikof, J.P. (2001). Precipitation Scenarios over Iberia: A Comparison between Direct GCM Output and Different Downscaling Techniques. J. Clim. 2001, 14, 4422–4446. DOI: 10.1175/1520-0442(2001)014<4422:PSOIAC>2.0.CO;2

Von Storch, H., and Zwiers, F.W. (1984). Statistical Analysis in Climate Research; Amsterdam University Press: Amsterdam, The Netherlands, Volume 484.

Wake, C.P. (1989). Glaciochemical Investigations as a Tool for Determining the Spatial and Seasonal Variation of Snow Accumulation in the Central Karakoram, Northern Pakistan. Ann. Glaciol. 1989,13, 279–284. DOI**:** https://doi.org/10.3189/S0260305500008053

WGMS. Global Glacier Change Bulletin No. 3 (2016–2017); Publication Based on Database Version; World Glacier Monitoring Service: Zurich, Switzerland, 2020; p. 274.

Wijngaard, J.B., Tank, A.M.G.K., Können, G.P. (2003). Homogeneity of 20th century European daily temperature and precipitation series. Int. J. Clim. 2003, 23, 679–692. https://doi.org/10.1002/joc.906

Wilcoxon, F. (1945). Individual Comparisons by Ranking Methods. In Breakthroughs in Statistics; Springer: New York, NY, USA, 1945; Volume 1, p. 80

Wilks, S. (2006). Statistical Methods in the Atmospheric Sciences; Academic press: Cambridge, MA, USA, p. 91.

Wu, J., Zha, J., Zhao, D. (2016). Evaluating the effects of land use and cover change on the decrease of surface wind speed over China in recent 30 years using a statistical downscaling method. Clim. Dyn. 2016, 48, 131–149. https://doi.org/10.1007/s00382-016-3065-z

Yaseen, M., Ahmad, I., Guo, J., Azam, M.I., et al., (2020). Spatiotemporal Variability in the Hydrometeorological Time-Series over Upper Indus River Basin of Pakistan. Adv. Meteorol. 2020, 2020, 5852760. https://doi.org/10.1155/2020/5852760

Zemp, M., Huss, M., Thibert, E., Eckert, N., et al., (2016). Global glacier mass changes and their contributions to sea-level rise from 1961 to 2016. Nature 2019, 568, 382–386. https://doi.org/10.1038/s41586-019-1071-0

Zhao, A., Bollasina, M.A., and Stevenson, D.S. (2019). Strong Influence of Aerosol Reductions on Future Heatwaves. Geophys. Res. Lett. 2019,46, 4913–4923. 10.1029/2019GL082269

## Supporting Information

**Table S1.** Overview of study stations…. …….(Same as **Table 1 in article 1** of this thesis).

**Table S2.** The seasonal outcome of S-Mode PCA over different predictor fields. PCs are the number of retained principal components, and Exp. Var denotes the percentage of total predictor variance, as explained by the retained PCs

| Predictors | WS | | PMS | | MS | |
|---|---|---|---|---|---|---|
| | **PCs (Nos)** | **Exp.Var (%)** | **PCs (Nos)** | **Exp.Var (%)** | **PCs (Nos)** | **Exp.Var (%)** |
| zg200 | 8 | 89 | 3 | 92 | 4 | 88 |
| va200 | 12 | 90 | 12 | 87 | 15 | 86 |
| ua200 | 10 | 88 | 9 | 88 | 10 | 89 |
| zg500 | 8 | 88 | 3 | 82 | 8 | 86 |
| va500 | 10 | 83 | 13 | 83 | 20 | 83 |
| ua500 | 10 | 85 | 9 | 84 | 11 | 79 |
| zg700 | 9 | 91 | 6 | 87 | 7 | 84 |
| va700 | 10 | 76 | 14 | 79 | 19 | 79 |
| ua700 | 11 | 83 | 9 | 79 | 12 | 81 |
| hus700 | 2 | 85 | 2 | 90 | 5 | 92 |
| hur700 | 3 | 79 | 4 | 80 | 4 | 77 |
| va850 | 16 | 83 | 15 | 79 | 19 | 80 |
| ua850 | 11 | 81 | 13 | 80 | 11 | 79 |
| ta850 | 6 | 86 | 4 | 85 | 7 | 82 |
| hus1000 | 3 | 85 | 4 | 90 | 2 | 92 |
| hur1000 | 5 | 80 | 3 | 76 | 7 | 77 |
| psl | 5 | 87 | 7 | 88 | 6 | 87 |
| Average | **8** | **84** | **8** | **84** | **10** | **84** |

**Table S3.** GCM used in the study……. **(**Same as **Table 2** in **Article 2** of this thesis).

**Table S4.** Same as **Table 2** in **Article 3** of this thesis but for $T_{min}$ models under the basin-wide regionalization experiment

***WS Models***

| Reg. Alt | RR | Mean Obs. $T_{min}$ | Predictors | PCs | RMSE (C°) | | MSESS (%) | | $R^2$ | |
|---|---|---|---|---|---|---|---|---|---|---|
| (m-amsl) | | (C°) | (Name) | (Nos) | Cal | Val | Cal | Val | Cal | Val |
| 2223 (1251 -3200) | Chilas | 4.30 | hus1000 | 2 | 1.01 | 1.04 | 87.95 | 86.65 | 0.88 | 0.90 |
| 1173.5 (308-2744) | Kakul | 2.79 | hus1000 | 2 | 0.89 | 0.91 | 85.91 | 84.69 | 0.86 | 0.88 |
| 3266 (2156-4030) | Gupis | -2.82 | hus1000 | 2 | 1.50 | 1.54 | 77.90 | 75.90 | 0.78 | 0.80 |
| *266 (35-1097)* | Jacobabad | 11.04 | hus1000 | 3 | 1.25 | 1.30 | 87.80 | 86.39 | 0.88 | 0.89 |
| 365 (122-1405) | Jehlum | 8.26 | hus1000 | 3 | 0.95 | 0.99 | 90.98 | 89.98 | 0.91 | 0.92 |
| | *Avg. Basin* | | | 2 | 1.12 | 1.16 | 86.11 | 84.72 | 0.86 | 0.88 |
| | *Avg. UIB* | | | 2 | 1.13 | 1.16 | 83.92 | 82.41 | 0.84 | 0.86 |
| | *Avg. Lower Indus* | | | 3 | 1.10 | 1.15 | 89.39 | 88.19 | 0.90 | 0.91 |

***PMS Models***

| | | | | | | | | | | |
|---|---|---|---|---|---|---|---|---|---|---|
| 2627) (1251-4030) | Astore | 7.63 | hus1000 | 4 | 0.89 | 0.95 | 92.05 | 90.64 | 0.92 | 0.93 |
| 1327 (508-2168) | Ghari Duputta | 16.22 | ua500 | 7 | 1.20 | 1.29 | 87.98 | 85.54 | 0.88 | 0.89 |
| 1281 (353-2591) | Dir | 11.41 | hus1000 | 3 | 1.25 | 1.31 | 87.29 | 85.52 | 0.87 | 0.89 |
| 961 (961) | Saidu Sharif | 16.39 | ua850 | 6 | 1.00 | 1.10 | 92.03 | 90.12 | 0.92 | 0.93 |
| 419 (187-1097) | Sialkot | 21.81 | va700 | 8 | 1.03 | 1.17 | 91.49 | 88.76 | 0.91 | 0.92 |
| 259 (28-1405) | DI Khan | 22.56 | hus1000 | 4 | 1.08 | 1.16 | 89.63 | 87.45 | 0.90 | 0.90 |
| | ***Avg. Basin*** | | | ***5*** | ***1.08*** | ***1.16*** | ***90.08*** | ***88.01*** | ***0.90*** | ***0.91*** |
| | ***Avg. UIB*** | | | ***5*** | ***1.09*** | ***1.16*** | ***89.84*** | ***87.96*** | ***0.90*** | ***0.91*** |
| | *Avg. Lower Indus* | | | 6 | 1.06 | 1.17 | 90.56 | 88.11 | 0.91 | 0.91 |

***MS Models***

| | | | | | | | | | | |
|---|---|---|---|---|---|---|---|---|---|---|
| 2218 (1251-4030) | Sakardu | 14.07 | ua850 | 5 | 0.95 | 1.03 | 86.74 | 84.02 | 0.87 | 0.89 |
| 746.25 (122-2591) | Jehlum | 24.99 | va500 | 13 | 0.52 | 0.61 | 84.74 | 78.28 | 0.85 | 0.87 |
| 2868 (1464-3719) | Darosh | *20.49* | *va850* | *7* | 1.42 | 1.52 | 75.02 | 70.50 | 0.75 | 0.78 |
| *961 (961)* | Saidu Sharif | 20.59 | va850 | 9 | 1.07 | 1.15 | 81.12 | 77.34 | 0.81 | 0.84 |
| 2892.5 (2156-4730) | Gupis | *15.35* | *va850* | *8* | 1.15 | 1.26 | 81.76 | 77.26 | 0.82 | 0.85 |
| *659 (172-1425)* | Risapur | 24.28 | va500 | 10 | 0.76 | 0.88 | 85.64 | 80.23 | 0.85 | 0.87 |
| 52 (9-122) | Hyderabad | 26.42 | hus1000+va500 | 9 | 0.53 | 0.60 | 78.45 | 72.07 | 0.78 | 0.81 |
| | ***Avg. Basin*** | | | ***9*** | ***0.91*** | ***1.01*** | ***81.92*** | ***77.10*** | ***0.82*** | ***0.84*** |
| | ***Avg. UIB*** | | | ***8*** | ***1.02*** | ***1.11*** | ***81.88*** | ***77.48*** | ***0.82*** | ***0.85*** |
| | *Avg. Lower Indus* | | | 10 | 0.65 | 0.74 | 82.05 | 76.15 | 0.82 | 0.84 |

**Table S5.** Same as **Table 4 in article 3** of this thesis, but shows the GCM and ERA-Interim reanalysis predictor correspondence for the $T_{min}$.

| Seasons | Regions | CMCC-CMS | CMCC-CM | CNRM-CM5 | Can-ESM2 | MPI-ESM-LR | MPI-ESM-MR | Nor-ESM1-ME | Nor-ESM1-M | Model Ensemble |
|---|---|---|---|---|---|---|---|---|---|---|
| | **UIB** | | | | | | | | | |
| WS | R1 | 0.79 | 0.80 | **0.82** | 0.79 | 0.70 | 0.71 | *0.68* | 0.71 | 0.75 |
| | R3 | 0.79 | 0.80 | **0.82** | 0.79 | 0.70 | 0.71 | *0.68* | 0.71 | 0.75 |
| | R5 | 0.76 | 0.79 | **0.82** | 0.78 | 0.67 | 0.67 | *0.66* | 0.69 | 0.73 |
| | Avg. over UIB | 0.78 | 0.80 | **0.82** | 0.79 | 0.69 | 0.70 | *0.67* | 0.70 | 0.74 |
| | UIB Uncertainity (in %) | 22.00 | 20.33 | **18** | 21.33 | 31.00 | 30.33 | *32.67* | 29.67 | 25.67 |
| | **Lower Indus** | | | | | | | | | |
| | R4 | 0.79 | 0.8 | **0.82** | 0.79 | 0.70 | 0.71 | *0.68* | 0.71 | 0.75 |
| | R6 | 0.67 | 0.74 | **0.81** | 0.69 | 0.6 | 0.61 | *0.59* | 0.62 | 0.67 |
| | Avg. over Lower Indus | 0.73 | 0.77 | **0.82** | 0.74 | 0.65 | 0.66 | *0.64* | 0.67 | 0.71 |
| | Lower Indus Uncertainity (in %) | 27 | 23 | **18.5** | 26 | 35 | 34 | *36.5* | 33.50 | 29.19 |
| PMS | **UIB** | | | | | | | | | |
| | R1 | 0.59 | 0.65 | **0.72** | 0.48 | 0.60 | 0.59 | 0.46 | *0.41* | 0.56 |
| | R3 | **0.80** | 0.71 | *0.66* | 0.73 | 0.69 | 0.74 | 0.69 | 0.68 | 0.71 |
| | R5 | 0.60 | 0.66 | **0.72** | 0.50 | 0.62 | 0.60 | 0.47 | *0.43* | 0.58 |
| | R7 | *0.64* | 0.65 | 0.67 | 0.69 | **0.71** | 0.67 | 0.66 | 0.67 | 0.67 |
| | Avg. over UIB | 0.66 | 0.67 | **0.69** | 0.60 | 0.66 | 0.65 | *0.57* | 0.55 | 0.63 |
| | UIB Uncertainity (in %) | 34.25 | 33.25 | **30.75** | 40.00 | 34.5 | 35 | *43* | 45.25 | 37.00 |
| | **Lower Indus** | | | | | | | | | |
| | R4 | **0.62** | 0.59 | 0.55 | 0.52 | 0.61 | 0.53 | 0.57 | 0.56 | 0.57 |
| | R6 | 0.57 | 0.64 | **0.72** | 0.51 | 0.6 | 0.56 | 0.48 | *0.45* | 0.57 |
| | Avg. over Lower Indus | 0.60 | 0.62 | **0.64** | 0.52 | 0.61 | 0.55 | 0.53 | *0.51* | 0.57 |
| | Lower Indus Uncertainity (in %) | 40.50 | 38.50 | **36.5** | 48.5 | 39.5 | 45.5 | 47.50 | *49.5* | 43.25 |
| MS | **UIB** | | | | | | | | | |
| | R1 | *0.54* | **0.64** | 0.59 | 0.61 | 0.60 | 0.56 | 0.56 | 0.60 | 0.59 |
| | R3 | **0.43** | 0.42 | 0.41 | 0.39 | 0.42 | **0.43** | 0.39 | *0.35* | 0.41 |
| | R4 | 0.50 | 0.52 | 0.49 | 0.46 | **0.55** | 0.48 | *0.42* | *0.42* | 0.48 |
| | R5 | 0.54 | 0.54 | 0.51 | 0.47 | **0.58** | 0.50 | 0.46 | *0.43* | 0.50 |
| | R7 | 0.49 | 0.49 | 0.48 | **0.42** | **0.54** | 0.45 | 0.44 | *0.42* | 0.47 |
| | Avg. over UIB | 0.50 | 0.52 | 0.50 | 0.47 | **0.54** | 0.48 | 0.45 | *0.44* | 0.49 |
| | UIB Uncertainity (in %) | 50 | 47.80 | 50.40 | 53.00 | **46.2** | 51.6 | 54.6 | *55.6* | 51.15 |
| | **Lower Indus** | | | | | | | | | |
| | R2 | 0.42 | **0.46** | 0.40 | *0.18* | 0.45 | 0.45 | 0.39 | 0.47 | 0.40 |
| | R6 | 0.40 | 0.40 | 0.41 | 0.39 | **0.43** | 0.41 | 0.36 | *0.33* | 0.39 |
| | Avg. over Lower Indus | 0.41 | **0.43** | 0.41 | *0.29* | **0.44** | **0.43** | *0.38* | 0.40 | 0.40 |
| | Lower Indus Uncertainity (in %) | 59 | 57 | 59.5 | 71.5 | 56 | 57 | *62.5* | 60 | 60.31 |

**Table S6.** P-values of the Wilcoxon signed-rank test to estimate the statistical significance of seasonal $T_{max}$ and $T_{min}$ changes during 2071-2100 relative to 1976-2005 under both RCP scenarios. Results are statistically significant, where the p-value is less than 0.05.

| Seasons | **Sub-regions** | RCP4.5 | | RCP8.5 | |
|---|---|---|---|---|---|
| **WS** | | **$T_{max}$** | **$T_{min}$** | **$T_{max}$** | **$T_{min}$** |
| | **UIB** | | | | |
| | R1 | 1.64E-05 | 7.28E-256 | 7.34E-05 | 3.12E-293 |
| | R3 | 6.06E-09 | 1.96E-264 | 0.00012 | 3.29E-298 |
| | R5 | 3.63E-120 | 6.25E-218 | 2.04E-218 | 2.07E-268 |
| | Lower Indus | | | | |
| | R4 | 9.25E-144 | 3.22E-258 | 5.27E-183 | 3.50E-292 |
| | R6 | 6.06E-09 | 3.57E-261 | 2.30E-268 | 2.49E-294 |
| **PMS** | **UIB** | | | | |
| | R1 | 0.07312 | 2.17E-23 | 0.006488627 | 1.61E-55 |
| | R3 | 2.99E-10 | 0.41789 | 1.27E-24 | 0.76316 |
| | R5 | 1.66E-05 | 1.32E-23 | 2.56E-12 | 5.03E-56 |
| | R7 | 5.60E-06 | 0.01265 | 3.60E-13 | 0.0014186 |
| | Lower Indus | | | | |
| | R4 | 1.63E-119 | 0.07357 | 2.52E-180 | 0.0541761 |
| | R6 | 5.37E-11 | 2.84E-26 | 2.96E-27 | 1.34E-64 |
| **MS** | **UIB** | | | | |
| | R1 | 0.01770 | 0.00393 | 2.05E-13 | 0.0001706 |
| | R3 | 8.63E-109 | 0.00122 | 3.30E-23 | 2.94E-14 |
| | R4 | 1.43E-06 | 0.05359 | 7.05E-17 | 5.99E-05 |
| | R5 | 2.69E-05 | 0.10281 | 2.48E-13 | 0.002231 |
| | R7 | 0.1134584 | 0.18033 | 3.94E-06 | 0.0674985 |
| | **Lower Indus** | | | | |
| | R2 | 1.65E-174 | 1.14E-179 | 8.93E-217 | 2.59E-232 |
| | R6 | 4.47E-56 | 0.00233 | 2.27E-142 | 2.80E-13 |

**Appendix S1**. GCM Ranking Procedure……..(same as **Section 3.5 in article 2** of this thesis).